GHENT UNIVERSITY
Faculty of Sciences
Department of Organic Chemistry
Polymer Chemistry & Biomaterials Research Group

Cell-Interactive Biopolymer-based Hydrogels designed for Tissue Engineering

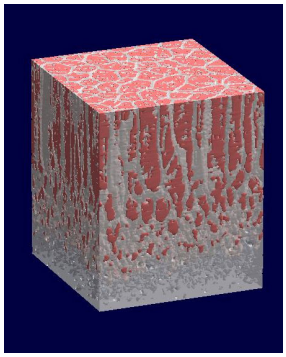

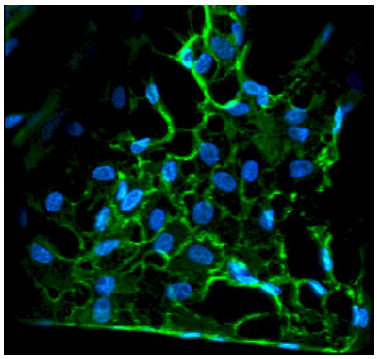

Proefschrift voorgelegd tot het behalen van de graad van Doctor in de Wetenschappen, Groep Scheikunde

Sandra Van Vlierberghe

Promotor: Prof. Dr. E. Schacht

GHENT UNIVERSITY
Faculty of Sciences
Department of Organic Chemistry
Polymer Chemistry & Biomaterials Research Group

Cell-Interactive Biopolymer-based Hydrogels designed for Tissue Engineering

Proefschrift voorgelegd tot het behalen van de graad van Doctor in de Wetenschappen, Groep Scheikunde

Sandra Van Vlierberghe

Promotor: Prof. Dr. E. Schacht

Dankwoord

Bij het afronden van dit doctoraatswerk ben ik een aantal mensen een woordje van dank verschuldigd.

In de eerste plaats wil ik graag mijn promotor, Prof. Etienne Schacht, bedanken omdat hij mij de kans geboden heeft om dit doctoraat aan te vatten. Daarnaast heb ik steeds beroep kunnen doen op zijn kennis en ervaring en heb ik het geluk gehad om met allerlei onderdelen van een doctoraat (o.a. doceren, congressen bijwonen, etc) uitgebreid kennis te maken!

Prof. Peter Dubruel wens ik eveneens te bedanken. Hij heeft niet alleen de *in vitro* biocompatibiliteit van de geproduceerde stalen geëvalueerd als toenmalige post-doc, maar bovendien kon ik steeds bij hem terecht zowel voor wetenschappelijke als niet-wetenschappelijke kwaaltjes.

De financiële steun van het IWT was onontbeerlijk.

Verder sta ik eveneens in het krijt bij alle mensen van het administratief en het technisch personeel en in het bijzonder bij Joris (tevens mijn loopmaatje), Mario, Marc, Philomain, Frank en Tim. Voor elk probleem bedachten zij wel een praktische oplossing… Mannen, jullie hebben er nog enen te goed van mij!

Ook wil ik alle collega's van de PBM groep bedanken voor de aangename samenwerking:

- ✓ Mijn labogenootjes Els en Jorg: We hebben op korte tijd -Jorg is nog niet zo lang in ons midden- toch al heel wat afgelachen!
- ✓ Mijn 'pseudo-chef' Vincent en Veska: De samenwerking op PolExGene verloopt vlot en onze wetenschappelijke uitstapjes zijn steeds heel aangenaam…
- ✓ Alle andere huidige en ex-collega's met wie ik mij de voorbije jaren geamuseerd heb of op wie ik kon rekenen voor wetenschappelijk advies.

Bovendien wil ik Prof. Luc Van Hoorebeke, Prof. Patric Jacobs, Dr. Veerle Cnudde en Dr. Bert Masschaele bedanken voor de micro-CT bijdrage. In addition, I would like to acknowledge Prof. James Kirkpatrick and Dr. Ron Unger for the *in vitro* biocompatibility assays. Mijn oprechte dank gaat eveneens uit naar Prof. Ria Cornelissen en Drs. Evi Lippens voor de *in vitro* evaluatie van de hydrogelen gesynthetiseerd in dit werk. Olivier Janssens dank ik voor de SEM-analyses en Drs. Els Vanderleyden en Drs. Nele De Smet voor de XPS-metingen.

En zoals men zegt ‘last but not least’:

Bedankt aan alle familieleden en vrienden die ik tijdens de volgende opsomming vergeten ben!

Ilse, Griet en Tinie, bedankt voor jullie vriendschap. Het is fijn om te weten dat je vrienden hebt waar je altijd op kan rekenen!

(Schoon)mama en schoonpapa, bedankt voor alle steun die jullie me gegeven hebben, niet alleen tijdens mijn doctoraat maar ook tijdens de jaren die eraan vooraf gegaan zijn.

Kathleen, het is super om een zus te hebben zoals jij die tevens mijn beste vriendin geworden is. Bedankt voor ALLES!

Tim, zonder jou had ik nooit gestaan waar ik nu sta. Telkens ik het moeilijk had, monterde jij me weer op. Bedankt om er altijd te zijn voor mij! Ik kijk al uit naar het volgende hoofdstuk in ons leven…

Sandra

Table of contents

Chapter I: Introduction

Chapter II:

Synthesis and Characterization of the Hydrogel Precursors

Chapter III:

Preparation and Characterization of Hydrogel Films

Chapter IV:

Preparation and Characterization of Gelatin Scaffolds

Chapter V:

Scaffolds Based on Gelatin and Chondroitin Sulphate

Chapter VI: Alternative Crosslinking Methods

Chapter VII: Interaction between Gelatin and Extra-Cellular Matrix Components

Chapter VIII: Biological Evaluation

Chapter I: Introduction

1 Problem statement and objectives

One of the most frequent, expensive and serious problems facing human health care, is the loss or failure of organs or tissues. The medical need for tissue and organ substitutes can arise from trauma, infectious, inherited or age-related diseases, or organ failure. Estimates of the total U.S. healthcare costs for patients with tissue loss or organ failure exceed $400 billion annually.[1] Every year, 21 million people in the United States suffer from failing tissues that need to be replaced or repaired.[2] In Europe, nearly 10 people a day die waiting for vital organs. As a result, there is a need for new, innovating technologies in the field of regenerative medicine in order to overcome these problems.[3, 4]

Regenerative medicine comprises different technologies that have a major impact on the human body and enable the repair of malfunctioning tissues.[5] It is often, however not exclusively, applied to treat elderly people. The two major application areas are at both ends of life.[6] One is at the beginning of life, when the processes of embryogenesis and foetal formation go wrong. They deal with how we can restructure, reform and rebuild those tissues. The second occurs during aging and deals with how we can approach the repair of key functions.

There are four major disciplines that comprise regenerative medicine, of which one discipline is applied in the present work.[7]

The first is the use of our own genes, proteins and antibodies to restore failing tissues. The latter is the most gentle approach. Namely, the addition or removal of a human protein where it is needed.[8] A second set of technologies has to do with the use of individual adult cells as therapy (i.e. tissue engineering), which will be the topic of the present work.[9] The third field is embryo research or the use of stem cells for medicine.[10] The final aspect of regenerative medicine, is the use of prosthetic devices to substitute organ or tissue function.

The final goal of the present work is to develop porous, biodegradable hydrogel scaffolds, possessing specific (pore) characteristics, suitable for a large variety of tissue engineering applications.

2 Definition and concept of tissue engineering

In literature, tissue engineering has often been defined.[11,12] However, a widely spread definition of tissue engineering was stated by Langer and Vacanti:[13]

"*Tissue engineering combines the principles and methods of the life sciences with those of engineering to elucidate fundamental understanding of structure-function relationships in normal and diseased tissues, to develop materials and methods to repair damaged or diseased tissues, and to create entire tissue replacements."*

There are three approaches in tissue engineering:[14]

1) The use of isolated cells or cell substitutes at the location of a defect.
2) The delivery of tissue-inducing substances, such as growth and differentiation factors, to targeted locations.
3) Growing cells in three-dimensional scaffolds, either *in vivo* or *in vitro*.

A common approach is the third one. Specific cells can be isolated through a biopsy from a patient. The cells are then grown into a three-dimensional scaffold under controlled culture conditions. Subsequently, the construct is delivered to the desired site in the patient's body (figure 1-1).[11]
When applying the third approach, a substrate material is required, possessing suitable characteristics.[15] It should exhibit good biocompatibility, meaning that it should not evoke an unresolved inflammatory response, nor demonstrate extreme immunogenicity or cytotoxicity. In addition, the mechanical properties of the scaffold must be sufficient. The mechanical strength required depends to a great extent on the site of the defect. Two tissue categories can be distinguished including hard (e.g. bone) and soft (e.g. skin) tissue.

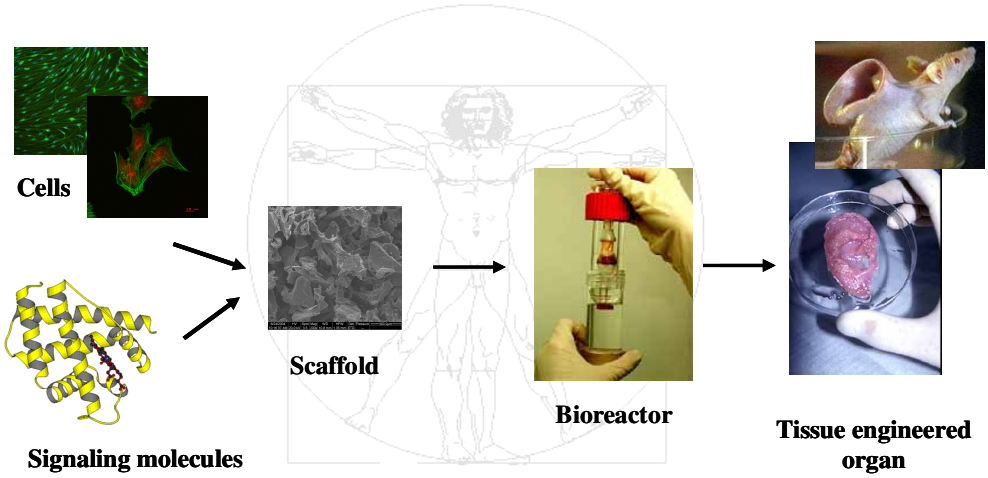

Figure 1-1: The strategy of tissue engineering.

Table 1-1 shows an overview of some common tissues with their respective mechanical properties as indicated by their elastic moduli.[16] Finally, the three-dimensional scaffolds developed should be easy to sterilize.

HARD TISSUE	MODULUS (GPa)	SOFT TISSUE	MODULUS (MPa)
Cortical bone	12.8	Skin	0.1
Cancellous bone	0.4	Intraocular lens	5.6
Enamel	84.3	Articular cartilage	10.5
Dentine	11.0	Tendon	401.5

Table 1-1: Mechanical properties of hard and soft tissues.

Investigations into synthetic and natural inorganic ceramic materials (e.g. hydroxyapatite and tricalcium phosphate) as candidate scaffold material have been aimed mostly at bone tissue engineering.[17-19] Synthetic and natural polymers, however, are an attractive alternative and versatile in their applications to the growth of most tissues. Aliphatic polyesters such as polyglycolic acid (PGA), polylactic acid (PLA) and polycaprolactone (PCL) are the most commonly used synthetic polymers, functioning as scaffolds for tissue engineering.[20-22] Naturally derived protein or carbohydrate polymers have been used as carriers for the growth of several tissue types.[23, 24] Collagen is, in this regard, the most often used natural polymer.[25-27]

3 Composition of the extra-cellular matrix

Extracellular matrices (ECM) are made up of an insoluble meshwork of proteins and carbohydrates that is deposited by cells and that fills most of the intercellular spaces.[28] Matrices at different locations in the body consist of different combinations of the three major classes of biomolecules:

- ✓ Structural proteins: collagen and elastin
- ✓ Specialized proteins: e.g. fibrillin, fibronectin and laminin
- ✓ Proteoglycans, which are composed of a protein core to which glycosaminoglycans are attached, forming extremely complex, high molecular weight components of the ECM.

Most of the extracellular matrix glycoproteins and collagens that have been identified, interact with cells and cellular behaviour often appears to originate in response to these interactions.[12] The easiest observable result of the interaction of cells with the extracellular matrix is cell adhesion.[29] The adhesive properties of the extracellular matrix proteins can be easily demonstrated *in vitro* by plating cells on a surface coated with extracellular matrix material. The cells will rapidly adhere to such a surface and spread on it.[30] However, the adhesive proteins not only promote adhesion, but they also stimulate cell migration.[31]

A more complex way in which ECMs influence cells, is their promotion of cell differentiation.[32] Probably the most important effect of matrices on cells is illustrated by the fact that normal cells require attachment to a substrate to enable survival and growth.[33] The most abundant components of the ECM are described in the following paragraphs.

3.1 Fibronectin

Fibronectin is a large multidomain glycoprotein possessing a molecular weight of ~500,000 Da and an iso-electric point of approximately 6. It is localized in connective tissue, on cell surfaces and in plasma and other body fluids.[34] Fibronectin interacts with a variety of macromolecules, including components of the cytoskeleton and the

extracellular matrix[35], with blood components[36] and with cell-surface receptors on a variety of cells including fibroblasts, neurons, phagocytes and bacteria.[35, 37] Fibronectin also forms inter- and intramolecular interactions, forming fibrillar entities whose structure is poorly understood.[38] In addition, it binds several small molecules such as sugars and Ca-ions.[39] These diverse recognition functions are located on domains, of which many have been expressed in recombinant form or isolated from proteolytic digests with retention of specific binding properties. The amino acid sequence of fibronectin typically reveals three types of internally homologous repeats or modules separated by short connecting sequences. There are 12 type I, 2 type II and 15 type III modules.[40] Each module constitutes an independently folded unit, often referred to as a domain, but not to be confused with 'functional domains' that frequently contain more than one module. 'Functional domains' retain the ability to interact with other macromolecules, e.g. collagen, glycosaminoglycans, proteoglycans etc (figure 1-2).[41] Type I and II modules each contain four conserved cysteines comprising two disulfide bonds that are crucial for stability and function.[42]

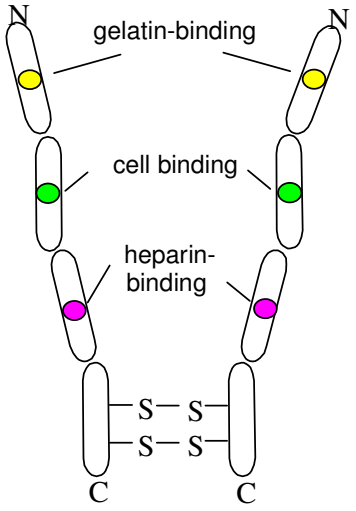

Figure 1-2: Binding sites, present on fibronectin.

A functional domain, responsible for cell-binding activity has been isolated from proteolytic fragments and its amino acid sequence has been determined. Synthetic peptides, corresponding to different segments of this domain were prepared and used to localize the cell-binding activity to a specific tripeptide sequence (Arg-Gly-Asp, or RGD).[43] The RGD sequence is a common motif in a variety of extracellular

adhesive proteins and it is recognized by a family of cell-surface receptors that bind these proteins.[44] Despite the common tripeptide sequence, found at the sites recognized by these receptors, each receptor specifically recognizes its own small set of adhesive molecules. Thus, receptor binding must also depend on other parts of the adhesive protein sequence.[45]

Fibronectin is not only important for cell adhesion, but also for cell migration by helping cells attach to the matrix.[31] The effect must be delicately balanced so that the migrating cells get a grip on the matrix without becoming immobilized on it.[46]

3.2 Collagen

Collagen is the major protein comprising the ECM and possesses a molecular weight of approximately 300,000 Da. The latter varies significantly according to the collagen type and the living species. There are at least 12 types of collagen.[47] Types I, II and III are the most abundant and form fibrils of similar structure. Type IV collagen forms a two-dimensional reticulum and is a major component of the basal lamina. Collagens are predominantly synthesized by fibroblasts, but epithelial cells also synthesize these proteins.[48]

The fundamental structure of collagens is a long and thin diameter rod-like protein.[27] Type I collagen for instance is 300 nm long, 1.5 nm in diameter and consists of three coiled subunits, composed of α-chains.[49] Each chain consists of 1050 amino acids, wound around each other in a characteristic right-handed triple helix.[48]

Collagens are also rich in proline and hydroxyproline.[50] They are synthesized as longer precursor proteins, called procollagens. These pro-domains are globular and form multiple intrachain disulfide bonds. The disulfides stabilize the proprotein allowing the triple helical section to form.[51] Collagen fibres are assembled in the ER and Golgi complexes.[52]

In table 1-2, an overview is presented of the different collagen types and their localization.[53-60]

COLLAGEN TYPE	LOCALIZATION
I	skin, tendon, bone
II	cartilage, vitreous humor
III	skin, muscle, frequently associated with type I
IV	all basal lamina
V	most interstitial tissue, associated with type I
VI	most interstitial tissue, associated with type I
VII	epithelia
VIII	some endothelial cells
IX	cartilage, associated with type II
X	hypertrophic and mineralizing cartilage
XI	cartilage
XII	cartilage, interacts with types I and III

Table 1-2: Overview of the different collagen types, localized in various tissues.

3.3 Glycosaminoglycans and proteoglycans

The most abundant polysaccharides in the body are the glycosaminoglycans (GAGs).[61] These molecules are long, unbranched polysaccharides, containing a repeating disaccharide unit. The disaccharide units consist of N-acetylgalactosamine or N-acetylglucosamine and a uronic acid such as glucuronate or iduronate.[62] GAGs are highly negatively charged, with a large hydrodynamic radius, resulting in viscous solutions.[63] GAGs are common constituents of cell surfaces and extracellular matrices.[64] They are characterized by a low compressibility, making them ideal as a lubricating fluid in the joints.[65] Moreover, their rigidity provides structural integrity to cells and pathways allowing cell migration. Biocharacteristics of GAGs include the binding and modulation of enzymes, protease inhibitors and cytokines.[66] The specific GAGs of physiological significance are hyaluronic acid, dermatan sulphate, chondroitin sulphate, heparin, heparan sulphate and keratin sulphate.[67] Hyaluronan is the only GAG that does not contain any sulphate and is not covalently attached to proteins forming a proteoglycan.[68] It is a component of non-covalently formed complexes with proteoglycans in the ECM. Hyaluronic acid polymers are very large (100,000 to 10,000,000 Da) and can contain a large volume of water.[69] This property makes them excellent shock absorbers.[70] Heparan sulphate binds to a variety of

extracellular matrix and basement membrane components including fibronectin, laminin and collagen, and promotes interactions of these components with integrins.[71] Heparan sulphate also functions as co-receptors for many growth factors including fibroblast growth factors and vascular endothelial growth factors.[72] These biocharacteristics implicate a major role for GAGs in phenomena like cell adhesion, migration, proliferation and differentiation.[73]

The majority of GAGs in the body are linked to core proteins, forming proteoglycans (i.e. mucopolysaccharides) (figure 1-3). The GAGs extend perpendicularly from the core in a brush-like structure.[62] The linkage of GAGs to the protein core involves a specific trisaccharide composed of two galactose residues and a xylulose residue. The trisaccharide linker is coupled to the protein core through an O-glycosidic bond to an S-residue in the protein.[74]

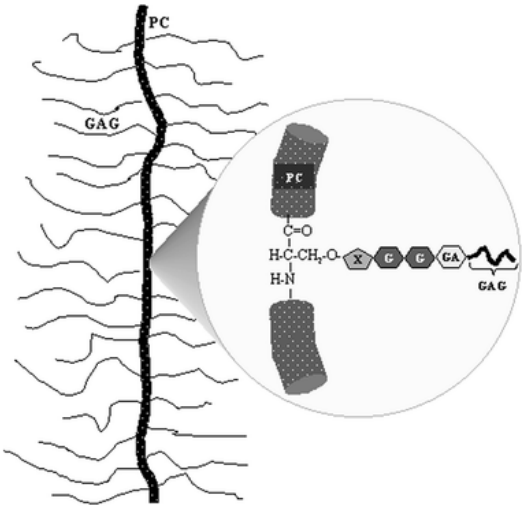

Figure 1-3: Schematic representation of a proteoglycan. Chains of glycosaminoglycans (GAG) are covalently attached to a protein core (PC). The GAG chain is bound to serine residues of the PC through a linkage region consisting of a xylosyl group (X), two D-galactose residues (G) and one D-glucuronic acid (GA).

Proteoglycans and GAGs perform numerous vital functions within the body, some of which still remain to be studied. One well-defined function of heparin is its role in preventing blood coagulation.[75] Heparin is abundant in granules of mast cells that line blood vessels. The release of heparin from these granules, in response to injury, and its subsequent entry into the serum leads to an inhibition of blood clotting, in the following manner. Free heparin complexes with and activates antithrombin III, which in turn inhibits all the serine proteases of the coagulation cascade.[76]

4 Hydrogels

4.1 Definition and properties

Hydrogels are hydrophilic polymer networks, able to absorb a large amount of water (i.e. one tenth to thousand times their dry weight).[77] Hydrophilic groups or domains, which are hydrated in an aqueous dissolution, are present in the network, creating the hydrogel structure.[78] In order to avoid the dissolution of the hydrophilic polymer chains in the aqueous phase, crosslinks need to be incorporated. The introduced crosslinks can be either physical or chemical.[24] Unstable bonds are often introduced in the gels, since it can be advantageous for many applications that the hydrogels are biodegradable.[79] These bonds can be broken either enzymatically or chemically. In the latter case, this mostly occurs via hydrolysis.[80]

Physical or reversible gels are formed by secondary forces such as ionic, hydrophobic interactions or hydrogen bonds. Irreversible or chemical hydrogels are covalently crosslinked networks.[81]

Besides biodegradability, biocompatibility also is very important.[79] When hydrogels are in contact with the body, the degradation products should not be toxic. This means that the components formed, should be metabolized into harmless products, or that they should be excreted from the body. Consequently, the starting products should be selected carefully.[82] Interestingly, the irritation of the surrounding tissue is also limited because of the soft and rubbery nature of hydrogels.[83]

4.2 Physical hydrogels

Formation of physical hydrogels can occur via different mechanisms.

A first method is crosslinking through ionic interaction. Polycations crosslink via anions and vice versa. Alginate is a well-known example of a polymer which can be crosslinked by ionic interactions. It is a polysaccharide with mannuronic acid and glucuronic acid residues and crosslinking occurs via calcium ions. Hydrogels can also be obtained by complexation of polyanions with polycations.[84]

A second procedure is crosslinking by crystallization. When an aqueous solution of, for example, poly(vinylalcohol) (PVA) is stored at room temperature, a gel with high elasticity is formed gradually. This gel formation is ascribed to the presence of PVA crystals, acting as junction zones in the network.[85]

Alternatively, physical gels can also be prepared from block- and graftcopolymers. The mixing of two different polymers and the synthesis of blockcopolymers can lead to the formation of interesting gels with good biocompatibility and interesting mechanical and swelling properties. The biodegradability of poly(lactic acid) and the biocompatibility of poly(ethylene glycol) for example, form a suitable combination.[86] This copolymer is often applied in wound bandages.

There exist also thermally induced networks. Cooling a polymer solution in order to form a gel (e.g. agarose or gelatin in water) is occurring most frequently.[87] However, heating a solution to induce gel formation also exists (e.g. PEO-PPO-PEO blockcopolymers in water).[79]

Several other methods are reported in literature (e.g. protein interactions and antigen-antibody interactions).[88]

4.3 Chemical hydrogels

Chemical crosslinking can also be subdivided into different categories.

A first method is the radical polymerization of monomers in the presence of crosslinkers (e.g. poly(2-hydroxyethyl methacrylate) (pHEMA). pHEMA is obtained by polymerisation of HEMA in the presence of a suitable crosslinker, such as ethylene glycol dimethacrylate (figure 1-4).[89]

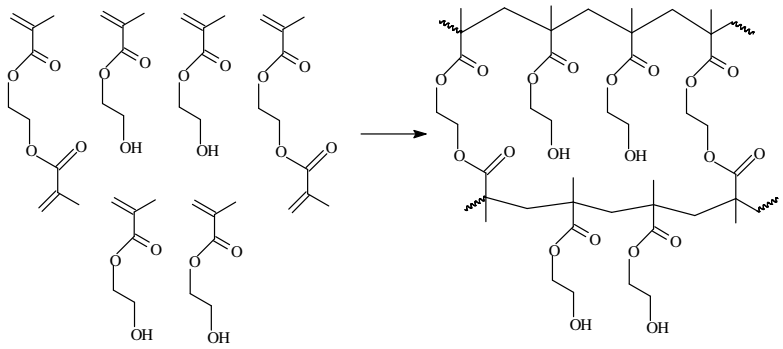

Figure 1-4: Synthesis of poly(2-hydroxyethyl methacrylate).

A large variety of hydrogels can be obtained by applying the same procedure.
Beside the radical polymerization of mixtures of vinyl monomers, chemical gels can also be obtained by radical polymerization of water soluble polymers, derivatized with polymerizable side groups (e.g. dextran).[90]

A second method is the hydrogel formation via chemical reaction of complementary groups. Watersoluble polymers owe their solubility to the presence of functional groups (especially OH, COOH, NH_2), which can be used to synthesize hydrogels. Covalent bonds between the polymer chains can arise by the reaction of functional groups with complementary reactivity, such as an amine with an aldehyde.[77]

Alternatively, high energy irradiation can be used to polymerize compounds.[91] For example, polymers derivatized with vinyl groups, can be transferred into hydrogels. Moreover, the presence of vinyl groups is not always necessary to induce gel formation. During the irradiation, radicals can be formed on the polymer chain by, for example, homolytic splitting of C-H bonds. An example of a polymer that can be crosslinked using this method is PVA.[92]

Finally, crosslinking can also occur by means of enzymes. Interaction of enzymes such as transglutaminase with, for instance, PEG can result in hydrogel formation.[93]

4.4 Applications

There exist a large variety of applications for hydrogels because of their interesting properties, as already mentioned earlier:

- ✓ Drug delivery systems[94]
- ✓ Contact lenses[95]
- ✓ Artificial organs[96]
- ✓ Synthetic cartilage[97]
- ✓ Coatings for catheters[98]
- ✓ Wound treatment[99]

5 Building blocks

In the present work, gelatin will be applied as the starting product for the hydrogel production. The major goal of the present work was to develop porous hydrogel scaffolds, to function as tissue engineering devices. Depending on the specific application (i.e. cell type etc.), chondroitin sulphate or hyaluronic acid should be co-crosslinked within the gelatin hydrogels developed.

5.1 Gelatin

Gelatin is derived from the latin word 'gelatus', which means 'frozen' or 'thickened'. It is a water-soluble protein, composed of a variety of amino acids (table 1-3)[100], connected via amide bonds, resulting in a linear polymer with a molecular weight varying between 15,000 and 250,000 Da.[101]
Gelatin is obtained by hydrolysis of collagen, which was already described in paragraph 3.2.[50]

Two types of gelatin can be distinguished according to their production process (figure 1-5).[102]

1. Type A gelatin (pH 3.8-6; iso-electric point (pH at which the net charge of the polymer is 0) 6-8) is obtained by acidic hydrolysis of collagen.
2. Type B gelatin (pH 5-7.4; iso-electric point 4.7-5.3) is produced by alkaline treatment of collagen.

Type B gelatin differs from type A by the hydrolysis of the amide groups. By this amidolysis, aspartine and glutamine are converted to aspartic acid and glutamic acid. The extra acid groups reduce the iso-electric point of gelatin. The iso-electric point of type A gelatin is higher than that of type B since amides are converted to carboxylate, while this does not happen or slowly happens in acidic medium. Also arginine can be hydrolysed to ornithine in alkaline conditions.[103]

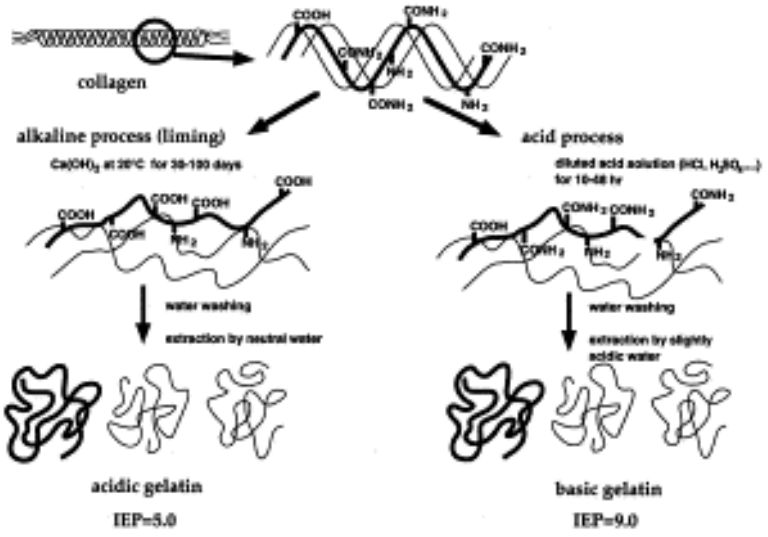

Figure 1-5: Synthesis of gelatin starting from collagen.

	Gelatin		
Amino acid	Type A	Type B	**Type I Collagen**
alanine	10.5	11.7	11.4
arginine*	4.9	4.8	5.1
asparagine	1.6	-	1.6
aspartic acid	2.9	4.6	2.9
cysteine	-	-	<0.1
phenylalanine*	1.4	1.4	1.3
glutamine	2.5	-	2.5
glutamic acid	4.8	7.2	4.8
glycine	31.1	33.0	33.2
histidine*	0.5	0.4	0.4
hydroxylysine	0.7	0.4	0.5
hydroxyproline	10.1	9.3	10.4
isoleucine*	1.0	1.1	1.1
leucine*	2.4	2.4	2.4
lysine*	2.9	2.8	2.8
methionine*	0.5	0.4	0.6
proline	14.2	12.4	11.5
serine	3.5	3.3	3.5
threonine*	1.8	1.8	1.7
tryptophan*	-	-	-
tyrosine	0.3	1.2	0.4
valine*	2.6	2.2	2.2

Table 1-3: The average amino acid composition (mol%) in gelatin and collagen.

The principal raw materials used in the gelatin production today are cattle bones, cattle hides, and pork skins.[104, 105] Substances, such as minerals (in the case of bone), fats and albuminoids (found in skin), are removed by chemical and physical treatment resulting in purified collagen. These pre-treated materials are then hydrolyzed to gelatin (figure 1-6).

The so-called 'green bone' is cleaned, degreased, dried and crushed to a particle size of about 1-2 cm. The pieces of bone are then treated with dilute hydrochloric acid to remove mineral salts. The resulting sponge-like material is called ossein. From this point on in the manufacture of type B gelatin, both cattle hides and ossein receive similar treatment. For the production of type B gelatin, both ossein and cattle hides are subjected to treatment with an alkali (usually lime) and water at room temperature. Depending on the previous treatment, the nature of the material, the size of the pieces, and the exact temperature, liming takes 5 to 20 weeks, usually 8 to 12. The process is controlled by the degree of alkalinity, as determined by titration with acid.

Next, the raw material is thoroughly washed with cold water to remove excess lime. The pH is adjusted with acid and the product is extracted with hot water to recover the soluble gelatin.

Pork skin is currently the most significant raw material source for the production of edible gelatin in North America. When pork skins are utilized for the production of type A gelatin, they are washed with cold water and then soaked in cold dilute mineral acid for several hours, until maximum swelling has occurred. Hydrochloric acid and sulfuric acid are most commonly employed. The remaining acid is then drained off and the material is again washed several times with cold water. The pork skins are then ready for extraction with hot water.

The dilute gelatin solutions from the various hot water extractions are filtered, deionized, and concentrated by cross-flow membrane filtration and/or vacuum evaporation. The gelatin solution is then chilled and either cut into ribbons or extruded, and the gelled material is deposited onto a stainless steel belt. The belt is passed through a drying chamber, which is divided into zones in each of which the temperature and humidity of the drying air is accurately controlled. Typical temperatures range from about 30°C in the initial zone up to about 70°C in the final zone.

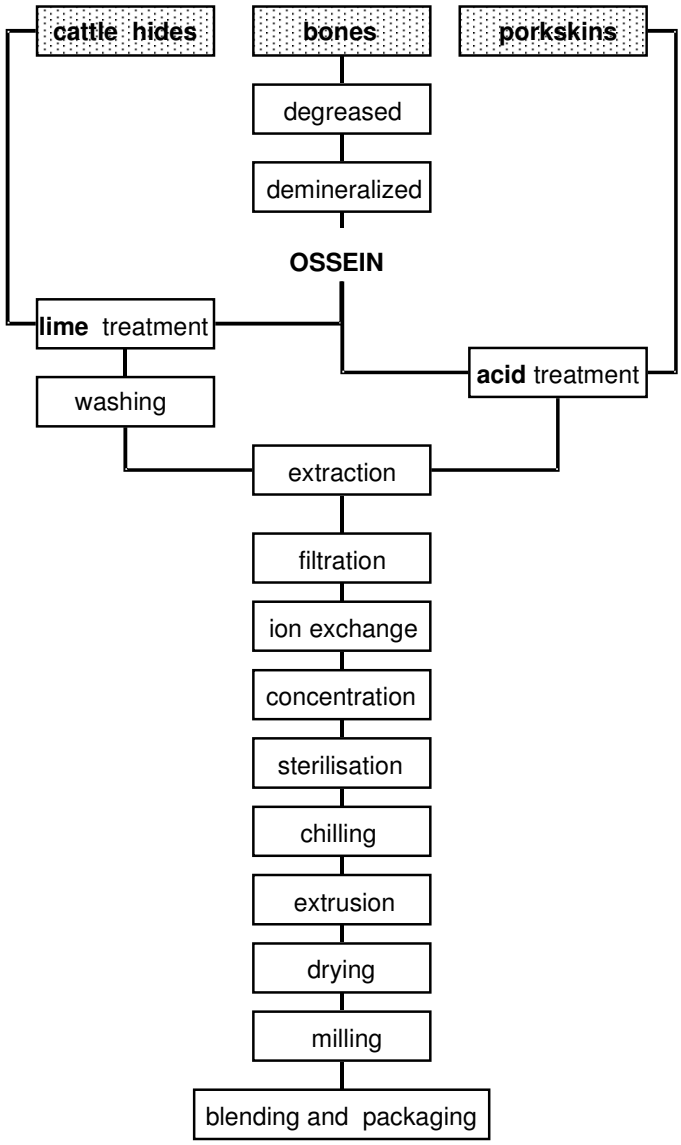

Figure 1-6: Production process of gelatin.

Gelatin is a vitreous, brittle solid that is coloured yellow to white and is nearly tasteless and odourless. It contains 84-90% protein, 1-2% mineral salts and 8-15% water.

Gelatin has since long been used in the food industry as clarification agent, stabilizer and protective coating material. It is used especially in desserts, candies, bakery products, ice cream and dairy products.[106] In the pharmaceutical industry, gelatin is applied in the manufacture of pharmaceutical capsules, tablets and emulsions.[107] Gelatin also finds application in cosmetics, photography and some specialized industries.[108]

5.2 Chondroitin sulphate

Chondroitin sulphate (CS) is a GAG, composed of a chain of alternating sugars (i.e. N-acetyl-D-galactosamine and D-glucuronic acid).[62] The chemical structure of one sub-class of CS is shown in figure 1-7. It is usually found, attached to proteins as part of a proteoglycan, as already disussed in paragraph 3.3. CS can consist of over 100 individual sugars, each of which can be sulphated in variable positions and quantities. There exist different types of CS:[109-111]

- ✓ Chondroitin sulphate A is predominantly sulphated at carbon-4 of the N-acetylgalactosamine (GalNAc) sugar and is also known as chondroitin-4-sulphate.
- ✓ Chondroitin sulphate B is also referred to as dermatan sulphate. Glucuronic acid (GlcA) residues are in this case epimerized into L-iduronic acid (IdoA).
- ✓ Chondroitin sulphate C is predominantly sulphated at carbon-6 of the GalNAc sugar (chondroitin-6-sulphate).
- ✓ Chondroitin sulphate D is predominantly sulphated at carbon-2 of the glucuronic acid and at carbon-6 of the GalNAc sugar (chondroitin-2,6-sulphate).
- ✓ Chondroitin sulphate E is predominantly sulphated at carbons-4 and -6 of the GalNAc sugar (chondroitin-4,6-sulphate).

CS is an important structural component of cartilage and provides much of its resistance to compression.[112] Furthermore, CS has biocharacteristics that include the binding and modulation of growth factors and cytokines, and the inhibition of proteases.[64] Consequently, the incorporation of CS in scaffolds designed for tissue engineering could be extremely valuable.

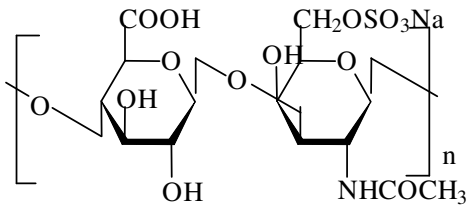

Figure 1-7: Chemical structure of chondroitin sulphate C.

5.3 Hyaluronic acid

Hyaluronic acid (HA) is derived from 'hyalos' (Greek for vitreous) and 'uronic acid', because it was first isolated from the vitreous humor and possesses a high uronic acid content.[113] Hyaluronan is a non-sulphated GAG, distributed widely throughout connective, epithelial, and neural tissue.[114] It is one of the major components of the extracellular matrix and it contributes significantly to cell proliferation and migration.[67] Hyaluronan is a polymer of disaccharides, composed of D-glucuronic acid and D-N-acetylglucosamine, linked together via alternating β-1,4 and β-1,3 glycosidic bonds (figure 1-8).[70]

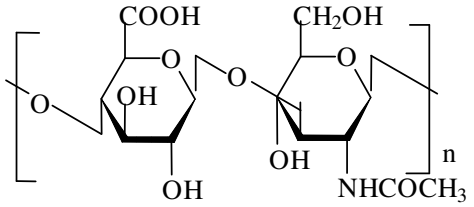

Figure 1-8: Chemical structure of hyaluronic acid.

The molecular weight of hyaluronan can range from 100,000 to 10,000,000 Da *in vivo*.[115] Hyaluronan is energetically stable because of the stereochemistry of the disaccharides present. Bulky groups on each sugar molecule are in sterically favored positions, while the smaller hydrogens are positioned on the less favorable axial positions.[116]

Hyaluronan is synthesized by a class of integral membrane proteins called hyaluronan synthases, of which vertebrates have three types: HAS1, HAS2, and HAS3. These enzymes increase the length of the hyaluronan chains by repeatedly adding glucuronic acid and N-acetylglucosamine to the polysaccharide as it is extruded through the cell membrane into the extracellular space.[117]

Hyaluronan is naturally found in many tissues of the body such as skin, cartilage, and the vitreous humor.[118] It is therefore well suited for biomedical applications, targeting these tissues.[61, 119]

The first hyaluronan-based biomedical product (Healon) was developed in the 1970s and 1980s and is approved for the use in eye surgery (e.g. corneal transplantation).[120]

Hyaluronan is also used to treat osteoarthritis of the knee.[69] It has also been suggested that hyaluronan has positive biochemical effects on cartilage cells.[66]

Due to its biocompatibility and its presence in the extracellular matrix, hyaluronan is often used as a scaffold in tissue engineering research.[121]

Hyaluronan is often used as a tumor marker for prostate and breast cancer. It may also be used to monitor the progression of the disease. [122, 123]

Hyaluronan may also be used postoperatively to induce tissue healing.[68] Current models of wound healing propose that HA with higher molecular weight appear to physically make room for white blood cells, which mediate the immune response.[124]

Hyaluronan also is a common ingredient in skin care products.[125]

6 PhD outline

The goal of the present work is the development of bio-interactive materials that can function as scaffolds for tissue engineering, which represents the second discipline in regenerative medicine. The self-structuring biopolymer gelatin will be combined with glycosaminoglycans (chondroitin sulphate and hyaluronic acid) and cell-adhesive polymers (e.g. fibronectin). Gelatin will introduce mechanical strength and the glycosaminoglycans and cell-adhesive polymers will function in cell adhesion, cell proliferation and cell migration processes. In order to avoid the dissolution of the biopolymers at body temperature, gelatin, chondroitin sulphate and hyaluronic acid are modified with functional groups, enabling crosslinking and formation of interpenetrating networks (figure 1-9).

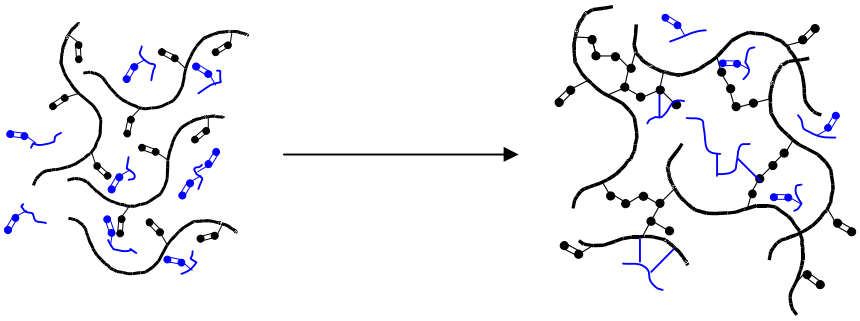

Figure 1-9: The formation of a chemically crosslinked hydrogel network based on modified gelatin and GAGs.

In order to crosslink gelatin, two approaches are selected (figure 1-10). On the one hand, polymerizable methacrylamide side chains will be incorporated to enable chemical crosslinking. Alternatively, the primary amines of gelatin will be modified with thiol side groups, enabling inter- and intramolecular disulfide formation through oxidation. The latter concept offers the possibility to prepare hydrogels that can be solubilised by reduction, which opens perspectives to isolate cells, cultured in the hydrogel carriers.

The hydrogels will be prepared as films and scaffolds. Bio-interactive hydrogels are also of interest to function as cell carrier material, or to combine with materials, less suitable for cell culture, yet possessing interesting (mechanical) properties.

The hydrogels developed will be characterized for their mechanical and physical properties and their biodegradability.

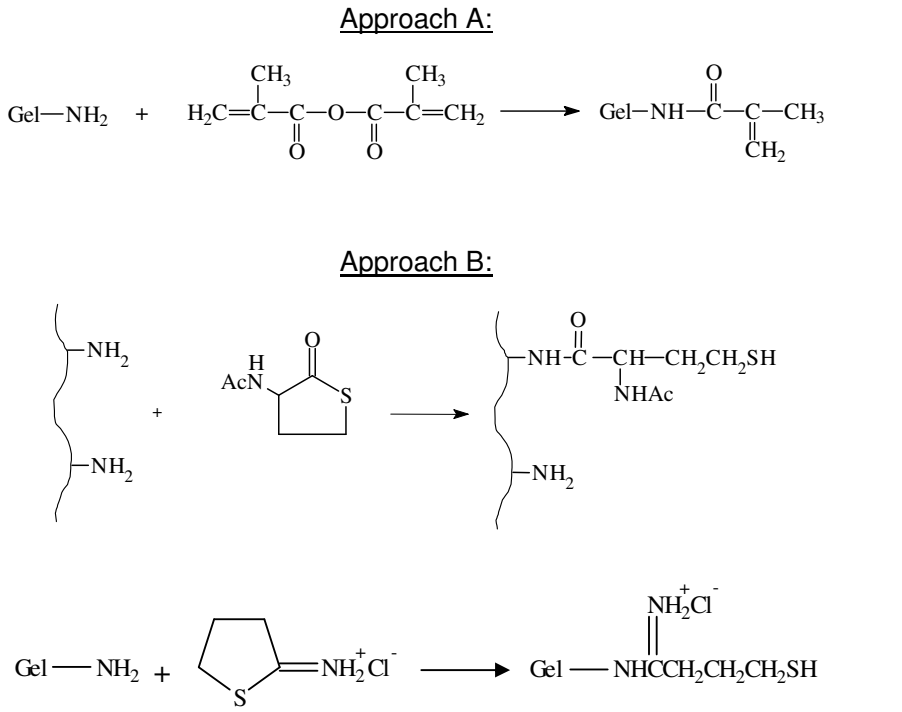

Figure 1-10: Derivatization of gelatin with crosslinkable side groups.

Since it is essential that the cells implanted, are both provided with nutrients and that metabolites are removed, a porous structure is introduced into the hydrogels developed, via a cryogenic treatment, followed by lyophilization (figure 1-11).

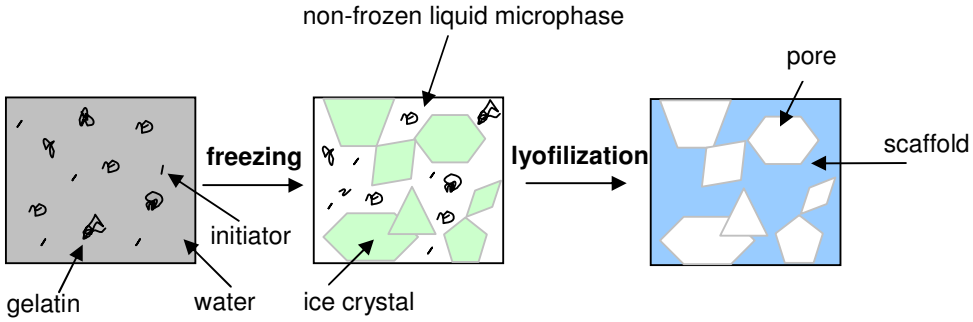

Figure 1-11: Cryogenic treatment of gelatin hydrogel, followed by lyofilization.

The synthesis and characterization of the hydrogel precursors will be described in depth in chapter 2. Both the modification degree and the molecular weight of the derivatives will be determined. Next, the influence of reaction conditions etc. will be investigated.

In chapter 3, the preparation and characterization of hydrogel films, composed of different combinations of modified gelatin and chondroitin sulphate will be discussed. For different types of materials, the contributions of both the physical and the chemical structuring to the total network strength is investigated. A study on the influence of varying parameters (e.g. polymer concentration, modification degree, cryogenic treatment) on the properties of the hydrogels developed, is performed by means of rheology, texturometry and swelling experiments.

The production of porous gelatin scaffolds by applying a cryogenic treatment, is dealt with in chapter 4. The influence of varying parameters including the cooling rate, applying a temperature gradient and the gelatin concentration on the pore morphology, the pore size and the porosity of the matrices developed, is studied using different techniques (e.g. micro-computed tomography, helium-pycnometry, scanning electron microscopy, etc).

In chapter 5, hydrogel scaffolds composed of both gelatin and chondroitin sulphate are described, since this combination has a potential application for some specific applications (i.e. tissue engineering of cartilage).

Next, alternatives in order to crosslink gelatin hydrogels, after lyophilization of the cryo-treated gelatin hydrogels are discussed in depth in chapter 6.

Chapter 7 deals with the interaction between gelatin and extracellular matrix components. Since cells can only survive when anchored, the interaction between its anchorage points (i.e. compounds of the extracellular matrix) and the scaffold material (i.e. gelatin) can play a tremendous role on the ability of the matrices to function as cell carriers. Moreover, when culturing cells *in vitro,* often serum, containing a variation of proteins is added to the medium. Possibly, the interaction between gelatin and some of the serum constituents could also affect the results of the cell interaction studies.

In chapter 8, the *in vitro* biocompatibility of the scaffolds developed is discussed. Furthermore, the suitability of hydrogels with different pore characteristics, to function as cell carriers, is investigated for a large variety of human cells.

References

1. Bottaro, D. P.; Heidaran, M. A., Engineered extracellurlar matrices: a biological solution for tissue repair, regeneration, and replacement. *e-biomed* **2001,** 2, 9-12.
2. Stock, U. A.; Vacanti, J. P., Tissue engineering: Current state and prospects. *Annual Review of Medicine* **2001,** 52, 443-451.
3. Tang, S.; Lui, S. L.; Lo, C. Y.; Lo, W. K.; Cheng, I. K. P.; Lai, K. N.; Chan, T. M., Spousal renal donor transplantation in Chinese subjects: a 10 year experience from a single centre. *Nephrol. Dial. Transplant.* **2004,** 19, (1), 203-206.
4. Collignon, F. P.; Holland, E. C.; Feng, S., Minireview Organ Donors with Malignant Gliomas: An Update. *American Journal of Transplantation* **2004,** 4, (1), 15-21.
5. Haseltine, W. A., Regenerative Medicine 2003: An Overview. *The Journal of Regenerative Medicine* **2003,** 4, 15-18.
6. Lagasse, E.; Shizuru, J. A.; Uchida, N.; Tsukamoto, A.; Weissman, I. L., Toward regenerative medicine. *Immunity* **2001,** 14, (4), 425-436.
7. Yannas, I. V., *Tissue and organ regeneration in adults*. 2001.
8. Williams, D., Benefit and risk in tissue engineering. *Materials today* **2004,** 7, (5), 24-29.
9. Griffith, L. G.; Naughton, G., Tissue engineering - Current challenges and expanding opportunities. *Science* **2002,** 295, (5557), 1009-1014.
10. Noel, D.; Djouad, F.; Jorgense, C., Regenerative medicine through mesenchymal stem cells for bone and cartilage repair. *Curr Opin Investig Drugs* **2002** 3, (7), 1000-1004.
11. Rezwan, K.; Chen, Q. Z.; Blaker, J. J.; Boccaccini, A. R., Biodegradable and bioactive porous polymer/inorganic composite scaffolds for bone tissue engineering. *Biomaterials* **2006,** 27, (18), 3413-3431.
12. Hubbell, J. A., Biomaterials in Tissue Engineering. *Bio-Technology* **1995,** 13, (6), 565-576.
13. Langer, R.; Vacanti, J. P., Tissue engineering. *Science* **1993,** 260, 920-926
14. Ma, P. X., Scaffolds for tissue engineering. *Materials today* **2004,** 7, (5), 30-40.
15. Mikos, A. G.; Temenoff, J. S., Formation of highly porous biodegradable scaffolds for tissue engineering. *Electronic journal of Biotechnology* **2000,** 3, (2).
16. Ramakrishna, S.; Mayer, J.; Wintermantel, E.; Leong, K. W., Biomedical applications of polymer-composite materials: a review. *Composites Science and Technology* **2001,** 61, (9), 1189-1224.
17. Burg, K. J. L.; Porter, S.; Kellam, J. F., Biomaterial developments for bone tissue engineering. *Biomaterials* **2000,** 21, (23), 2347-2359.
18. Beruto, D. T.; Mezzasalma, S. A.; Capurro, M.; Botter, R.; Cirillo, P., Use of alpha-tricalcium phosphate (TCP) as powders and as an aqueous dispersion to modify processing, microstructure, and mechanical properties of polymethylmetacrylate (PMMA) bone cements and to produce bone-substitute compounds. *Journal of Biomedical Materials Research* **1999,** 49, (4), 498-505.

19. Yaylaoglu, M. B.; Korkusuz, P.; Ors, U.; Korkusuz, F.; Hasirci, V., Development of a calcium phosphate-gelatin composite as a bone substitute and its use in drug release. *Biomaterials* **1999,** 20, (8), 711-719.
20. Pulapura, S.; Kohn, J., Trends in the development of bioresorbable polymers for medical applications. *Journal of Biomaterials Applications* **1992,** 6, (3), 216-50.
21. Cannizzaro, S. M.; Padera, R. F.; Langer, R.; Rogers, R. A.; Black, F. E.; Davies, M. C.; Tendler, S. J. B.; Shakesheff, K. M., A novel biotinylated degradable polymer for cell-interactive applications. *Biotechnology and Bioengineering* **1998,** 58, (5), 529-535.
22. Hou, Q. P.; Grijpma, D. W.; Feijen, J., Preparation of interconnected highly porous polymeric structures by a replication and freeze-drying process. *Journal of Biomedical Materials Research Part B-Applied Biomaterials* **2003,** 67B, (2), 732-740.
23. Bloch, K.; Lozinsky, V. I.; Galaev, I. Y.; Yavriyanz, K.; Vorobeychik, M.; Azarov, D.; Damshkaln, L. G.; Mattiasson, B.; Vardi, P., Functional activity of insulinoma cells (INS-1E) and pancreatic islets cultured in agarose cryogel sponges. *Journal of Biomedical Materials Research Part A* **2005,** 75A, (4), 802-809.
24. Drury, J. L.; Mooney, D. J., Hydrogels for tissue engineering: scaffold design variables and applications. *Biomaterials* **2003,** 24, (24), 4337-4351.
25. Boland, E. D.; Matthews, J. A.; Pawlowski, K. J.; Simpson, D. G.; Wnek, G. E.; Bowlin, G. L., Electrospinning collagen and elastin: Preliminary vascular tissue engineering. *Frontiers in Bioscience* **2004,** 9, 1422-1432.
26. Chen, G. P.; Liu, D. C.; Maruyama, N.; Oligushi, H.; Tanaka, J.; Tateishi, T., Cell adhesion of bone marrow cells, chondrocytes, ligament cells and synovial cells on a PLGA-collagen hybrid mesh. *Materials Science & Engineering C-Biomimetic and Supramolecular Systems* **2004,** 24, (6-8), 867-873.
27. Chvapil, M., Collagen Sponge - Theory and Practice of Medical Applications. *Journal of Biomedical Materials Research* **1977,** 11, (5), 721-741.
28. Griffith, L. G., Polymeric biomaterials. *Acta Materialia* **2000,** 48, (1), 263-277.
29. Anselme, K., Osteoblast adhesion on biomaterials. *Biomaterials* **2000,** 21, (7), 667-81.
30. Yamato, M.; Okano, T., Cell sheet engineering. *Materials today* **2004,** 7, (5), 42-47.
31. Neff, J. A.; Tresco, P. A.; Caldwell, K. D., Surface modification for controlled studies of cell-ligand interactions. *Biomaterials* **1999,** 20, (23-24), 2377-2393.
32. Adams, J. C.; Watt, F. M., Regulation of Development and Differentiation by the Extracellular-Matrix. *Development* **1993,** 117, (4), 1183-1198.
33. Diener, A.; Nebe, B.; Luthen, F.; Becker, P.; Beck, U.; Neumann, H. G.; Rychly, J., Control of focal adhesion dynamics by material surface characteristics. *Biomaterials* **2005,** 26, (4), 383-392.
34. Vogel, V., Fibronectin in a surface-adsorbed state. In *Proteins at interfaces II, fundamentals and applications*, Horbett, T. A.; Brash, J. L., Eds. 1995.
35. Vuento, M.; Vaheri, A., Dissociation of Fibronectin from Gelatin-Agarose by Amino-Compounds. *Biochemical Journal* **1978,** 175, (1), 333-336.

36. Haas, R.; Culp, L. A., Binding of Fibronectin to Gelatin and Heparin - Effect of Surface Denaturation and Detergents. *Febs Letters* **1984,** 174, (2), 279-283.
37. Wittmer, C. R.; Van Tassel, P. R., Probing adsorbed fibronectin layer structure by kinetic analysis of monoclonal antibody binding. *Colloids and Surfaces B-Biointerfaces* **2005,** 41, (2-3), 103-109.
38. Chung, C. Y.; Erickson, H. P., Glycosaminoglycans modulate fibronectin matrix assembly and are essential for matrix incorporation of tenascin-C. *Journal of Cell Science* **1997,** 110, 1413-1419.
39. Illario, M.; Cavallo, A. L.; Monaco, S.; Di Vito, E.; Mueller, F.; Marzano, L. A.; Troncone, G.; Fenzi, G.; Rossi, G.; Vitale, M., Fibronectin-induced proliferation in thyroid cells is mediated by alpha v beta 3 integrin through Ras/Raf-1/MEK/ERK and calcium/CaMKII signals. *Journal of Clinical Endocrinology and Metabolism* **2005,** 90, (5), 2865-2873.
40. Katagiri, Y.; Brew, S. A.; Ingham, K. C., All six modules of the gelatin-binding domain of fibronectin are required for full affinity. *Journal of Biological Chemistry* **2003,** 278, (14), 11897-11902.
41. Greiling, D.; Clark, R. A. F., Fibronectin provides a conduit for fibroblast transmigration from collagenous stroma into fibrin clot provisional matrix. *Journal of Cell Science* **1997,** 110, 861-870.
42. Vartio, T.; Kuusela, P., Disulfide-Bonded Dimerization of Fibronectin Invitro. *European Journal of Biochemistry* **1991,** 202, (2), 597-604.
43. Tiwari, A.; Kidane, A.; Salacinski, H.; Punshon, G.; Hamilton, G.; Seifalian, A. M., Improving endothelial cell retention for single stage seeding of prosthetic grafts: Use of polymer sequences of arginine-glycine-aspartate. *European Journal of Vascular and Endovascular Surgery* **2003,** 25, (4), 325-329.
44. Lebaron, R. G.; Athanasiou, K. A., Extracellular matrix cell adhesion peptides: Functional applications in orthopedic materials. *Tissue Engineering* **2000,** 6, (2), 85-103.
45. Dsouza, S. E.; Ginsberg, M. H.; Plow, E. F., Arginyl-Glycyl-Aspartic Acid (RGD) - a Cell-Adhesion Motif. *Trends in Biochemical Sciences* **1991,** 16, (7), 246-250.
46. Hersel, U.; Dahmen, C.; Kessler, H., RGD modified polymers: biomaterials for stimulated cell adhesion and beyond. *Biomaterials* **2003,** 24, (24), 4385-4415.
47. Lee, J. E.; Park, J. C.; Hwang, Y. S.; Kim, J. K.; Kim, J. G.; Suh, H., Characterization of UV-irradiated dense/porous collagen membranes: Morphology, enzymatic degradation, and mechanical properties. *Yonsei Medical Journal* **2001,** 42, (2), 172-179.
48. Darnell, J.; Matsudaira, P.; Zipursky, L.; Lodish, H.; Berk, A.; Baltimore, D., *Molecular cell biology*. 1999.
49. Yamamoto, S.; Nakamura, F.; Hitomi, J.; Shigeno, M.; Sawaguchi, S.; Abe, H.; Ushiki, T., Atomic force microscopy of intact and digested collagen molecules. *Journal of Electron Microscopy* **2000,** 49, (3), 423-427.
50. Kozlov, P. V.; Burdygina, G. I., The Structure and Properties of Solid Gelatin and the Principles of Their Modification. *Polymer* **1983,** 24, (6), 651-666.

51. Koide, T.; Asada, S.; Takahara, Y.; Nishikawa, Y.; Nagata, K.; Kitagawa, K., Specific recognition of the collagen triple helix by chaperone HSP47 - Minimal structural requirement and spatial molecular orientation. *Journal of Biological Chemistry* **2006,** 281, (6), 3432-3438.
52. Horstmann, H.; Ng, C. P.; Tang, B. L.; Hong, W. J., Ultrastructural characterization of endoplasmic reticulum - Golgi transport containers (EGTC). *Journal of Cell Science* **2002,** 115, (22), 4263-4273.
53. Henson, F. M. D.; Davies, M. E.; Schofield, P. N.; Jeffcott, L. B., Expression of types II, VI and X collagen in equine growth cartilage during development. *Equine Veterinary Journal* **1996,** 28, (3), 189-198.
54. Hurst, P. R.; Palmay, R. D.; Myers, D. B., Localization and synthesis of collagen types III and V during remodelling and decidualization in rat uterus. *Reproduction Fertility and Development* **1997,** 9, (4), 403-409.
55. Smith, L. T., Patterns of Type-Vi Collagen Compared to Type-I, Type-Iii and Type-V Collagen in Human Embryonic and Fetal Skin and in Fetal Skin-Derived Cell-Cultures. *Matrix Biology* **1994,** 14, (2), 159-170.
56. Berry, S. D. K.; Howard, R. D.; Akers, R. M., Mammary localization and abundance of laminin, fibronectin, and collagen IV proteins in prepubertal heifers. *Journal of Dairy Science* **2003,** 86, (9), 2864-2874.
57. Wetzels, R. H. W.; Robben, H. C. M.; Leigh, I. M.; Schaafsma, H. E.; Vooijs, G. P.; Ramaekers, F. C. S., Distribution Patterns of Type-Vii Collagen in Normal and Malignant Human Tissues. *American Journal of Pathology* **1991,** 139, (2), 451-459.
58. Sawada, H.; Konomi, H., The Alpha-1 Chain of Type-Viii Collagen Is Associated with Many but Not All Microfibrils of Elastic Fiber System. *Cell Structure and Function* **1991,** 16, (6), 455-466.
59. Gregory, K. E.; Keene, D. R.; Tufa, S. F.; Lunstrum, G. P.; Morris, N. P., Developmental distribution of collagen type XII in cartilage: Association with articular cartilage and the growth plate. *Journal of Bone and Mineral Research* **2001,** 16, (11), 2005-2016.
60. Holmes, D. F.; Kadler, K. E., The 10+4 microfibril structure of thin cartilage fibrils. *Proceedings of the National Academy of Sciences of the United States of America* **2006,** 103, (46), 17249-17254.
61. Shu, X. Z.; Liu, Y. C.; Palumbo, F.; Prestwich, G. D., Disulfide-crosslinked hyaluronan-gelatin hydrogel films: a covalent mimic of the extracellular matrix for in vitro cell growth. *Biomaterials* **2003,** 24, (21), 3825-3834.
62. Jackson, R. L.; Busch, S. J.; Cardin, A. D., Glycosaminoglycans - Molecular-Properties, Protein Interactions, and Role in Physiological Processes. *Physiological Reviews* **1991,** 71, (2), 481-539.
63. Zhong, S. P.; Teo, W. E.; Zhu, X.; Beuerman, R.; Ramakrishna, S.; Yung, L. Y. L., Formation of collagen-glycosaminoglycan blended nanofibrous scaffolds and their biological properties. *Biomacromolecules* **2005,** 6, (6), 2998-3004.
64. Lee, J. E.; Kim, K. E.; Kwon, I. C.; Ahn, H. J.; Lee, S. H.; Cho, H. C.; Kim, H. J.; Seong, S. C.; Lee, M. C., Effects of the controlled-released TGF-beta 1 from chitosan microspheres on

chondrocytes cultured in a collagen/chitosan/glycosaminoglycan scaffold. *Biomaterials* **2004,** 25, (18), 4163-4173.

65. Luo, Y.; Kirker, K. R.; Prestwich, G. D., Cross-linked hyaluronic acid hydrogel films: new biomaterials for drug delivery. *Journal of Controlled Release* **2000,** 69, (1), 169-184.
66. Yoo, H. S.; Lee, E. A.; Yoon, J. J.; Park, T. G., Hyaluronic acid modified biodegradable scaffolds for cartilage tissue engineering. *Biomaterials* **2005,** 26, (14), 1925-1933.
67. Liu, H. F.; Mao, J. S.; Yao, K. D.; Yang, G. H.; Cui, L.; Cao, Y. L., A study on a chitosan-gelatin-hyaluronic acid scaffold as artificial skin in vitro and its tissue engineering applications. *Journal of Biomaterials Science-Polymer Edition* **2004,** 15, (1), 25-40.
68. Kirker, K. R.; Luo, Y.; Nielson, J. H.; Shelby, J.; Prestwich, G. D., Glycosaminoglycan hydrogel films as bio-interactive dressings for wound healing. *Biomaterials* **2002,** 23, (17), 3661-3671.
69. Liu, H. F.; Yin, Y. J.; Yao, K. D.; Ma, D. R.; Cui, L.; Cao, Y. L., Influence of the concentrations of hyaluronic acid on the properties and biocompatibility of Cs-Gel-HA membranes. *Biomaterials* **2004,** 25, (17), 3523-3530.
70. Mao, J. S.; Liu, H. F.; Yin, Y. J.; Yao, K. D., The properties of chitosan-gelatin membranes and scaffolds modified with hyaluronic acid by different methods. *Biomaterials* **2003,** 24, (9), 1621-1629.
71. Pieper, J. S.; van Wachem, P. B.; van Luyn, M. J. A.; Brouwer, L. A.; Hafmans, T.; Veerkamp, J. H.; van Kuppevelt, T. H., Attachment of glycosaminoglycans to collagenous matrices modulates the tissue response in rats. *Biomaterials* **2000,** 21, (16), 1689-1699.
72. Zaia, J.; Costello, C. E., Tandem mass spectrometric sequencing of heparin and heparan sulfate oligosaccharides. *Abstracts of Papers of the American Chemical Society* **2002,** 224, U132-U132.
73. Pieper, J. S.; Hafmans, T.; Veerkamp, J. H.; van Kuppevelt, T. H., Development of tailor-made collagen-glycosaminoglycan matrices: EDC/NHS crosslinking, and ultrastructural aspects. *Biomaterials* **2000,** 21, (6), 581-593.
74. Vynios, D. H.; Papageorgakopoulou, N.; Sazakli, H.; Tsiganos, C. P., The interactions of cartilage proteoglycans with collagens are determined by their structures. *Biochimie* **2001,** 83, (9), 899-906.
75. Alban, S.; Franz, G., Partial synthetic glucan sulfates as potential new antithrombotics: A review. *Biomacromolecules* **2001,** 2, (2), 354-361.
76. Matsuda, T.; Magoshi, T., Terminally alkylated heparin. 1. Antithrombogenic surface modifier. *Biomacromolecules* **2001,** 2, (4), 1169-1177.
77. Hennink, W. E.; van Nostrum, C. F., Novel crosslinking methods to design hydrogels. *Advanced Drug Delivery Reviews* **2002,** 54, (1), 13-36.
78. Gupta, P.; Vermani, K.; Garg, S., Hydrogels: from controlled release to pH-responsive drug delivery. *Drug Discovery Today* **2002,** 7, (10), 569-579.
79. Jeong, B.; Kim, S. W.; Bae, Y. H., Thermosensitive sol-gel reversible hydrogels. *Advanced Drug Delivery Reviews* **2002,** 54, (1), 37-51.

80. Gombotz, W. R.; Pettit, D. K., Biodegradable Polymers for Protein and Peptide Drug-Delivery. *Bioconjugate Chemistry* **1995,** 6, (4), 332-351.
81. Peppas, N. A.; Bures, P.; Leobandung, W.; Ichikawa, H., Hydrogels in pharmaceutical formulations. *European Journal of Pharmaceutics and Biopharmaceutics* **2000,** 50, (1), 27-46.
82. Landers, R.; Hubner, U.; Schmelzeisen, R.; Mulhaupt, R., Rapid prototyping of scaffolds derived from thermoreversible hydrogels and tailored for applications in tissue engineering. *Biomaterials* **2002,** 23, (23), 4437-4447.
83. Hoffman, A. S., Hydrogels for biomedical applications. *Advanced Drug Delivery Reviews* **2002,** 43, (1), 3-12.
84. Hoffman, A. S., Hydrogels for biomedical applications. *Advanced Drug Delivery Reviews* **2002,** 54, (1), 3-12.
85. Hassan, C. M.; Peppas, N. A., Structure and applications of poly(vinyl alcohol) hydrogels produced by conventional crosslinking or by freezing/thawing methods. In *Biopolymers/Pva Hydrogels/Anionic Polymerisation Nanocomposites*, 2000; Vol. 153, pp 37-65.
86. Li, F.; Li, S. M.; Vert, M., Synthesis and rheological properties of polylactide/poly(ethylene glycol) multiblock copolymers. *Macromolecular Bioscience* **2005,** 5, (11), 1125-1131.
87. Petka, W. A.; Harden, J. L.; McGrath, K. P.; Wirtz, D.; Tirrell, D. A., Reversible hydrogels from self-assembling artificial proteins. *Science* **1998,** 281, (5375), 389-392.
88. Miyata, T.; Asami, N.; Uragami, T., Preparation of an antigen-sensitive hydrogel using antigen-antibody bindings. *Macromolecules* **1999,** 32, (6), 2082-2084.
89. Huang, C. W.; Sun, Y. M.; Huang, W. F., Curing kinetics of the synthesis of poly(2-hydroxyethyl methacrylate) (PHEMA) with ethylene glycol dimethacrylate (EGDMA) as a crosslinking agent. *Journal of Polymer Science Part a-Polymer Chemistry* **1997,** 35, (10), 1873-1889.
90. vanDijkWolthuis, W. N. E.; Tsang, S. K. Y.; KettenesvandenBosch, J. J.; Hennink, W. E., A new class of polymerizable dextrans with hydrolyzable groups: hydroxyethyl methacrylated dextran with and without oligolactate spacer. *Polymer* **1997,** 38, (25), 6235-6242.
91. Hua, F. J.; Qian, M. P., Synthesis of self-crosslinking sodium polyacrylate hydrogel and water-absorbing mechanism. *Journal of Materials Science* **2001,** 36, (3), 731-738.
92. El-Din, H. M. N.; Abd Alla, S. G.; El-Naggar, A. W. M., Swelling, thermal and mechanical properties of poly(vinylalcohol)/sodium alginate hydrogels synthesized by electron beam irradiation. *Journal of Macromolecular Science Part a-Pure and Applied Chemistry* **2007,** 44, (3), 291-297.
93. Kolodziejska, I.; Piotrowska, B.; Bulge, M.; Tylingo, R., Effect of transglutaminase and 1-ethyl-3-(3-dimethylaminopropyl) carbodiimide on the solubility of fish gelatin-chitosan films. *Carbohydrate Polymers* **2006,** 65, (4), 404-409.
94. Kimura, M.; Takai, M.; Ishihara, K., Biocompatibility and drug release behavior of spontaneously formed phospholipid polymer hydrogels. *Journal of Biomedical Materials Research Part A* **2007,** 80A, (1), 45-54.

95. Xiang, Y. Q.; Zhang, Y.; Chen, D. J., Novel dually responsive hydrogel with rapid des welling rate. *Polymer International* **2006,** 55, (12), 1407-1412.
96. Risbud, M. V.; Karamuk, E.; Moser, R.; Mayer, J., Hydrogel-coated textile scaffolds as three-dimensional growth support for human umbilical vein endothelial cells (HUVECs): Possibilities as coculture system in liver tissue engineering. *Cell Transplantation* **2002,** 11, (4), 369-377.
97. Suh, J. K. F.; Matthew, H. W. T., Application of chitosan-based polysaccharide biomaterials in cartilage tissue engineering: a review. *Biomaterials* **2000,** 21, (24), 2589-2598.
98. Park, S.; Bearinger, J. P.; Lautenschlager, E. P.; Castner, D. G.; Healy, K. E., Surface modification of poly(ethylene terephthalate) angioplasty balloons with a hydrophilic poly(acrylamide-co-ethylene glycol) interpenetrating polymer network coating. *Journal of Biomedical Materials Research* **2000,** 53, (5), 568-576.
99. Lopergolo, L. C.; Lugao, A. B.; Catalaini, L. H., Development of a poly(N-vinyl-2-pyrrolidone)/poly (ethylene glycol) hydrogel membrane reinforced with methyl methacrylate-grafted polypropylene fibers for possible use as wound dressing. *Journal of Applied Polymer Science* **2002,** 86, (3), 662-666.
100. Eastoe, J. E.; Leach, A. A.; , Chemical constitution of gelatin. In *The science and technology of gelatin*, Academic Press: New York, 1977; Vol. Chapter 3.
101. Lee, S. B.; Jeon, H. W.; Lee, Y. W.; Lee, Y. M.; Song, K. W.; Park, M. H.; Nam, Y. S.; Ahn, H. C., Bio-artificial skin composed of gelatin and (1 -> 3), (1 -> 6)-beta-glucan. *Biomaterials* **2003,** 24, (14), 2503-2511.
102. Lin, L. H.; Chen, K. M., Preparation and surface activity of gelatin derivative surfactants. *Colloids and Surfaces a-Physicochemical and Engineering Aspects* **2006,** 272, (1-2), 8-14.
103. Johns, P.; Courts, A., Relationship between collagen and gelatin. In *The science and technology of gelatin*, Academic Press: New York, 1977.
104. Kuhne, M.; Weidenberg, E.; Schulze, F.; Lhafi, S. K., Food processing effects on tetracycline residues in gelatin derived from bones: Methodology and comparison of manufacturing conditions. *Archiv Fur Lebensmittelhygiene* **2006,** 57, (1), 8-10.
105. Hinterwaldner, R., Technology of gelatin manufacture. In *The science and technology of gelatin*, Academic Press: New York, 1977; Vol. Chapter 10.
106. Kojima, T.; Bessho, M.; Furuta, M.; Okuda, S.; Hara, M., Characterization of biopolymer hydrogels produced by gamma-ray irradiation. *Radiation Physics and Chemistry* **2004,** 71, (1-2), 235-238.
107. Ciper, M.; Bodmeier, R., Modified conventional hard gelatin capsules as fast disintegrating dosage form in the oral cavity. *European Journal of Pharmaceutics and Biopharmaceutics* **2006,** 62, (2), 178-184.
108. Boudet, C.; Iliopoulos, I.; Poncelet, O.; Cloitre, M., Control of the chemical cross-linking of gelatin by a thermosensitive polymer: example of switchable reactivity. *Biomacromolecules* **2005,** 6, 3073-3078.

109. Rovenska, E.; Michalka, P.; Papincak, J.; Durdik, S.; Jakubovsky, J., Chondroitin sulphates A, B and C, collagen types I-IV and fibronectin in venous sinus of the red pulp in human spleen. *International Journal of Tissue Reactions-Experimental and Clinical Aspects* **2005,** 27, (1), 1-7.
110. Rumsby, M.; Ichihara-Tanaka, K.; Kimura, T.; Scott, M.; Haynes, L.; Muramatsu, T., Bipolar undifferentiated CG-4 oligodendroglial line cells adhere, extend processes and disperse on midkine, a heparin-binding growth factor: Orthovanadate and chondroitin sulphate E inhibit cell attachment. *Neuroscience Research Communications* **2001,** 28, (1), 31-39.
111. Sugahara, K.; Nadanaka, S.; Takeda, K.; Kojima, T., Structural analysis of unsaturated hexasaccharides isolated from shark cartilage chondroitin sulfate D that are substrates for the exolytic action of chondroitin ABC lyase. *Eur J Biochem* **1996,** 239, (3), 871-880.
112. Chahine, N. O.; Chen, F. H.; Hung, C. T.; Ateshian, G. A., Direct measurement of osmotic pressure of glycosaminoglycan solutions by membrane osmometry at room temperature. *Biophysical Journal* **2005,** 89, (3), 1543-1550.
113. George, E., Intra-articular hyaluronan treatment for osteoarthritis. *Ann Rheum Dis* **1998,** 57, (11), 637-640.
114. Cai, S. S.; Liu, Y. C.; Shu, X. Z.; Prestwich, G. D., Injectable glycosaminoglycan hydrogels for controlled release of human basic fibroblast growth factor. *Biomaterials* **2005,** 26, (30), 6054-6067.
115. Adam, N.; Ghosh, P., Hyaluronan molecular weight and polydispersity in some commercial intra-articular injectable preparations and in synovial fluid. *Inflammation Research* **2001,** V50, (6), 294-299.
116. Brown, M. B.; Jones, S. A., Hyaluronic acid: a unique topical vehicle for the localized delivery of drugs to the skin. *Journal of the European Academy of Dermatology and Venereology* **2005,** 19, (3), 308-318.
117. Stern, R., Hyaluronan catabolism: a new metabolic pathway. *European Journal of Cell Biology* **2004,** 83, (7), 317-325.
118. Ghosh, P.; Guidolin, D., Potential mechanism of action of intra-articular hyaluronan therapy in osteoarthritis: Are the effects molecular weight dependent? *Seminars in Arthritis and Rheumatism* **2002,** 32, (1), 10-37.
119. Liu, Y. C.; Shu, X. Z.; Prestwich, G. D., Biocompatibility and stability of disulfide-crosslinked hyaluronan films. *Biomaterials* **2005,** 26, (23), 4737-4746.
120. Cavallini, G. M.; Campi, L.; Delvecchio, G.; Lazzerini, A.; Longanesi, L., Comparison of the clinical performance of Healon 5 and Healon in phacoemulsification. *European Journal of Ophthalmology* **2002,** 12, (3), 205-211.
121. Liu, Y. C.; Shu, X. Z.; Gray, S. D.; Prestwich, G. D., Disulfide-crosslinked hyaluronan-gelatin sponge: growth of fibrous tissue in vivo. *Journal of Biomedical Materials Research Part A* **2004,** 68A, (1), 142-149.
122. Toole, B. P.; Hascall, V. C., Hyaluronan and tumor growth. *American Journal of Pathology* **2002,** 161, (3), 745-747.

123. Toole, B. P., Hyaluronan promotes the malignant phenotype. *Glycobiology* **2002,** 12, (3), 37R-42.

124. Chen, W. Y. J.; Abatangelo, G., Functions of hyaluronan in wound repair. *Wound Repair and Regeneration* **1999,** 7, (2), 79-89.

125. Kakehi, K.; Kinoshita, M.; Yasueda, S., Hyaluronic acid: separation and biological implications. *Journal of Chromatography B-Analytical Technologies in the Biomedical and Life Sciences* **2003,** 797, (1-2), 347-355.

Chapter II:

Synthesis and Characterization of the Hydrogel Precursors

1 Introduction

The present work deals with hydrogels based on gelatin and glycosaminoglycans to function as cell carriers for tissue engineering applications. The materials should be crosslinked chemically in order to obtain stable hydrogels with suitable mechanical properties at body temperature.

In the following sections, the chemical modification of the individual compounds (i.e. gelatin, chondroitin sulphate and hyaluronic acid) with crosslinkable side groups, are discussed thoroughly. Preferably, all hydrogel constituents should be co-crosslinkable, meaning that the incorporated side chains should be identical, since in a forthcoming part of the present work, hydrogels composed of different combinations of the precursors, are prepared.

Initially, double bonds were selected as crosslinkable side groups. After the preparation, the modified polymers were characterized using attenuated total reflection infrared spectroscopy (ATR-IR), nuclear magnetic resonance spectoscopy (^{1}H-NMR) and size exclusion chromatography (SEC).

In most cases, chemical crosslinking is irreversible. However, since the prepared materials will function as cell carriers for tissue engineering, it could be useful to implement a reversible crosslinking method (e.g. by incorporation of thiols). In this way, cells could be released from the matrix by adding a reduction agent (e.g.

dithiothreitol) to cleave disulfide linkages with the formation of thiols. For this reason, beside incorporation of double bonds, gelatin was also substituted using thiolating compounds. Spectrometric methods were utilized to estimate the degree of substitution and SEC experiments led to the determination of the average molecular weight of the thiolated gelatin.

2 Synthesis and characterization of modified gelatin

Since gelatin has a sol-gel transition temperature of ± 30°C, gelatin hydrogels should be crosslinked chemically to avoid dissolution at body temperature.[1] Gelatin is a protein, which is comprised of a large variety of side chains, that can be modified with different components.[2] Consequently, a large number of studies was and still is devoted to the chemical crosslinking of gelatin hydrogels.[3] The choice of potential reagents is limited to water-stable ones, since gelatin only dissolves in water and in a few alcohols.[4] In order to avoid the destruction of gelatin molecules during the modification, the reaction temperature should not exceed 80°C, the pH should be in the range of 3 to 10 and reaction times should be kept short. In most cases, bifunctional reagents such as glutaraldehyde[5,6] and diisocyanates[7], as well as carbodiimides[8,9], polyepoxycompounds[10] and acyl azides[11] are used. The derivatization occurs mostly via the amine groups (figure 2-1) of lysine and hydroxylysine.[12] The guanidinium group of arginine will be protonated in mild basic conditions, which makes the reaction (nucleophilic attack) impossible. The imidazole group of histidine will react, but with the formation of unstable products.[13] Boudet et al achieved chemical cross-linking using a thermosensitive reactive copolymer based on N-isopropylacrylamide.[14] The copolymer consists of acrylic acid units which form amide bonds with the amino groups of gelatin in the presence of a water-soluble carbodiimide. By setting the temperature above or below the LCST, it is possible to switch off or on the reactivity of the system and control the gelation process. Butler et al applied a natural crosslinking reagent, namely Genipin.[15] The crosslinking mechanism of Genipin with gelatin is still under investigation. A proposed mechanism is the nucleophilic attack of amines of gelatin inducing ring opening of the dihydropyran ring of Genipin. A second amine can then react subsequently with the

resulting aldehyde. Another possibility is to obtain chemically crosslinked hydrogels through high-energy irradiation, such as ebeam and gamma-ray.[16,17] The major advantage of the latter technique is that the reaction is reagent- and solvent-free. Moreover, sterilization can occur simultaneous during high-energy irradiation.[18,19] The latter is particularly interesting in view of future applications since the production process is then shortened by combining crosslinking and sterilization in one step.

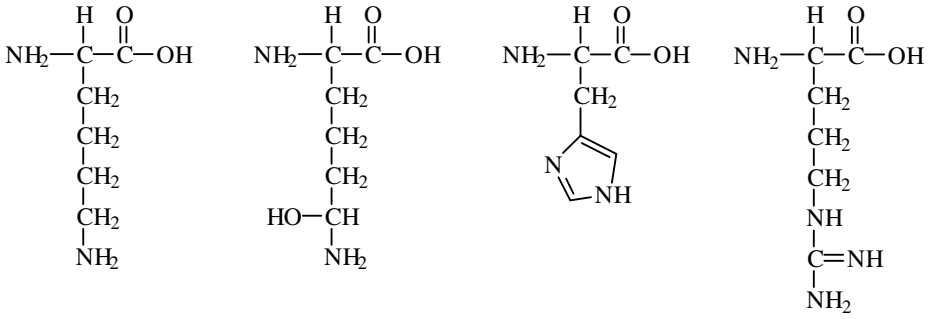

Lysine **Hydroxylysine** **Histidine** **Arginine**

Figure 2-1: Building blocks of gelatin consisting of amine groups.

However, the present work is focussing on the modification of amines into methacrylamide side groups, since this method enables separate derivatization, followed by subsequent crosslinking. Moreover, mechanically stable and biocompatible hydrogels were obtained using this approach, as described in the PhD and publications of Dr. A. Van Den Bulcke.[13, 20]

2.1 Synthesis of methacrylamide modified gelatin

In the present work, methacrylic anhydride was chosen to modify gelatin (figure 2-2). The reaction is performed in aqueous solution (pH 7.5) at 40°C. An excess of methacrylic anhydride is added while vigorously stirring, since the reagent does not dissolve in water and the reaction is interfacial. After 1 hour, the methacrylamide modified gelatin (gel-MOD) is isolated by means of dialysis, followed by freeze-drying.

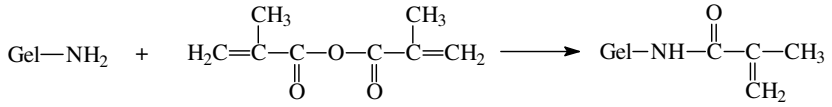

Figure 2-2: Synthesis of gel-MOD.

The amount of crosslinkable side groups can be adjusted by simply varying the amount of methacrylic anhydride added.[13]

2.2 Characterization of gel-MOD

Gel-MOD was already characterized extensively in the PhD of Dr. A. Van Den Bulcke (i.e. molecular weight, degree of substitution). For this reason, the present work only describes one method in order to determine the degree of modification.

^{1}H-NMR spectroscopy at elevated temperature (40°C) was applied, since the latter appeared to be a simple, yet accurate method to determine the methacrylamide substituents on the gelatin in D_2O. The ^{1}H-NMR spectrum of the synthesized methacrylamide gelatin is shown in the figure below.

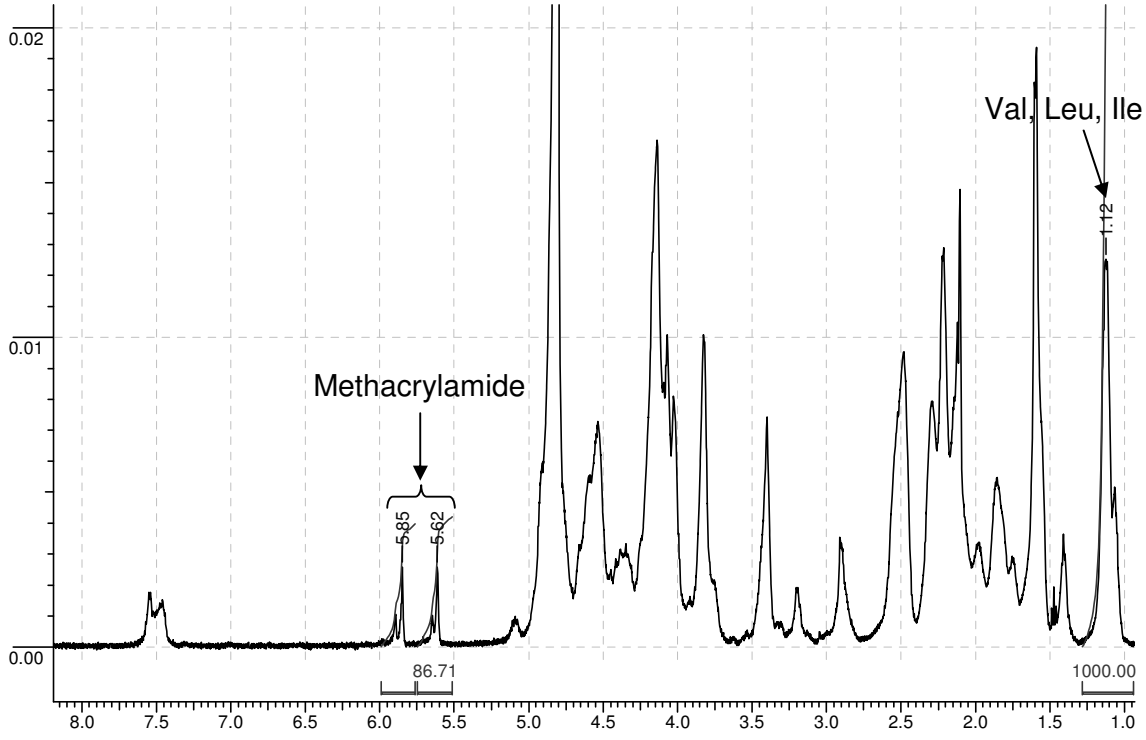

Figure 2-3: ^{1}H-NMR spectrum of gel-MOD with a degree of substitution of 86%, recorded in D_2O at 40°C.

The NMR-spectrum, represented in figure 2-3, is extremely complex since gelatin is composed of more than 20 different amino acids, as already described in chapter 1

(table 1-2). The structure of these amino acid building blocks is: -NH-CHR-CO-, in which the side chain (R) varies and possesses different functional groups. Complete analysis of the spectrum was out of the scope of the present study. Only attributing one peak to a component, that cannot be modified, was essential in order to calculate the degree of substitution.

The signal at 1.12 ppm could be ascribed to the resonance in the valine (Val), leucine (Leu) and isoleucine (Ile) side chain, by recording ^{1}H-NMR spectra of the different amino acids. The hydrophobic alkyl side chains of valine, leucine and isoleucine can be considered chemically inert. Based on the known composition (0.023 mol Val + 0.026 mol Leu + 0.015 mol Ile in 100 g gelatin), it can be calculated that the integration of this peak (18 protons) corresponds to 0.3836 mol/100g.

Also the total amount of available amine groups in gelatin (0.0385 mol/100g) needs to be considered, since we would like to define the degree of substitution as a function of the initial amount of free amine groups in gelatin:

$$\text{DS (\%)} =$$

$$0.3836 \text{ mol} \times (\text{integration at } 5.7 \text{ ppm} / \text{integration at } 1.1 \text{ ppm}) \times (100 / 0.0385 \text{ mol})$$

In the example, the integration at 1.1 ppm is 1000 and that at 5.7 ppm is 86.71. The degree of substitution (DS) is thus 86%. This corresponds to 8 double bonds per 10 amines (lysine + hydroxylysine).

In addition to ^{1}H-NMR-spectroscopy, the degree of substitution can also be obtained using the decrease in amine content after modification with methacrylic anhydride. The latter can be obtained spectrometric after reaction of the amines present with trinitrobenzenesulfonic acid (TNBS). This method was already evaluated and described in depth in the PhD of Dr. A. Van Den Bulcke and the obtained modification degrees were in good correlation with the results obtained using ^{1}H-NMR-spectroscopy.[13]

3 Synthesis and characterization of thiolated gelatin

The disadvantage of most chemical crosslinking procedures is the fact that they are irreversible.[21,22] This may be unfavourable when applying the materials developed as cell carriers in bioreactors.[23] Crosslinking via disulfide bond formation by oxidation of thiolated compounds could offer a solution for this problem, since this process is reversible.[24] Cleavage of the disulfide linkages via reducing agents (e.g. dithiothreitol) again results in thiolated, soluble reagents.[25]

In literature, numerous thiolating agents have been described. Dithioglycolide was first introduced by Schöberl.[26] However, this reagent has the disadvantage that it easily polymerizes to form polythioglycolides. Thiolation of RNAse has been investigated in this respect.[27] Benesch et al originally employed benzoyl homocysteine thiolactone for thiolation.[28] However, they eventually selected the acetyl derivative because of its greater solubility in water. Klotz et al used sodium thioparaconate, but the obtained results were similar to those obtained with alternative thiolating reagents.[29]

In the present work, two thiolating agents were applied and compared, namely N-acetylhomocysteine thiolactone and Traut's reagent.

Introduction of a sulfhydryl group occurs by aminolysis of the thiolactone bond of N-acetylhomocysteine thiolactone.[30] This method was patented in 1961, after which the product was used for the thiolation of numerous amine-containing compounds (e.g. ribonuclease).[31, 32]

Traut's reagent or 2-iminothiolane is a cyclic thioimidate compound for sulfhydryl addition.[33] It reacts spontaneously and efficiently with primary amines at pH 7-9.[34] The reagent can also react with aliphatic and phenolic hydroxyl groups, especially at high pH.[35] However, the rate of these reactions is 1000-fold less than with amino groups and will not occur when amines are present and with reaction times not exceeding 24 hours.[36]

3.1 Synthesis of thiolated gelatin

Gelatin was dissolved at 40°C in degassed buffer (pH 10), in the presence of EDTA. The latter was included to chelate divalent metals in the solution that may catalyze

thiol oxidation (i.e. formation of disulfide bonds).[37,38] Consequently, N-acetyl homocysteine thiolactone (figure 2-4) or Traut's reagent (figure 2-5) was added and the reaction proceeded for respectively three hours or 45 minutes under argon atmosphere. Purification of the obtained products occurred via dialysis in the presence of argon in order to prevent disulfide formation by redox reaction with oxygen, followed by freeze-drying.

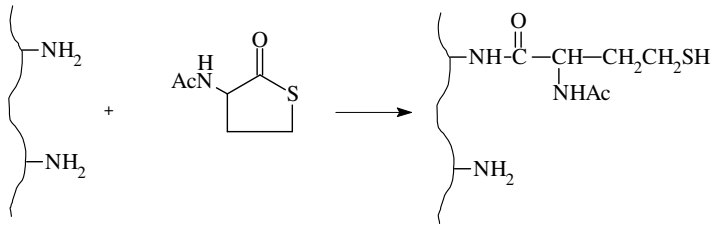

Figure 2-4: Reaction scheme to prepare thiolated gelatin by means of N-acetyl-homocysteine thiolactone.

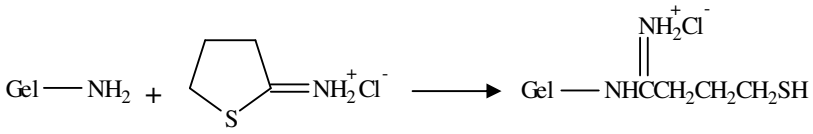

Figure 2-5: Synthesis of thiolated gelatin with 2-iminothiolane as reagent.

3.2 Characterization of the thiolated gelatin derivatives

3.2.1 Quantification of the thiol groups

There exist two possible pathways to determine the amount of incorporated thiol groups in gelatin, either **directly** or **indirectly**.

The direct approach involves the use of Ellman's reagent. Already in 1959, Ellman introduced 5,5'-dithio-bis-(2-nitrobenzoic acid) (DTNB) as a versatile water-soluble compound for quantifying free sulfhydryl groups in solution.[39] A solution of this compound produces a yellow-coloured product when it reacts with thiol groups. This compound possesses a high specificity for thiols at neutral pH values and is characterized by a high molar extinction coefficient and short reaction times.[40]

DTNB reacts with a free sulfhydryl group yielding a mixed disulfide and 2-nitro-5-thiobenzoic acid (TNB), as depicted in figure 2-6. TNB is the coloured species, produced in this reaction and has a high molar extinction coefficient in the visible range (14150 $M^{-1}cm^{-1}$ at 412 nm).[41,42] The extinction coefficient of TNB is not affected by changes in pH between 7.6 and 8.6, but varies under different solvent conditions.[42]

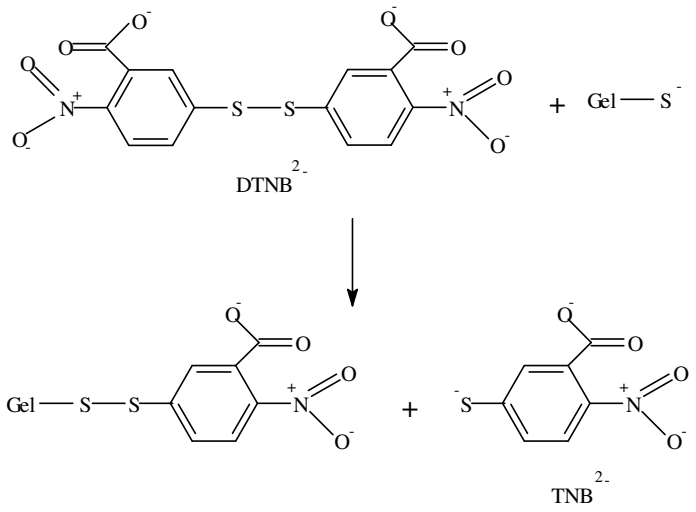

Figure 2-6: Reduction of Ellman's reagent.

Thiol groups were quantified by comparison with a standard curve obtained from solutions containing known concentrations of cysteine.

The indirect method involves the determination of the difference between the amine content in gelatin before and after modification.

The amine concentration was determined spectrometrically by means of ortho-phthalic dialdehyde or 1,2-benzenedicarboxaldehyde (OPA) (figure 2-7). Iso-indol chromophores originate during the derivatization, which possess a maximum absorbance at 335 nm ($\varepsilon = \pm 10^4$ $M^{-1}cm^{-1}$). The reaction proceeds fast and amine concentrations were obtained by comparison with a calibration curve based on n-butylamine.

After derivatization with N-acetylhomocysteine thiolactone or Traut's reagent, the amount of free amines in gelatin decreases. Consequently, less amines will be available for reaction with OPA, which will lead to lower absorbances at 335 nm. The difference in absorbance is proportional with the amount of amines that is modified

with thiol groups. The degree of substitution is defined as the ratio of the amount of modified amines to the amount of total amines originally (i.e. before modification) present in gelatin.

In literature, many alternative methods have been described to determine amine concentrations in solutions (e.g. 2,4,6-trinitrobenzenesulfonic acid (TNBS) and ninhydrin).[43,44,45] However, TNBS could not be used since it also reacted with the incorporated thiol groups, yielding compounds that showed absorbance at the same wavelength as the chromophores originated from the reaction of the amines with TNBS.

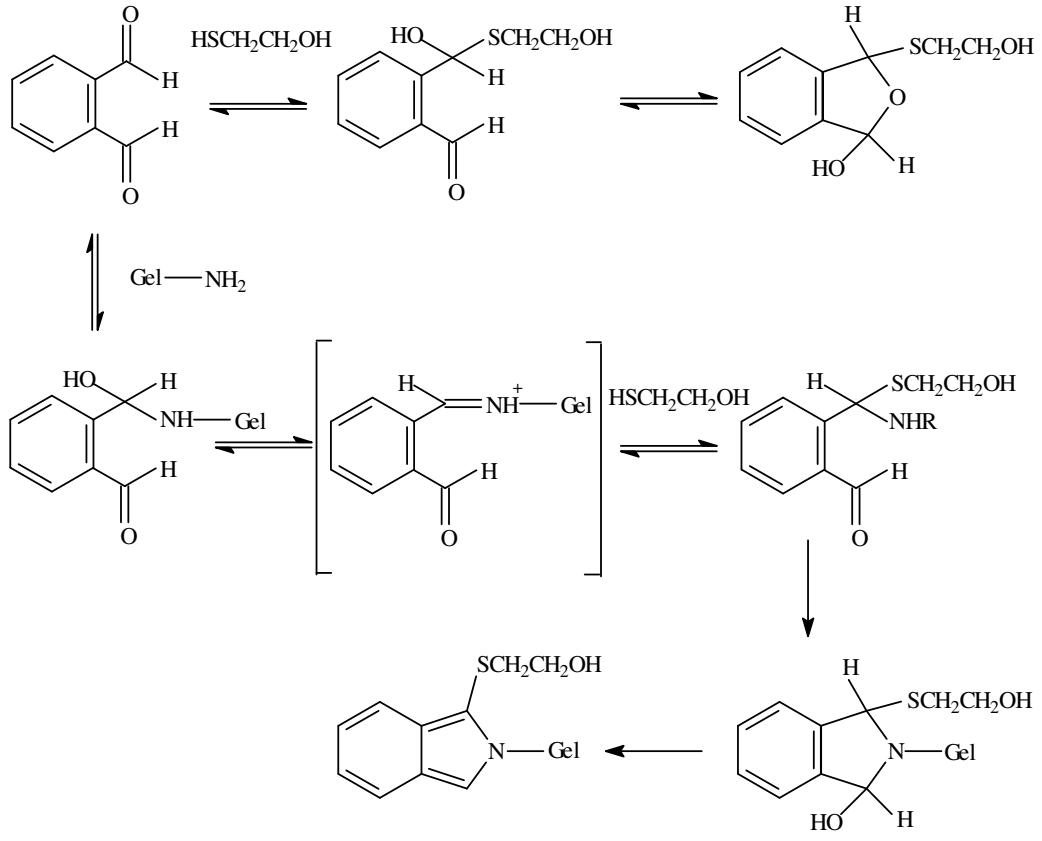

Figure 2-7: Reaction mechanism of ortho-phtalic dialdehyde with the primary amines of gelatin.

Both the direct and indirect method were compared, after modification of gelatin with N-acetylhomocysteine thiolactone. All experiments were performed in triplicate. The results, shown in figure 2-8, demonstrate a significantly higher degree of substitution

when using OPA compared to Ellman's reagent. Hence, less thiol groups were detected with Ellman's reagent than there were present in gelatin. Probably, oxidation of some incorporated thiol groups occurred in the presence of oxygen, thereby forming disulfide linkages. Since disulfides can not be detected using Ellman's reagent, this method probably underestimates the thiol concentration. OPA thus appears to be the best method to determine the degree of substitution of gelatin, despite the fact that it is an indirect method.

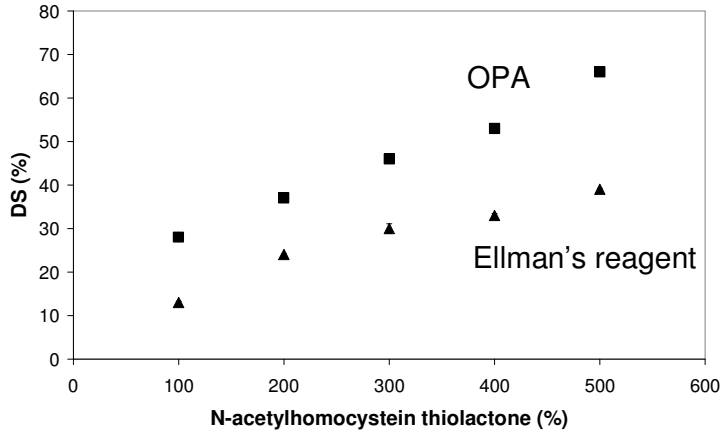

Figure 2-8: Degree of substitution of gelatin as a function of the amount of added thiolactone (n = 3).

The degree of modification is proportional to the added amount of thiolactone. The maximum obtainable degree of substitution is 65%, after the addition of five equivalents of N-acetylhomocysteine thiolactone.

3.2.2 Determination of the average molecular weight of gel-SH

The molecular weight and the molecular weight dispersity of the gelatin derivatives were determined by means of size exclusion chromatography (SEC) at 50°C, using buffer as eluens. Pullulan standards were utilized for calibration. Gelatin with a weight-average molecular weight of 190000 Da and a polydispersity of 2.5 were used for the modification reaction. The table below indicates that the molecular weight of the thiolated gelatin is significantly higher. In order to investigate whether these results were due to crosslinking of incorporated thiol groups, a reducing agent dithiothreitol (DTT) was added, followed by SEC. It was observed that the molecular

weight decreased, but still remained higher than the molecular weight of unmodified gelatin (i.e. 190,000 Da). There exist different possible explanations for the latter phenomenon. The first one is that DTT could not react with all the present disulfides, because of the conformation of certain gelatin chains. A second possibility is the influence of the thiolation on the hydrodynamic volume of the molecules. The last option is related to the purification process. During dialysis, gelatin molecules having a molecular weight lower than the molecular weight cut off (MWCO) of the membranes, are removed from the solution, resulting in a relatively higher fraction of polymers with higher molecular weight. As a result, the polydispersity decreases. However, since the polydispersity of the thiolated gelatin is higher than that of unmodified gelatin, the latter explanation can be excluded.

	Mw		**δ**	
		+ DTT		+ DTT
Gel	190000 Da	190000 Da	2.5	2.5
Gel-SH (thiolactone)	280000 Da	260000 Da	2.7	2.8
Gel-SH (Traut's reagent)	330000 Da	200000 Da	3.2	3.5

Table 2-1: Weight-average molecular weights and polydispersities of gelatin and thiolated gelatin.

The increase in polydispersity after modification is also due to the formation of disulfides.

3.3 Influence of the pH on the degree of substitution

The pH of the reaction buffer plays an important role in the derivatization of gelatin.
The equilibrium between the free amines of (hydroxy-)lysine and their conjugated acid shifts when the pH changes. In less basic media, a smaller amount of primary amines is available for the reaction with N-acetylhomocysteine thiolactone, since more amines are protonated.
In addition, the competition with already incorporated thiols should not be underestimated either. In this way, the sulfhydryl groups present in gelatin can, at elevated pH, react as a nucleophile with the thiolactone and thus compete with the primary amines of the polymer. Reaction buffers with three different pH's (9, 10 and

11) resulted in the formation of thiolated gelatin, but the optimal reaction medium appeared to be a carbonate buffer (pH 10) (figure 2-9).

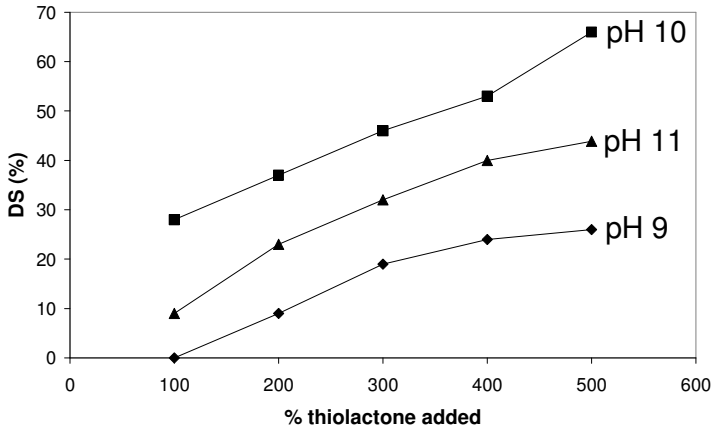

Figure 2-9: Influence of pH on the degree of substitution of gelatin.

3.4 Influence of the reagent on the degree of substitution

As already mentioned in a previous paragraph (§ 3.1), beside N-acetylhomocysteine thiolactone, alternative thiolating agents such as Traut's reagent exist (figure 2-10). In the present work, a comparative study was made on the efficiency of both compounds.

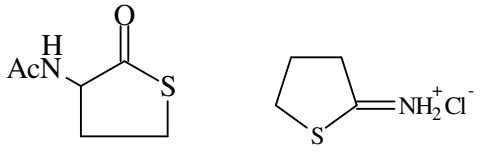

Figure 2-10: Chemical structure of N-acetylhomocysteine thiolactone (left part) and Traut's reagent (right part).

Varying amounts of both reagents (i.e. 1 and 2 equivalents) were applied and the corresponding modification degrees were determined using OPA. The results for Traut's reagent are shown in white and those for thiolactone are depicted in grey (figure 2-11).

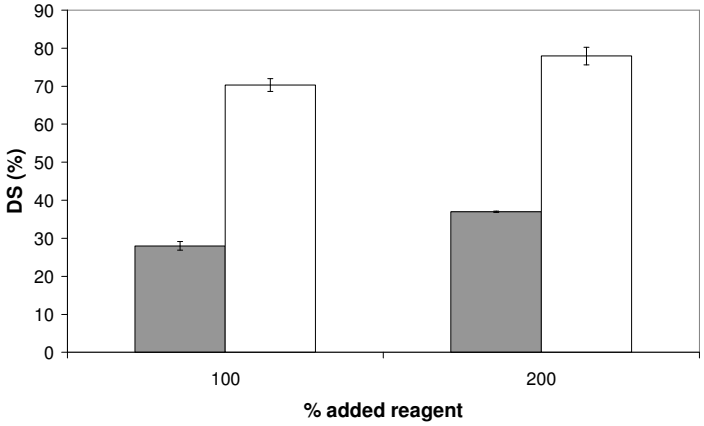

Figure 2-11: Influence of the applied reagent on the degree of substitution of gelatin (Traut's reagent: white; thiolactone: grey).

From the results in figure 2-11, it can be concluded that the reactivity of Traut's reagent is significantly higher than that of thiolactone. When applying one equivalent 2-iminothiolane, the obtained modification degree is already 70%, compared to 30% when using thiolactone. Moreover, the reaction with Traut's reagent only proceeds for 45 minutes (pH 8).

4 Synthesis and characterization of methacrylate-modified chondroitin sulphate

Chondroitin sulphate (CS) is a glycosaminoglycan, which is comprised of alternating units of β-1,3-linked glucuronic acid and (β-1,4) N-acetyl-galactosamine and is sulphated on either the 4- or 6-position of the N-acetyl-galactosamine residues.[46] Since natural CS is readily water-soluble, a chemical crosslinking step is necessary in order to retain CS within hydrogel films and/or scaffolds.[47]

In literature, a variety of methods was already described to graft CS onto different components. Güdemez et al activated the alcoholic groups within a polyhydroxyethyl methacrylate membrane to prepare it for covalent coupling with chondroitin sulphate. Epoxy groups were incorporated covalently onto the membrane by the nucleophilic reaction between the chloride groups of epichlorohydrin and the hydroxyl groups of the pHEMA.[48] Kirker et al prepared biocompatible hydrogel films using the adipic dihydrazide derivative of chondroitin sulphate, in which a pendant hydrazide

functionality permits generation of a gel using a small molecule[49] or macromolecular crosslinkers[50] (e.g. poly(ethylene glycol)-propiondialdehyde).[46] The most frequently utilized crosslinking reagents are 1-ethyl-3-(3-dimethyl aminopropyl)carbodiimide (EDC) and N-hydroxysuccinimide (NHS).[51,52,53] The crosslinking reaction occurs often in the presence of collagen[54,55] or other amine-containing reagents (e.g. 1,12-diaminododecane).[56] However, using EDC as crosslinking method often results in (partial) matrix collapse when working in aqueous media. This can be (partly) prevented if crosslinking is carried out in the presence of ethanol to decrease the polymer solubility.[57]

Alternatively, thiol groups were incorporated into CS by EDC-mediated condensation with dithiobis(propionic acid), followed by dithiothreitol reduction. Next, thiol-modified CS was crosslinked with poly(ethylene glycol) diacrylate.[58]

Li et al utilized glycidyl methacrylate (GMA) in a homogeneous-phase system (DMSO) expecting epoxide ring-opening, but instead transesterification dominated the reaction. However, in their study concerning the different solubility of the water-soluble CS and the water-insoluble GMA, a slow heterogeneous-phase reaction of CS with GMA was designed and performed in aqueous medium regardless of GMAs potential side-reaction with water.[59]

The optimal strategy, used in the present work is equivalent to the synthesis of gel-MOD and results in the incorporation of methacrylate side groups. Subsequent light-induced polymerization of the structure enables co-crosslinking with gel-MOD.

4.1 Synthesis of methacrylate – modified chondroitin sulphate

Similar to the derivatization of gelatin, methacrylic anhydride was selected to introduce double bonds.[47] The synthesis of the methacrylate-modified chondroitin sulphate (CS-MOD) precursor is illustrated in figure 2-12. Part of the hydroxyl groups of CS were converted into methacrylate groups. As methacrylic acid (MA) is generated during the esterification, NaOH was added as neutralizing agent, avoiding possible acid catalysed degradation of the polysaccharide. The glycosaminoglycan containing crosslinkable methacrylate groups was purified by membrane dialysis against double distilled water for several days, followed by isolation via lyophilization.

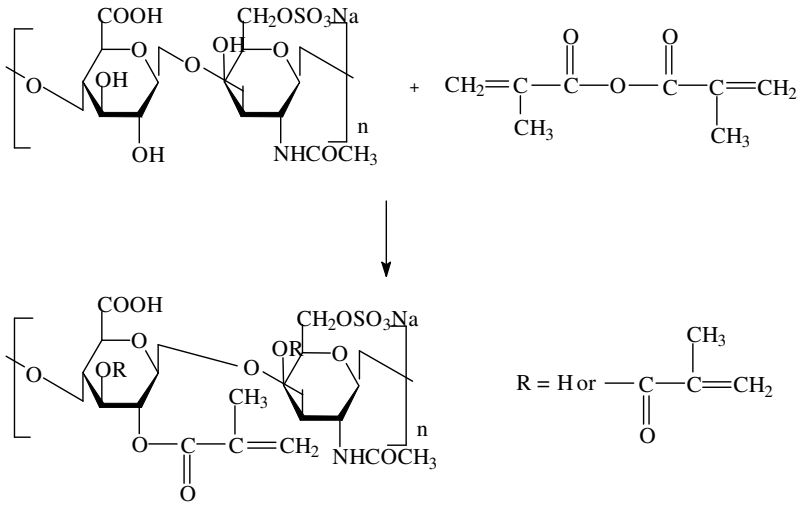

Figure 2-12: Synthesis of CS-MOD.

4.2 Characterization of CS-MOD

4.2.1 Attenuated total reflection – Infrared (ATR-IR)

The successful incorporation of methacrylate side groups on chondroitin sulphate was confirmed by ATR-IR. As shown in figure 2-13, the characteristic ester absorption band at 1705 cm^{-1} appeared after modification with methacrylic anhydride. The other infrared bands were assigned as follows.[60,61, 62]

The broad band in the region 3600-3000 cm^{-1} is due to the v(OH) stretching mode and partially to the v(N-H) stretching vibration of the N-acetyl side chain. The band at 1610 cm^{-1} is assigned to the amide I mode (mainly C=O stretching coupled with N-H bending). The shoulder at 1550 cm^{-1} can be assigned to the amide II band and the feature at 1410 cm^{-1} originates from the symmetrical COO^- vibration, $v_s(COO^-)$. The absorbance in the region 1100-950 cm^{-1} mainly results from different vibrations of the pyranose ring. Additional bands in the spectrum can be attributed to vibrations of the C-O-SO_3^--fragment. The intense band centred at 1226 cm^{-1} is due to the antisymmetrical stretching mode, $v_{as}(SO_3^-)$. A peak at 1124 cm^{-1} is probably due to the antisymmetrical C-O-S stretching.

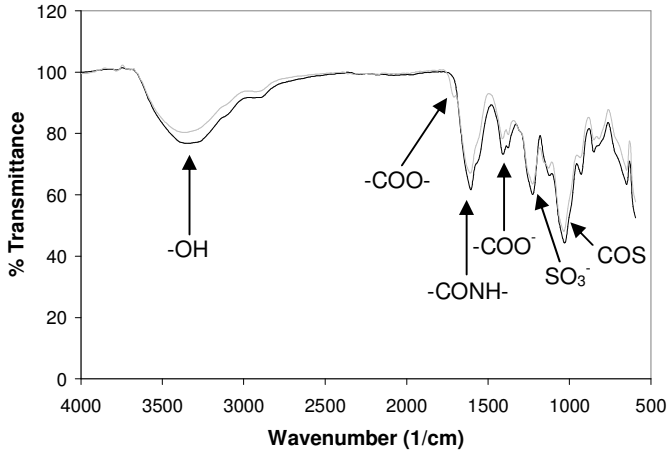

Figure 2-13: ATR-IR spectra of CS (black) and CS-MOD (grey).

Since infrared spectra only give qualitative and semi-quantitative information, an alternative method was needed to determine the amount of incorporated methacrylate groups (i.e. degree of substitution).[63]

4.2.2 Determination of degree of substitution using ^{1}H-NMR

The methacrylate substitution on CS was quantified using ^{1}H-NMR as shown in figure 2-14. Two distinctive peaks at 5.76 and 6.19 ppm can be attributed to the two protons attached to the double bond ($C=CH_2$) and the peak shown at 1.95 ppm, was ascribed to the methyl groups adjacent to the double bonds (CH_3-$C=CH_2$).

The ^{1}H-NMR region from 1.6 to 2.5 ppm was expanded and the peaks corresponding to the two methyl groups were deconvoluted and integrated. The peak intensity at 1.95 ppm to that at 2.04 ppm, corresponding to the methyl groups on native CS, was used to calculate the degree of substitution. The degree of substitution was expressed as the amount of modified repeating disaccharide units.

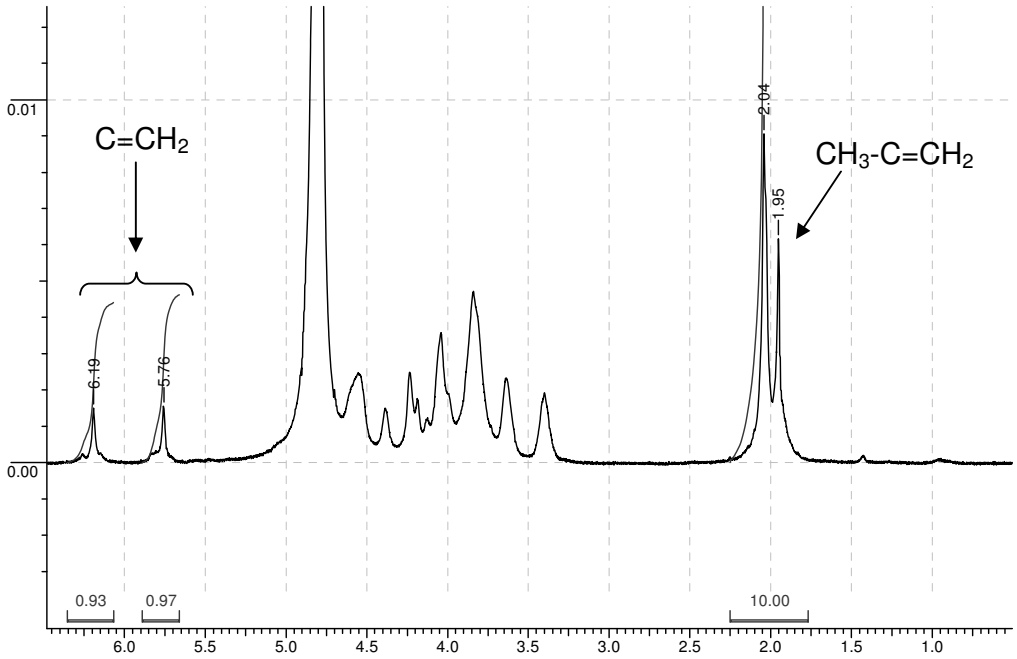

Figure 2-14: ^{1}H-NMR spectrum of CS-MOD.

The degree of substitution was calculated using the following equation:

DS (%) = 100 x (integration at 5.7 ppm) /
((sum of integrations at 1.95 and 2.04 ppm – 3 x (integration at 5.7 ppm)) / 3)

In the example, the integration at 5.7 ppm is 0.97 and the sum of the integrations at 1.95 and 2.04 ppm is 10. The degree of substitution is 41% meaning that 41% of the repeating disaccharide units are modified, which corresponds with 13.7% of the OH's.

The degree of substitution can be varied easily by adjusting the amount of added methacrylic anhydride. In figure 2-15, a master curve is shown for the modification of CS, showing the degree of substitution, obtained after adding different quantities of methacrylic anhydride.

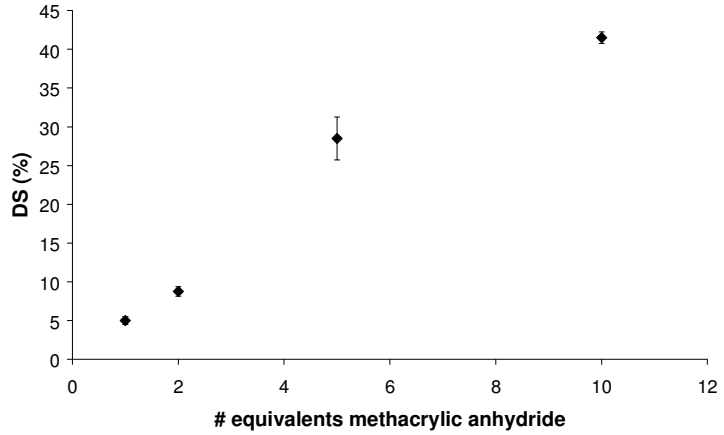

Figure 2-15: Master curve of CS showing the degree of substitution as a function of the amount of methacrylic anhydride added.

From the ^{1}H-NMR spectrum (figure 2-14), it can also be concluded that all detectable methacrylic acid was removed during dialysis. Otherwise a peak corresponding to the methyl group of methacrylic acid would be visible at 1.6 ppm.

4.2.3 Determination of average molecular weight

The molecular weight and the molecular weight dispersity of the synthesized derivatives were determined by means of size exclusion chromatography (SEC) at 50°C. Pullulan standards were used for calibration.
The weight-averaged molecular weight of native chondroitin sulphate was 118,000 Da with a polydispersity of 1.2. CS-MOD appeared to have a somewhat lower weight-averaged molecular weight of 111,000 Da and a polydispersity of 1.2.

5 Synthesis and characterization of methacrylate-modified hyaluronan

Hyaluronan (HA) is an attractive building block for new biocompatible and biodegradable polymers, applied in drug delivery and tissue engineering.

HA derivatives have physicochemical properties that may significantly differ from the native polymer (e.g. improved mechanical properties), but most derivatives retain their biocompatibility and biodegradability.

In literature, a lot of attention has been paid to the modification of HA. Esterified hyaluronan has been prepared by alkylation of the tetra(n-butyl)ammonium salt of hyaluronan with an alkyl halide in dimethylformamide (DMF).[64] At high percentages of esterification, the resulting materials became insoluble in water. These polymers showed good mechanical strength when dry, but the hydrated materials were less robust.

The chemical modification of the carboxylic functions of hyaluronan with amine-containing compounds using carbodiimide compounds is generally performed in water at pH 4.75. At this pH, the carboxylic acid is protonated, but a small percentage of the amine base may remain in nucleophilic form to produce a covalent adduct.[65]

Alternatively, hydrazides can also couple to carbodiimide-activated glucuronic acid residues of HA at pH 4.75.[49] Consequently, the use of dihydrazide compounds, such as adipic dihydrazide, can provide multiple pendant hydrazide groups for crosslinking agents.

Other carbodiimide-mediated reactions of hyaluronan employ hydroxylamine-containing species to obtain hyaluronan-activated esters.

Furthermore, reactive bisaldehyde functionalities have been generated from the vicinal secondary alcohol functions on hyaluronan by oxidation with sodium periodate. Consequent crosslinking occurred via reductive coupling with multifunctional primary amines.

Different strategies exist in order to obtain chemically crosslinked hyaluronan-based materials.[66,67] For example, Intergel® is a hydrogel formulation of hyaluronan, formed by chelation with ferric hydroxide. A similar procedure has been the basis of synthesis using copper, zinc, calcium, barium and other chelating metals.

Laurent et al prepared a crosslinked gel in dilute NaOH using bisepoxybutane and sodium borohydride, a strategy first developed for crosslinking of agarose.[68]

In the present work, photocrosslinking of a methacrylate derivative of hyaluronic acid (HA-MOD) will be applied.

5.1 Synthesis of HA-MOD

Methacrylic anhydride was selected in order to modify the hydroxyl groups of hyaluronic acid with methacrylate groups. The modification procedure applied, was similar to that used for the synthesis of CS-MOD. Hyaluronan was dissolved in double distilled water. Next, varying amounts of methacrylic anhydride were added, followed by adjusting the pH to 8 using NaOH. The reaction scheme is presented in figure 2-16.

Finally, the polymer derivatives were purified via dialysis and isolated by lyophilisation.

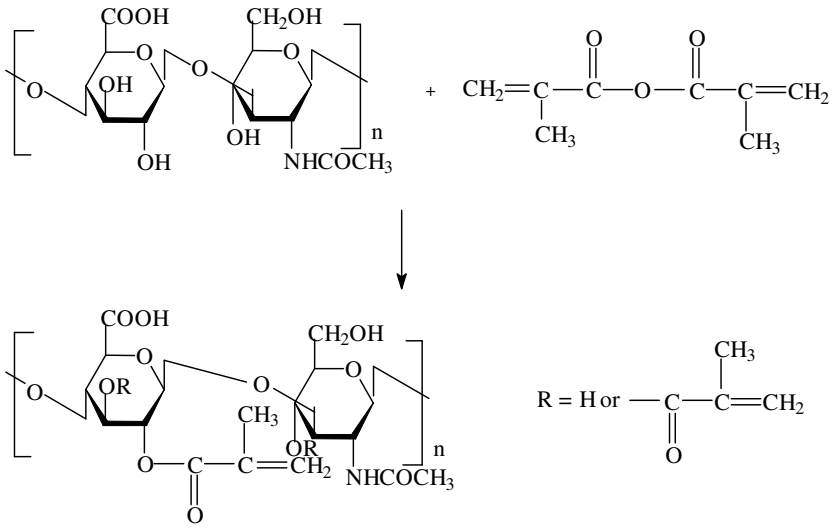

Figure 2-16: Modification of hyaluronic acid with methacrylic anhydride.

5.2 Characterization of HA-MOD

5.2.1 ATR-IR

The incorporation of methacrylate side groups was demonstrated by means of ATR-IR (figure 2-17), since a peak around 1720 cm^{-1} (indicated with an arrow) was present in the spectrum after reaction with methacrylic anhydride. Peak assignment was already performed in depth in § 4.2.1 for CS-MOD. Since both

glycosaminoglycans possess similar structures, beside the absence of sulphate groups in hyaluronan, peaks at analogous wavenumbers were expected and obtained.[69]

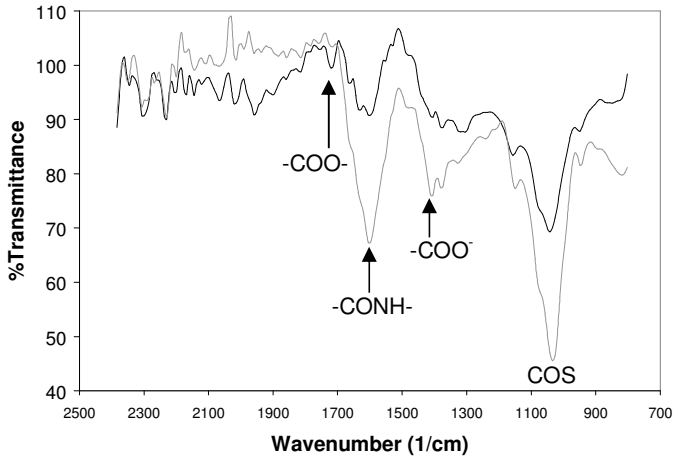

Figure 2-17: ATR-IR spectra of HA (grey) and HA-MOD (black).

5.2.2 Determination of degree of substitution using ^{1}H-NMR

The evidence of methacrylate substitution on hyaluronan was also observed by ^{1}H-NMR as shown in figure 2-18. Two distinctive peaks at 5.78 and 6.21 ppm were attributed to the two protons attached to the double bond ($C=CH_2$) and the peak shown at 1.98 ppm, was ascribed to the methyl group adjacent to the double bond (CH_3-$C=CH_2$).

The ^{1}H-NMR region from 1.7 to 2.3 ppm was expanded and the peaks corresponding to the two methyl groups were deconvoluted and integrated. The peak intensity ratio at 1.98 ppm to that at 2.06 ppm, corresponding to the methyl groups on native HA, were used to calculate the degree of substitution. The degree of substitution was expressed as the amount of modified repeating disaccharide units.

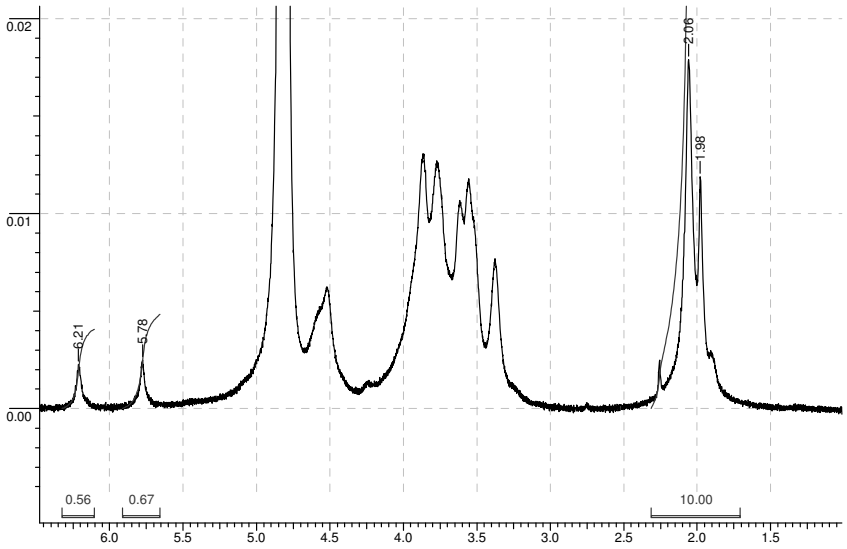

Figure 2-18: ^{1}H-NMR spectrum of modified hyaluronan.

The degree of substitution can thus be calculated using the following equation:

DS (%) = 100 x (integration at 5.78 ppm) /
((sum of integrations at 1.98 and 2.06 ppm – 3 x (integration at 5.78 ppm)) / 3)

In the example, the integration at 5.78 ppm is 0.615 and the sum of the integrations at 1.98 and 2.06 ppm is 10. The degree of substitution is thus 23%. This implies that in average 23% of the repeating disaccharide units are modified, which corresponds with 5.8% of the OH's.

The degree of substitution can be varied by simply adjusting the amount of added methacrylic anhydride. In figure 2-19, a master curve is represented for the modification of HA, showing the relation between the degree of substitution and the amount of added methacrylic anhydride. All data points are the average of minimum three experiments.

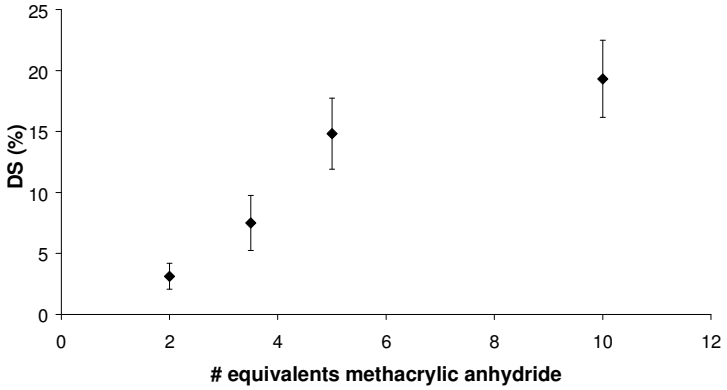

Figure 2-19: Influence of the amount of methacrylic anhydride added, on the modification degree of HA.

From the ^{1}H-NMR spectrum (figure 2-18), it can also be concluded that all methacrylic acid was removed during dialysis. Otherwise a peak corresponding to the methyl group of methacrylic acid would be visible at 1.6 ppm.

6 Conclusion

The present chapter has demonstrated that the polymer precursors can be easily prepared in various ways.

Methacrylic anhydride appears to be a very appropriate reagent for the modification of gelatin and glycosaminoglycans. The synthesis of all derivatives was performed in aqueous solution and the degree of substitution could be easily adjusted by simply varying the amount of added methacrylic anhydride. The degree of substitution was determined by means of ^{1}H-NMR-spectroscopy. The average molecular weight was determined by means of size exclusion chromatography.

An alternative for the derivatization of gelatin is thiolation. Both N-acetylhomocysteine thiolactone and Traut's reagent are suitable for the incorporation of thiol groups in gelatin. The degree of substitution was varied by changing the ratio of gelatin and thiolating reagent and could be obtained indirectly by determining the difference in amine content before and after substitution. Both the pH of the reaction medium and the type of thiolating agent can influence the modification degree significantly. Traut's reagent is more efficient since less excess is needed.

References

1. Gadomski, W.; Ratajska-Gadomska, B., Evolution of water structure in biopolymer solutions during the gelation process. *Chemical Physics Letters* **2004,** 399, (4-6), 471-474.
2. Ward, A. G.; Courts, A., *The science and technology of gelatin*. 1977.
3. Kuijpers, A. J.; Engbers, G. H. M.; Krijgsveld, J.; Zaat, S. A. J.; Dankert, J.; Feijen, J., Cross-linking and characterisation of gelatin matrices for biomedical applications. *Journal of Biomaterials Science-Polymer Edition* **2000,** 11, (3), 225-243.
4. Djagny, K. B.; Wang, Z.; Xu, S. Y., Gelatin: A valuable protein for food and pharmaceutical industries: Review. *Critical Reviews in Food Science and Nutrition* **2001,** 41, (6), 481-492.
5. Jayakrishnan, A.; Jameela, S. R., Glutaraldehyde as a fixative in bioprotheses and drug delivery matrices. *Biomaterials* **1996,** 17, 471-484.
6. Olde Damink, L. H.; Dijkstra, P. J.; Van Luyn, M. J.; van Wachem, P. B.; Nieuwenhuis, P.; Feijen, J., Glutaraldehyde as a cross-linking agent for collagen-based biomaterials. *Journal of Materials Science-Materials in Medicine* **1995,** 6, 460-472.
7. Olde Damink, L. H.; Dijkstra, P. J.; Van Luyn, M. J.; Van Wachem, P. B.; Nieuwenhuis, P.; Feijen, J., Cross-linking of dermal sheep collagen using hexamethylene diisocyanate. *Journal of Materials Science-Materials in Medicine* **1995,** 6, 429-434.
8. Ofner, C. M.; Bubnis, W. A., Chemical and swelling evaluations of amino group cross-linking in gelatin and modified gelatin matrices. *Pharmaceutical Research* **1996,** 13, 1821-1827.
9. Lee S, K. Y., Chong M, Hong S, Lee Y, Study of gelatin-containing artificial skin V: fabrication of gelatin scaffolds using a salt-leaching method. *biomaterials* **2005,** 26, (14), 1961-1968.
10. Sung, H.-W.; Hsu, H.-L.; Shih, C.-C.; Lin, D.-S., Cross-linking characteristics of biological tissues fixed with monofunctional or multifunctional epoxy compounds. *Biomaterials* **1996,** 17, 1405-1410.
11. Petite, H.; Rault, I.; Huc, A.; Mesnache, P.; Herbage, D., *Journal of Biomedical Materials Research* **1990,** 24, 179-188.
12. Aoki, H.; Taguchi, T.; Saito, H.; Kobayashi, H.; Kataoka, K.; Tanaka, J., Rheological evaluation of gelatin gels prepared with a citric acid derivative as a novel cross-linker. *Materials Science & Engineering C-Biomimetic and Supramolecular Systems* **2004,** 24, (6-8), 787-790.
13. Van Den Bulcke, A. Synthese en evaluatie van hydrogelen op basis van gelatine. 2000.
14. Boudet, C.; Iliopoulos, I.; Poncelet, O.; Cloitre, M., Control of the chemical cross-linking of gelatin by a thermosensitive polymer: example of switchable reactivity. *Biomacromolecules* **2005,** 6, 3073-3078.
15. Butler, M. F.; Ng, Y. F.; Pudney, P. D. A., Mechanism and kinetics of the crosslinking reaction between biopolymers containing primary amine groups and genipin. *Journal of Polymer Science Part a-Polymer Chemistry* **2003,** 41, (24), 3941-3953.

16. Kojima, T.; Bessho, M.; Furuta, M.; Okuda, S.; Hara, M., Characterization of biopolymer hydrogels produced by gamma-ray irradiation. *Radiation Physics and Chemistry* **2004,** 71, (1-2), 235-238.
17. Terao, K.; Nagasawa, N.; Nishida, H.; Furusawa, K.; Mori, Y.; Yoshii, F.; Dobashi, T., Reagent-free crosslinking of aqueous gelatin: manufacture and characteristics of gelatin gels irradiated with gamma-ray and electron beam. *Journal of Biomaterials Science-Polymer Edition* **2003,** 14, (11), 1197-1208.
18. Woolston, J., Irradiation sterilization of medical devices. *Med. Dev. Technol.* **1990**, 25-31.
19. Bruck, S. D.; Mueller, E. P., Radiation sterilization of polymeric implant materials. *Journal of Biomedical Materials Research, Applied Biomaterials* **1988,** 22, 133-144.
20. Van den Bulcke, A. I.; Bogdanov, B.; De Rooze, N.; Schacht, E. H.; Cornelissen, M.; Berghmans, H., Structural and rheological properties of methacrylamide modified gelatin hydrogels. *Biomacromolecules* **2000,** 1, (1), 31-38.
21. Martucci, J. F.; Ruseckaite, R. A.; Vazquez, A., Creep of glutaraldehyde-crosslinked gelatin films. *Materials Science and Engineering a-Structural Materials Properties Microstructure and Processing* **2006,** 435, 681-686.
22. Nickerson, M. T.; Patel, J.; Heyd, D. V.; Rousseau, D.; Paulson, A. T., Kinetic and mechanistic considerations in the gelation of genipin-crosslinked gelatin. *International Journal of Biological Macromolecules* **2006,** 39, (4-5), 298-302.
23. Bilodeau, K.; Mantovani, D., Bioreactors for tissue engineering: Focus on mechanical constraints. A comparative review. *Tissue Engineering* **2006,** 12, (8), 2367-2383.
24. Zelikin, A. N.; Quinn, J. F.; Caruso, F., Disulfide cross-linked polymer capsules: En route to biodeconstructible systems. *Biomacromolecules* **2006,** 7, (1), 27-30.
25. Di Stefano, G.; Lanza, M.; Kratz, F.; Merina, L.; Fiume, L., A novel method for coupling doxorubicin to lactosaminated human albumin by an acid sensitive hydrazone bond: synthesis, characterization and preliminary biological properties of the conjugate. *European Journal of Pharmaceutical Sciences* **2004,** 23, (4-5), 393-397.
26. Schöberl, A., *Angewandte Chemie* **1948,** 60, 7.
27. White, F. H., *Journal of Biological Chemistry* **1960,** 235, 383.
28. Benesch, R.; Benesch, R. E., *Journal of American chemical society* **1956,** 78, 1597.
29. Klotz, I. M.; Elfbaum, S. G., *Biochimica et biophysica acta* **1964,** 86, 100.
30. Mudd, S. H.; Finkelstein, J. D.; Refsum, H.; Ueland, P. M.; Malinow, M. R.; Lentz, S. R.; Jacobsen, D. W.; Brattstrom, L.; Wilcken, B.; Wilcken, D. E. L.; Blom, H. J.; Stabler, S. P.; Allen, R. H.; Selhub, J.; Rosenberg, I. H., Homocysteine and its disulfide derivatives - A suggested consensus terminology. *Arteriosclerosis Thrombosis and Vascular Biology* **2000,** 20, (7), 1704-1706.
31. Town, B. W. Thiolation of proteins by reaction with homocysteine thiolactone in the presence of tertiary amine. 1961.
32. White, F. H.; Sandoval, A., The thiolation of ribonuclease. *Biochemistry* **1962,** 1, (6), 938-946.

33. Traut, R. R.; Bollen, A.; Sun, T. T.; Hershey, J. W. B.; Sundberg, J.; Pierce, L. R., Methyl 4-Mercaptobutyrimidate as a Cleavable Crosslinking Reagent and Its Application to Escherichia-Coli 30s Ribosome. *Biochemistry* **1973,** 12, (17), 3266-3273.
34. Jue, R.; Lambert, J. M.; Pierce, L. R.; Traut, R. R., Addition of Sulfhydryl-Groups to Escherichia-Coli Ribosomes by Protein Modification with 2-Iminothiolane (Methyl 4-Mercaptobutyrimidate). *Biochemistry* **1978,** 17, (25), 5399-5406.
35. Alagon, A. C.; King, T. P., Activation of Polysaccharides with 2-Iminothiolane and Its Uses. *Biochemistry* **1980,** 19, (18), 4341-4345.
36. Tarentino, A. L.; Phelan, A. W.; Plummer, T. H., 2-Iminothiolane - a Reagent for the Introduction of Sulfhydryl-Groups into Oligosaccharides Derived from Asparagine-Linked Glycans. *Glycobiology* **1993,** 3, (3), 279-285.
37. do Nascimento, C. W. A., Organic acids effects on desorption of heavy metals from a contaminated soil. *Scientia Agricola* **2006,** 63, (3), 276-280.
38. Kudryavtseva, E. V.; Sidorova, M. V.; Ovchinnikov, M. V.; Bespalova, Z. D.; Bushuev, V. N., Comparative evaluation of different methods for disulfide bond formation in synthesis of the HIV-2 antigenic determinant. *Journal of Peptide Research* **1997,** 49, (1), 52-58.
39. Ellman, G. L., Tissue sulfhydryl groups. *Archives of Biochemistry and Biophysics* **1959,** 82, 70-77.
40. Butterworth, P. H. W.; Baum, H.; Porter, J. W., A modification of the Ellman procedure for the estimation of protein sulfhydryl groups. *Archives of Biochemistry and Biophysics* **1967,** 118, 716-723.
41. Riddles, P. W.; Blakeley, R. L.; Zerner, B., Reassessment of Ellman's reagent. *Meth. Enzymol.* **1983,** 91, 49-60.
42. Riddles, P. W.; Blakeley, R. L.; Zerner, B., Ellman's reagent: 5, 5'-dithiobis(2-nitrobenzoic acid) - a reexamination. *Analytical Biochemistry* **1979,** 94, 75-81.
43. Snyder, S. L.; Sobocinsky, P. Z., An improved 2,4,6-trinitrobenzenesulfonic acid method for the determination of amines. *Analytical Biochemistry* **1975,** 64, 284-288.
44. Haynes, R.; Osuga, D. T.; Feeney, R. E., Modification of aminogroups in inhibitors of proteolytic enzymes. *Biochem.* **1967,** 6, 541-547.
45. Raza, A.; Ansari, T. M.; Atta ur, R., Spectrophotometric determination of lisinopril in pure and pharmaceutical formulations. *Journal of the Chinese Chemical Society* **2005,** 52, (5), 1055-1059.
46. Kirker, K. R.; Luo, Y.; Nielson, J. H.; Shelby, J.; Prestwich, G. D., Glycosaminoglycan hydrogel films as bio-interactive dressings for wound healing. *Biomaterials* **2002,** 23, (17), 3661-3671.
47. Wang, L. F.; Shen, S. S.; Lu, S. C., Synthesis and characterization of chondroitin sulfate-methacrylate hydrogels. *Carbohydrate Polymers* **2003,** 52, (4), 389-396.
48. Gudemez, E.; Eksioglu, F.; Korkusuz, P.; Asan, E.; Gursel, I.; Hasirci, V., Chondroitin sulfate-coated polyhydroxyethyl methacrylate membrane prevents adhesion in full-thickness tendon tears of rabbits. *Journal of Hand Surgery-American Volume* **2002,** 27A, (2), 293-306.

49. Pouyani, T.; Harbison, G. S.; Prestwich, G. D., Novel Hydrogels of Hyaluronic-Acid - Synthesis, Surface-Morphology, and Solid-State Nmr. *Journal of the American Chemical Society* **1994,** 116, (17), 7515-7522.
50. Luo, Y.; Kirker, K. R.; Prestwich, G. D., Cross-linked hyaluronic acid hydrogel films: new biomaterials for drug delivery. *Journal of Controlled Release* **2000,** 69, (1), 169-184.
51. Daamen, W. F.; van Moerkerk, H. T. B.; Hafmans, T.; Buttafoco, L.; Poot, A. A.; Veerkamp, J. H.; van Kuppevelt, T. H., Preparation and evaluation of molecularly-defined collagen-elastin-glycosaminoglycan scaffolds for tissue engineering. *Biomaterials* **2003,** 24, (22), 4001-4009.
52. Pieper, J. S.; Hafmans, T.; Veerkamp, J. H.; van Kuppevelt, T. H., Development of tailor-made collagen-glycosaminoglycan matrices: EDC/NHS crosslinking, and ultrastructural aspects. *Biomaterials* **2000,** 21, (6), 581-593.
53. van Susante, J. L. C.; Pieper, J.; Buma, P.; van Kuppevelt, T. H.; van Beuningen, H.; van der Kraan, P. M.; Veerkamp, J. H.; van den Berg, W. B.; Veth, R. P. H., Linkage of chondroitin-sulfate to type I collagen scaffolds stimulates the bioactivity of seeded chondrocytes in vitro. *Biomaterials* **2001,** 22, (17), 2359-2369.
54. Pieper, J. S.; van Wachem, P. B.; van Luyn, M. J. A.; Brouwer, L. A.; Hafmans, T.; Veerkamp, J. H.; van Kuppevelt, T. H., Attachment of glycosaminoglycans to collagenous matrices modulates the tissue response in rats. *Biomaterials* **2000,** 21, (16), 1689-1699.
55. Pieper, J. S.; van der Kraan, P. M.; Hafmans, T.; Kamp, J.; Buma, P.; van Susante, J. L. C.; van den Berg, W. B.; Veerkamp, J. H.; van Kuppevelt, T. H., Crosslinked type II collagen matrices: preparation, characterization, and potential for cartilage engineering. *Biomaterials* **2002,** 23, (15), 3183-3192.
56. Sintov, A.; Dicapua, N.; Rubinstein, A., Cross-Linked Chondroitin Sulfate - Characterization for Drug-Delivery Purposes. *Biomaterials* **1995,** 16, (6), 473-478.
57. Pieper, J. S.; Oosterhof, A.; Dijkstra, P. J.; Veerkamp, J. H.; van Kuppevelt, T. H., Preparation and characterization of porous crosslinked collagenous matrices containing bioavailable chondroitin sulphate. *Biomaterials* **1999,** 20, (9), 847-858.
58. Cai, S. S.; Liu, Y. C.; Shu, X. Z.; Prestwich, G. D., Injectable glycosaminoglycan hydrogels for controlled release of human basic fibroblast growth factor. *Biomaterials* **2005,** 26, (30), 6054-6067.
59. Li, Q.; Wang, D. A.; Elisseeff, J. H., Heterogeneous-phase reaction of glycidyl methacrylate and chondroitin sulfate: Mechanism of ring-opening-transesterification competition. *Macromolecules* **2003,** 36, (7), 2556-2562.
60. Cael, J. J.; Isaac, D. H.; Blackwell, J.; Koenig, J. L.; Atkins, E. D. T.; Sheehan, J. K., Polarized Infrared-Spectra of Crystalline Glycosaminoglycans. *Carbohydrate Research* **1976,** 50, (2), 169-179.
61. Servaty, R.; Schiller, J.; Binder, H.; Arnold, K., Hydration of polymeric components of cartilage - an infrared spectroscopic study on hyaluronic acid and chondroitin sulfate. *International Journal of Biological Macromolecules* **2001,** 28, (2), 121-127.

62. Wang, S. C.; Chen, B. H.; Wang, L. F.; Chen, J. S., Characterization of chondroitin sulfate and its interpenetrating polymer network hydrogels for sustained-drug release. *International Journal of Pharmaceutics* **2007,** 329, (1-2), 103-109.
63. Workman, J. An introduction to near infrared spectroscopy. http://www.spectroscopynow.com/coi/cda/detail.cda?id=1881&type=EducationFeature&chId=2&page=1
64. Benedetti, L.; Cortivo, R.; Berti, T.; Berti, A.; Pea, F.; Mazzo, M.; Moras, M.; Abatangelo, G., Biocompatibility and Biodegradation of Different Hyaluronan Derivatives (Hyaff) Implanted in Rats. *Biomaterials* **1993,** 14, (15), 1154-1160.
65. Pouyani, T.; Kuo, J. W.; Harbison, G. S.; Prestwich, G. D., Solid-State Nmr of N-Acylureas Derived from the Reaction of Hyaluronic-Acid with Isotopically-Labeled Carbodiimides. *Journal of the American Chemical Society* **1992,** 114, (15), 5972-5976.
66. Kuo, J. W.; Swann, D. A.; Prestwich, G. D., Chemical Modification of Hyaluronic-Acid by Carbodiimides. *Bioconjugate Chemistry* **1991,** 2, (4), 232-241.
67. Larsen, N. E.; Leshchiner, E. A.; Parent, E. G.; Balazs, E. A., Hylan and Hylan Derivatives in Drug Delivery. *Abstracts of Papers of the American Chemical Society* **1990,** 200, 77-PMSE.
68. Laurent, T. C.; Hellsing, K.; Gelotte, B., Cross-linked gels of hyaluronic acid *Acta Chem. Scand.* **1964,** 18, 274-275.
69. Haxaire, K.; Marechal, Y.; Milas, M.; Rinaudo, A., Hydration of polysaccharide hyaluronan observed by IR spectrometry. I. Preliminary experiments and band assignments. *Biopolymers* **2003,** 72, (1), 10-20.

Chapter III:
Preparation and Characterization of Hydrogel Films

1 Introduction

The structure and mechanical behaviour of gelatin gels have already been widely studied in the past.[1,2] Gelatin normally dissolves in aqueous solutions at 40°C and above this temperature, the protein exists as flexible single coils, as demonstrated in figure 3-1.[3] On recooling, transparent gels are formed, if the concentration is higher than the critical gelation concentration.[4,5] These gels are formed by physical crosslinks, also called 'junction zones', originated from a partial transition to 'ordered' triple helical collagen-like sequences, separated by peptide residues in the 'disordered' conformation. The main evidence for this phenomenon came from optical rotation measurements.[6,7]

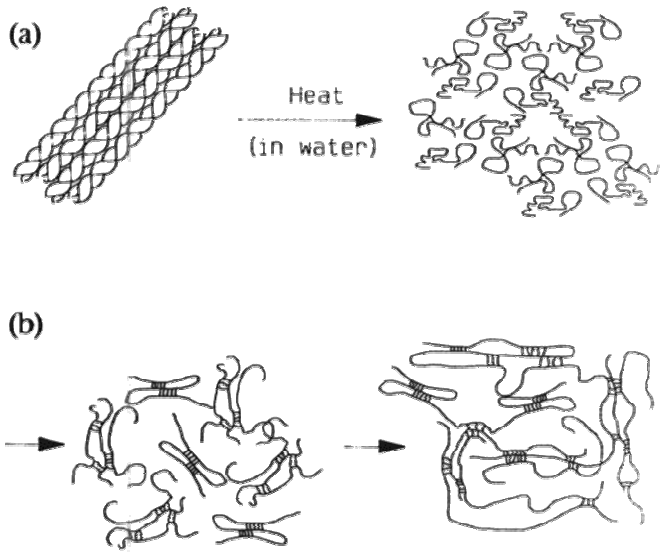

Figure 3-1: Thermo-reversible gelation of aqueous gelatin solutions.

In most biopolymer systems, including DNA and a number of polysaccharides (e.g. agarose), the coil to double helix transition occurs very fast and resembles a true first-order phase transition.[8,9] For gelatin, however, it is known that there is an initial phase (i.e. nucleation), lasting several hours, followed by a much slower process that appears to continue for a very long time (i.e. propagation). The latter phenomenon is called 'frustrated renaturation', since helices never stop growing and the gel state (i.e. solid-like) is never in equilibrium.[3]

Because of its unique gelation properties, gelatin is interesting to use as a hydrogel component.[10] The mechanical properties of gel-MOD hydrogels (type I) and thiolated gelatin hydrogels (type II) depend on the contributions of both the physical crosslinking, as already mentioned before, and the chemical crosslinking, respectively between double bonds (type I) and by disulfide formation (type II).

Above the sol-gel temperature (± 30°C), the gel strength only depends on the chemical network, since physical entanglements are then destroyed.

The contributions of both chemical and physical crosslinking in hydrogels depends strongly on the temperature, the storage time and the reaction conditions.[11,12] In the present chapter, the contributions of both the chemical and the physical crosslinking of gelatin hydrogels will be studied in depth by means of rheology, swelling experiments and texturometry.

1.1 *Rheology*

Rheology is the study of the deformation and flow of matter under the influence of an applied stress. The term was used for the first time by Eugene Bingham in 1920, inspired by Heraclitus's famous expression 'panta rei', which is Greek for 'everything flows'.

In practice, rheology is principly concerned with extending the "classical" principles of elasticity and Newtonian fluid mechanics to materials, whose mechanical behaviour cannot be described using the classical theories. Rheological behavior is particularly observed in materials containing polymer molecules.[13,14]

If a sample is loaded, it will deform. When the load is removed, an ideally viscous body (fluid) will remain deformed (damper model). The viscosity of a Newtonian (ideally viscous) substance does not depend on the load. The mathematical description of the flow curve according to Newton is:

$$\tau = \eta \times \dot{\gamma}$$

with τ = shear stress
η = viscosity
$\dot{\gamma}$ = shear rate

After deformation, an ideally elastic body will, upon removal of the load, fully return to its initial position (spring model). Ideally elastic substances behave according to Hooke's law:

$$\tau = G \times \gamma$$

with τ = shear stress
G = shear modulus
γ = strain

Visco-elastic fluids will reform with a delay and only partially; in visco-elastic bodies the reformation is (nearly) complete, but delayed.[15]

Oscillatory tests are used to examine all kinds of visco-elastic materials such as low-viscosity liquids[16], polymer solutions[17,18], melts[19], pastes[20], gels[21], elastomers[22], and even rigid solids[23]. This mode of testing is also referred to as "dynamic mechanical analysis".[24] The latter can be performed by means of a rheometer, which consists of two basic components, separated by the sample (figure 3-2). Beside the plate/plate measuring system, which was applied in the present work, cone/plate and concentric cylinder measuring systems also exist.
Tests with controlled shear strain are applied on visco-elastic materials in the form of oscillatory sine functions according to:

$$\gamma(t) = \gamma_0 \sin \omega t$$

with γ_0 = amplitude

ω = frequency

The shear stress corresponding to this deformation is a phase-shifted sine function:

$$\tau(t) = \tau_0 \sin(\omega t + \delta)$$

with the phase shift angle δ between the preset and the resulting curve, as illustrated in figure 3-2. The phase shift angle is always in the range from 0° to 90°. For idealelastic behaviour $\delta = 0°$, for idealviscous behaviour $\delta = 90°$ and for visco-elastic behaviour $0° < \delta < 90°$.

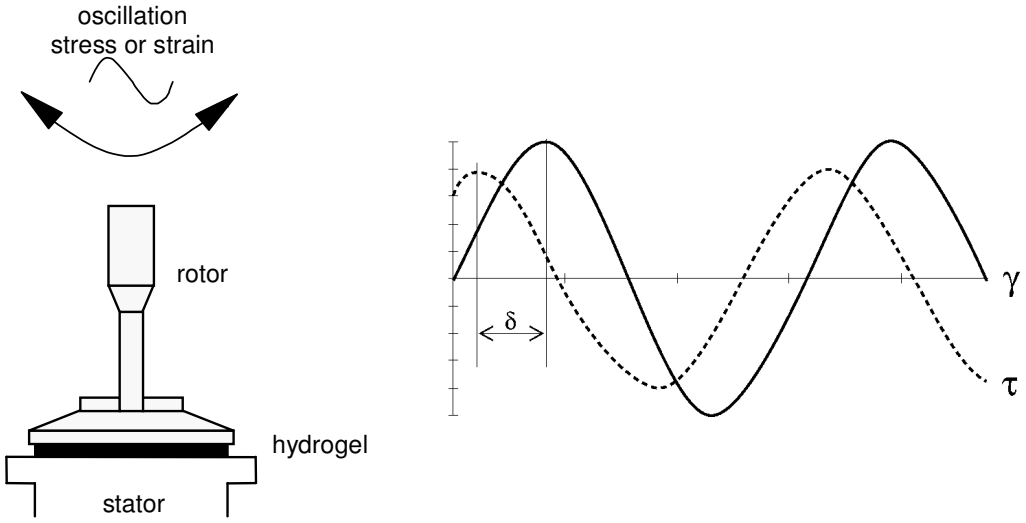

Figure 3-2: Preset shear strain function γ(t), and resulting shear stress function τ(t), applied during a rheological experiment.

Two important parameters exist, enabling the characterization of visco-elastic materials, namely the **storage modulus (G')** and the **loss modulus (G'')**.

The G'-value is a measure of the deformation energy, stored by the sample during the shear process. After the load is removed, this energy is completely available, now acting as the driving force for the reformation process, which partially or completely compensates the previously applied deformation of the structure. Materials which store the whole deformation energy, show completely reversible deformation

behaviour since they occur finally with an unchanged shape after a load cycle. Thus, G' represents the elastic behaviour of a test material:

$$G'(\omega) = \tau_0/\gamma_0 \cos\delta$$

The G''-value is a measure of the deformation energy consumed by the sample during the shear process and therefore afterwards, it is lost. This energy is spent during the process of changing the material's structure, e.g. when the sample is flowing. There exists relative motion between the molecules inducing frictional forces between these components and causing frictional heat. Energy is dissipated during this process. A part of this energy heats up the test material and another part may be lost to the surrounding environment. Energy losing materials are characterized by irreversible deformation behaviour, since their final shape is changed after a load cycle. Thus, G'' represents the viscous behaviour of a test material:

$$G'(\omega) = \tau_0/\gamma_0 \sin\delta$$

The loss factor (or damping factor) gives the ratio between the viscous and the elastic behaviour of a material:

$$\tan\delta = G''/G'$$

1.2 *Texturometry*

In contrast to dynamic oscillation measurements, measuring at small deformations[25], large deformations are also applied in order to have an idea on the mechanical properties of a material.[26] Usually tensile tests are performed[27]. However, these are less suitable for hydrogels since cracks can occur at the fixation points. Consequently, the majority of publications about large-deformation experiments on hydrogels is concerned with compression tests.[28,29]

In the present work, large deformation experiments were performed by means of a texturometer, enabling fast and simple determination of the hydrogel properties.

Texturometry analysis is mainly used in the food industry.[30, 31] However, nowadays it has also proven its use in pharmaceutical industry [32,33] and cosmetics [34,35].

By means of a plunjer or probe (cylindrical, sphere-shaped, etc.), which compresses the sample at a constant rate, a compression force is applied onto the testing material. Hydrogel films (1 mm thick) were positioned on a round opening in the bottom plate and fixed by the upper plate. (figure 3-3)

In the present work, different testing procedures were applied. A 'texture profile analysis test' (TPA-test) was performed in order to examine the 'recovery'-properties of the hydrogels developed after compression. Fatigue and fracture tests give additional information on polymer films.[36]

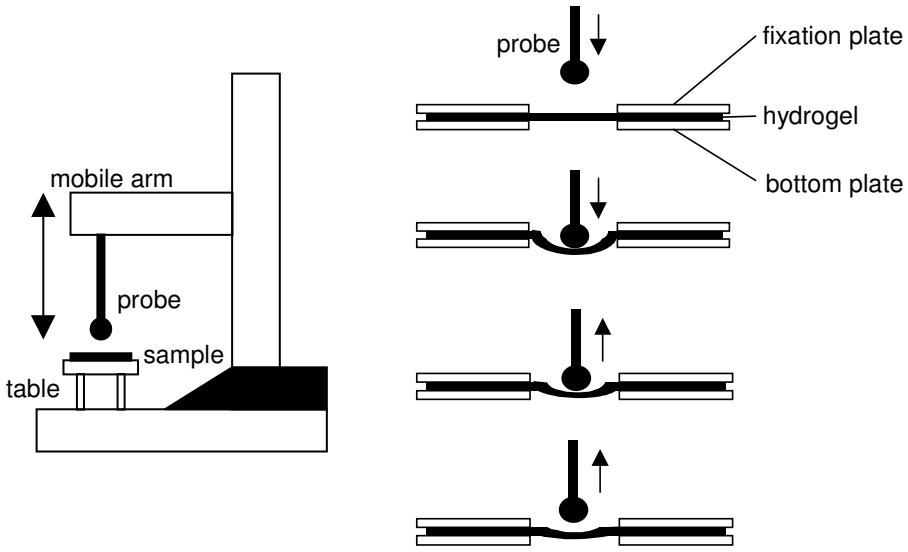

Figure 3-3: Scheme of the texturometer apparatus and the TPA-test procedure.

When performing the TPA-test, the sample is compressed twice by the plunjer, moving with the same speed. The theoretical curve, depicted in figure 3-4, always represents force as a function of time. From the surface areas below the curves and from the measured forces, different parameters can be calculated, as shown in table 3-1.

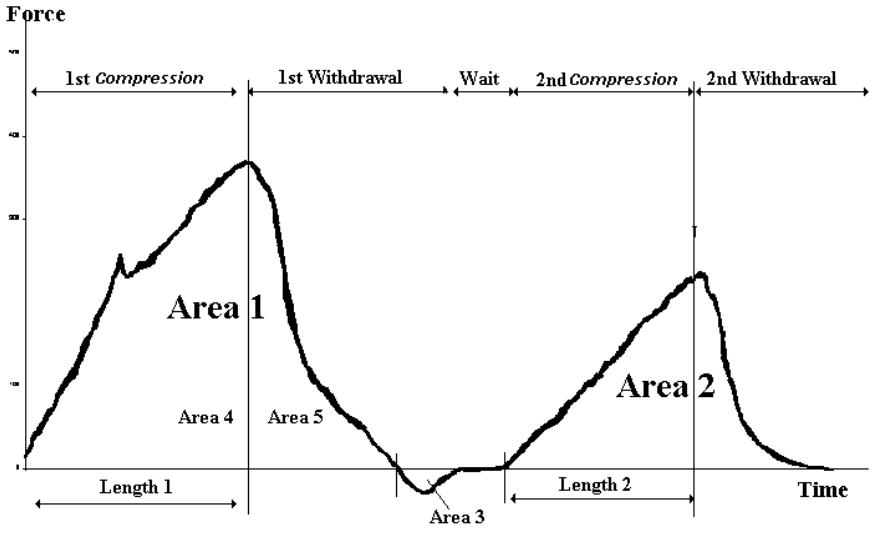

Figure 3-4: Standard TPA-test.

Parameter	Unit	Definition
Hardness	N	The hardness value is the peak force of the first compression of the product.
Fracturability	N	When a product fractures, the fracturability point occurs where the plot has its first significant peak (where the force falls off) during the probe's first compression of the product.
Cohesiveness	-	Cohesiveness is how well the product withstands a second deformation relative to how it behaved under the first deformation. It is measured as the area of work during the second compression divided by the area of work during the first compression. (i.e. Area 2/Area 1)
Springiness	-	Springiness is how well a product physically springs back after it has been deformed during the first compression. Springiness is typically measured by the distance of the detected height of the product after the second compression (i.e. Length 2), divided by the original compression distance (i.e. Length 1). The original definition of springiness used Length 2 only, however, comparison could then only be made among products which were identical in their original shape and height.
Chewiness	N	Chewiness only applies for solid products and is calculated as Gumminess x Springiness.
Gumminess	N	Gumminess only applies for semi-solid products and is Hardness x Cohesiveness.
Resilience	-	Resilience is how well a product "fights to regain its original position". You can think of it as instant springiness, since resilience is measured on the withdrawal of the first penetration, before the waiting period is started. (i.e. Area 5/Area 4)

Table 3-1: Texturometrical parameters that can be obtained from a TPA-experiment.

Fatigue tests are similar to TPA-tests. In contrast with TPA, where only two compression cycles are applied, hydrogel films then undergo a large amount of

cycles, in order to examine a possible change in mechanical properties after repeated loading.[37]

In fracture experiments, only one compression cycle is applied until the hydrogel breaks. Parameters such as fracture force and fracture deformation are obtained after performing these tests. Elastic materials will break fast and suddenly. Plastic materials however will break slowly.[38]

2 Gel-MOD hydrogels

The formation of hydrogels based on gel-MOD occurs in two steps. In a first part, gelatin is derivatised by the reaction with methacrylic anhydride, as already described in the previous chapter (§ 2.1). Next, the water-soluble gel-MOD is crosslinked via radical polymerisation. The crosslinking can be initiated by means of redox-initiators[39,40], heat[41], UV-treatment[42, 43], gamma-irradiation[44] or irradiation with high-energy electron beams[45-47].

The preparation of a chemically crosslinked gel-MOD hydrogel is depicted in figure 3-5.

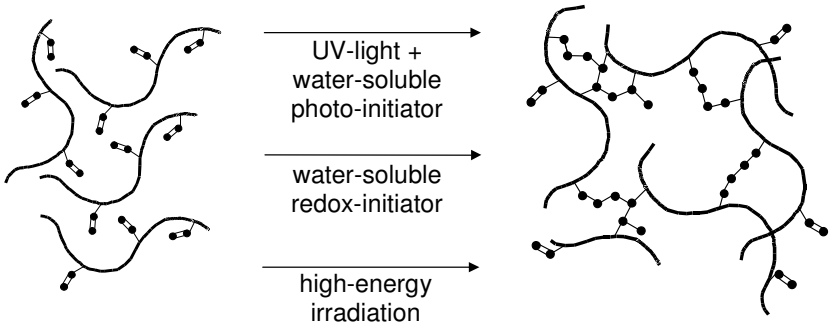

Figure 3-5: Chemical crosslinking of gel-MOD hydrogels.

In the present chapter, UV-irradiation in the presence of a water-soluble photo-initiator will be utilized to perform crosslinking.

Alternative approaches in order to obtain chemically crosslinked hydrogels (e.g. e-beam and redox-initiators) will be discussed thoroughly in chapter 6.

Photochemistry is concerned with chemical reactions induced by optical radiation. The radiation is most often ultraviolet (200-400 nm) or visible (400-800 nm) light, but sometimes also infrared (800-2500 nm) light. Photochemistry can be used to induce any number of chemical processes, from initiating a chemical reaction to degrading a compound. Two basic steps characterize photo-initiation: the absorption of light to excite a compound and the resulting photochemical reaction of the excited compound.[48]

A photoinitiator is an ingredient that absorbs light and is responsible for the production of free radicals in a free radical polymerized system or cations in a cationic photoinitiated system. An excited compound (AB*) can dissociate to fragments (A + B), react with another compound to yield a new compound (ABC), isomerize (BA), luminesce (AB + hv), ionize ($AB^+ + e^-$), or decay without radiation (AB).[49] All these processes are rapid, often occurring on the nanosecond scale.

For most photoinitiated polymerizations, the excited chromophore dissociates into radicals, and these radicals react with monomers to form radical species, which then propagate radical polymerization. There are two general classes of photoinitiators:

- ✓ Type I**:** photoinitiators undergo a unimolecular bond cleavage upon irradiation to yield free radicals
- ✓ Type II: photoinitiators undergo a bimolecular reaction where the excited state of the photoinitiator interacts with a second molecule (a coinitiator) to generate free radicals.

UV photoinitiators of both type I and type II are available. However, visible light photoinitiators belong almost exclusively to the type II class of photoinitiators.

The choice of photoinitiator is determined by the radiation source, the film thickness and the solvent.

In the present work, Irgacure® 2959 was applied since it is a water-soluble photo-initiator, having a rather low toxicity.[50] Photofragmentation occurs through the α-cleavage (Norrish type I) with formation of benzoyl radicals and carbon radicals, as shown in figure 3-6.[51]

The crosslinking degree and rate of the hydrogels developed are influenced by different parameters (e.g. polymer and initiator concentration, irradiation time, degree of substitution). The influence of various factors on the mechanical properties of the

hydrogel films will be studied by means of rheology, texturometry and swelling experiments.

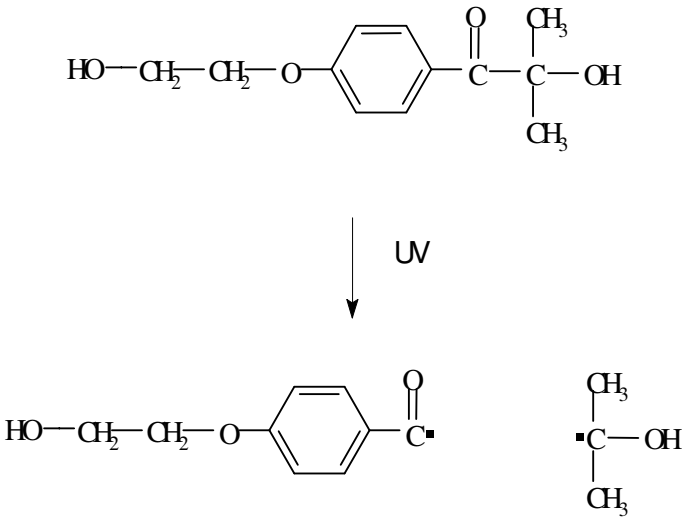

Figure 3-6: Photo-initiator: Irgacure ® 2959 (1-[4-(2-Hydroxyethoxy)-phenyl]-2-hydroxy-2-methyl-1-propane-1-one).

Gel-MOD hydrogel films with varying mechanical properties were already described in the PhD work of Dr. A. Van Den Bulcke.[52] Rheology, texturometry and swelling experiments were performed in order to investigate the influence of the degree of substitution, the gelatin concentration, the initiator concentration, the irradiation time and the storage time on the properties of the gel-MOD hydrogels. From the results, it appeared that the hydrogel properties could be adjusted by varying the modification degree, the initiator concentration, etc. The hydrogels developed were strong, flexible and transparent.[52]

Given that the gel-MOD hydrogels were already characterized fully in the PhD of Dr. A. Van Den Bulcke, the present work will only briefly summarize these results and focus on the *in situ* crosslinking of gel-MOD gels. 10 w/v% gelatin hydrogels (1 mm thick) with varying modification degree were UV-irradiated at 20°C during rheological evaluation, as demonstrated in figure 3-7. From the graph, it appeared that both the crosslinking degree and rate increased with increasing degree of substitution. Moreover, after UV-irradiation, G' and G'' still increased, indicating an after-curing period of 20 minutes during which the gel strength becomes higher.

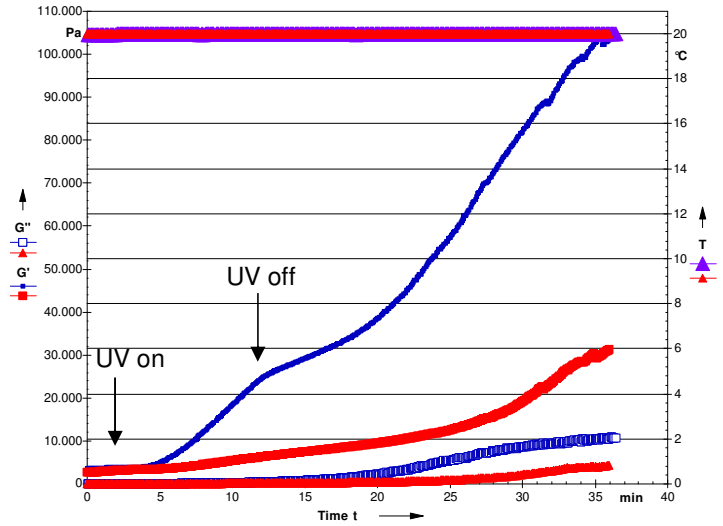

Figure 3-7: Rheological evaluation of gel-MOD with varying modification degree (DS 65% in blue and DS 25% in red) (1 Hz, 0.1% strain, F_N = 0.1 N).

In figure 3-8, the physical crosslinking is monitored rheologically in the first part, followed by UV-induced chemical crosslinking in the second part of the experiment. A characteristic 'cure' curve of log (G', G'') against time was obtained. Typically, this had an initial lag time, and both G'' and G' increased, but with G' increasing faster than G'', so that at a given time there was a 'cross-over' (i.e. gelation point), which is indicated with an arrow (figure 3-8).[53,54] Subsequently G' continued to increase until a plateau value of the modulus was obtained.

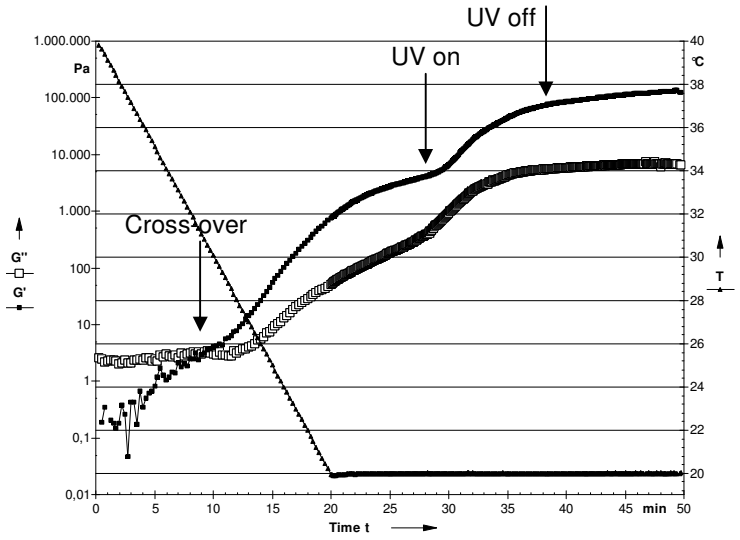

Figure 3-8: Physical crosslinking, followed by UV-irradiation of 10 w/v% gel-MOD hydrogels (DS 65%) (1 Hz, 0.1% strain, F_N = 0.1 N).

In a second part of the experiment, the physically crosslinked hydrogel was UV-irradiated. From figure 3-8, it appears that the contribution of the chemical crosslinking was higher than that of the physical entanglements.

3 Hydrogels based on thiolated gelatin

In the previous paragraph, chemical crosslinking was introduced by UV-irradiation of gel-MOD. The disadvantage of the latter approach is that the process is irreversible, as already mentioned before. Type II hydrogels, however, can be crosslinked reversibly via a two-step synthesis. First, thiol groups are incorporated into the gelatin side chains by the reaction with either N-acetyl homocysteine thiolactone or Traut's reagent, as already described in chapter 2 (§ 3.1). In a second step, disulfide bond formation can occur under mild conditions by air oxidation or with dilute oxidants (H_2O_2, $NaIO_4$, I_2).[55,56] Alternatively, thiol polymers can also be crosslinked using visible light as the initiator in the presence of certain dyes (e.g. eosin, fluorescein, methylene blue) as sensitizers.[57]

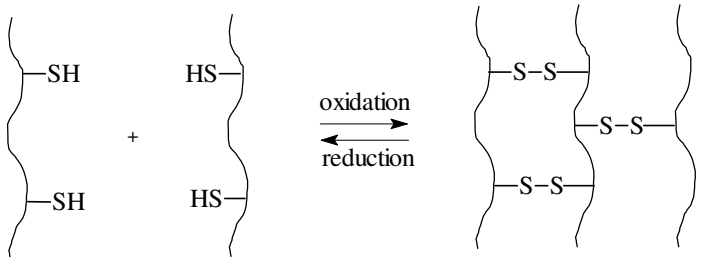

Figure 3-9: Formation of gelatin intermolecular disulfide bonds.

A disulfide bond is formed between free thiol groups under oxidizing conditions (figure 3-9). These covalent bonds are much stronger than hydrogen bonds, Van der Waals interactions and electrostatic interactions. However, they are weaker than the C-C bonds, formed in type I hydrogels (250 kJ/mole versus 350 kJ/mole). Disulfide bonds play an important role in increasing the stability of many native proteins.[58] Disulfide crosslinking are cleavable in a reducing environment (e.g. dithiotreitol).[59]

In the present work, dithiotreitol and hydrogen peroxide were used respectively as reducing and oxidizing agents. The influence of both additives on the physical gelation of gelatin was investigated by rheology. Next, the influence of the modification degree and the storage time on the mechanical properties of the hydrogels developed, was examined by means of rheology, texturometry and swelling experiments.

3.1 *Preparation and characterization of thiolated gelatin films*

The gelatin-disulfide hydrogels were prepared and evaluated as thin films (1 mm thick). This conformation was chosen in order to simplify rheological measurements. Moreover, hydrogel membranes can also be used as coatings in tissue engineering applications.[60,61]

The hydrogel films were prepared by mixing an aqueous solution of thiolated gelatin (at 40°C) with hydrogen peroxide, followed by injection of the mixture between two silanized glass plates, separated by a 1 mm-thick silicone spacer.

Quantitative information on the visco-elastic and rheological properties of the materials can be obtained by measuring the mechanical response of the hydrogels on the applied deformation. In general, the storage modulus G' and the loss modulus G'' are measured.

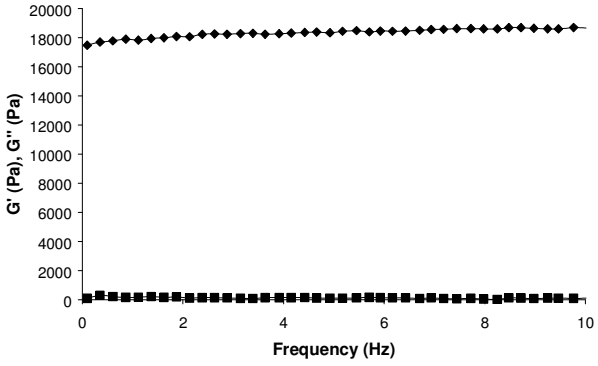

Figure 3-10: Mechanical spectrum of a type II hydrogel recorded at 20°C. The hydrogel (DS 70%, 15 w/v%) was stored at 5°C for 2 weeks (0.1% strain, gap = 900 µm).

In the mechanical spectrum (figure 3-10), G' and G'' are plotted as a function of the frequency. Both moduli display a pronounced plateau value in the frequency region

studied. Moreover, G' is about two orders of magnitude higher than G'', which is indicative for the formation of a well established network.[62]

In a further experiment, the influence of dithiotreitol and hydrogen peroxide on the gelation properties of unmodified gelatin was examined rheologically.

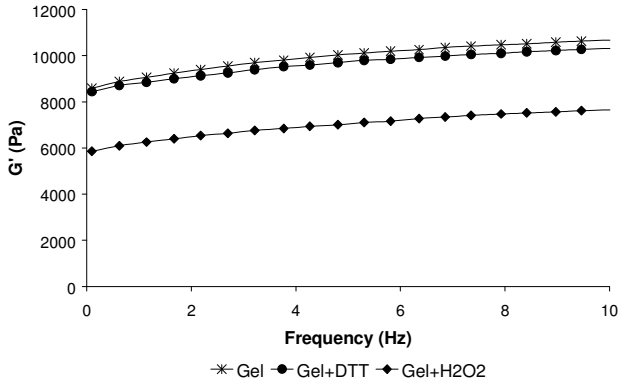

Figure 3-11: Influence of additives (DTT and H_2O_2) on G' of gelatin hydrogels (15 w/v%), stored at 5°C for 2 days (0.4% strain, gap = 900 µm, 21°C).

From the results in figure 3-11, it could be concluded that hydrogen peroxide influences the physical crosslinking of gelatin to some extent. However, this effect can be neglected since during crosslinking the triple-helix formation is disturbed anyhow. That is, the time span during which disulfide bond formation occurs, is a lot shorter than the time needed to enable physical crosslinking, as discussed in the following paragraph (§ 3.2).

3.2 *Influence of the degree of modification of thiolated gelatin on the hydrogel network properties*

The characteristics of type II hydrogels can also be fine tuned by the correct selection of parameters influencing the properties of the hydrogels developed.

An important factor affecting the mechanical strength is the degree of substitution of the thiolated gelatin. The modification degree (DS) was defined as the ratio of amine groups that was modified with sulfhydryls to the total amount of amines, present in gelatin (0.385 mmol/g), before the derivatization.

Thiolated gelatins with various modification degrees were prepared, as described in chapter 2 (§ 3.2.1). Next, hydrogel films composed of these gelatins were evaluated rheologically and compared with a hydrogel based on unmodified gelatin.

From figure 3-12, it appears that the storage modulus increases with increasing degree of substitution. The oxidation of thiol groups by hydrogen peroxide resulted in intermolecular and intramolecular disulfide bond formation. Interestingly, G' of unmodified gelatin is slightly higher than the storage modulus of gelatin with a degree of substitution of 15%. The chemical bonds were introduced by addition of an oxidant to the polymer solution in 'random state'. The oxidant was mixed with gelatin in the sol state. Consequently, no physical gelation could occur before the start of the chemical crosslinking. In literature, it was described that gelatin solutions, kept at room temperature, are rather slow structuring systems. Long induction periods are necessary in order to induce helix formation.[63] The chemical modification of gelatin with sulfhydryl groups will even prolong this induction time. The formation of disulfide bonds will further hinder the physical structuring. Consequently, it can be concluded that the physical contribution mainly originates from the storage at 5°C, after chemical crosslinking.

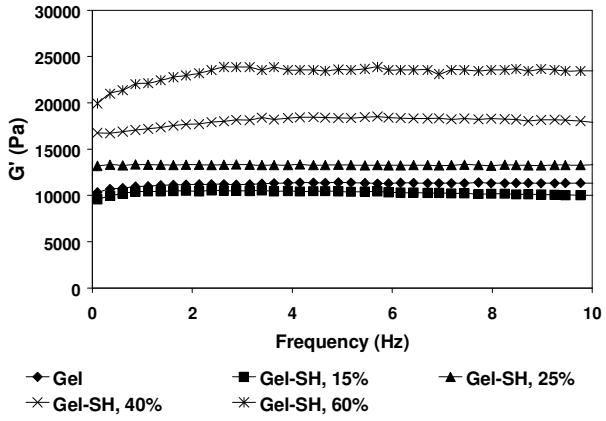

Figure 3-12: Influence of the degree of substitution on G' (0.1% strain, gap = 900 µm, 20°C).

In order to have an idea on the contributions of both physical and chemical crosslinking to the total gel strength, dynamic mechanical analysis was performed on the hydrogels developed, both at room temperature and above the sol-gel transition temperature (at 50°C).

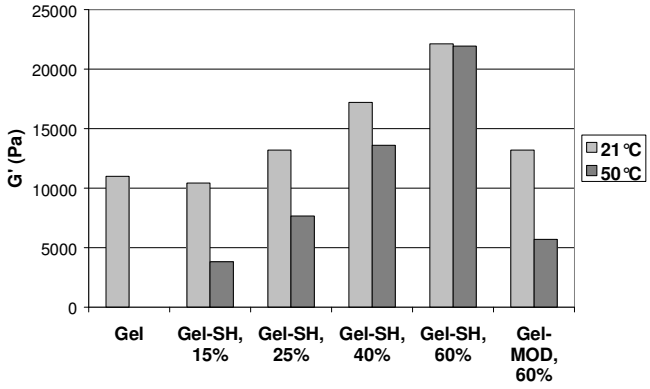

Figure 3-13: Effect of the modification degree on the temperature dependence of G'. Gel-SH hydrogels (15 w/v%) were stored for 3 days at 5°C (0.1% strain, gap = 900 µm).

When measuring at 21°C, the gel strength of the hydrogels developed, is influenced by both the physical and the chemical crosslinking (figure 3-13). However, when measuring at 50°C, thus above the sol-gel transition temperature, there is no contribution of physical entanglements, consequently only the disulfide bonds contribute to G'. From figure 3-13, it can be concluded that the physical contribution decreases with increasing modification degree. In hydrogels composed of highly modified gelatin, more chemical bonds are formed. A network with high density and high G', preserving its network properties above the transition temperature, is obtained. The decrease in storage modulus at elevated temperatures is more pronounced for hydrogels with lower degrees of substitution. The latter decrease can be ascribed to the destruction of the physical entanglements of the polymer chains. The amount of reactive thiol groups has thus a large impact on both the chemical and the physical contributions, although in an opposite way. For all gels (DS 15%, 25%, 40% and 60%), the contribution of the chemical crosslinking was sufficient to ensure strong materials, even at elevated temperatures.

When comparing type I and type II hydrogels, it seems that the physical contribution to the storage modulus of type I hydrogels is higher than that of type II hydrogels. This observation can be clarified as follows. Type I hydrogels are crosslinked chemically by UV-irradiation, after a 24 hours-storage period during which the triple-helix formation can occur. In case of type II hydrogels, an oxidant is added to the polymer solution, so disulfide bond formation occurs already above the sol-gel temperature, before physical entanglements can take place.

In figure 3-14, the impact of the modification on the crosslink phenomenon is presented schematically. When an unmodified gelatin solution undergoes a coil-helix transformation, a strong physical network is formed. Both a large amount of thiol side groups and the immediate disulfide bond formation will hinder the origin of a physical network, thus hydrogels with a limited physical contribution to the mechanical properties will be obtained. The network junctions are of physical origin (e.g. hydrogen bonds) and are thus subject to changes in temperature, pH, ion strength, etc. (i.e. 'non-permanent crosslinks').

In case of a low modification degree, both physical and chemical crosslinking can occur. After heating, the helices will dissolve, while the stable, chemical bonds form an unsolvable network. By the temperature increase, the portion of physically structured gelatins will melt; consequently the molecular weight between the junctions will increase. The latter will result in a higher mobility of the gelatin chains and a decrease of the storage modulus at elevated temperatures. In case of higher modification degrees, the chemical network formation will compete with the possible helix formation. Rheological measurements have confirmed that the presence of many covalent bonds (i.e. high DS) can hinder the subsequent physical structuring at cooling. Consequently, G' of the concerning hydrogels will remain constant when heating above the transition temperature (figure 3-13).

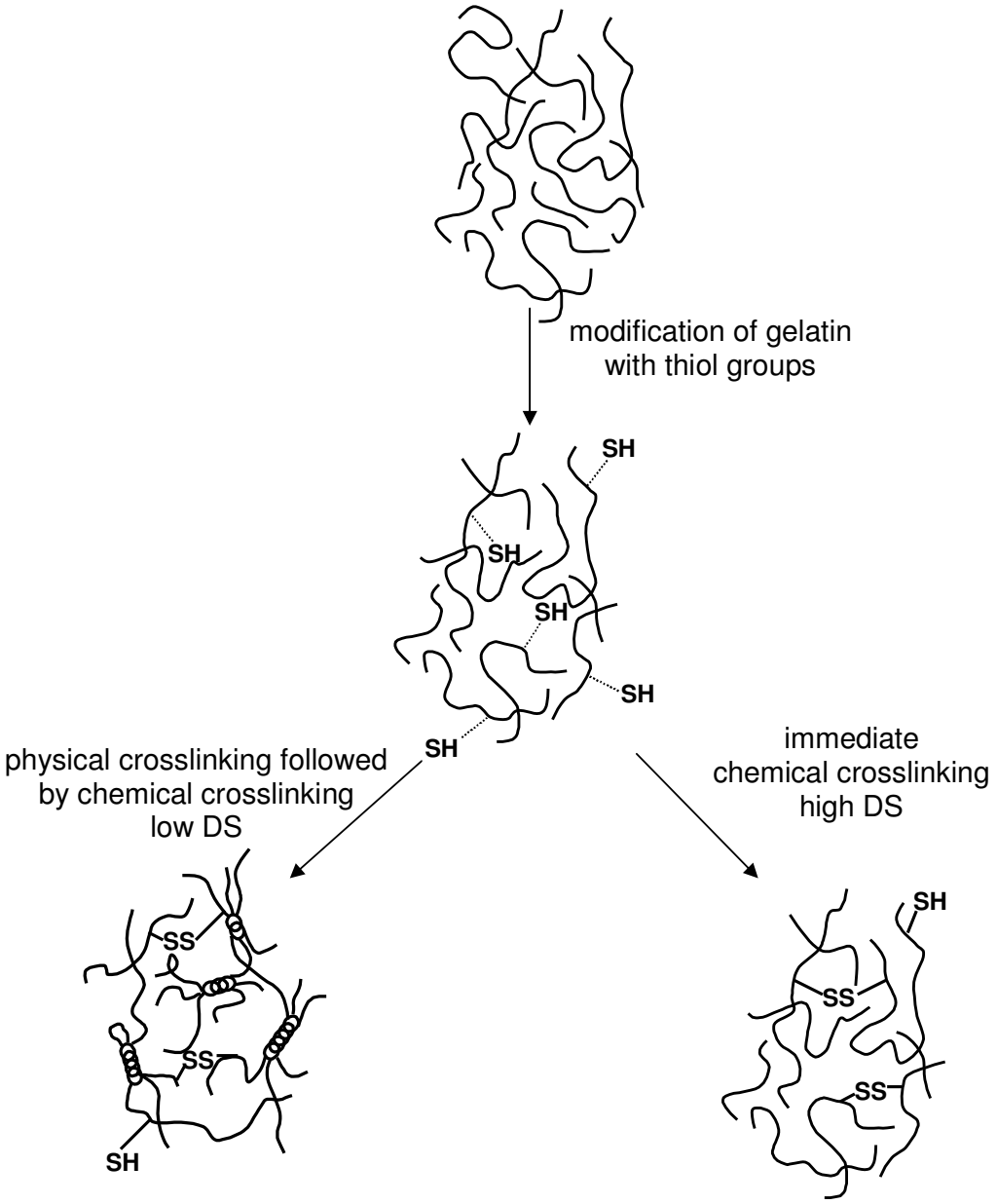

Figure 3-14: Schematic representation of the influence of the synthesis route on the formation of the gelatin network.

The swelling properties of the hydrogels developed, were examined by incubating the gels in double distilled water at 37°C. After predetermined time periods, the swollen polymer films were removed from the medium, dipped with a tissue and weighed.

The results are expressed as swelling percentage or water level and are calculated according to the following formulas:

$$\text{swelling (\%)} = [(W_{ht} - W_{d0}) / W_{d0}] \times 100\%$$
$$\text{water level (\%)} = [(W_{ht} - W_{d0}) / W_{ht}] \times 100\%$$

with W_{d0} = weight of dry gel at initial time
W_{ht} = weight of hydrated gel at time t

Other important parameters when characterizing hydrogel networks are the gel and sol fraction. By means of the dry weight after swelling, gel and sol fractions can be calculated. These can be defined as respectively the percentage of dry polymer, remaining in the hydrogel after swelling and the ratio of polymer dissolving during incubation. In general, a higher gel fraction, thus improved crosslinking, suppresses the swelling capacity. The calculation of the gel and sol fraction occurs by means of the following formulas:

$$\text{gel fraction (\%)} = (W_{de} / W_{d0}) \times 100\%$$
$$\text{sol fraction (\%)} = 100\% - \text{gel fraction}$$

with W_{de} = dry weight after swelling
W_{d0} = dry weight before swelling

For all hydrogels studied, equilibrium swelling was reached after incubation overnight (data not shown). Both the swelling at equilibrium and the gel fraction are represented in figure 3-15. With increasing degree of substitution, the equilibrium swelling decreased drastically. The degree of derivatization thus influences the swelling properties to a large extent.

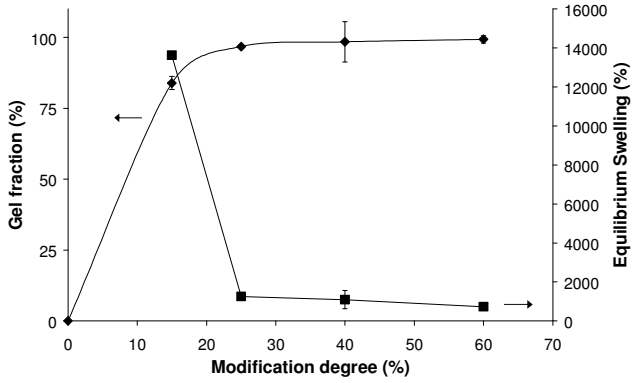

Figure 3-15: Swelling at equilibrium and gel fraction of thiolated gelatin hydrogels with increasing degree of substitution. The thiolated gelatin hydrogels (15 w/v%) were stored for 10 days at 5°C.

Since the hydrogels were stored at 5°C after disulfide bond formation, physical structuring of free gelatin chains could occur. Subsequent incubation at 37°C will cause destruction of the physical network. The changes in mass measured, could thus be ascribed to both water uptake and loss of gelatin fractions.

The insolubility of the type II hydrogels is caused by three-dimensional network formation, via interchain crosslinking. The gelatin fraction, which is not anchored chemically through disulfide bonds, will dissolve at 37°C by the melting of the physical entanglements. The unsolvable weight fraction of the initial hydrogel is the gel fraction. The polymer fraction that leaches out, is called 'sol fraction'.

The gel fraction increases with increasing degree of derivatization (figure 3-15). In order to obtain high gel fractions (i.e. 90%), at least 8 crosslinkable side groups should be present per 1000 amino acids. This corresponds to a degree of substitution of 25%.

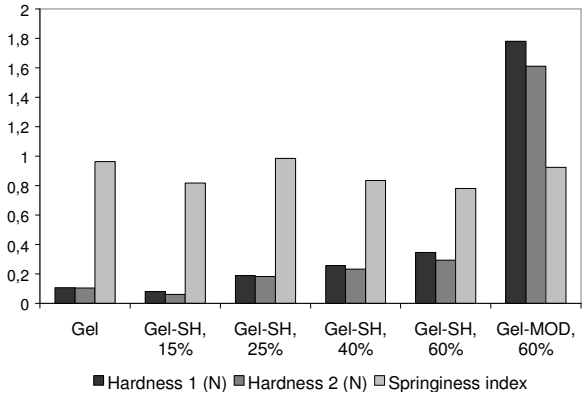

Figure 3-16: Influence of the modification degree on texture parameters. 15 W/v% gelatin hydrogels were stored for 2 days at 5°C. Texturometrical parameters: test rate = 20 mm/min, trigger = 0.1 N, 100% compression, T = 21°C.

In figure 3-16, some texture parameters of the crosslinked gelatin hydrogels, obtained by means of TPA, are plotted. Hardness 1 and hardness 2 represent the maximum force during respectively the first and the second compression. The springiness index is the ratio of the distance over which the sample recovers after the first compression in comparison with the distance at maximum compression. The parameter is an indication of the recovery properties of the material. A value of 1 implies that the material has fully returned to its original position after one compression cycle.

With increasing modification degree of the thiolated gelatin hydrogels, the hardness also increases, while the springiness index barely changes (figure 3-16). The texture changes in the hydrogels are probably caused by the increased amount of chemical bonds in the hydrogel matrix. These measurements demonstrate that the modification degree of thiolated gelatin influences the intermolecular bonds of the hydrogel network directly, as a result of which the force needed for hydrogel deformation changes. The springiness index of about 0.9 implies that the hydrogels almost recover completely. A small decrease of the force, necessary to compress the gel a second time (hardness 2 in comparison with hardness 1), indicates a small weakening of the hydrogel structure, as a result of the compression.

From the results in figure 3-16, it can also be concluded that the hardness of type I hydrogels is higher than that of type II hydrogels. A possible explanation for the latter phenomenon is the disulfide exchange in type II hydrogels, which was already observed before in literature.[64,65] For type I hydrogels, interchain bond formation

occurs randomly and indefinitely, possibly giving rise to more brittle structures compared to type II hydrogels in which disulfide bonds are broken and restored randomly after the crosslink procedure.

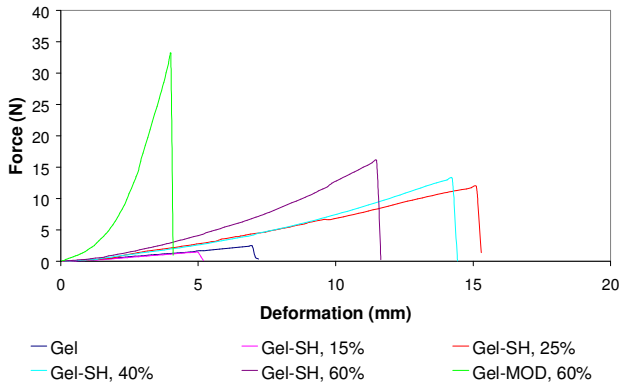

Figure 3-17: Force-deformation curve of type I and type II gelatin hydrogels with increasing degree of substitution (15% to 60% DS) (test rate = 20 mm/min, T = 21°C).

In figure 3-17, the force-deformation curves of type I and type II gelatin hydrogels are plotted. All samples display a typical curvature with a nice fracture. The plots were obtained by a compression-until-fracture setup, in which deformations exceeding 100% are possible. With increasing derivatization degree, an increase in force at fracture was observed. Hydrogels, based on thiolated gelatin with a low degree of substitution display a large deformation at fracture, indicating their flexibility. Gelatin films, possessing a higher modification degree, display lower deformation properties in contrast to their higher fracture force. Consequently, these hydrogels are more brittle. The observation that type II hydrogels were less brittle than type I materials, is again confirmed by the force-fracture setup (figure 3-17). The deformation at fracture of type II hydrogels is about the double of that for the type I hydrogels.

3.3 *Influence of the storage time on the mechanical properties*

In figure 3-18, the storage modulus of gelatin hydrogels, stored at 4°C after chemical crosslinking, is plotted against the storage time. Unmodified gelatin hydrogels were compared with type I and type II hydrogels.

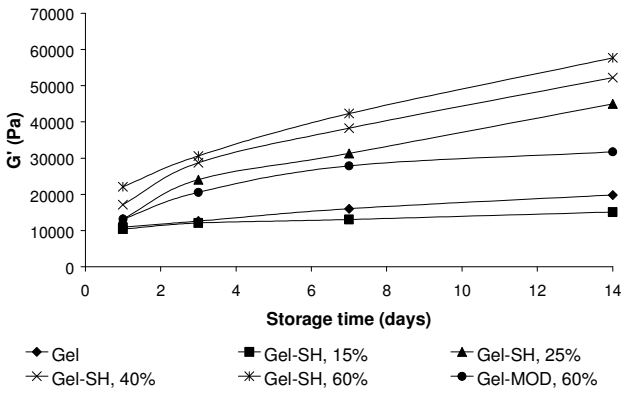

Figure 3-18: The influence of the storage time after chemical crosslinking on the mechanical properties of the hydrogels (15 w/v%) developed (0.1% strain, gap = 900 µm, 20°C).

From the graph, it can be concluded that the physical crosslinking increases with increasing storage time, since G' of unmodified gelatin increases with time. For thiolated gelatin hydrogels, the improvement in mechanical properties is more pronounced compared to type I hydrogels and unmodified gelatins. Consequently, both the chemical and the physical contributions to the gel strength increase. The latter can be ascribed to disulfide exchange, occurring during the storage time, as already mentioned earlier.[65] Conversely, carbon-carbon bonds, formed during UV-irradiation of type I hydrogels cannot be broken and reformed afterwards. As a result, the chemical contribution to the mechanical properties of type I hydrogels cannot increase when stored longer. In that case, only extra triple-helices, formed during the storage time, influence the shift in G' during storage.

4 Hydrogels based on CS-MOD

Proteins of the extracellular matrix (ECM) such as collagens (i.e. starting product of gelatin synthesis) and glycosaminoglycans (GAGs) are among the most abundant in the body. They are widely utilized to fabricate scaffolds, serving as an active analogue of native ECM.[66] Collagen-GAG scaffolds have been used extensively for *in vitro* studies of cell-ECM interactions and as a platform for tissue biosynthesis including *in vivo* studies of tissue or organ regeneration.[67, 68] Favourable characteristics of scaffolds from these natural materials encourage host cells to

repopulate and form new tissues that closely simulate the native organization.[69, 70] Additionally, they enhance biological interactions with cells and speed up tissue regeneration by introducing cell-specific ligands or extracellular signalling molecules, such as peptides and oligosaccharides.[71]

In the present work, collagen was replaced by gelatin, its soluble derivative. It has been successfully used for a range of applications, including burn dressings, cardiovascular surgery and 3D scaffolds for tissue engineering of skin, bone, cartilage, and other tissues.[72] The combination of gelatin and GAGs is often used in skin regeneration since gelatin or GAGs alone cannot heal full thickness wounds.[73] GAGs have also been reported to significantly affect cellular response, morphology and stiffness of the combination scaffolds.[74, 75]

Since type I hydrogels were prepared by UV-irradiation of gel-MOD (§ 2), it was convenient to utilize CS-MOD, enabling co-crosslinking within the gelatin hydrogels. In a first step, the derivatization of chondroitin sulphate occurs by the reaction with methacrylic anhydride, as described in chapter 2 (§ 4.1). Subsequent crosslinking takes place by UV-irradation of the aqueous CS-MOD solution, in the presence of Irgacure® 2959. Alternatively, mixtures of gel-MOD and CS-MOD can also be crosslinked by UV-irradiation in the presence of a water-soluble photoinitiator (figure 3-19).

The crosslinking degree and rate of the hydrogels developed, depend on different factors such as the polymer concentrations, the modification degree of the polymer precursors applied, etc. The effect of different parameters on the resulting hydrogel properties were evaluated by means of rheology.

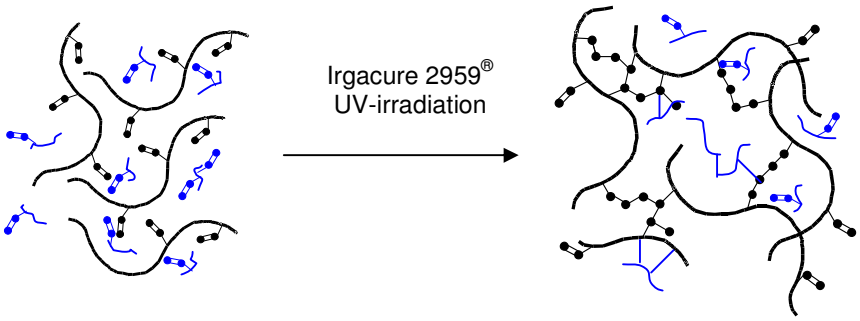

Figure 3-19: Chemical crosslinking of gel-MOD (black) and CS-MOD (blue).

4.1 *Preparation and characterization of CS-based films*

Both the combination hydrogels and the hydrogels composed of only CS-MOD were prepared and evaluated as thin films, similar to the previously studied type I and type II hydrogels. The hydrogel films were prepared by mixing an aqueous solution of the hydrogel precursors (at 40°C) with the photoinitiator, followed by injection between two silanized glass plates, separated by a 1 mm silicone spacer. Chemical crosslinking occurred via UV-irradiation (279 nm). First, the linear visco-elastic region of the hydrogels developed was determined, by means of an amplitudescan (i.e. rheology) (data not shown). Next, mechanical spectra were recorded, from which it could be concluded that well-structured networks were obtained by the applied procedure (data not shown).

4.2 *Influence of the modification degree on the mechanical properties*

CS-MOD hydrogels with varying modification degrees were crosslinked *in situ* during rheological evaluation. In contrast to gelatin-based hydrogels, where the total hydrogel network strength is the sum of both the physical and the chemical crosslinking, the strength of chondroitin sulphate hydrogels only depends on the chemical contribution, since CS has no gelling properties. However, by derivatization and subsequent irradiation, hydrogels with storage moduli up to 20,000 could be obtained (figure 3-20).

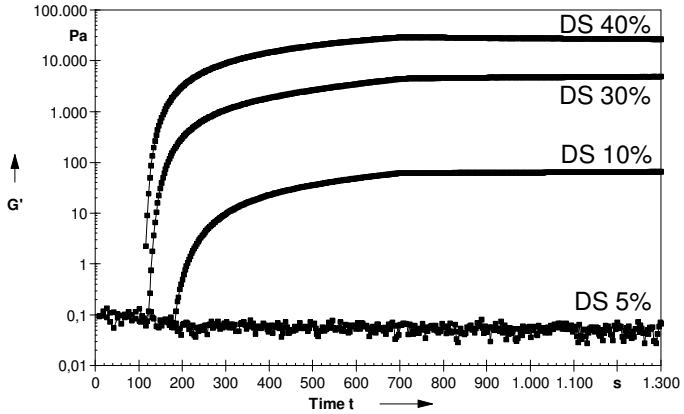

Figure 3-20: Influence of the modification degree of CS-MOD on the mechanical properties of the hydrogels developed (0.5% strain, 1 Hz, F_N = 0.01 N, T = 21°C).

The mechanical strength of the combination hydrogels (gelatin and chondroitin sulphate) was also studied using rheology. In this case, the total hydrogel network strength was the sum of the following contributions:

- ✓ The physical gelation of gelatin as a consequence of the presence of triple helices,
- ✓ The chemical network strength caused by gelatin, modified with methacrylamide side groups,
- ✓ The chemical network strength due to CS-MOD.

The last two factors can also be described as the total chemical network strength, which is thermostable, since no distinction can be made between double bonds in protein or glycosaminoglycan side chains during the crosslinking process.
A large variety of gelatin and chondroitin sulphate derivatives with different modification degrees can be synthesized, enabling the production of a broad selection of hydrogel materials with varying mechanical properties. An overview of the polymer films developed and their resulting storage moduli are presented in table 3-2.

When comparing the results, it can be concluded that:
With constant gelatin concentrations, having identical modification degrees, an increase in derivatization of the chondroitin sulphate component (DS 5% versus 40%) results in a high increase of the storage modulus (G' x 2).
All hydrogels developed were crosslinked very efficiently. The moduli remained the same at elevated temperatures (40°C) (data not shown), implying that the physical contribution to the hydrogel network strength was reduced to a minimum. Dr. A. Van Den Bulcke already showed in her PhD work that the presence of covalent bonds hinders the physical structuring of gelatin. G' of 15 w/v% gelatin hydrogels (DS 40%) already remained constant upon heating the hydrogels to temperatures higher than the sol-gel transition temperature. [52]

Composition		G' (20°C) Pa
Gel-MOD	**CS-MOD**	
10 w/v%, DS 65%	0.5 w/v%, DS 40%	17540
10 w/v%, DS 65%	2 w/v%, DS 40%	42275
10 w/v%, DS 65%	5 w/v%, DS 40%	98141
10 w/v%, DS 65%	0.5 w/v%, DS 5%	9737
10 w/v%, DS 65%	2 w/v%, DS 5%	15844
10 w/v%, DS 65%	5 w/v%, DS 5%	44599
7 w/v%, DS 65%	5 w/v%, DS 40%	89420
10 w/v%, DS 65%	5 w/v%, DS 40%	101463
15 w/v%, DS 65%	5 w/v%, DS 40%	190018
7 w/v%, DS 65%	5 w/v%, DS 5%	27883
10 w/v%, DS 65%	5 w/v%, DS 5%	39370
15 w/v%, DS 65%	5 w/v%, DS 5%	61666

Table 3-2: Composition of the gelatin-chondroitin sulphate hydrogels and their mechanical strength, obtained by means of rheology (0.5% strain, 1 Hz, F_N = 0.01 N, T = 21°C).

4.3 *Influence of the polymer concentration on the mechanical properties*

In figure 3-21, the *in situ* crosslinking of CS-MOD hydrogels, composed of varying polymer concentrations is monitored using rheology. From the results, it appeared that both the crosslinking degree and rate increased with increasing concentration. However, the increase in mechanical strength was higher than expected, based on the increase in CS concentration, in comparison with type I hydrogels. The latter phenomenon was also observed for the combination hydrogels composed of gelatin and chondroitin sulphate (table 3-2).

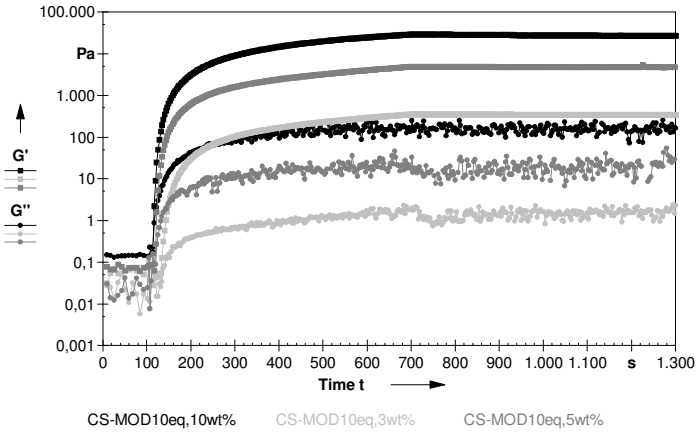

Figure 3-21: Influence of the glycosaminoglycan concentration on the storage modulus (0.5% strain, 1 Hz, F_N = 0.01 N, T = 21°C).

The higher the polymer concentration, the more pronounced the influence of the modification on the rheological properties becomes.

5 Influence of cryogenic treatment

Cryotropic gelation is a specific type of gelation, taking place upon cryogenic treatment of gel-forming systems. A requirement for the processes resulting in the formation of cryogels, is crystallisation of the bulk of the low-molecular-weight liquid present in the initial system.[76] Due to the crystallisation of the pure solvent, the total volume of the non-frozen liquid microphase (NFLMP) is lower than the initial reaction volume. Consequently, the concentration of polymer or monomer in the NFLMP is higher than the initial concentration. The polymer gel phase can be formed during one of the stages of cryogenic treatment: during freezing of the initial system, during storage of the samples in the frozen state or during thawing of the frozen specimens.[76-79]

Recently, the structuring of different polymers by cryogenic treatment has attracted a lot of attention. This is illustrated below with some examples. For a thiol-containing poly(acryl amide) derivative, the conditions were optimized in order to obtain an insoluble gel after freezing-thawing. The gel retained the shape of the cryo-mould. A solution of this polymer kept at room temperature remained liquid.[80] The reaction rate and yield to transform macromolecular thiols into the corresponding disulphides were

increased by freeze-thawing of aqueous solutions of thiol-containing polymers in the presence of oxidants.[81]

The processes of cryo-induced association and aggregation of β-glucans resulted in the formation of soft or hard matter depending on the amount of applied freeze-thaw cycles.[82] Multiple freezing cycles also influenced the structure of poly(vinyl alcohol) (PVA) hydrogels in such a way that secondary crystallites were superimposed on primary crystallites which were formed after one temperature cycle. This resulted in materials with improved mechanical properties.[83]

Cryogels have a broad application field.[84] Macroporous PVA cryogels were proposed as cell immobilizing carriers via cell entrapment techniques.[85-88] Agarose cryogel sponges were evaluated as scaffolds for culturing both isolated pancreatic islets and insulinoma cells.[85] Blends of poly(vinyl alcohol) with different biological macromolecules, such as hyaluronic acid, dextran and gelatin were used to produce bioartificial hydrogels functioning as potential tissue engineering scaffolds.[89] Macroporous gels, based on agarose, poly(acrylamide) or polymethacrylates were patented as separation media for application within the field of chromatography.[90, 91] Poly(vinyl alcohol) cryogels were proposed as temperature sensors, making them applicable for monitoring the temperature distribution induced by a heat source used for hyperthermic therapy.[92]

In the present work, we applied the principle of cryogelation on gelatin. Some preliminary evidence for such behaviour was described earlier.[93] However, the present study aims an in depth rheological investigation of the influence of freeze-thaw cycles, by evaluating possible effects of the number of cryogenic cycles, the cooling rate and the thawing rate on the mechanical properties of the resulting cryogels.

A profound understanding of the cryogenic parameters affecting the final material properties is of great importance, since in a subsequent part of the present work, a cryogenic treatment will be applied in order to develop porous scaffolds, suitable for tissue engineering purposes.

To distinguish between physical and chemical cross-linking phenomena, the cryogelation of gelatin and gel-MOD were also compared.

5.1 *Experimental procedure*

Using a novel cryo-setup, developed in our laboratory, the temperature of freezing and the cooling rate were programmed automatically (figure 3-22).

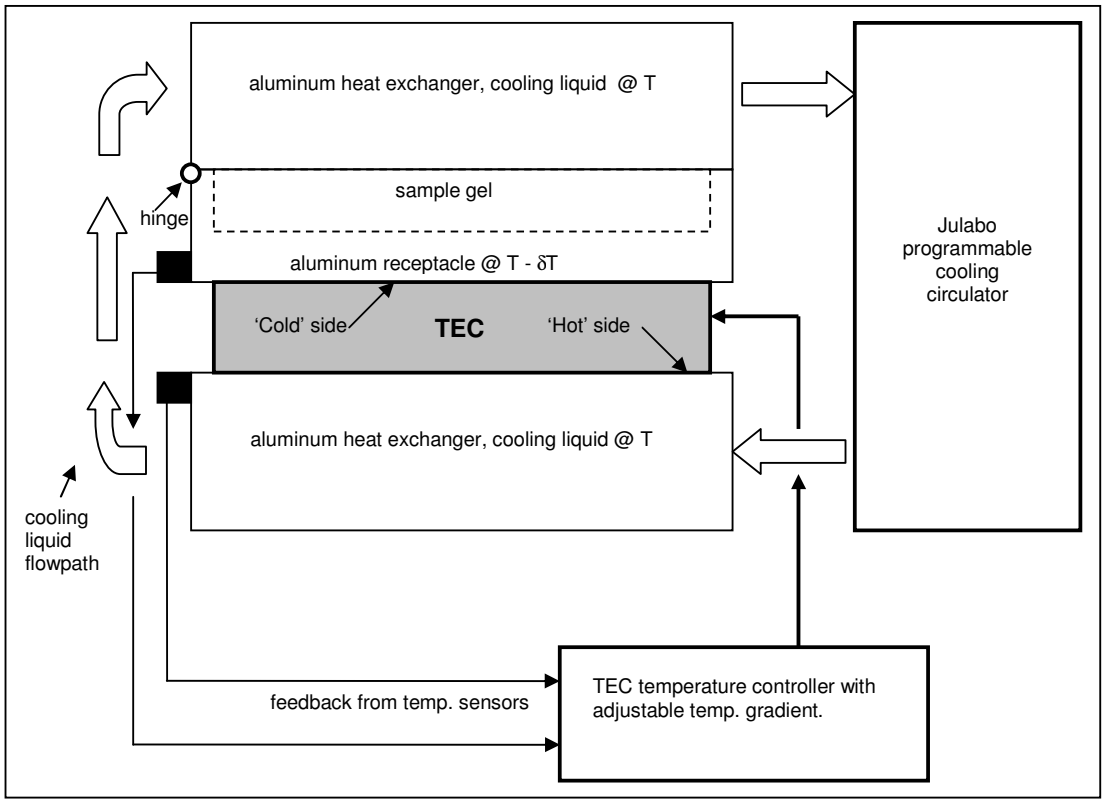

Figure 3-22: Schematic overview of the programmable cryo-unit.

Under the bottom of the mold, a Peltier element (also known as thermo electric cooler, TEC) was positioned. Thermoelectric modules are solid-state heat pumps that operate on the Peltier effect. A thermoelectric module consists of an array of p- and n-type semiconductor elements, heavily doped with electrical carriers. The array of elements is electrically connected in series and thermally connected in parallel. This array is then attached to two ceramic substrates, one on each side of the elements (figure 3-23). Heat transfer occurs as electrons flow through one pair of n- and p-type elements (often referred to as a "couple") within the thermoelectric module as follows: Electrons can travel freely in the copper conductors but not so freely in the semiconductor. As the electrons leave the copper and enter the hot-side of the p-type, they must fill a "hole" in order to move through the p-type. When the electrons fill a hole, they drop down to a lower energy level and release heat in the process.

Essentially the holes in the p-type are moving from the cold side to the hot side. Then, as the electrons move from the p-type into the copper conductor on the cold side, the electrons are bumped back to a higher energy level and absorb heat in the process. Next, the electrons move freely through the copper until they reach the cold side of the n-type semiconductor. When the electrons move into the n-type, they must bump up an energy level in order to move through the semiconductor. Heat is absorbed when this occurs. Finally, when the electrons leave the hot-side of the n-type, they can move freely in the copper. They drop down to a lower energy level and release heat in the process.

In summary, heat is always absorbed at the cold side of the n- and p- type elements. The electrical charge carriers (holes in the p-type and electrons in the n-type) always travel from the cold side to the hot side, and heat is always released at the hot side of thermoelectric element. The heat pumping capacity of a module is proportional to the current and is dependent on the element geometry, number of couples, and material properties.

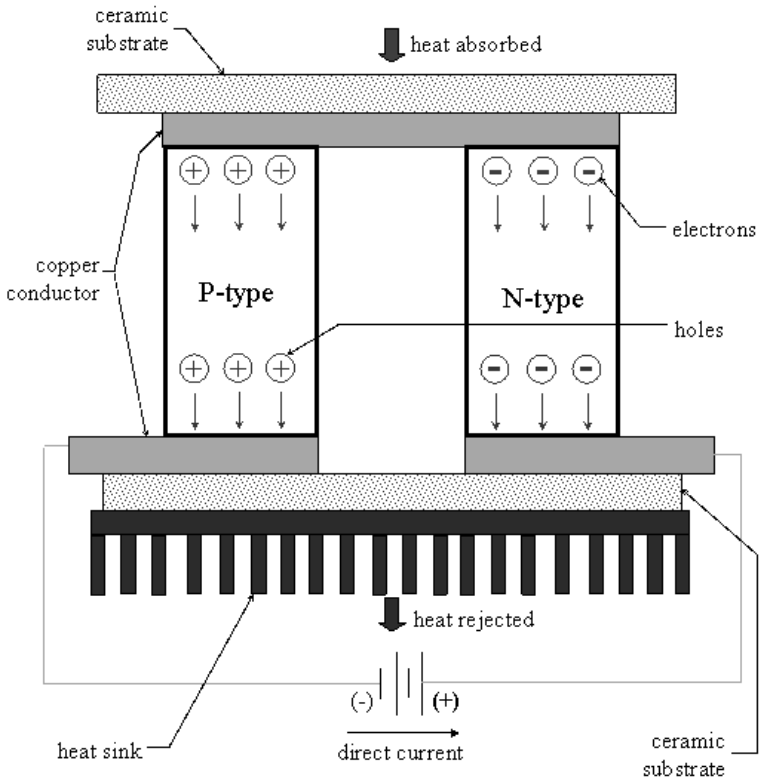

Figure 3-23: Working principle of thermo-electric coolers (i.e. Peltier elements).

The Peltier element enables a temperature gradient of maximum 30°C to be established between the top and the bottom of the mould. For the samples obtained by applying a temperature gradient, the temperature at the top of the mould was the highest. The temperature gradient was only applied to create porous scaffolds with predetermined pore morphologies, which will be discussed in depth in chapter 4.

5.2 *Cryogenic treatment of gelatin*

5.2.1 Effect of the gelatin concentration

In a first part of the work, the influence of the gelatin concentration on the mechanical properties of gelatin hydrogels and cryogels was compared. Since knowledge of the linear visco-elastic range of a material is required prior to rheological measurements, we first performed an amplitude scan of the different gels. The results are summarised in figure 3-24.

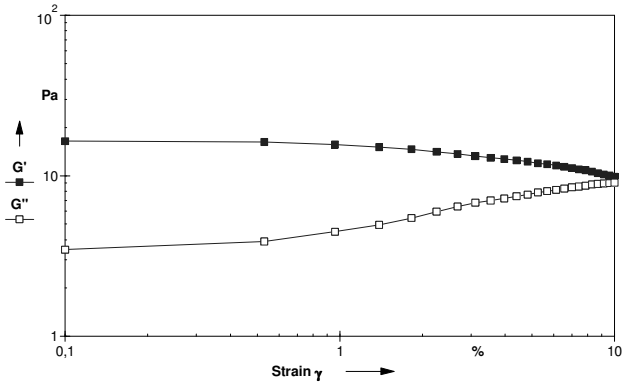

Figure 3-24: Determination of the linear visco-elastic range of an unfrozen 0.5w/v% gelatin solution (1 Hz, 5°C, gap 0.5 mm).

A strain of 0.5% was selected for all further measurements, since this is the highest strain, still part of the linear visco-elastic range. Next, the mechanical spectra of the gels were recorded. These tests showed a limited frequency-dependence of the storage modulus (figure 3-25).

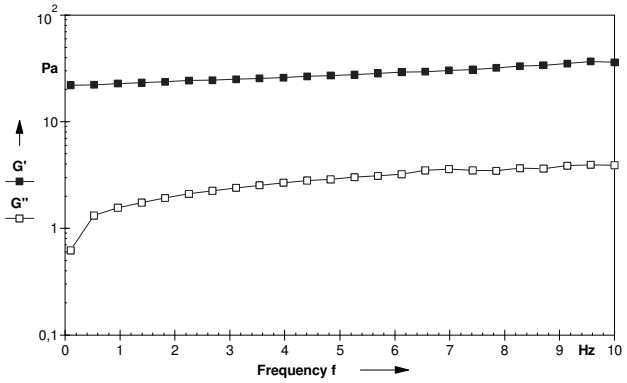

Figure 3-25: Mechanical spectrum of an unfrozen 1w/v% gelatin solution (0.5% strain, 5°C, gap 0.5 mm).

The influence of the gelatin concentration on the cryogenic treatment was studied by applying one freeze-thaw cycle on gelatin samples with concentrations varying from 0.2 to 2 w/v %. These cryogels were compared with unfrozen hydrogels with the same concentration and storage time. Figure 3-26 shows the storage moduli corresponding to the different gelatin concentrations. From the results, it can be concluded that the storage moduli (G') of the cryogels (after a single freezing cycle) were higher than G' of the non-frozen hydrogels, irrespective of the applied gelatin concentration (0.2 - 2 w/v %).

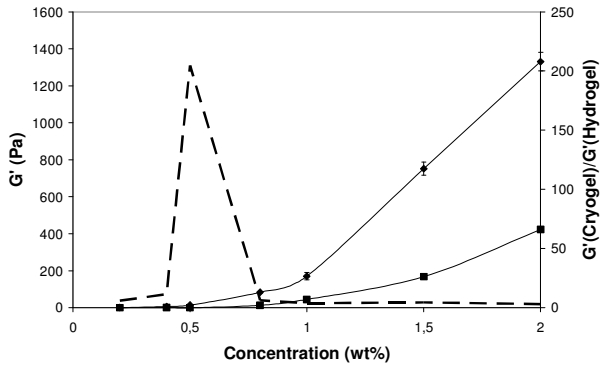

Figure 3-26: Influence of gelatin concentration (w/v%) on G' (0.5% strain, 0.85 Hz, 5°C, gap 0.5 mm) for unfrozen gelatin solutions (■) and for gelatin cryogels formed by a single cycle of freezing to -30°C (◆) (*$P < 0.05$).

Furthermore, the ratio of the storage moduli of the cryogels and the hydrogels revealed a maximum at a gelatin concentration of 0.5 w/v %. This corresponds with a cryogel in the "gel" state, as indicated in figure 3-27, and a "hydrogel" in the "sol" state. The storage and loss moduli of a 0.5 w/v% hydrogel are very low (i.e.

respectively 0.05 and 0.2 Pa), while G' of the cryogel is three times higher than G'' (see figure 3-27). This indicates that a cryogenic treatment leads to gel formation at gelatin concentrations that are below the gelation concentration. It should be noted that the observed decrease in gelation concentration is only apparent, since the polymer chains are accumulated in the gelation region (non-frozen liquid micro-phase), resulting in a local increase of the gelatin concentration. This effect has been observed for any type of cryotropic gelation.[76] The structuring of gelatin upon cryogenic treatment is very similar to the freeze-thaw behaviour of cereal β-glucans and xanthan.[62, 82] The gelatin gels, obtained after the cryogenic treatment, also belong to the category of physically crosslinked gels whose three-dimensional structure is mainly stabilized by multiple hydrogen bonds and hydrophobic interactions in the junction zones of the polymeric network.[82]

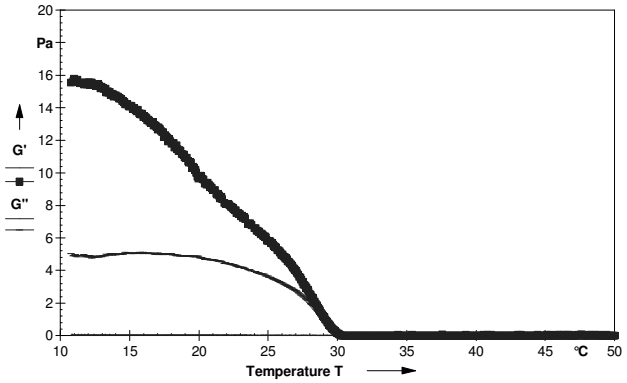

Figure 3-27: Temperature scan (0.5% strain, 0.85 Hz, F_N 0 N) of a 0.5 w/v% gelatin cryogel after applying one freeze-thaw cycle.

5.2.2 Effect of the number of cryogenic cycles

In addition to the gelatin concentration, we also investigated the effect of the number of cryogenic cycles applied, on the mechanical properties of the obtained cryogels. For these measurements, 0.5 w/v % and 2 w/v % gelatin hydrogels were selected. In figure 3-28, the storage moduli are plotted as a function of the gelatin concentration and the number of freeze-thaw cycles. From the results, it can be concluded that the mechanical properties of cryogels can be improved by increasing the number of cryogenic cycles. This trend was observed for both gelatin concentrations studied. The latter can be explained by the formation of additional cross-links during repeated freezing/thawing cycles. The physical gelation of gelatin is a dynamic process in

which bonds are broken and formed continuously. With an increasing incubation time, a more stable conformation is formed. However, due to physical limitations, equilibrium is never reached. The latter phenomenon is called "frustrated renaturation".[3, 94]

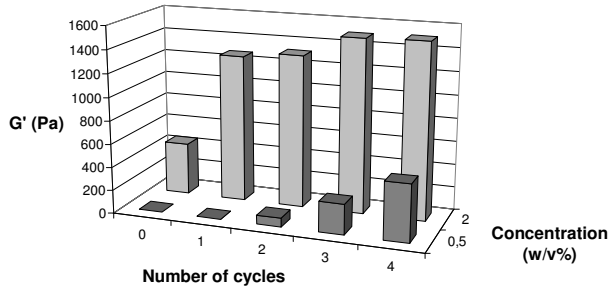

**Figure 3-28: Effect of the number of freeze-thaw cycles on G'
(0.5% strain, 0.85 Hz, 5°C, gap 0.5 mm) for two gelatin concentrations (0.5 and 2 w/v%).**

With the parameters applied in the present work, a kinetic competition exists between the self-gelling process at the sol-gel temperature (± 30°C) and the freezing process below 0°C. There are thus two possible explanations for the improved mechanical properties of cryo-treated gelatin gels. A first possibility is that the freezing rate is faster than the rate of physical gelation. This implies that cryotropic gelation could occur on gelatin in the sol-state. A second possibility is that physical gelation takes place faster than cryotropic gelation. Sufficient chain mobility apparently remains within the hydrogel in order to enable further chain entanglement resulting in a gel with improved mechanical properties. Kinetics of the freezing and the self-gelling process could also be comparable, however distinguishing both phenomena is very difficult, if not impossible. A progressive increase in mechanical properties after multiple freezing/thawing cycles has been reported for xanthan[62] and poly(vinyl alcohol) cryogels.[76] This was ascribed to the formation of microcrystalline zones acting as junction knots in the supramolecular polymer network. The dimensions of the micro crystallites formed, were influenced by the number of applied freezing/thawing cycles.[76, 95]

The observed variations in mechanical properties could potentially affect the degradation behaviour of the scaffolds developed. It can be anticipated that increased mechanical properties, related to a more efficient physical crosslinking (i.e.

triple helix formation), would adversely affect the degradation rate. This is of relevance in the field of tissue engineering, since, ideally, the degradation time of the scaffolds should match the time required for new tissue formation.

5.2.3 Influence of the cooling rate during the freezing step

Experiments using PVA based cryogels have indicated that over a wide range of freezing rates (0.1°C/min to 17°C/min), the effect of the freezing rate on the physical characteristics of the gels was relatively low.[86] However, for blends of amylopectin and amylose, the effect of the freezing rate seemed to have a more pronounced influence on the material properties.[78] In that study, hydrogel samples were stored at different incubation temperatures for similar incubation times and thawed subsequently at the same rate. The cryogels developed, could be distinguished by their appearance and their swelling properties. However, the observed differences were attributed to the storage in the frozen state, despite the fact that a different cooling rate was applied during the treatment.

For gelatin, we anticipated that the freezing rate would influence the mechanical properties since gelation occurs via triple helix formation. These helices act as junction zones within the network.[94] A faster cooling process could hinder the triple helix formation, and thus the degree of physical gelation.

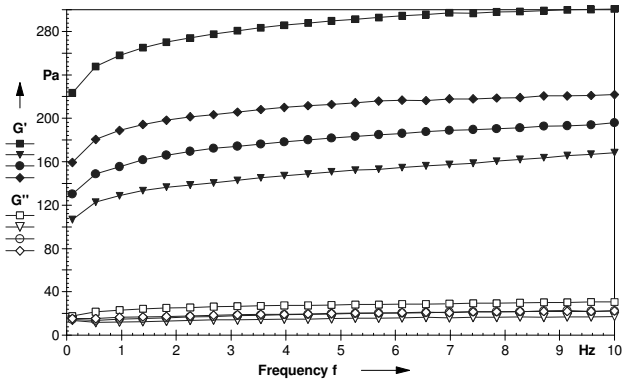

Figure 3-29: Mechanical spectra (0.5% strain, 5°C, gap 0.5 mm) showing the influence of the cooling rate on G' (filled symbols) and G'' (open symbols) of a 1 w/v% gelatin solution. The applied cooling rates were 0.1°C/min (■), 0.3°C/min (◆), 0.5°C/min (●) and 1°C/min (▼).

From the results (figure 3-29), it can be concluded that for 1 w/v % hydrogels, the storage modulus decreased with an increasing cooling rate. A higher freezing rate does indeed disturb the formation of chain entanglements and thus the physical gelation. A similar trend was observed for 10 w/v % hydrogels indicating that within the concentration range investigated, the gelatin concentration does not affect the kinetic effects observed at low concentrations (data not shown).

5.2.4 Effect of the thawing rate

The above results clearly indicate that the conditions applied for the development of cryogels, strongly affect the final material mechanical properties. For the effect of the thawing rate, it has been shown that the influence depends on the type of cross-links within the hydrogel network.[76] For cryogels cross-linked by covalent or ionic bonds, the conditions of thawing of specimens usually have little influence on the material properties. However, for cryogels in which hydrogen bond formation is the predominant cross-linking mechanism, the resulting gels often are sensitive to the thawing conditions applied.[76] In our work, we have varied the thawing rate from 0.06 to 1°C/min. The results of the mechanical studies (figure 3-30), indicated a decrease in G' with an increasing thawing rate.

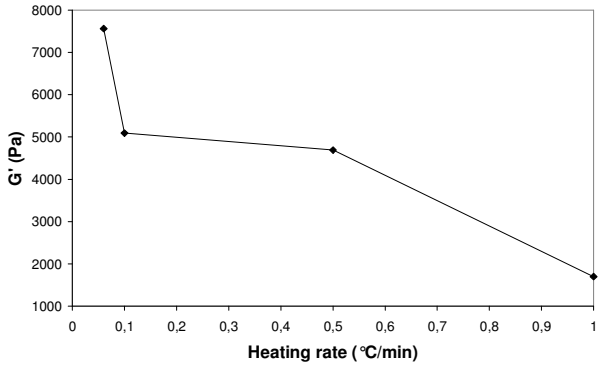

Figure 3-30: Effect of the thawing rate on the storage modulus (G') of 10 w/v% hydrogels (0.5% strain, 5°C, gap 0.5 mm).

This trend, observed earlier for PVA, is typical for thermally reversible cryogels in which hydrogen bonding is the predominant type of intermolecular contacts, stabilising the polymer network junction knots.[76, 77, 86]

5.3 *Cryogenic treatment of gel-MOD*

From the above results, it can be concluded that the cryogenic treatment enhanced the triple helix formation of gelatin chains. In addition to this effect, we also anticipated an influence on a subsequent chemical crosslinking step. The latter is affected by the separation between the different methacrylamide side groups as well as their mobility. In figure 3-31, storage moduli before and after UV-treatment, for a 10 w/v% non-frozen gelatin hydrogel were compared with those from a cryogel, developed by applying one freeze-thaw cycle.

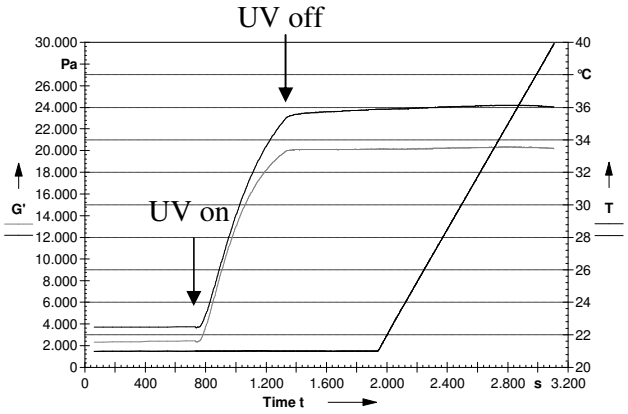

Figure 3-31: Influence of UV-irradiation and temperature increase on G' of 10 w/v% unfrozen gel-MOD hydrogels (grey) and cryogels formed by one freeze-thaw cycle (black) (0.5% strain, 1 Hz, gap 1 mm, $F_N = 0.2$ N).

In accordance with non-modified gels, G' of the cryogel before UV-irradiation was higher than that of the hydrogel. However, the increase in storage modulus during the chemical crosslinking was also higher for the cryogel compared to the non-frozen hydrogel. The latter is a first indication that freeze-thawing has a favourable effect on the crosslinking efficiency of 10 w/v% gel-MOD. During the cryo-treatment, phase separation occurs which probably reduces the distance between neighbouring vinyl bonds and thus facilitates the chemical crosslinking. On the other hand, a change in gelatin concentration alters the mobility of the polymer chains. Therefore, 15 w/v% gelatin hydrogels were also freeze-thawed and their mechanical properties before and after UV-curing were compared with non-frozen hydrogels (figure 3-32).

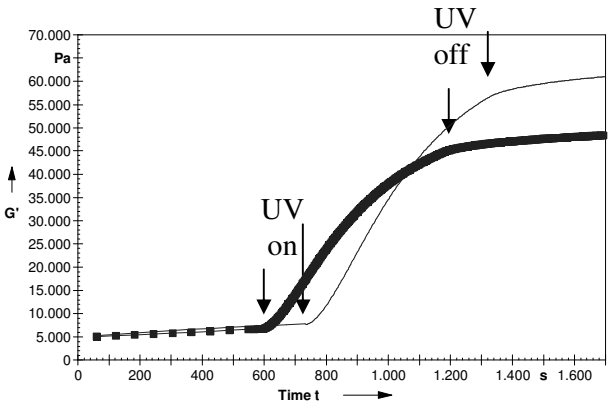

Figure 3-32: G' at different time points of 15 w/v% unfrozen hydrogels (–) and of cryogels after applying one cryo-treatment (■). The gels were in situ UV-cured during 10 minutes at 5°C (0.5% strain, 1 Hz, gap 1 mm, F_N = 0.2 N).

Before chemical crosslinking, G' of both hydrogel types were in the same range. This is probably due to a lack of chain mobility below the sol-gel temperature, which hinders phase separation below the solvent crystallisation temperature, thus avoiding an increase in the concentration of polymer chains within the "non-frozen (yet solidified) liquid microphase". After UV-treatment, the storage modulus of the hydrogel is higher than that of the cryogel, which can be explained by a possible phase separation of the initiator molecules and the methacrylamide side groups due to the cryo-treatment.

6 Conclusion

The present chapter indicates that gelatin is very suitable as polymer precursor for hydrogel preparation. The physical structuring, inherent to gelatin, contributes to a large extent to the mechanical properties. However, the chemical crosslinking of all hydrogel types developed, mostly determines the final properties of the end product and can be controlled to a large extent.

The gelatin gels (type I and II) are flexible, strong and transparent. Since the hydrogels are prepared, starting from natural, hydrophilic polymer chains, no monomer residues have to be removed before use. Moreover, type I gelatin and chondroitin sulphate hydrogels were prepared by means of a two-step production process, without the addition of a crosslinker. After modification of gelatin and chondroitin sulphate with respectively methacrylamide and methacrylate groups, the radical crosslink polymerization can occur. A major advantage of type II hydrogels is the fact that the chemical crosslinking is reversible. Disulfide bonds can be reduced again to thiol groups by means of a mild reducing agent such as dithiotreitol. The latter could be interesting in view of future applications as cell carriers in tissue engineering.

The mechanical properties of the hydrogels developed, depend on many parameters, such as the storage time, the polymer concentration, the modification degree etc. The final network strength depends on the contribution of two factors: the physical gelation and the chemical crosslinking. The effect of the different parameters on the respective contributions of the physical and the chemical crosslinking could be followed by means of rheology, by measurements above and below the melting point of gelatin. From the results, it could be concluded that the physical gelation was disturbed more in type II hydrogels compared to type I hydrogels. However, the disulfide bond formation resulted in more flexible and less brittle hydrogels (type II) than radical polymerisation of double bonds in type I hydrogels.

Gelatin cryogels, developed by freeze-thaw treatments, possess a lower critical gelation concentration compared to regular hydrogels, formed at room temperature. This implies that lower gelatin concentrations can be applied for developing gels with similar mechanical properties. The present work demonstrates that the self-gelling

properties of gelatin (below the sol-gel temperature) do not necessarily limit certain processing possibilities. Cryogelation of materials can reduce the required amount of material to a great extent, which benefits not only the cost, but also offers the possibility of decreasing the amount of added initiator.

The present work also indicates that the concept is limited to gelatin concentrations for which the chain mobility below the sol-gel temperature is sufficient to allow phase separation and cryo-concentration within the non-frozen liquid microphase.

The observed findings are of importance in the field of tissue engineering since variation of the cryogenic parameters affects the mechanical properties of the resulting hydrogels. The latter probably influence the degradation profile of the (cell seeded) scaffolds which, ideally, should match the rate of new tissue formation. Without any doubt, this process can and will be applied on a large number of (natural) polymers.

References

1. Djagny, K. B.; Wang, Z.; Xu, S. Y., Gelatin: A valuable protein for food and pharmaceutical industries: Review. *Critical Reviews in Food Science and Nutrition* **2001,** 41, (6), 481-492.
2. Chatterjee, S.; Bohidar, H. B., Effect of cationic size on gelation temperature and properties of gelatin hydrogels. *International Journal of Biological Macromolecules* **2005,** 35, (1-2), 81-88.
3. Djabourov, M., Architecture of Gelatin Gels. *Contemporary Physics* **1988,** 29, (3), 273-297.
4. Marangoni, A. G.; Tosh, S. M., On the nature of the maximum gelation temperature in polymer gels. *Biophysical Chemistry* **2005,** 113, (3), 265-267.
5. Tanaka, T.; Swislow, G.; Ohmine, I., Phase-Separation and Gelation in Gelatin Gels. *Physical Review Letters* **1979,** 42, (23), 1556-1559.
6. Mackie, A. R.; Gunning, A. P.; Ridout, M. J.; Morris, V. J., Gelation of gelatin observation in the bulk and at the air-water interface. *Biopolymers* **1998,** 46, (4), 245-252.
7. Todd, A., Rigidity factor of gelatin gels. *Nature* **1961,** 191, 567-569.
8. Aymard, P.; Martin, D. R.; Plucknett, K.; Foster, T. J.; Clark, A. H.; Norton, I. T., Influence of thermal history on the structural and mechanical properties of agarose gels. *Biopolymers* **2001,** 59, (3), 131-144.
9. Righetti, P. G., Of Matrices and Men. *Journal of Biochemical and Biophysical Methods* **1989,** 19, (1), 1-20.
10. Fukunaka, Y.; Iwanaga, K.; Morimoto, K.; Kakemi, M.; Tabata, Y., Controlled release of plasmid DNA from cationized gelatin hydrogels based on hydrogel degradation. *Journal of Controlled Release* **2002,** 80, (1-3), 333-343.
11. Veerman, C.; Rajagopal, K.; Palla, C. S.; Pochan, D. J.; Schneider, J. P.; Furst, E. M., Gelation kinetics of beta-hairpin peptide hydrogel networks. *Macromolecules* **2006,** 39, (19), 6608-6614.
12. Orozco-Guareno, E.; Almaraz, A. N. C.; Reyes, G. I.; Lopez-Ureta, L. C.; Gonzalez-Alvarez, A., Characterization of structured acrylamide/acrylic acid hydrogels by TMDSC and microscopy. *Journal of Thermal Analysis and Calorimetry* **2006,** 86, (2), 511-516.
13. Lohse, D. J., The Influence of Chemical Structure on Polyolefin Melt Rheology and Miscibility. *Polymer Reviews* **2005,** 45, (4), 289 - 308.
14. Seema, A.; Kutty, S. K. N., Rheology of Short Nylon-6 Fiber Reinforced Styrene-Butadiene Rubber. *International Journal of Polymeric Materials* **2005,** 54, (10), 933 - 948.
15. Schurz, J., Rheology of Synovial Fluids and Substitute Polymers. *Journal of Macromolecular Science, Part A* **1996,** 33, (9), 1249 - 1262.
16. Nijenhuis, K. T.; Winter, H. H., Mechanical-Properties at the Gel Point of a Crystallizing Polyvinyl-Chloride) Solution. *Macromolecules* **1989,** 22, (1), 411-414.
17. Bindal, A.; Narsimhan, G.; Hem, S. L.; Kulshreshtha, A., Effect of Steam Sterilization on the Rheology of Polymer Solutions. *Pharmaceutical Development and Technology* **2003,** 8, (3), 219 - 228.

18. Chambon, F.; Petrovic, Z. S.; Macknight, W. J.; Winter, H. H., Rheology of Model Polyurethanes at the Gel Point. *Macromolecules* **1986,** 19, (8), 2146-2149.
19. Li, Y.; Ke, W.; Gao, X.; Yuan, Y.; Shen, K., Effect of Melt Vibration on Mechanical Properties of Injection Molding and Rheology. *Journal of Macromolecular Science, Part B* **2005,** 44, (2), 289 - 301.
20. Rasteiro, M. G.; Antunes, E., Correlating the Rheology of PVC-Based Pastes with Particle Characteristics. *Particulate Science and Technology* **2005,** 23, (4), 361 - 375.
21. Ramakrishnan, S.; Gerardin, C.; Prud; apos; homme, R. K., Syneresis of Carrageenan Gels: NMR and Rheology. *Soft Materials* **2004,** 2, (2), 145 - 153.
22. Shin, I.; Szamosi, J.; Tobing, S., Two-Level Factorial Study of the Rheology and Foaming of Bromobutyl Rubber Solutions. *International Journal of Polymeric Materials* **1991,** 15, (2), 103 - 106.
23. Telis, V. R. N.; Telis-Romero, J.; Gabas, A. L., Solids Rheology for Dehydrated Food and Biological Materials. *Drying Technology* **2005,** 23, (4), 759 - 780.
24. Wolfe, S. V.; Tod, D. A.; Rarde, Characterization of Engineering Polymers by Dynamic Mechanical Analysis. *Journal of Macromolecular Science, Part A* **1989,** 26, (1), 249 - 272.
25. Osaki, K., Polymer Dynamics and Rheology. *International Journal of Polymeric Materials* **1993,** 20, (3), 265 - 269.
26. Nunes, M. C.; Raymundo, A.; Sousa, I., Rheological behaviour and microstructure of pea protein/[kappa]-carrageenan/starch gels with different setting conditions. *Food Hydrocolloids* **2006,** 20, (1), 106-113.
27. Stern, C.; Frick, A.; Weickert, G., Relationship between the structure and mechanical properties of polypropylene: Effects of the molecular weight and shear-induced structure. *Journal of Applied Polymer Science* **2007,** 103, (1), 519-533.
28. Iritani, E.; Katagiri, N.; Yamaguchi, K.; Cho, J. H., Compression-permeability properties of compressed bed of superabsorbent hydrogel particles. *Drying Technology* **2006,** 24, (10), 1243-1249.
29. Bartkowiak, A.; Brylak, W., Hydrogel microcapsules containing natural and chemically modified oligochitosan - Mechanical properties and porosity. *Polimery* **2006,** 51, (7-8), 547-554.
30. Alasalvar, C.; Taylor, K. D. A.; Oksuz, A.; Garthwaite, T.; Alexis, M. N.; Grigorakis, K., Freshness assessment of cultured sea bream (Sparus aurata) by chemical, physical and sensory methods. *Food Chemistry* **2001,** 72, (1), 33-40.
31. Soeda, T., The Function on Food-Processing for the Cold-Gel Prepared from Heated Soy Protein Isolate - Studies on the Gelation of Soy Protein During the Cold-Storage .4. *Journal of the Japanese Society for Food Science and Technology-Nippon Shokuhin Kagaku Kogaku Kaishi* **1995,** 42, (9), 672-676.
32. Johnson, F. A.; Craig, D. Q. M.; Mercer, A. D.; Chauhan, S., The effects of alginate molecular structure and formulation variables on the physical characteristics of alginate raft systems. *International Journal of Pharmaceutics* **1997,** 159, (1), 35-42.

33. Pillay, V.; Fassihi, R., A new method for dissolution studies of lipid-filled capsules employing nifedipine as a model drug. *Pharmaceutical Research* **1999,** 16, (2), 333-337.
34. JACHOWICZ, J.; YAO, K., Dynamic hairspray analysis. I. Instrumentation and preliminary results *J. Soc. Cosmet. Chem.* **1996,** 47, 73-84.
35. SMEWING, J., Analysing the textural properties of cosmetics. *Cosmetics and Toiletries Manufacture Worldwide* **1998**, 249-253.
36. Tanahashi, M.; Kohsaka, N.; Mori, M.; Hatao, T.; Katsumura, A.; Takeda, K., Fatigue-fracture surface of polycarbonate subjected to heating/cooling cycles under longitudinal confinement. *Kobunshi Ronbunshu* **2006,** 63, (12), 767-773.
37. Cheng, H. C.; Hwu, F. S., Fatigue reliability analysis of composites based on residual strength. *Advanced Composite Materials* **2006,** 15, (4), 385-402.
38. Bastun, V. N.; Nizhnik, S. B.; Usikova, G. I., Structural approach to enhance the fracture resistance of high-strength metallic materials. *International Applied Mechanics* **2006,** 42, (8), 904-912.
39. Barros, J. A. G.; Fechine, G. J. M.; Alcantara, M. R.; Catalani, L. H., Poly (N-vinyl-2-pyrrolidone) hydrogels produced by Fenton reaction. *Polymer* **2006,** 47, (26), 8414-8419.
40. Zhu, W.; Ding, J. D., Synthesis and characterization of a redox-initiated, injectable, biodegradable hydrogel. *Journal of Applied Polymer Science* **2006,** 99, (5), 2375-2383.
41. Liou, F. J.; Wang, Y. J., Preparation and characterization of crosslinked and heat-treated PVA-MA films. *Journal of Applied Polymer Science* **1996,** 59, (9), 1395-1403.
42. Chao, G. T.; Deng, H. X.; Huang, Q.; Jia, W. J.; Huang, W. X.; Gu, Y. C.; Tan, H. P.; Fan, L. Y.; Liu, C. B.; Huang, A. L.; Lei, K.; Gong, C. Y.; Tu, M. J.; Qian, Z. Y., Preparation and characterization of pH sensitive semi-interpenetrating network hydrogel based on methacrylic acid, bovine serum albumin (BSA), and PEG. *Journal of Polymer Research* **2006,** 13, (5), 349-355.
43. Wei, H. L.; Yu, H. Q.; Zhu, K. Q.; Qian, L. J.; Zhang, A. Y.; Feng, Z. G., Preparation of thermosensitive and supramolecular structured hydrogel by copolymerization of photocurable polypseudorotaxanes based on alpha-cyclodextrins with N-isopropylacrylamide and its characterization. *Acta Polymerica Sinica* **2006**, (4), 581-587.
44. Fei, I.; Wach, R. A.; Mitomo, H.; Yoshii, F.; Kume, T., Hydrogel of biodegradable cellulose derivatives. I. Radiation-induced crosslinking of CMC. *Journal of Applied Polymer Science* **2000,** 78, (2), 278-283.
45. El-Din, H. M. N.; Abd Alla, S. G.; El-Naggar, A. W. M., Swelling, thermal and mechanical properties of poly(vinylalcohol)/sodium alginate hydrogels synthesized by electron beam irradiation. *Journal of Macromolecular Science Part a-Pure and Applied Chemistry* **2007,** 44, (3), 291-297.
46. Abd El-Rehim, H. A.; Hegazy, E. S. A.; Diaa, D. A., Characterization of super-absorbent material based on carboxymethylcellulose sodium salt prepared by electron beam irradiation. *Journal of Macromolecular Science-Pure and Applied Chemistry* **2006,** A43, (1), 101-113.

47. El-Naggar, A. W. M.; Alla, S. G. A.; Said, H. M., Temperature and pH responsive behaviours of CMC/AAc hydrogels prepared by electron beam irradiation. *Materials Chemistry and Physics* **2006,** 95, (1), 158-163.
48. Fisher, J. P.; Dean, D.; Engel, P. S.; Mikos, A. G., Photoinitiated polymerization of biomaterials. *Annual Review of Materials Research* **2001,** 31, 171-181.
49. Kameta, K.; Kouchi, N.; Hatano, Y., *4 Cross sections for photoabsorption, photoionization, neutral dissociation of molecules*. 2003; p 4001-4061.
50. Williams, C. G.; Malik, A. N.; Kim, T. K.; Manson, P. N.; Elisseeff, J. H., Variable cytocompatibility of six cell lines with photoinitiators used for polymerizing hydrogels and cell encapsulation. *Biomaterials* **2005,** 26, (11), 1211-1218.
51. O. Soppera, C. C.-B., Real-time Fourier transform infrared study of the free-radical ultraviolet-induced polymerization of a hybrid sol-gel. II. The effect of physicochemical parameters on the photopolymerization kinetics. *Journal of Polymer Science Part A: Polymer Chemistry* **2003,** 41, (6), 831-840.
52. Van Den Bulcke, A. Synthese en evaluatie van hydrogelen op basis van gelatine. 2000.
53. Hiroshi Yoshioka, Y. M. S. T. S. K., Thermoreversible gelation on cooling and on heating of an aqueous gelatin-poly(<I>N</I>-isopropylacrylamide) conjugate. *Polymers for Advanced Technologies* **1998,** 9, (2), 155-158.
54. Kavanagh, G. M.; Ross-Murphy, S. B., Rheological characterisation of polymer gels. *Progress in Polymer Science* **1998,** 23, (3), 533-562.
55. Liu, Y. C.; Shu, X. Z.; Prestwich, G. D., Biocompatibility and stability of disulfide-crosslinked hyaluronan films. *Biomaterials* **2005,** 26, (23), 4737-4746.
56. Shu, X. Z.; Liu, Y. C.; Palumbo, F.; Prestwich, G. D., Disulfide-crosslinked hyaluronan-gelatin hydrogel films: a covalent mimic of the extracellular matrix for in vitro cell growth. *Biomaterials* **2003,** 24, (21), 3825-3834.
57. Kallmann, G.; Oster, G. Optical or Photographic Cross-linking of Thiol Polymers. 1962.
58. Zhong, Y.; Li, B. Y.; Haynie, D. T., Control of stability of polypeptide multilayer nanofilms by quantitative control of disulfide bond formation. *Nanotechnology* **2006,** 17, (23), 5726-5734.
59. Han, K. K.; Richard, C.; Delacourte, A., Chemical Cross-Links of Proteins by Using Bifunctional Reagents. *International Journal of Biochemistry* **1984,** 16, (2), 129-145.
60. Zilberman, M., Novel composite fiber structures to provide drug/protein delivery for medical implants and tissue regeneration. *Acta Biomaterialia* **2007,** 3, (1), 51-57.
61. Sales, V. L.; Engelmayr, G. C.; Gottlieb, D.; Johnson, J. A.; Gao, J.; Wang, Y.; Sacks, M. S.; Mayer, J. E., Protein pre-coating of elastomeric tissue-engineering scaffolds: extracellular matrix formation and phenotypic changes of circulating endothelial progenitor cells. *Circulation* **2006,** 114, (18), 402-402.
62. Giannouli, P.; Morris, E. R., Cryogelation of xanthan. *Food Hydrocolloids* **2003,** 17, (4), 495-501.
63. Te Nijenhuis, K. Dynamic mechanical studies on thermo-reversible aging processes in gels of polyvinylchloride and of gelatin. 1979.

64. Zelikin, A. N.; Quinn, J. F.; Caruso, F., Disulfide cross-linked polymer capsules: En route to biodeconstructible systems. *Biomacromolecules* **2006,** 7, (1), 27-30.
65. White, F. H.; Sandoval, A., The thiolation of ribonuclease. *Biochemistry* **1962,** 1, (6), 938-946.
66. Wang, T. W.; Sun, J. S.; Huang, Y. C.; Wu, H. C.; Chen, L. T.; Lin, F. H., Skin basement membrane and extracellular matrix proteins characterization and quantification by real time RT-PCR. *Biomaterials* **2006,** 27, (29), 5059-5068.
67. Pek, Y. S.; Spector, M.; Yannas, I. V.; Gibson, L. J., Degradation of a collagen-chondroltin-6-sulfate matrix by collagenase and by chondroitinase. *Biomaterials* **2004,** 25, (3), 473-482.
68. Lee, C. R.; Grodzinsky, A. J.; Spector, M., The effects of cross-linking of collagen-glycosaminoglycan scaffolds on compressive stiffness, chondrocyte-mediated contraction, proliferation and biosynthesis. *Biomaterials* **2001,** 22, (23), 3145-3154.
69. Spilker, M. H.; Asano, K.; Yannas, I. V.; Spector, M., Contraction of collagen-glycosaminoglycan matrices by peripheral nerve cells in vitro. *Biomaterials* **2001,** 22, (10), 1085-1093.
70. Torres, D. S.; Freyman, T. M.; Yannas, I. V.; Spector, M., Tendon cell contraction of collagen-GAG matrices in vitro: effect of cross-linking. *Biomaterials* **2000,** 21, (15), 1607-1619.
71. Moghaddam, M. J.; Matsuda, T., Molecular Design of 3-Dimensional Artificial Extracellular-Matrix - Photosensitive Polymers Containing Cell Adhesive Peptide. *Journal of Polymer Science Part a-Polymer Chemistry* **1993,** 31, (6), 1589-1597.
72. Liu, Y. C.; Shu, X. Z.; Gray, S. D.; Prestwich, G. D., Disulfide-crosslinked hyaluronan-gelatin sponge: growth of fibrous tissue in vivo. *Journal of Biomedical Materials Research Part A* **2004,** 68A, (1), 142-149.
73. Choi, Y. S.; Hong, S. R.; Lee, Y. M.; Song, K. W.; Park, M. H.; Nam, Y. S., Study on gelatin-containing artificial skin: I. Preparation and characteristics of novel gelatin-alginate sponge. *Biomaterials* **1999,** 20, (5), 409-417.
74. Pieper, J. S.; Hafmans, T.; Veerkamp, J. H.; van Kuppevelt, T. H., Development of tailor-made collagen-glycosaminoglycan matrices: EDC/NHS crosslinking, and ultrastructural aspects. *Biomaterials* **2000,** 21, (6), 581-593.
75. Osborne, C. S.; Reid, W. H.; Grant, M. H., Investigation into the biological stability of collagen/chondroitin-6-sulphate gels and their contraction by fibroblasts and keratinocytes: the effect of crosslinking agents and diamines. *Biomaterials* **1999,** 20, (3), 283-290.
76. Lozinsky, V. I., Cryogels on the basis of natural and synthetic polymers: Preparation, properties and application. *Uspekhi Khimii* **2002,** 71, (6), 559-585.
77. Lozinsky, V. I.; Damshkaln, L. G., Study of cryostructuration of polymer systems. XVII. Poly(vinyl alcohol) cryogels: Dynamics of the cryotropic gel formation. *Journal of Applied Polymer Science* **2000,** 77, (9), 2017-2023.
78. Lozinsky, V. I.; Damshkaln, L. G.; Brown, R.; Norton, I. T., Study of cryostructuration of polymer systems. XVIII. Freeze-thaw influence on water-solubilized artificial mixtures of amylopectin and amylose. *Journal of Applied Polymer Science* **2000,** 78, (2), 371-381.

79. Podorozhko, E. A.; Kurskaya, E. A.; Kulakova, V. K.; Lozinsky, V. I., Cryotropic structuring of aqueous dispersions of fibrous collagen: influence of the initial pH values. *Food Hydrocolloids* **2000,** 14, (2), 111-120.
80. Vainerman, E. S.; Lozinsky, V. I.; Rogozhin, S. V., Study of Cryostructurization of Polymer Systems .I. Structure Formation in Solutions of Thiol-Containing Polymers under Freezing-Thawing. *Colloid and Polymer Science* **1981,** 259, (12), 1198-1201.
81. Lozinsky, V. I.; Golovina, T. O.; Gusev, D. G., Study of cryostructuration of polymer systems: XIII. Some characteristic features of the behaviour of macromolecular thiols in frozen aqueous solutions. *Polymer* **2000,** 41, (1), 35-47.
82. Lazaridou, A.; Biliaderis, C. G., Cryogelation of cereal beta-glucans: structure and molecular size effects. *Food Hydrocolloids* **2004,** 18, (6), 933-947.
83. Willcox, P. J.; Howie, D. W.; Schmidt-Rohr, K.; Hoagland, D. A.; Gido, S. P.; Pudjijanto, S.; Kleiner, L. W.; Venkatraman, S., Microstructure of poly(vinyl alcohol) hydrogels produced by freeze/thaw cycling. *Journal of Polymer Science Part B-Polymer Physics* **1999,** 37, (24), 3438-3454.
84. Lozinsky, V. I.; Galaev, I. Y.; Plieva, F. M.; Savinal, I. N.; Jungvid, H.; Mattiasson, B., Polymeric cryogels as promising materials of biotechnological interest. *Trends in Biotechnology* **2003,** 21, (10), 445-451.
85. Bloch, K.; Lozinsky, V. I.; Galaev, I. Y.; Yavriyanz, K.; Vorobeychik, M.; Azarov, D.; Damshkaln, L. G.; Mattiasson, B.; Vardi, P., Functional activity of insulinoma cells (INS-1E) and pancreatic islets cultured in agarose cryogel sponges. *Journal of Biomedical Materials Research Part A* **2005,** 75A, (4), 802-809.
86. Lozinsky, V. I.; Plieva, F. M., Poly(vinyl alcohol) cryogels employed as matrices for cell immobilization. 3. Overview of recent research and developments. *Enzyme and Microbial Technology* **1998,** 23, (3-4), 227-242.
87. Lozinsky, V. I.; Zubov, A. L.; Titova, E. F., Swelling behavior of poly(vinyl alcohol) cryogels employed as matrices for cell immobilization. *Enzyme and Microbial Technology* **1996,** 18, (8), 561-569.
88. Lozinsky, V. I.; Zubov, A. L.; Titova, E. F., Poly(vinyl alcohol) cryogels employed as matrices for cell immobilization .2. Entrapped cells resemble porous fillers in their effects on the properties of PVA-cryogel carrier. *Enzyme and Microbial Technology* **1997,** 20, (3), 182-190.
89. Cascone, M. G.; Lazzeri, L.; Sparvoli, E.; Scatena, M.; Serino, L. P.; Danti, S., Morphological evaluation of bioartificial hydrogels as potential tissue engineering scaffolds. *Journal of Materials Science-Materials in Medicine* **2004,** 15, (12), 1309-1313.
90. Plieva, F.; Oknianska, A.; Degerman, E.; Galaev, I. Y.; Mattiasson, B., Novel supermacroporous dextran gels. *Journal of Biomaterials Science-Polymer Edition* **2006,** 17, (10), 1075-1092.
91. Dainiak, M. B.; Galaev, I. Y.; Mattiasson, B., Affinity cryogel monoliths for screening for optimal separation conditions and chromatographic separation of cells. *Journal of Chromatography A* **2006,** 1123, (2), 145-150.

92. Lukas, L. A.; Surry, K. J. M.; Peters, T. M., Temperature dosimetry using MR relaxation characteristics of poly(vinyl alcohol) cryogel (PVA-C). *Magnetic Resonance in Medicine* **2001,** 46, (5), 1006-1013.
93. Lozinsky, V. I.; Plieva, F. M.; Galaev, I. Y.; Mattiasson, B., The potential of polymeric cryogels in bioseparation. *Bioseparation* **2001,** 10, (4-5), 163-188.
94. Tosh, S. M.; Marangoni, A. G.; Hallett, F. R.; Britt, I. J., Aging dynamics in gelatin gel microstructure. *Food Hydrocolloids* **2003,** 17, (4), 503-513.
95. Hassan, C. M.; Ward, J. H.; Peppas, N. A., Modeling of crystal dissolution of poly(vinyl alcohol) gels produced by freezing/thawing processes. *Polymer* **2000,** 41, (18), 6729-6739.

Chapter IV:
Preparation and Characterization of Gelatin Scaffolds

1 Introduction

A frequently applied approach in the domain of tissue engineering, is the development of porous scaffolds containing bioactive compounds such as glycosaminoglycans and/or growth factors.[1-4] Autologous or allogenic cells can be seeded and cultured on these materials resulting in newly formed tissue *in vitro*[5] or *in vivo*[5, 6]. In the past, a large number of materials, synthetic as well as natural, have been proposed as cell carriers. The most frequently used synthetic polymers include poly(glycolic acid), poly(DL-lactic acid) and poly(DL-lactic-co-glycolic acid) copolymers.[7, 8] Common natural cell matrices include chitosan[9, 10], collagen[10, 11] and gelatin[12-14]. In the present work, gelatin was selected, since it is a self-assembling, non-toxic, biodegradable, inexpensive and non-immunogenic material.[14] It has been widely applied in medicine as a wound dressing and as an adhesive and absorbent pad for surgical use.[15] Moreover, in previous studies on gelatin-based sponges, it was shown that acellular sponges containing gelatin have potential applications in the field of tissue engineering.[6] The gel-sol transition temperature of gelatin is about 30°C, as already described in chapter 3. In the present work, gelatin was derivatized with methacrylamide side chains enabling chemical crosslinking to avoid dissolution at body temperature (37°C), as discussed in chapter 2 (§ 2.1).[16]

A material to be applied as scaffold should fulfil certain requirements. First, high porosity is required in order to support diffusion of oxygen and nutrients towards the cells and drainage of waste products from the matrix. In addition, pore interconnectivity is important to promote phenomena such as cell migration and

angiogenesis. Secondly, the porous biomaterials should be biocompatible and in some cases also biodegradable.[12, 17]

The pore size required for cell ingrowth depends on the cell type seeded on the matrix.[8] For porous silicon nitride scaffolds, endothelial cells bind preferentially to scaffolds with pores smaller than 80 µm, while fibroblasts preferentially bind to larger pores (>90µm).[10] A pore size gradient through the scaffold could be favourable in some cases to mimic the complex architectures of tissues. Porous scaffolds with spatially variable pore size can influence the location and mechanical properties required by tissue interfaces. Pore size gradients can also impact cell migration *in vitro* and *in vivo*, which is a significant advantage for generating the complex tissue interfaces required for functional tissue regeneration.[18]

At present, different techniques exist to fabricate porous scaffolds including porogen leaching[12, 19], phase separation, emulsion freeze drying[8, 20], solvent evaporation[21], gas foaming[22] and fibre bonding[23].

One of the most common and straightforward techniques to prepare porous scaffolds is the particulate leaching method, which involves the selective leaching of a mineral, usually NaCl salt or of an organic compound such as saccharose to generate the pores.[24, 25]

Phase separation can result in scaffolds with porosities up to 95%.[26] Basically, the polymer is dissolved in a solvent and phase separation is induced by lowering the solution temperature or by adding a non-solvent to the solution. The presence of polymer solvent or non-solvent residues in the scaffolds can, however, represent a limitation of phase separation techniques.[27] In the present work, water is used as solvent, so the disadvantage of residual (toxic) solvents, is excluded.

An alternative, proposed for the fabrication of porous polymer scaffolds, is emulsion freeze-drying. Poly(DL-lactic-co-glycolic acid), for example, is dissolved in methylene chloride and then distilled water is added to form an emulsion. The polymer/water mixture is cast into a mould and quenched by placing it in liquid nitrogen. After quenching, the scaffolds are freeze-dried at -55°C, resulting in the removal of the dispersed water and polymer solvents. Scaffolds with large porosities (up to 95%), but small pore sizes (13-35 µm) have been fabricated using this technique. These parameters are very dependent on factors such as the ratio of polymer solution to water and the viscosity of the emulsion, as these values influence the emulsion's stability prior to quenching. Therefore, with further adjustment, it is possible that pore

size could be increased. However, although this technique is advantageous since it does not require an extra washing/leaching step, the use of organic solvents remains a concern for the inclusion of cells and bioactive molecules.[28]

Solvent casting/particulate leaching involves the casting of a polymer solution and dispersed porogen particulates in a mould, the removal of the polymer solvent, followed by leaching out the porogen.[29, 30] Because of the casting and the solvent evaporation step, this technique is only suitable for thin scaffolds. A drawback of this technique is the use of organic solvents, which can be difficult to completely remove from the scaffolds during the drying process.

In order to circumvent this problem, several authors proposed to replace solvent casting by melt-moulding, resulting in the melt moulding/particulate leaching method. Briefly, the melt-moulding step consists of premixing polymer powder and solid porogen particulates and hot-pressing them together. The samples are then subjected to the same solid porogen leaching step as for the solvent-cast samples.[31, 32]

Gas foaming is another alternative for the fabrication of porous polymer scaffolds. It is carried out by dissolving a gas at elevated pressure (i.e. physical blowing agent) or by incorporating a chemical that yields gaseous decomposition products (i.e. chemical blowing agent). The foaming technique generally leads to pore structures that are not fully interconnective.[27]

Fibre bonding typically requires high temperatures (above the transition temperature of the polymer) and is not applicable for the processing of amorphous polymers. The high temperatures used in this process also are likely to denature any biologically active molecules one might wish to incorporate into the matrix.[33]

Unlike the conventional fabrication techniques, solid freeform fabrication has no restriction on shape control. The latter is a computerized fabrication technique that can rapidly produce highly complex three-dimensional objects using data from computer medical imaging equipment such as MRI and CT scans, which will be discussed in paragraph 3.1.1. The prototyping material is deposited to build the final structure in a layer-by-layer process.[34, 35]

In the present study, a combination of phase separation and freeze-drying was used to induce pore formation within gelatin hydrogels. When an aqueous gelatin solution is solidified (i.e. frozen), phase separation occurs between the growing ice crystals

and the concentrated gelatin solution (non-frozen liquid micro-phase).[36, 37] After sublimation of the ice crystals (freeze-drying), a porous scaffold originates. Using a novel cryo-setup, developed in our laboratory, as shown in chapter 3 (figure 3-22), the cooling rate, the temperature gradient and the final freezing temperature during the cryogenic treatment can be varied in a controlled manner. In addition, we also varied the gelatin concentration.

Scanning electron microscopy (SEM), helium pycnometry (He-pycnometry), micro-computed tomography (μ-CT) and light microscopy analysis were applied in order to evaluate the pore size, the pore morphology and the porosity of the gelatin hydrogels developed. Next, swelling experiments, dynamic vapour sorption, compression tests and *in vitro* degradation studies were performed on a selection of the scaffolds developed.

2 Experimental procedure for the preparation of gel-MOD scaffolds

2.1 Influence of the initiator concentration on the hydrogel properties

An important parameter, influencing the properties of the hydrogels developed, is the initiator concentration. For some applications, it is necessary to obtain sufficient chemical crosslinking within a short irradiation time. In this case, higher initiator concentrations should be used. An increase in photo-initiator concentration leads to a higher energy uptake by the component, which is caused by the increase of the optical density. The latter gives rise to an increase of the polymerization degree until a constant value is obtained. On the other hand, the amount of recombination reactions also increases with higher initiator concentrations.[38]

Chemically crosslinked hydrogel scaffolds were prepared by adding a predetermined amount of initiator, calculated to the amount of methacrylamide side chains present. The homogeneous solution was then injected into the mould of the cryo-unit,

schematically shown in figure 3-22, after which the solution was allowed to gel for 1 hour at room temperature. In a final curing step, the hydrogel was exposed to UV-light (279 nm, 10 mW/cm^2) for two hours. The scaffolds obtained, were evaluated by swelling experiments and compression tests, since the hydrogel thickness (i.e. 5 mm) ruled out the use of rheology (figure 4-1).

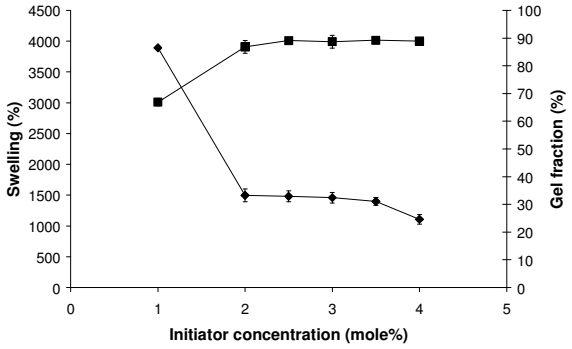

Figure 4-1: Influence of the initiator concentration on %swelling and gel fraction.

From the data, depicted in figure 4-1, it appeared that initiator concentrations, exceeding 2 mol% did not result in hydrogel scaffolds, possessing higher gel fractions. Consequently, an initiator concentration of 2 mol% was utilized for further experiments.

By means of texturometry, the influence of the initiator concentration on the compression modulus was also studied. From figure 4-2, it was observed that the compression modulus, in contrast to the gel fraction, increased for the entire initiator concentration range applied. The latter can be explained by the higher crosslinking degree of the top layer when applying higher initiator concentrations. A similar effect was, in contrast to what we anticipated, not observed for the gel fraction. The limited penetration depth of UV-light can result in heterogeneous crosslinking (i.e. between surface and bulk) of the scaffolds at elevated initiator concentrations. The increase in crosslinking at higher initiator concentrations is probably limited to the hydrogel surface, as demonstrated by compression tests (figure 4-2). Depth-dependent UV-penetration was already observed previously for dextran-methacrylate hydrogels. Even though the concerning hydrogels were thinner in that work (3 mm versus 5 mm), they were thick enough to produce differential UV-penetration through the material.[39, 40]

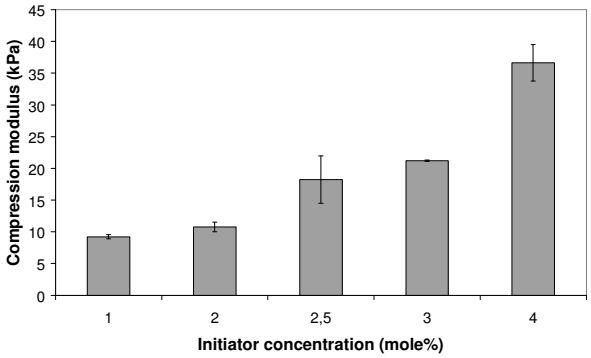

Figure 4-2: Influence of the initiator concentration on the compression modulus (20% strain, 21°C, sample size = 10 mm x 10 mm).

2.2 Influence of the irradiation time on the hydrogel properties

Beside the initiator concentration, the irradiation time also influences the strength of photo-crosslinked hydrogels.[41]

In order to investigate the effect of the irradiation time on the properties of the hydrogels developed, swelling experiments were performed, followed by determining the gel fraction (figure 4-3).

The gel fraction increased with increasing irradiation time, up to 1.5 hours UV-irradiation. When further increasing the irradiation time up to 5 hours, the gel fraction decreased slightly. The latter is probably due to the degradation of gelatin when exposed to UV-light for longer time periods. This phenomenon was already observed for a variety of polymers.[42, 43] Consequently, an irradiation time of two hours was selected to perform all further experiments.

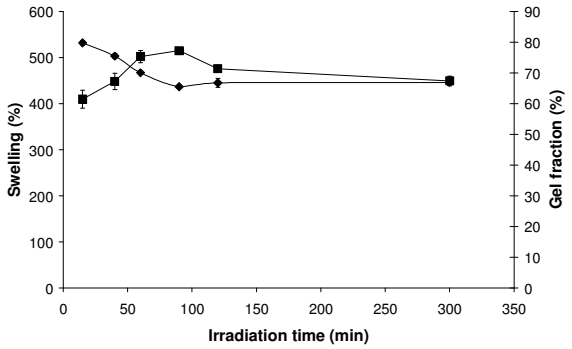

Figure 4-3: Effect of the irradiation time on the swelling properties and the gel fraction.

2.3 Cryogenic treatment

In a next part, porous gelatin scaffolds were generated by a cryogenic treatment of a chemically crosslinked gel-MOD hydrogel. The reaction mixture, containing gel-forming agents (i.e. gelatin) is frozen at temperatures below the solvent (i.e. water) crystallization point. The frozen system, despite its appearance as a single solid block, remains essentially heterogeneous and contains so-called unfrozen liquid microphase (UFLMP) along with the crystals of the frozen solvent (figure 4-4).[36, 37]

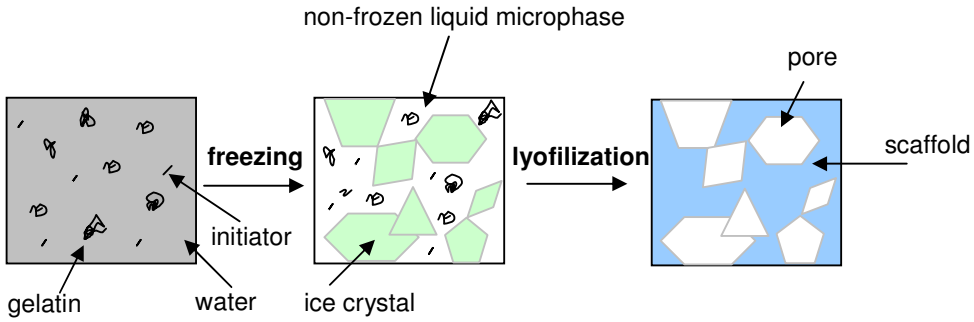

Figure 4-4: Cryogenic treatment of gelatin hydrogel, followed by lyofilization.

Gel-forming reagents are concentrated in the UFLMP, that is, **cryoconcentration** takes place, as already discussed in the previous chapter (§ 5). Since the UFLMP presents only a small portion of the total initial volume in which the concentration of gel precursors has increased dramatically, gel-formation is promoted. In fact, due to cryoconcentration, the gel formation in such frozen systems proceeds sometimes faster than in liquid medium, when using the same initial concentration of precursors.[44, 45]

The crystals of frozen solvent perform as pore-forming agents. When melted or freeze-dried, they leave voids or macropores. The surface tension between the solvent and the gel phase rounds the shape of the pores, making the pore surfaces smoother. During freezing, solvent crystals grow until they meet other crystals, so after thawing/lyophilization, a system of interconnected pores arises inside the gel.

The dimensions and shape of the pores depend on many factors, of which the most important are the precursor concentrations and the freezing regime.

In table 4-1, an overview is presented, showing a variety of materials, able to form cryogels with their respective applications.

Gel-forming reagents	Application
polyacrylamide[46, 47]	bioseparation[37, 48, 49]
poly(N-isopropyl-acrylamide)	drug release[50]
poly(vinyl alcohol)[51-54]	drug delivery, cell matrix[55, 56]
poly(acrylic acid)	drug delivery[57]
cellulose[45]	food
β-glucans[58]	food preparations[59]
xanthan[60]	food thickener[61]
agarose	cell carrier[62]
amylose/amylopectin[63]	food
collagen	medicine and food[64]

Table 4-1: Fields of application of cryotropic gelation processes and materials based on polymeric cryogels.

In the present work, porous structures were obtained by lyophilization. For the development of different porous hydrogels, a special designed cryo-unit was applied. The setup, as depicted in figure 3-22 (chapter 3), enabled us to vary different parameters during the cryogenic treatment: cooling rate, temperature gradient and final freezing temperature. In addition, also the effect of the gelatin concentration on the material properties was studied. The materials were analyzed for their pore size, pore geometry and their overall porosity by µ-CT, He-pycnometry, SEM and optical microscopy. Both µ-CT and SEM have been widely applied before for evaluating porous, 3D scaffolds.[7, 19, 65, 66]

2.4 Procedure in order to avoid skin formation

We noticed by SEM of freeze-dried scaffolds of cryogenically treated hydrogels, that the treatment resulted in the formation of hydrogels with a less porous skin with a thickness of 100-200 µm (figure 4-5). The latter is a problem for cell ingrowth studies. Therefore, a simple and novel technique enabling the elimination of skin formation was elaborated. The hydrogels, prepared as described above (§ 2.1), were coated on top and bottom side by a 0.5 mm thick layer of uncrosslinked gelatin. After cryogenic treatment, the uncrosslinked top and bottom layers were dissolved by incubation in water (40°C, 5 hours).

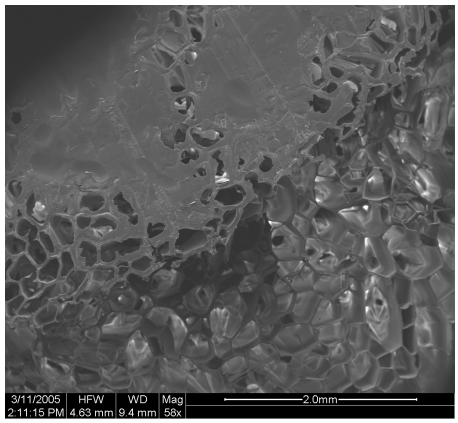

Figure 4-5: Skin formation on lyophilized scaffolds, visualized by SEM.

Microscopic analysis of freeze-sections (cross-sections) of hydrogel scaffolds, incubated at 37°C, clearly demonstrated that this approach allowed to avoid the problem of skin formation (figure 4-6). This procedure was then adapted as standard treatment in the preparation of all cryogenic hydrogels described in this work.

Hydrogel with skin **Hydrogel without skin**

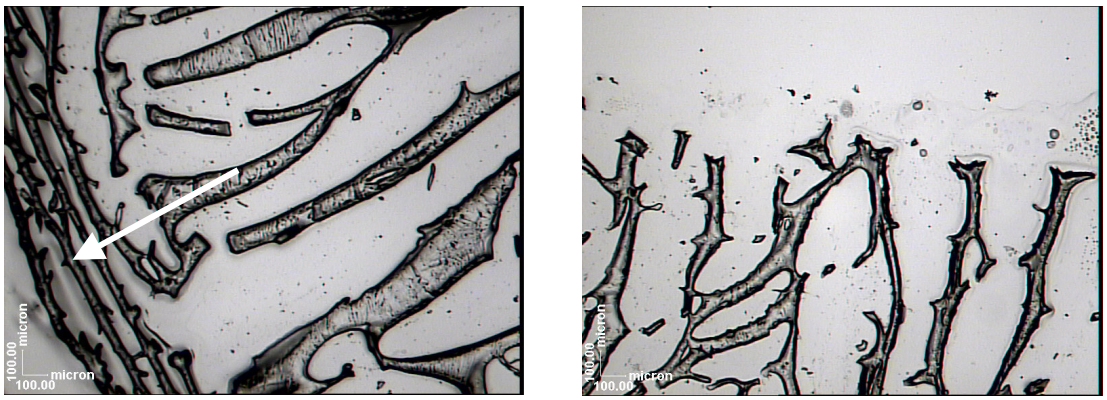

Figure 4-6: Optical microscopy visualisation of hydrogel freeze sections obtained using a microtome. The left and right panel represent a hydrogel respectively with and without a non porous skin. The skin present on the left hydrogel is indicated by the white arrow. The scale bars represent 100 µm.

3 Characterization of the porous scaffolds

3.1 Techniques

3.1.1 Micro-computed tomography (µCT)

Radiography is the recording of a shadow image of an optically opaque object, using penetrating radiation and a recording medium.[67]

Tomography is an extension of radiography. In general terms, it is a non-destructive technique to investigate the inner structure of an object in 3D. Basically, the 3D object is reconstructed, based on a set of 2D projections (or radiographies), taken from different angles by rotating the sample around a defined axis (figure 4-7).[68] The original mathematical framework was developed by Radon in 1917. It provided the solution for the reconstruction of a distribution of a given parameter based on its projections, taken with a parallel beam of penetrating radiation.[67]

More recently, X-ray tomography has become an important technique for non-destructive testing in various research fields, such as biology, geology, archaeology, industry, etc.[69] Over the years, the resolution of CT imaging systems has steadily improved. Modern medical scanners now have a resolution of a few hundred

microns. The reason for this limitation is the fact that for medical purposes the radiation dose has to be as low as possible and the radiation energy is generally limited to about 100 keV, resulting in relatively large detector elements. Non-medical devices do not suffer from dose or energy restrictions. Resolving powers below 1 micron have already been achieved.[67]

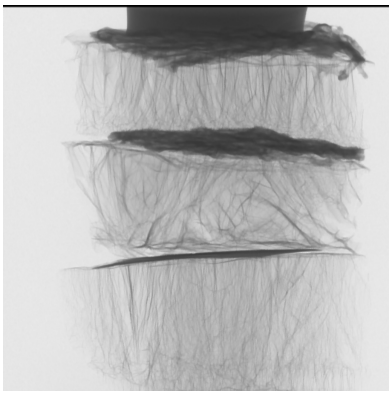

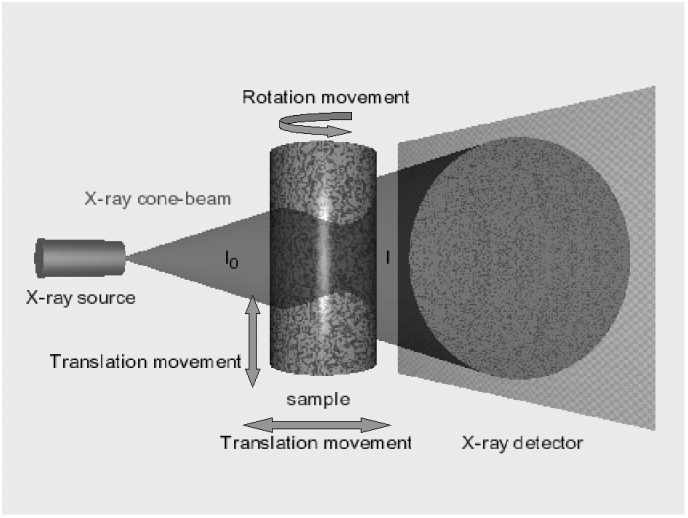

Figure 4-7: Overview of µ-CT setup.

In the present study, a "Skyscan 1072" X-ray micro-tomograph was used. This compact desktop system, consisting of an X-ray shadow microscopic system and a computer with tomographic reconstruction software, generates high-resolution images for small samples (7 mm diameter). During a measurement, both the X-ray source and the detector are fixed while the sample rotates around a stable vertical axis (figure 4-7). Random movement and multiple-frame averaging were used to minimise the Poisson noise in the images. The spot size of the Hamamatsu micro-focus tube limits the spatial resolution of the reconstructed slices to 10 µm in the X, Y and Z directions. During acquisition, X-ray radiographs are recorded at different angles during step-wise rotation between 0° and 180° around the vertical axis. The attenuation of the X-rays passing through a sample when scanning is performed, depends on the atomic number of the material and its density. These two features are crucial in the resulting contrast of the images.

After reconstruction of the 2D cross-sections, 3D software µCTanalySIS was used in order to segment the images and determine their 3D porosity and pore size distribution.[70, 71] For the determination of the pore size distribution, each pore was filled with the largest sphere possible (the so-called 'maximum opening'). The total

volume filled by this maximum sphere, was determined during the analysis. Subsequently, the software filled the total volume of each pore with a smaller sphere, while its total filling volume was determined. This process continued until the total volume of each pore was comprised with the smallest inscribed sphere, with a size of one voxel (figure 4-8). From this analysis, data of all pores were acquired.

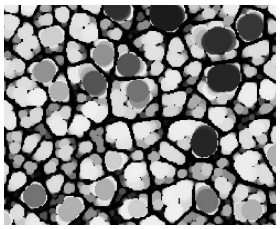

Figure 4-8: Principle of the pore analysis performed by µCTanalySIS.

Another software program (Octopus), was also used to analyse certain images and to show the similarity with micrographs generated using SEM.[72, 73] Octopus is a server/client tomography reconstruction package for parallel and cone beam geometry.

3.1.2 Helium pycnometry

A pycnometer allows to measure the volume and the density of solid objects in a non-destructive manner. The latter is accomplished by employing Archimedes' principle of fluid displacement and Boyle's law of volume-pressure relationships respectively for liquid and gas pycnometers.[74] Archimedes' principle is that an object totally or partially immersed in a fluid, is lifted up by a force, equal to the weight of the fluid that is displaced.

Ideally, a gas is used as the displacing fluid since it penetrates the finest pores, allowing maximum accuracy. That is why helium is used preferentially, since its small atomic dimension enables entry into pores approaching one Ängström (10^{-10} m). Its behaviour as an ideal gas is also desirable. Other gases such as nitrogen could also be used, often with no measurable differences.

In the present work, a 'constant-volume' gas pycnometer was used (figure 4-9).[75] The latter is composed of a sample chamber, a tank and an absolute pressure transducer, which is positioned in a thermostatically controlled environment.

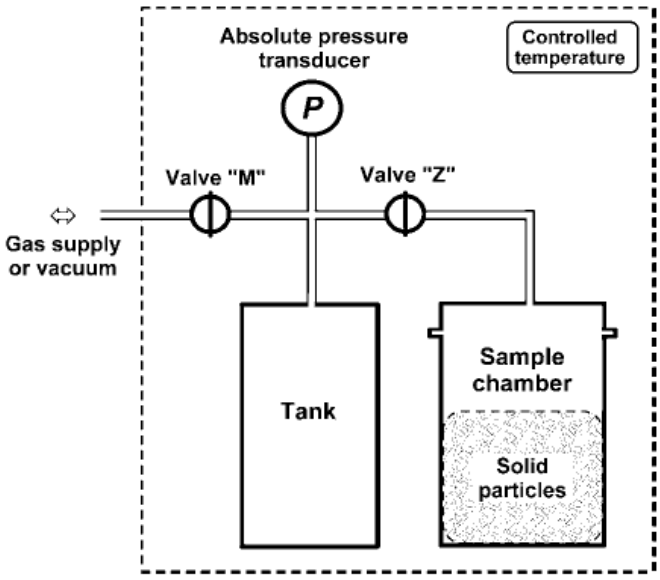

Figure 4-9: Diagram of a constant-volume gas pycnometer.

In order to determine the volume of a sample, the following procedure is applied:

1. the sample is positioned in the sample chamber
2. valves 'Z' and 'M' are opened and the pycnometer is filled with gas
3. valve 'M' is closed and the absolute pressure transducer is used to measure the initial gas pressure in the pycnometer (P_i)
4. valve 'Z' is closed to isolate the sample chamber
5. valve 'M' is opened and some gas is introduced into the tank (or removed from it)
6. valve 'M' is closed again and the gas pressure into the tank is measured (P_j)
7. valve 'Z' is opened so that the gas can expand from the tank to the sample chamber (or vice versa)
8. the final gas pressure is measured (P_f) when the gas expansion is finished

Based on the hypotheses that the gas behaves ideally and that the expanding gas quickly reaches equilibrium, the following equation can be deduced:

$$V_s = V_c + V_t (P_f - P_j) / (P_f - P_i)$$

with V_s = sample volume

V_c = sample chamber volume

V_t = tank (i.e. reservoir) volume

Pycnometers are used for research and quality control in a broad application field, such as ceramics, petrochemicals, fibers, pharmaceuticals, cosmetics, etc.[76, 77]

3.1.3 Dynamic Vapour Sorption Analysis

A dynamic vapour sorption (DVS) apparatus regulates the temperature and humidity of the environment surrounding a sample, allowing any weight changes in a sample due to sorption or desorption of water vapour to be accurately measured (figure 4-10).

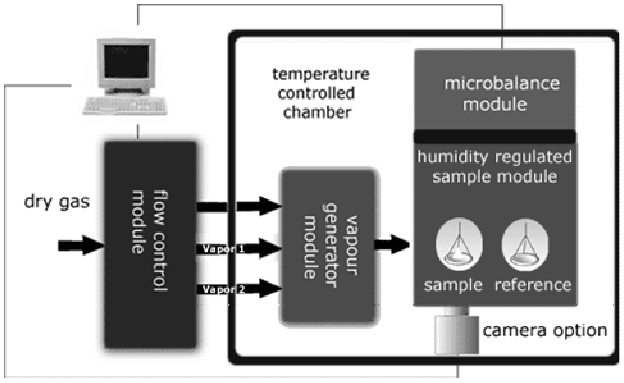

Figure 4-10: Overview of the dynamic vapour sorption apparatus.

The DVS utilizes a dry carrier gas (i.e. nitrogen). Precise control of the ratio of saturated and dry carrier gas flows is enabled with mass flow control. Samples can be subjected to a controlled cycle of changing relative humidity, beginning with an initial drying phase at 0% relative humidity. Mass changes can be measured by means of a recording ultra-microbalance, which measures the weight change caused by sorption or desorption of the vapour molecule.

A DVS is a valuable tool to measure sorption/desorption isotherms and kinetics, surface energies, diffusion coefficients, amorphous content in polymers, etc. It is often used for the analysis of pharmaceuticals[78], food components[79] and polymers[80, 81].

3.2 Influence of parameter variations on the pore size and porosity

3.2.1 Influence of the gelatin concentration

As a first variable for the preparation of hydrogels, the gelatin concentration (expressed as w/v%) was varied. The conditions used for the hydrogel preparation, as well as the pore analysis data obtained using µ-CT, He-pycnometry and SEM are listed in table 4-2. The pore size of hydrogel types GI_a and GI_c, as visualized by µ-CT and SEM analysis are shown in figure 4-11.

Sample	Type GI_a	Type GI_b	Type GI_c
Gelatin concentration	**5 w/v%**	**10 w/v%**	**15 w/v%**
Cooling rate	0.15°C/min	0.15°C/min	0.15°C/min
Final freezing temperature	-30°C	-30°C	-30°C
Temperature gradient	0°C	0°C	0°C
Porosity (µ-CT)	86 ± 0.68%	83 ± 2.63%	82 ± 1.33%
Average pore diameter (µ-CT)	160 µm	135 µm	105 µm
Average pore diameter (SEM)	147 ± 41 µm	117 ± 37 µm	70 ± 24 µm
Porosity (Pycnometry)	96 ± 0.4%	91 ± 0.7%	78 ± 0.6%

Table 4-2: Experimental parameters and pore analysis data of scaffolds type GI_a, GI_b and GI_c.

From the results, it can be concluded that both the porosity and the pore size decreased with an increasing amount of gelatin. There are two possible explanations for the observed findings.

First, a higher gelatin concentration could result in an increasing nucleation rate and thus in a larger number of pores. Nucleation depends on the instability of the liquid phase and on the diffusion of atoms into clusters. The former increases with decreasing temperature, the latter increases with increasing temperatures. A higher gelatin concentration resulted in a decrease of the freezing temperature of the solvent (in this case water). As a consequence, the mobility of the atoms to diffuse into clusters was higher and the nucleation rate increased.

Secondly, comparing the 5-15 w/v% scaffolds, the more concentrated hydrogels could possess a decreased heat and protein transfer and thus result in smaller pores. A combination of both is most likely the most plausible explanation.

The pore sizes, measured using SEM were somewhat lower than the pore sizes obtained using µ-CT (table 4-2, figure 4-11). This is due to the fact that, in the case of µ-CT, pore diameters are calculated based on the amount of pixels present on the pore diameter. Thus, when taking into account the pixels of the pore wall itself, the pore size obtained will be at least 20 µm higher (since one pixel corresponded with 10 µm), depending on the pore wall thickness.

A combination of different techniques, both with its advantages and disadvantages (destructive (SEM) versus non-destructive (µ-CT), objective (SEM) versus subjective (choice of thresholding parameters using µ-CT), 100 nm resolution (SEM) versus 10 µm resolution (µ-CT), 2-D (SEM) versus 3-D imaging (µ-CT)), is thus essential to obtain a complete material analysis.

The difference in porosity between the scaffolds was studied by He-pycnometry and µ-CT analysis. The µ-CT data showed a smaller variation between the porosities of the samples compared to pycnometry-measurements (table 4-2). In our opinion, the porosities obtained from pycnometry experiments are more realistic. The latter technique is not limited to a resolution of 10 µm since it is based on the intrusion of helium in the porous scaffolds. In the present work, we have selected the µ-CT

tresholding parameters in such a way that no scaffold material was excluded. The disadvantage of the latter approach was that some noise voxels were then considered as material, leading to a lower decrease in porosity. The higher porosity of the 5 w/v% gelatin compared to the 15 w/v% gelatin, is clearly illustrated in figure 4-11 (first and second row).

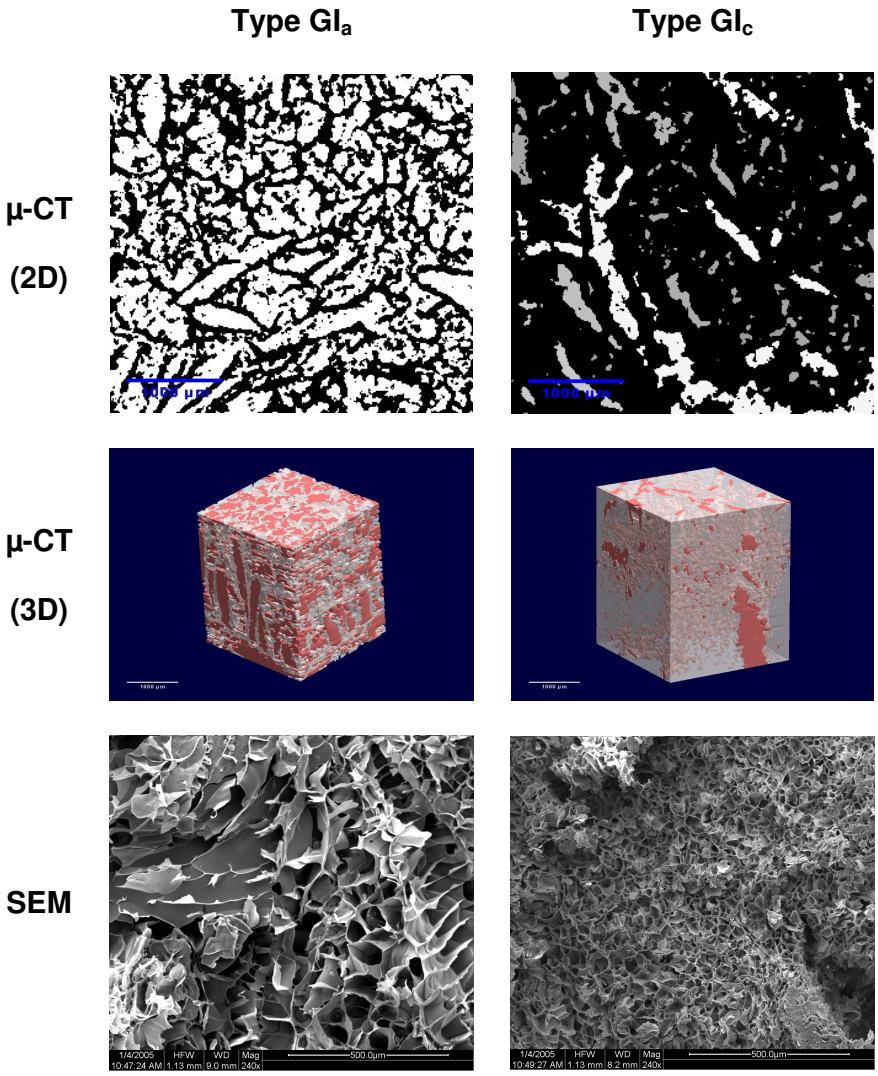

Figure 4-11: µ-CT (2D and 3D) and SEM analysis of the 5 w/v% (Type GI$_a$) and the 15 w/v% gelatin (Type GI$_c$). For the µ-CT (3D) pictures, the pores are coloured red and the material is grey transparent. The scale bars represent 1000 µm (µ-CT) and 500 µm (SEM).

An important prerequisite for a scaffold to be applied as a biomaterial is the fact that the material should possess interconnecting pores. Pore interconnectivity can be studied by µ-CT.

To analyse the reconstructed images, double thresholding based on the greyvalue histogram of the images, had to be performed using µCTanalySIS.[68] After thresholding, each pore detected inside the binary images was labelled and analysed in 3D. Based on the maximum opening of each pore, the binary images were then rewritten, labelling each pore with a certain greyvalue corresponding to a certain maximum opening. The grey value of a pore in the 2-D segmentations (figure 4-11, top row) indicated the diameter of the largest inscribed sphere in the concerning pore network. Figure 4-11 illustrates two cross-sections after analysis with µCTanalySIS. A low contrast between the material borders and the pores, in combination with small amounts of noise, containing similar greyvalues as the material borders, led to small errors in the resulting thresholded images. Figure 4-11 (top left) suggested that the pores of the 5 w/v% scaffold were interconnecting. The complete pore network was labelled in white, thus either belonging to the same pore network or belonging to different pore networks with the same maximum opening. In the 15 w/v% gelatin (figure 4-11, top right) more individual pores were detected, each belonging to a different pore network.

3.2.2 Influence of the cooling rate

In addition to the gelatin concentration, the cooling rate of the gelatin solution was also varied. Literature data describes the influence of the cooling rate on the nucleation and growth of ice crystals and thus on the resulting pore size.[10-14] In most studies, the samples were incubated in a freezer for several hours at different temperatures. These studies indicated that the pore size decreased with a decreasing freezing temperature.[10, 12, 13] Whether the underlying cause of this phenomenon was the actual final freezing temperature, the cooling rate, or a combination of both has never been studied before. The present work demonstrates that the underlying cause is actually the phenomenon of undercooling. In another publication, a complex setup was used to control the cooling rate of a collagen solution.[11] In that study, it was shown that the pore size in collagen matrices decreased with an increasing cooling rate.

Our study aimed to implement a procedure to examine the effect of the cooling rate on the pore size and morphology in gelatin scaffolds. The experimental conditions applied in the present work and the results obtained are summarized in table 4-3. For these experiments, a gelatin concentration of 10 w/v% was selected.

Sample	Type GI_b	Type GII_b
Gelatin concentration	10 w/v%	10 w/v%
Cooling rate	**0.15°C/min**	**0.83°C/min**
Final temperature of freezing	-30°C	-30°C
Temperature gradient	0	0
Porosity (µ-CT)	83 ± 2.63%	84 ± 1.73%
Average pore diameter (µ-CT)	135 µm	65 µm
Average pore diameter (SEM)	117 ± 37 µm	48 ± 6 µm
Porosity (Pycnometry)	91 ± 0.7%	89 ± 3%

Table 4-3: Experimental parameters and pore data of matrices type GI_b and GII_b.

Summarising the results (table 4-3), it can be concluded that a decrease of the cooling rate from 0.83°C/min to 0.15°C/min resulted in an increase in average pore diameter from 65 µm to 135 µm. The difference in median pore size between the rapidly and the slowly cooled gelatin, as analysed by µ-CT and SEM, is shown in figure 4-12. Thus, the slower the cooling rate, the lower the undercooling (difference between the freezing temperature and the actual temperature of the material) and the nucleation rate and the higher the rate of heat and protein transfer. This leads to a lower amount of large pores.[10]

The porosity of both types of hydrogels were identical as shown by µ-CT and He-pycnometry. Again, the porosity values, obtained by µ-CT, were lower compared to He-pycnometry (respectively ±80% versus ±90%).

From figure 4-12 (top row), it can also be concluded that the pore interconnectivity was not influenced by the cooling rate. The pores of both types of hydrogels were interconnected, since all pores were labelled in white after performing a 3-D analysis. A 3-D image of the rapidly cooled gelatin (figure 4-12, centre right), visualized very

clearly a central sample region where the porosity decreased. This corresponded with the zone where the two cooling surfaces (started from top and bottom of the sample) coincide. A plausible explanation for the observation that the pore diameters in the central region are smaller is a decreased heat and protein transfer. Ice crystals are normally formed in the direction of heat transfer.[82] Since the resolution of the µ-CT technique is 10 µm, small pores in the central region were not detected, giving rise to a local decrease in porosity (data not shown).

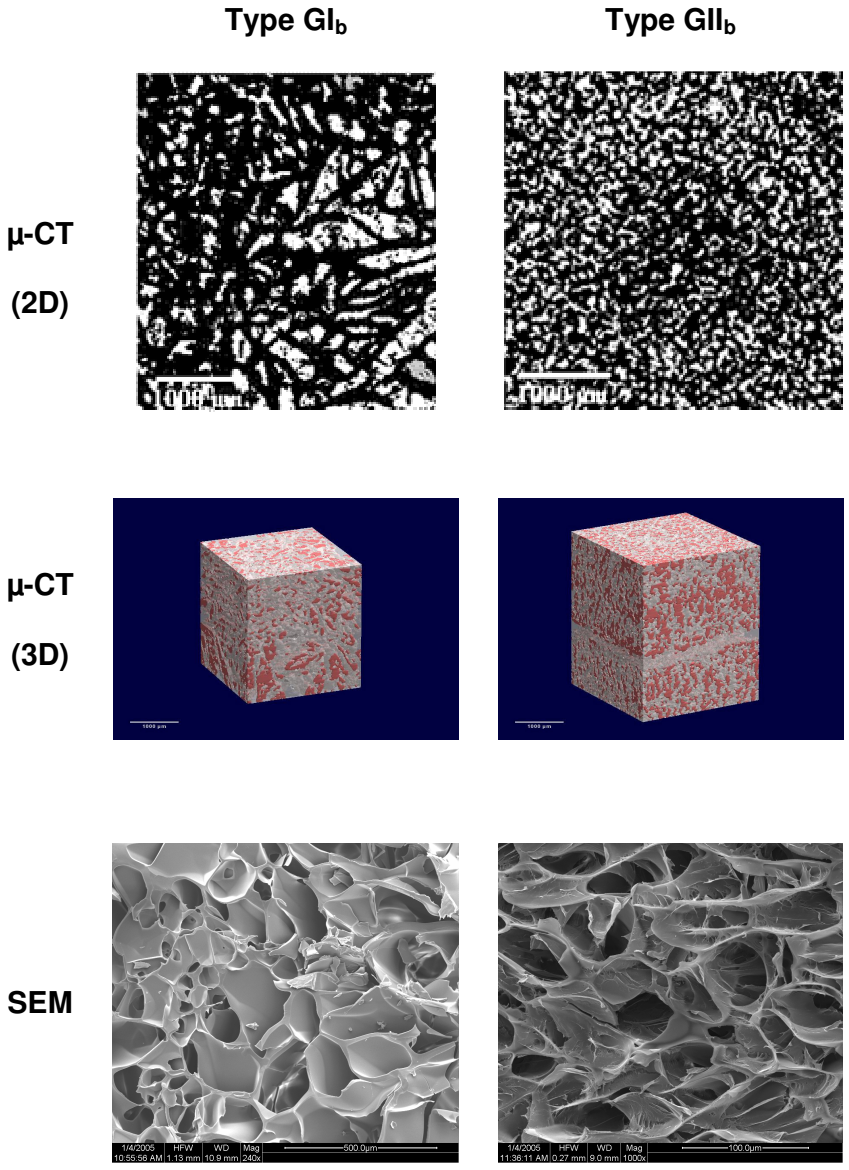

Figure 4-12: Images of the rapidly cooled gelatin (Type GII_b) and the slowly cooled gelatin (Type GI_b), obtained using µ-CT and SEM. The scale bars represent 1000 µm (µ-CT), 100 µm and 500 µm (SEM).

The 3-D reconstruction for the slowly cooled hydrogel type was similar compared to the rapidly cooled gelatin, except that no zone was observed where the porosity decreased (figure 4-12, centre left). Probably, the effect of the coinciding cooling surfaces on the pore structure is more pronounced for the rapidly cooled scaffold, since the undercooling is higher in the latter case.

3.2.3 Effect of applying a temperature gradient

Using the cryogenic unit, developed in our laboratory (figure 3-22, chapter 3), it was also possible to establish a temperature gradient between the top and the bottom of the mould during the freezing step. During the applied temperature gradients, the temperature at the top of the mould was the highest. In the present work, two gradients were applied and compared (10°C and 30°C). The results are summarized in table 4-4.

Sample	Type GIV_b	Type $GIII_b$
Gelatin concentration	10 w/v%	10 w/v%
Cooling rate	0.15°C/min	0.15°C/min
Final freezing temperature	-30°C	-30°C
Temperature gradient	**10°C**	**30°C**
Porosity (µ-CT)	76 ± 4.67%	75 ± 3.54%
Average pore diameter top	116 µm	330 µm
(µ-CT) bottom	20-30 µm	20-30 µm
Average pore diameter (SEM)	96 ± 10 µm	283 ± 48 µm
Porosity (Pycnometry)	92 ± 1.4%	94 ± 0.2%

Table 4-4: Experimental parameters and pore analysis data of the low (type GIV_b) and high (Type $GIII_b$) gradient scaffolds.

From the data in table 4-4 and figure 4-13, it can be concluded that the high temperature gradient (ΔT = 30°C) resulted in a pore size gradient throughout the scaffold. The pore morphology of the hydrogel is shown in the 3-D µ-CT reconstruction and the SEM picture in figure 4-13 (top right and bottom right picture).

The pictures clearly indicate the presence of transversal pore channels in the direction of heat transfer. From the data (table 4-4), it can be concluded that the pore size decreased from 330 µm to 20-30 µm when moving through the scaffold from top to bottom. The smallest pores were formed at the side exposed to the lowest temperature (i.e. the bottom of the mould). As discussed in § 3.2.1, this is related to an increased nucleation and reduced heat and protein transfer phenomena.

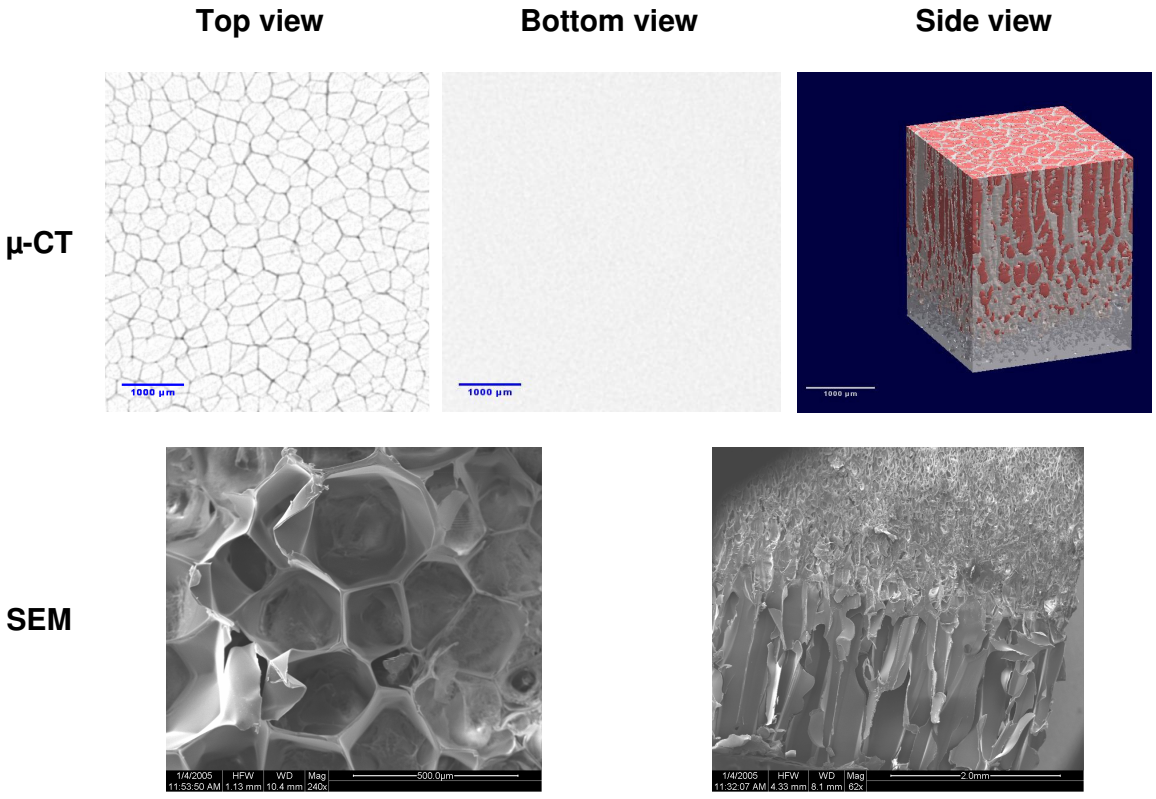

Figure 4-13: µ-CT and SEM analysis of the top, the bottom and the side of the scaffold exposed to a temperature gradient of 30°C (type GIII$_b$). The scale bars represent 1000 µm (µ-CT), 500 µm and 2 mm (SEM).

The applied temperature gradient also resulted in a decrease in porosity, when moving from top to bottom of the scaffold, from 82% to 61%.

When applying a temperature gradient of 10°C, the effect on the pore size and the porosity was less pronounced compared to the high temperature (30°C) gradient. The pore size decreased from top (116 µm) to bottom (20-30 µm) without altering the porosity. A few cracks were visualized both in the 3-D reconstruction and the SEM image (figure 4-14, right), which resulted in a local increase of the porosity.

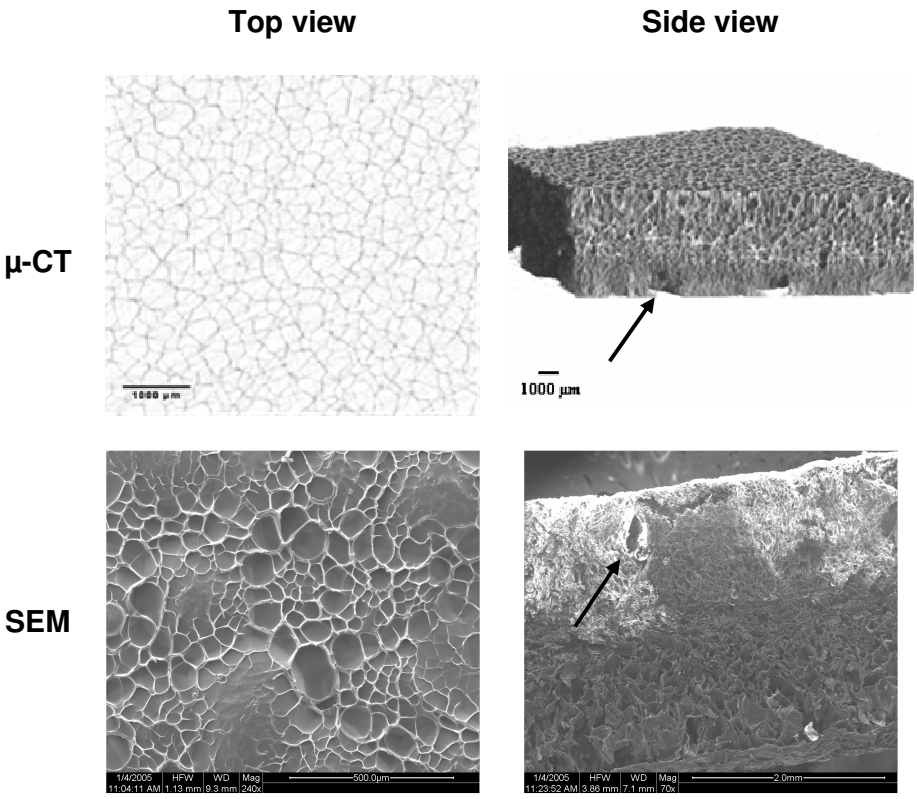

Figure 4-14: Top views and side views of the low gradient scaffold (type GIV_b) obtained using µ-CT and SEM. The scale bars represent 1000 µm (µ-CT), 500 µm and 2000 µm (SEM). A crack present in the scaffold is indicated with an arrow.

In contrast to the pore size, the porosity of the materials was not affected by the applied temperature gradient. The porosity of both scaffolds, as measured by µ-CT and He-pycnometry was in the range of 75% and 90% respectively (table 4-4). The porosities for both types of hydrogels, were similar since the same amount of water was removed through lyophilization. In our opinion, this is the first time that porous gelatin hydrogels were prepared by applying a controlled temperature gradient during the freezing step. This enabled us to develop porous materials containing a pore morphology and pore size that can be fine-tuned by the cryogenic parameters.

Up to now, pore size gradients were created by the spatial arrangement of porogen size. Porous silk gradient systems, for example, were obtained by arranging the porogens from smallest to largest size in a container. After adding the silk solution and removing the solvent, the porogens were dissolved, creating a scaffold with a pore gradient system.[18] The latter approach, however, is rather labour intensive and impractical, consequently the cryo-approach, utilized in the present work, could be used as an interesting alternative.

3.2.4 Influence of final freezing temperature

As a last cryo-parameter, we varied the final freezing temperature (-10°C versus -30°C) while keeping the cooling rate constant (0.2°C/min). The results, as shown in table 4-5, indicated that the final freezing temperature did not significantly influence the hydrogel pore size and porosity.

Sample	Type GV_b	Type GVI_b
Gelatin concentration	10 w/v%	10 w/v%
Cooling rate	0.2°C/min	0.2°C/min
Final temperature of freezing	**-10°C**	**-30°C**
Temperature gradient	0°C	0°C
Porosity (µ-CT)	85 ± 3.67%	83 ± 2.65%
Average pore diameter (µ-CT)	138 µm	147 µm
Average pore diameter (SEM)	181 ± 60 µm	182 ± 47 µm
Porosity (Pycnometer)	92 ± 2%	89 ± 0.9%

Table 4-5: Experimental parameters and pore data of hydrogels type GV_b and type GVI_b.

The pores were homogeneously distributed in the scaffold that was treated cryogenically to a final freezing temperature of -10°C, as shown in figure 4-15. Similar results were obtained for the hydrogel that was cooled to -30°C (data not shown).

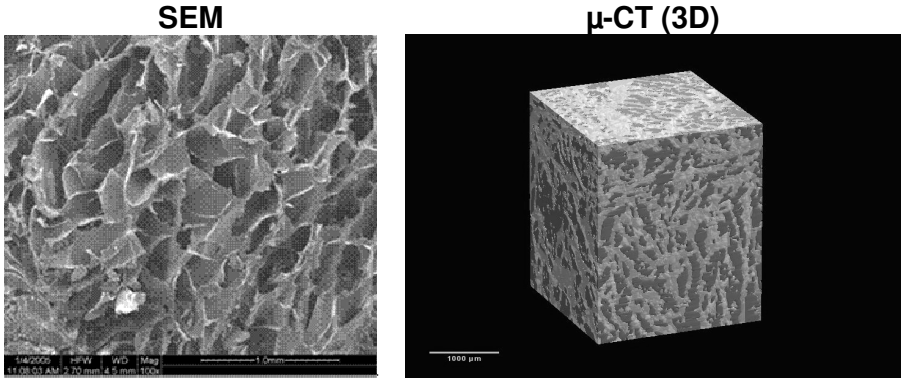

Figure 4-15: Effect of final freezing temperature on the scaffold structure as visualized by µ-CT and SEM. The structures represent the gelatin scaffold using a final freezing temperature of -10°C (Type GV_b). The scale bars represent 1000 µm.

The data indicate that, of all the parameters varied, the gelatin concentration, the cooling rate and the applied temperature gradient have the largest effect on the pore size and geometry. The final freezing temperature has a negligible effect.
The gelatin concentration, the cooling rate and the temperature gradient affect the pore diameter, whereas the pore geometry and the overall porosity depend mostly on the applied temperature gradient and the gelatin concentration respectively.

3.3 Study of physico-chemical properties of scaffolds developed

Next, a detailed study was performed on the correlation between the cryogenic parameters applied and the physico-chemical properties of the materials. This is relevant since a clear correlation between the structure and the physico-chemical properties of different types of hydrogels was reported before.[28, 83] Lee reported on porous scaffolds composed of gelatin and β-glucan as a wound dressing.[6] The average pore size was in the range of 90-150 µm and the swelling capacity of the material increased with decreasing pore size/porosity. The latter was due to a decrease in gelatin/β-glucan ratio. In contrast to those results, Kang found that the water uptake of porous gelatin matrices increased with an increasing pore size.[84] Another group reported on a scaffold concentration dependant maximum in water absorption of chitosan-gelatin scaffolds.[85]

These contradictory results indicated the need to perform a study to establish the relation between the pore size and the overall porosity of gelatin scaffolds and their water uptake. In addition, possible effects of the pore-inducing method (i.e. cryogenic treatment) on the mechanical properties were also considered. As a last part of the structure/properties relation, the effect of the porous structure on the *in vitro* degradation in the presence of collagenase was studied.

Hydrogel Type	Pore size (porosity)			Pore morphology
	5 w/v %(a)	10 w/v %(b)	15 w/v %(c)	
GIII	–	330 → 20 µm (94%)	–	cone, pore size decreasing from top to bottom
GI	160 µm (96%)	135 µm (91%)	105 µm (78%)	spherical, uniform pore size throughout entire scaffold
GII	–	65 µm (89%)	–	spherical, uniform pore size throughout entire scaffold

Table 4-6: Summary of the hydrogel characteristics (pore size, pore morphology and porosity) of the developed hydrogels as studied by µ-CT (pore size and morphology) and He-pycnometry (porosity).

The physico-chemical evaluation of a series of porous gelatin cryogels to be applied in the field of tissue engineering was performed. Hydrogels with varying pore size, pore geometry and porosity were prepared as reported earlier (§ 3.2) and compared in terms of their physico-chemical properties including swelling, water vapour uptake, mechanical properties and *in vitro* degradation behaviour. A summary of the materials included in this study, as well as their pore size/morphology characteristics are summarised in table 4-6. Type GIII hydrogels contain top bottom transversal channels with a decreasing pore size from top to bottom (330-20 µm). Type GI and type GII scaffolds contain spherical pores in the range from 65-160 µm, depending on the freezing parameters and the gelatin concentration applied.

3.3.1 Water uptake capacity

Since the developed scaffolds are intended to be used as cell carriers for tissue engineering applications, it is important to study the swelling capacity of the hydrogels. Therefore, the different scaffold types developed were immersed in double distilled water at 37°C. At regular time points, the swelling degree of the hydrogels was determined.

The pictures in figure 4-16 represent type $GIII_b$ hydrogels at different immersion times (0 minutes, 15 minutes and 1 day). The maximum swelling (equilibrium swelling) was obtained after 1 day. The volume increase of the hydrogels during swelling was rather limited (14% swelling).

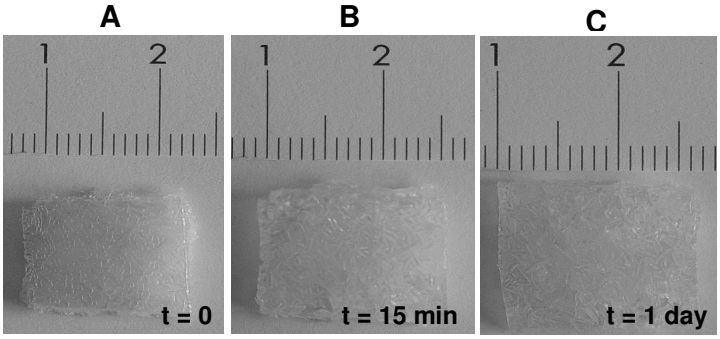

Figure 4-16: Type GIII$_b$ hydrogels (10 w/v%) in dry state (part A), after 15 minutes immersion in double distilled water at 37°C (part B) and at equilibrium swelling (1 day, part C).

As a first parameter, the influence of the gelatin concentration on the swelling capacity was investigated by immersing type GI scaffolds with varying w/v % (5, 10 and 15 w/v %) in water. From the obtained results (figure 4-17), it can be concluded that the swelling ratio decreases with increasing gelatin concentration. The gelatin concentration affects two parameters of the hydrogel. First, the gelatin concentration is related to the degree of cross-linking. The higher the w/v % gelatin, the higher the amount of cross-linkable groups and the lower the swelling ratio of the resulting hydrogel.[86-89] Secondly, the gelatin concentration affects the porosity (table 4-6). The higher the w/v % gelatin, the lower the porosity and thus the lower the swelling ratio. Both effects are thus synergistic.

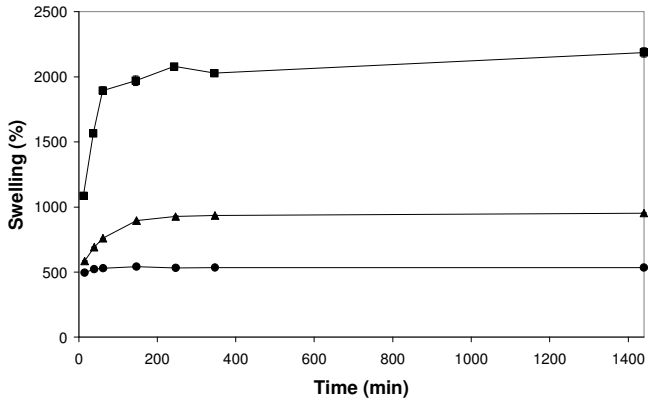

Figure 4-17: Swelling ratio as a function of time for type GI scaffolds with gelatin concentrations of 5 w/v% (■), 10 w/v% (▲) and 15 w/v% (●).

In addition to the effect of the gelatin concentration, a possible effect of the pore size and pore geometry on the water uptake was also investigated. Type GI_b, GII_b and $GIII_b$ hydrogels were immersed in water and the swelling ratios were determined at regular time points. The results, shown in figure 4-18, demonstrate that type $GIII_b$ hydrogels possessed the highest degree of swelling. This can be attributed to the pore geometry and pore size of type $GIII_b$ scaffolds, consisting of top-bottom honeycomb structured pores with a diameter decreasing from 330 µm to 20-30 µm when moving from top to the bottom of the scaffold.[73] This pore geometry (i.e. channel) thus clearly facilitates the water uptake, resulting in a higher degree of swelling.

Next to the effect of the pore geometry, a possible influence of the pore size on the swelling properties was also investigated. Since type GI_b hydrogels possess larger pores compared to type GII_b scaffolds (135 versus 65 µm), a reduced water uptake capacity for type GII_b hydrogels was anticipated. However, the water uptake at equilibrium was similar for both systems (figure 4-18 and inset). This can most likely be ascribed to two counterbalancing effects. A smaller pore size indeed leads to a lower swelling degree for type GII_b hydrogels. However, the faster cooling applied for preparing GII_b hydrogels, results in less gelatin chain entanglements, giving rise to a lower degree of physical cross linking. The latter results in a higher water uptake capacity for type GII_b hydrogels.[90] Due to these counterbalancing effects, both scaffolds possess a similar swelling degree.

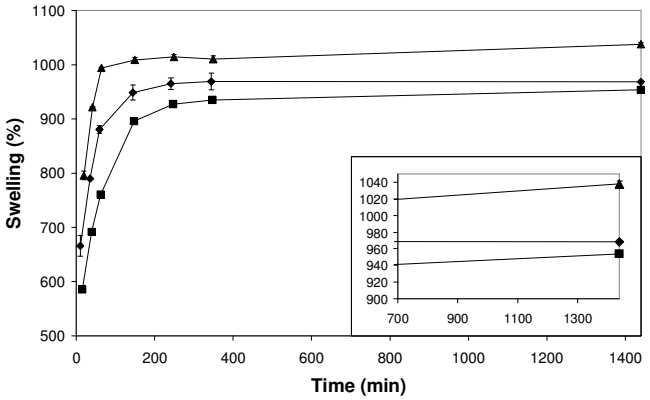

Figure 4-18: Degree of swelling as a function of time for 10 w/v% hydrogels type $GIII_b$ (▲), type GI_b (■) and type GII_b (◆).

Similar results were obtained for the 5 and 15 w/v% hydrogels (data not shown).

For some applications, not only the swelling capacity is important, but also the swelling rate can influence the applicability of materials. For certain *in vivo* applications, knowledge of the swelling rate is important since it provides information on how quick a certain defect can be filled during or after a surgical procedure.[91] Therefore, the **swelling kinetics** of the hydrogels developed, were also investigated.
Although the change in swelling rate rapidly decreases over time for all hydrogels developed (see figures 4-17 and 4-18), the experimental data could not be fitted using simple power law expressions. A suitable alternative was provided by the Voigt model, which consists of a spring and a dashpot in parallel (figure 4-19).[92-94] The spring and dashpot respectively provide the immediate elastic and delayed viscous strain responses to an externally applied stress. Any number of arrangements of these elements can be applied to simulate a particular kind of time dependence. In molecular terms, the elastic responses are the fast, reversible changes in bond length, shape and orientation which occur when stress is applied to a polymer chain. The viscous responses are the slower, irreversible, energy dissipating processes which occur as a result of the molecular movements.

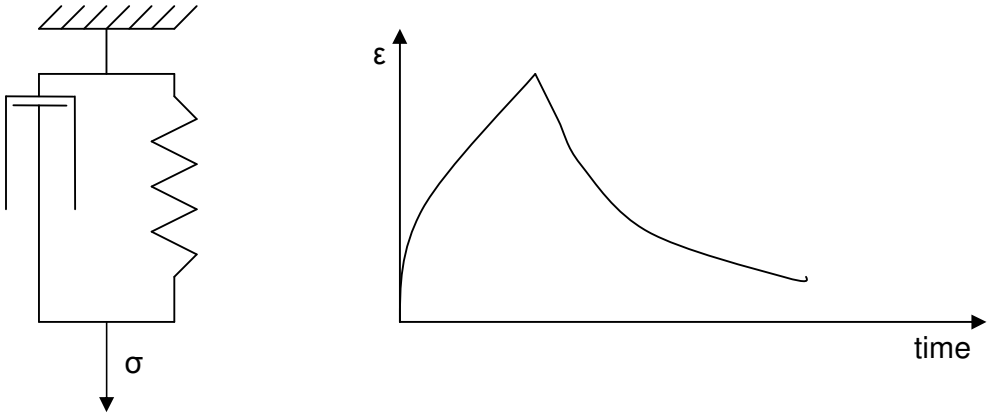

Figure 4-19: Elongation of a Voigt-element as a function of time.

In this case, there is no externally applied stress. Instead, stress is exerted on the gelatin network by interaction with water.
When a stress σ_0 is applied at time t_0, the strain response ε of the model with Young's modulus E is given at time t by the following expression:

$$\varepsilon(t) = \sigma_0/E[1-\exp\{(t_0-t)/\tau_0\}]$$

where τ_0 is known as the retardation time and determines the influence of the dashpot.[92] The system differs fundamentally from the stretching of a dry rubber in that the volume drastically increases and the number of chain entanglements decreases with time. Consequently, the modulus in the equation mentioned above, cannot have the same significance for absorbents, although Flory referred to an inverse relationship between the equilibrium swelling of a rubber by a solvent and the modulus of the rubber. However, the time dependence of swelling was not discussed.[92]

The experimental swelling data follow a typical exponential relationship which has two characteristic constants, i.e. σ_0/E and τ_0. The quantitative value of the former can be estimated from the values of the steady state swelling of the individual samples, since the water transport is diffusion-controlled.[93] For the latter, minus the reciprocal value of the slope of the plot of $\ln[1-S_t/S_\infty]$ against time was used (S_∞ is equilibrium or steady state swelling). Since such a plot possesses a typical first order relationship, the slope is a measure of the characteristic time (τ_0) for the individual scaffolds (figure 4-20). The Voigt-based equation can thus be rewritten as follows:[94]

$$S_t = S_e(1-e^{-t/\tau})$$

where S_t is swelling at time t, S_e is equilibrium swelling and τ stands for the rate parameter.

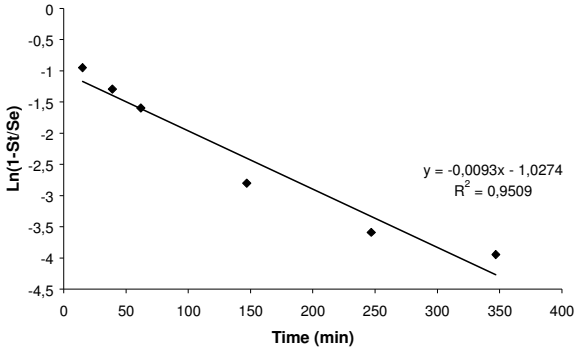

Figure 4-20: Determination of τ as derived from the linear relationship between $\ln[1-S_t/S_\infty]$ and time for type GI_b hydrogels.

Starting from this model, the rate parameter τ for a hydrogel matrix, which is a measure for the swelling rate, can be determined.

The rate parameters of the different scaffold types are shown in table 4-7, clearly indicating that both the gelatin concentration (i.e. the porosity and pore size) and the cryogenic parameters applied (i.e. the pore geometry and the pore size) influence τ. From the results, it can be derived that τ decreases with an increasing gelatin concentration. The latter effect is similar to what was reported earlier for absorbent polymers for which the swelling kinetics were significantly influenced by the particle size of the absorbents.[95] Using these materials, a lower particle size resulted in a higher water uptake rate. Based on these results, an increase in the absorption rate would be expected from the increase in surface area with decreasing particle size of an absorbent. For the hydrogel developed in the present work, this implies that with an increasing surface area (and thus with an increasing gelatin concentration), the rate parameter decreases, as demonstrated in table 4-7. A similar effect was observed changing the cryogenic parameters (i.e. going from type $GIII_b$ to type GII_b hydrogels).

Hydrogel Type	τ (min)	Surface area (m^2/g)
Type $GIII_b$	179	0.010
Type GI_a	182	0.031
Type GI_b	108	0.037
Type GI_c	84	0.048
Type GII_b	52	0.077

Table 4-7: The rate parameters and the surface areas of the gel-MOD hydrogels studied.

Although the swelling behaviour of gelatin-based hydrogels was already described previously by various models, the Voigt-based model, applied before for gelatin-graft-poly(sodium acrylate-co-acrylamide) and acrylic-based polymers, turned out to be the most suitable for the cryogenic treated scaffolds in the present work.[96, 97]

3.3.2 Dynamic vapour sorption analysis

In a first part, the influence of the gelatin concentration on the water vapour uptake was studied at 25°C. Increasing hydrogel masses during sorption were recorded as a function of the relative humidity (table 4-8). The water vapour uptake increased with decreasing gelatin concentration irrespective of the applied humidity. The latter can be attributed to the higher porosity of hydrogels prepared using low gelatin concentration.

Target RH (%)	Mass change (%) during sorption		
	Type GI_a	**Type GI_b**	**Type GI_c**
0	0	0	0
20	7.42	6.60	5.56
40	12.11	11.19	9.92
60	17.41	16.26	14.63
80	28.20	26.97	24.19

Table 4-8: Effect of gelatin concentration on the water vapour sorption of type GI hydrogels. Mass change (%) during sorption is expressed as a function of the relative humidity (RH, %).

Secondly, the effect of the pore geometry and pore size on the water vapour uptake was studied at 25°C at constant gelatin concentration (10 w/v %) (table 4-9). In contrast to what was anticipated, no differences were observed comparing the three hydrogel types. Apparently, the porosity and not the pore geometry nor the pore size, is the most important factor determining the water vapour uptake capacity.

Target RH (%)	Mass change (%) during sorption		
	Type $GIII_b$	**Type GI_b**	**Type GII_b**
0	0	0	0
20	6.36	6.60	6.79
40	10.68	11.19	11.34
60	15.67	16.26	16.26
80	26.39	26.97	26.45

Table 4-9: Effect of pore size and pore morphology on the water vapour sorption of 10 w/v% gel-MOD scaffolds.

Next, samples were also subjected to multiple sorption and desorption cycles (figure 4-21). However, no variation in dynamic vapour sorption profiles was found between the first and the second cycle indicating that the DVS measurements were extremely reproducible.

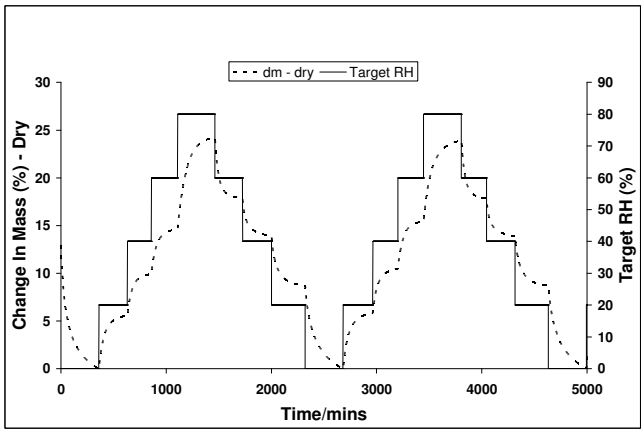

Figure 4-21: Dynamic vapour sorption study of type GI_c hydrogel at 25°C.

Interestingly, differences between sorption and desorption behaviour were observed in the isotherm plots (figure 4-22), clearly demonstrating hysteresis phenomena. This can be attributed to a structural change promoted by the distribution of water molecules among the polymer chains.[98] This plasticization effect limits the desorption of H_2O vapour due to a permanent deformation in the polymeric structure.[99] The role of water in modifying the properties of biopolymers has been studied extensively in the past. The hydration behaviour of proteins is of great relevance since it affects the protein secondary structure formation, as well as the chemical and enzymatic reactivities.[100]

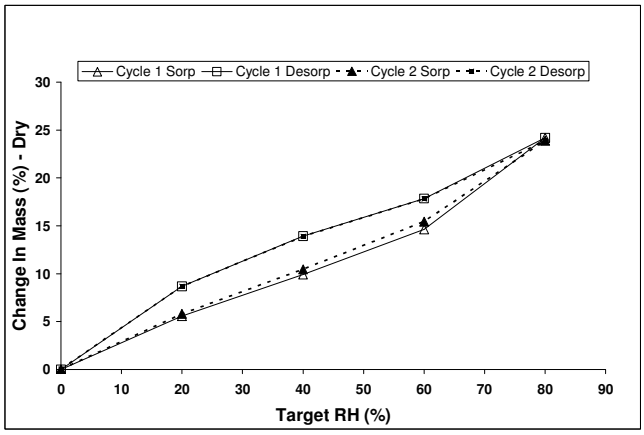

Figure 4-22: Water sorption (-▲-) and water desorption (■) isotherms of a type GI_c scaffold for two consecutive cycles (The open symbols represent the first cycle, the second cycle is represented by the closed symbols) at 25°C.

Finally, the influence of the temperature on the water vapour uptake was studied. From figure 4-23, it can be derived that the moisture uptake decreased with increasing temperature (37°C versus 25°C). The observed decrease can be attributed to the contribution of the physical entanglements, which are not present above the gel/sol temperature (± 30°C).

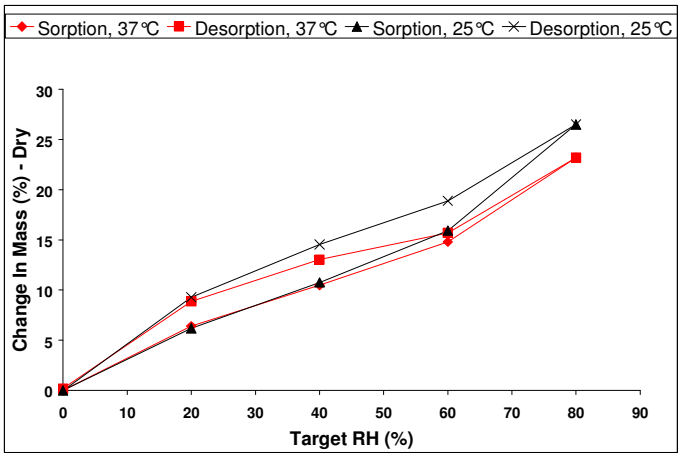

Figure 4-23: Influence of the temperature (25°C versus 37°C) on the water vapour uptake capacity of type $GIII_b$ hydrogels.

3.3.3 Mechanical testing

Irrespective of their final biomaterial application, the hydrogels developed should possess mechanical properties suited for a specific application. Hydrogels, implanted *in vivo* or applied as micro-carrier in a bioreactor are subjected to certain loads.[101, 102] The mechanical properties of the different scaffolds were studied by compression. Using the slope of the initial linear part of the stress-strain curves obtained, the compression moduli were calculated (figure 4-24). It can be concluded that the compression moduli increased with an increasing gelatin concentration. Furthermore, using the type G_b hydrogels we studied possible effect of the pore geometry and pore size on the mechanical properties. Type $GIII_b$ hydrogels possessed the lowest compression modulus ($P < 0.05$). This is due to the geometry of the pores, i.e. aligned parallel to the direction of compression.

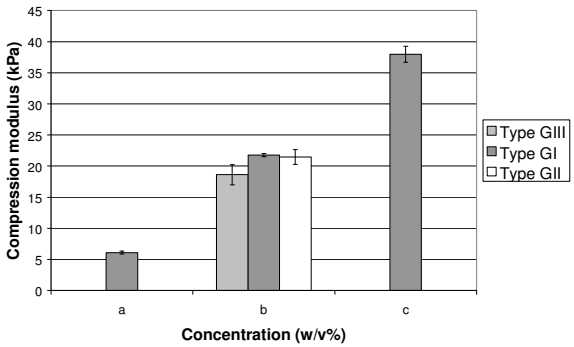

Figure 4-24: Effect of the gelatin concentration and the scaffold type on the compression modulus (20% strain, 21°C).

Comparing type GI_b and GII_b hydrogels, no statistically significant differences in compression moduli were observed (P = 0.46). This is most likely due to the small differences in pore size between type GI_b and GII_b scaffolds (135 versus 65 µm, table 4-6).

When comparing the obtained compression moduli (see figure 4-24) with the mechanical properties of tissues (see table 1-1), it can be concluded that the obtained values are more than a ten-fold lower. The mechanical properties of the hydrogels developed could be improved by for example adding synthetic polymers including polyesters, possessing higher compression moduli. However, this approach was beyond the scope of this PhD work.

3.3.4 Determination of effective network density

The suitability of hydrogels as biomedical materials and their performance in a particular application depend to a large extent on their bulk structure. The most important parameters used to characterize the network structure of hydrogels are the polymer volume fraction in the swollen state ($v_{2,s}$), the molecular weight of the polymer chain between two neighbouring crosslinking points (M_c) and the corresponding mesh size (ξ). These parameters, which are interrelated can be determined through the use of the equilibrium-swelling theory and the rubber-elasticity theory.[103, 104] Since the rubber-elasticity theory is utilized in the present work, a short introduction to the model is presented below.

Rubber elasticity theory

Hydrogels resemble natural rubbers in their remarkable property to elastically respond to applied stresses. A hydrogel, subjected to a relatively small deformation (i.e. less than 20%) will fully and rapidly recover to the original dimensions. This elastic behaviour of hydrogels can be used to elucidate their structure by utilizing the rubber-elasticity theory. Interestingly, rubber-elasticity theory has been used not only to analyze chemically and physically crosslinked hydrogels, but also hydrogels exhibiting temporary crosslinks due to hydrogen bonding.[105]

In the present work, only the form of the rubber-elasticity theory used to analyze the structure of hydrogels prepared in the presence of a solvent is presented. Detailed derivations can be found in literature.[106] The equation correlates the applied stress with the network junctions.

$$\tau = \frac{\rho RT}{M_c}\left(1 - \frac{2M_c}{M_n}\right)\left(\alpha - \frac{1}{\alpha^2}\right)\left(\frac{v_{2,s}}{v_{2,r}}\right)^{1/3}$$

Here, τ is the stress applied to the polymer sample, ρ is the density of the polymer, R is the universal gas constant, T is the absolute experimental temperature and M_c is the molecular weight between crosslinks. The hydrogel structure can thus be investigated using the rubber-elasticity theory, which requires tensile testing experiments to be performed.

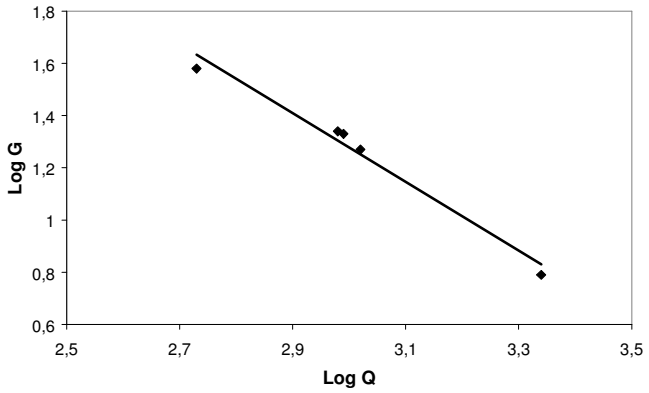

Figure 4-25: Log G versus log Q plot of hydrogel types used in the experiment.

The applicability of the Gaussian model to the hydrogels developed, was investigated by studying a possible linear correlation between the log of the compression modulus (G) and the log of the equilibrium swelling (Q) (see figure 4-25), according to the following equation:[107]

$$G = cRT/M_c(1-2M_c/M_n)Q^{-1/3}$$

The mechanical properties of hydrogels are strongly related to their swelling degree, which is related to the crosslink density of the hydrogels.[108] The effective network density of some of the hydrogel scaffolds developed (table 4-10), was determined by measuring the modulus of elasticity in compression as described earlier for other hydrogel systems.[107, 108] For these experiments, the hydrogels were incubated in double distilled water at 37°C for one day, followed by determining their equilibrium heights at various compressive stresses, using a texturometer. The elasticity modulus at equilibrium was derived using the following equation:

$$F/A = -G(\lambda-\lambda^{-2})$$

F/A = compressive stress applied,
G = equilibrium elasticity modulus,
λ = the relative compression l/l_0,
l_0, l = height of respectively original and deformed gel.

The elasticity modulus (G) was obtained from the slope of the linear plot of F/A versus $-(\lambda-\lambda^{-2})$. Using the value of the elasticity modulus, the effective network density was calculated using the following equation:[104]

$$v_e = G/(RTv_{2,s}^{1/3}\langle\alpha\rangle^2)$$

v_e = effective network density (mol/m^3),
R = universal gas constant,
T = absolute temperature,
$v_{2,s}$ = polymer volume fraction of the hydrogel at equilibrium swelling,
$\langle\alpha\rangle$ = isotropic dilation factor ($\sim v_{2,r}^{1/3}$),

$v_{2,r}$ = polymer volume fraction in the relaxed state.

Since this equation also requires the density of the individual scaffolds, pycnometry measurements were performed. The effective network densities and related parameters for the different hydrogels are summarized in table 4-10.

Hydrogel Type	$v_{2,s}$	G (Pa)	v_e (mmol/cm^3)
Type GIII$_b$	0.046 ± 0.001	18630	0.138 ± 0.001
Type GI$_a$	0.027 ± 0.001	6100	0.078 ± 0.001
Type GI$_b$	0.062 ± 0.005	21770	0.120 ± 0.003
Type GI$_c$	0.086 ± 0.003	38000	0.156 ± 0.002
Type GII$_b$	0.063 ± 0.003	21450	0.118 ± 0.002

Table 4-10: Network parameters for the hydrogels developed.

From table 4-10, it can be concluded that the crosslink density increases with increasing gelatin concentration. A higher concentration of polymer precursors, obviously corresponds to a higher amount of available crosslinkable side groups. When comparing type GIII$_b$, GI$_b$ and GII$_b$ scaffolds, type GIII$_b$ hydrogels have a significantly higher crosslink density compared to type GI$_b$ and GII$_b$ hydrogels (i.e. 0.138 mmol/cm^3 versus 0.118-0.120 mmol/cm^3) ($P < 0.05$). The similar crosslink density for type GI$_b$ and type GII$_b$ hydrogels was also reflected by the similarities in swelling and mechanical properties of both types of scaffolds (see § 3.3.1 and 3.3.3). However, the crosslinking density of 0.138 mmol/cm^3, observed for type GIII$_b$ hydrogels was not anticipated based on the highest equilibrium swelling degree obtained for those scaffolds (see § 3.3.1). The channel-like pore morphology, observed for these scaffolds, leading to a high water uptake, thus compensates for the high crosslink density, which would normally lead to lower swelling capacities.

The amount of junction knots, calculated from the above equation, are lower compared to the amount of double bonds available for crosslinking (i.e. 0.118-0.138 mmol/cm^3 versus 0.255 mmol/cm^3 for 10 w/v% gelatins). The observed experimental values are lower than the theoretically calculated numbers since it can be anticipated

that a fraction of the double bonds present in the gelatin side groups are crosslinked during UV irradiation.

3.3.5 In vitro degradation experiments

To study possible differences in the degradation profile of the materials, the scaffolds were immersed in PBS in the presence of collagenase. At regular time intervals, the samples were removed and both the compression modulus and the gel fraction were determined. Possible effects of the gelatin concentration, the pore size and the pore geometry were investigated.

3.3.5.1 Effect of w/v% gelatin

The degradation profiles of type GI scaffolds with varying w/v % gelatin are shown in figure 4-26. It can be observed that the degradation time increased with increasing gelatin concentration. At higher gelatin concentrations, the degree of cross-linking increases, which slows down the degradation process. The penetration of collagenase into the hydrogel network is thus hindered by a higher number of cross-links between the gelatin molecules. A reduced enzyme penetration causes a distinct decrease of the surface which is available for enzymatic degradation.

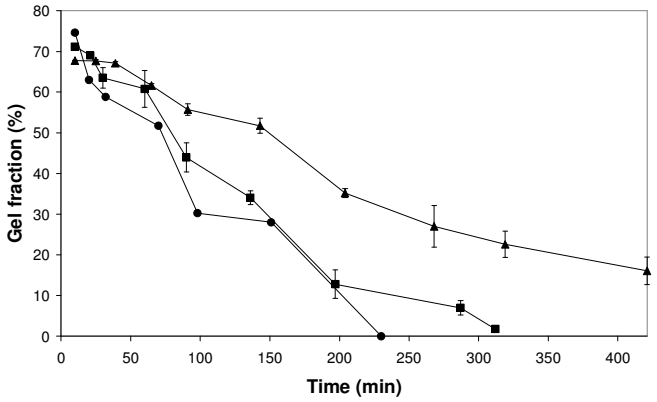

Figure 4-26: *In vitro* degradation behaviour of 5 w/v%$_{(a)}$ (●), 10 w/v%$_{(b)}$ (■) and 15 w/v%$_{(c)}$ (▲) type GI gelatin scaffolds. The degradation was studied at 37°C in the presence of collagenase.

3.3.5.2 Effect of pore size and geometry

Next, possible effects of the pore geometry and pore size on the degradation of the scaffolds (10 w/v%) were investigated. Again, the compression modulus and the gel fraction were determined at regular time intervals. The data are summarized in figures 4-27 and 4-28.

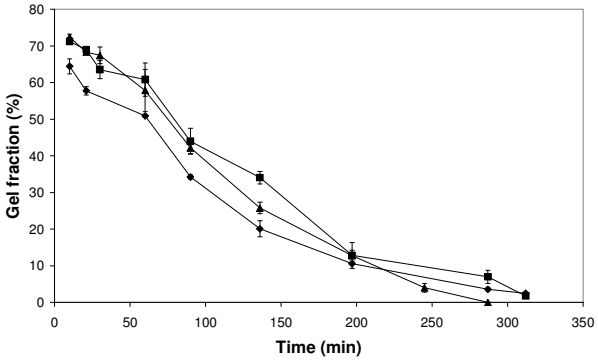

Figure 4-27: Influence of *in vitro* degradation on the gel fraction of hydrogels type $GIII_b$ (▲), type GI_b (■) and type GII_b (◆) (* *P* < 0.01).

From the gel fraction data (figure 4-27), it can be concluded that type $GIII_b$ hydrogels possess the fastest degradation profile. This can again be attributed to the elongated pore structure throughout the scaffold, enabling a faster influx of fluids. This assumption is supported by the higher swelling rate and swelling degree observed for these materials (see § 3.3.1).

Comparing type GI_b and GII_b hydrogels, no difference in degradation rate was observed (figure 4-27), what can be related to the similar swelling properties for both types of scaffolds (see § 3.3.1).

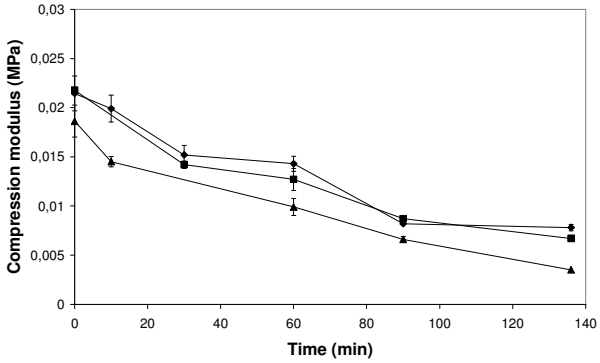

Figure 4-28: Influence of *in vitro* degradation on the compression modulus of hydrogels type $GIII_b$ (▲), type GI_b (■) and type GII_b (◆) (* *P* < 0.01).

Figure 4-28 represents the compression moduli of type GI-GIII hydrogels as a function of time. In contrast to what we anticipated, no differences in compression moduli during degradation were observed comparing the different scaffolds. The latter effect can presumably be explained by considering the possible degradation mechanisms involved.[109] Two different degradation mechanisms can be distinguished: heterogeneous degradation (i.e. surface degradation) and homogeneous degradation (i.e. bulk degradation). In the former case, the polymer matrix preserves its original geometrical shape, but decreases in size as a function of time. In the latter case, the degradation reaction occurs randomly. For bulk degradation, the scaffold size will remain similar during a relatively long time period. In case of surface erosion, the polymers are expected to preserve their mechanical properties (reflected by their compression moduli) longer. Most likely, surface degradation occurs to a large extent for all hydrogel types, since the observed decreases in compression moduli are relatively slow, all showing a similar slope. This assumption is also supported by the appearance of the hydrogels (i.e. decreasing dimensions) as a function of time.

4 Conclusion

Scaffold porosity was induced by a combination of phase separation and freeze-drying. The novel cryo-unit enabled us to produce, in a controlled manner, three-dimensional porous scaffolds in which the pore size, the pore geometry and the porosity can be easily fine-tuned by variation of the cryogenic parameters. In addition, the pore characteristics induced by applying a cryogenic treatment on chemically crosslinked hydrogels are sustained after re-swelling. Three experimental conditions influenced the characteristics of porous gelatin scaffolds: (1) the cooling rate, (2) the polymer concentration and (3) the implemented temperature gradient. The problem of skin formation during cryogenic treatment was solved by applying a soluble layer of uncrosslinked gelatin onto the preformed hydrogel, prior to cryogenic treatment. The formed skin can be easily removed by aqueous treatment above the gel-sol transition temperature of gelatin.

The results obtained in the present study will be a valuable tool for research on porous scaffolds, including pore creation techniques as well as non-destructive structure analysis techniques.

It was also observed that an increasing w/v % gelatin results in a decrease of the degradation and the swelling ratio and in an increase of the compression modulus of the resulting hydrogels. However, when studying the influence of the pore size on these parameters, we found that the correlations were less straightforward than expected based on literature data. We found that a cryogenic treatment influenced both the pore size and the extent of gelatin cross-linking. Obviously, the latter significantly influences the physico-chemical properties of gelatin scaffolds.

From the results, it was also shown that the water uptake of the porous gelatin scaffolds developed, could be fitted to a Voigt-based model. The latter offers valuable information regarding swelling kinetics.

Based on the theory of rubber elasticity, it was also demonstrated that type $GIII_b$ hydrogel scaffolds possessed the highest crosslink density in comparison with type GI_b and type GII_b matrices. The latter was not anticipated, based on the swelling experiments. Consequently, a large variety of experimental techniques needs to be applied to perform an in depth study of material characteristics.

References

1. Freyman, T. M.; Yannas, I. V.; Yokoo, R.; Gibson, L. J., Fibroblast contraction of a collagen-GAG matrix. *Biomaterials* **2001,** 22, (21), 2883-2891.
2. Ellis, D. L.; Yannas, I. V., Recent advances in tissue synthesis in vivo by use of collagen-glycosaminoglycan copolymers. *Biomaterials* **1996,** 17, (3), 291-299.
3. Zaleskas, J. M.; Kinner, B.; Freyman, T. M.; Yannas, I. V.; Gibson, L. J.; Spector, M., Contractile forces generated by articular chondrocytes in collagen-glycosaminoglycan matrices. *Biomaterials* **2004,** 25, (7-8), 1299-1308.
4. Pek, Y. S.; Spector, M.; Yannas, I. V.; Gibson, L. J., Degradation of a collagen-chondroltin-6-sulfate matrix by collagenase and by chondroitinase. *Biomaterials* **2004,** 25, (3), 473-482.
5. Nehrer, S.; Breinan, H. A.; Ramappa, A.; Young, G.; Shortkroff, S.; Louie, L. K.; Sledge, C. B.; Yannas, I. V.; Spector, M., Matrix collagen type and pore size influence behaviour of seeded canine chondrocytes. *Biomaterials* **1997,** 18, (11), 769-776.
6. Lee, S. B.; Jeon, H. W.; Lee, Y. W.; Lee, Y. M.; Song, K. W.; Park, M. H.; Nam, Y. S.; Ahn, H. C., Bio-artificial skin composed of gelatin and (1 -> 3), (1 -> 6)-beta-glucan. *Biomaterials* **2003,** 24, (14), 2503-2511.
7. Chen, G. P.; Ushida, T.; Tateishi, T., Development of biodegradable porous scaffolds for tissue engineering. *Materials Science & Engineering C-Biomimetic and Supramolecular Systems* **2001,** 17, (1-2), 63-69.
8. Whang, K.; Thomas, C. H.; Healy, K. E.; Nuber, G., A Novel Method to Fabricate Bioabsorbable Scaffolds. *Polymer* **1995,** 36, (4), 837-842.
9. Lee, J. E.; Kim, S. E.; Kwon, I. C.; Ahn, H. J.; Cho, H.; Lee, S. H.; Kim, H. J.; Seong, S. C.; Lee, M. C., Effects of a chitosan scaffold containing TGF-beta 1 encapsulated chitosan microspheres on in vitro chondrocyte culture. *Artificial Organs* **2004,** 28, (9), 829-839.
10. O'Brien, F. J.; Harley, B. A.; Yannas, I. V.; Gibson, L. J., The effect of pore size on cell adhesion in collagen-GAG scaffolds. *Biomaterials* **2005,** 26, (4), 433-441.
11. Schoof, H.; Apel, J.; Heschel, I.; Rau, G., Control of pore structure and size in freeze-dried collagen sponges. *Journal of Biomedical Materials Research* **2001,** 58, (4), 352-357.
12. Kang, H. W.; Tabata, Y.; Ikada, Y., Fabrication of porous gelatin scaffolds for tissue engineering. *Biomaterials* **1999,** 20, (14), 1339-1344.
13. Ren, L.; Tsuru, K.; Hayakawa, S.; Osaka, A., Sol-gel preparation and in vitro deposition of apatite on porous gelatin-siloxane hybrids. *Journal of Non-Crystalline Solids* **2001,** 285, (1-3), 116-122.
14. Ulubayram, K.; Eroglu, I.; Hasirci, N., Gelatin microspheres and sponges for delivery of macromolecules. *Journal of Biomaterials Applications* **2002,** 16, (3), 227-241.
15. Choi, Y. S.; Lee, S. B.; Hong, S. R.; Lee, Y. M.; Song, K. W.; Park, M. H., Studies on gelatin-based sponges. Part III: A comparative study of cross-linked gelatin/alginate, gelatin/hyaluronate and chitosan/hyaluronate sponges and their application as a wound

dressing in full-thickness skin defect of rat. *Journal of Materials Science-Materials in Medicine* **2001,** 12, (1), 67-73.

16. Van den Bulcke, A. I.; Bogdanov, B.; De Rooze, N.; Schacht, E. H.; Cornelissen, M.; Berghmans, H., Structural and rheological properties of methacrylamide modified gelatin hydrogels. *Biomacromolecules* **2000,** 1, (1), 31-38.
17. O'Brien, F. J.; Harley, B. A.; Yannas, I. V.; Gibson, L., Influence of freezing rate on pore structure in freeze-dried collagen-GAG scaffolds. *Biomaterials* **2004,** 25, (6), 1077-1086.
18. Wang, X.; Kim, H. J.; Wong, C.; Vepari, C.; Matsumoto, A.; Kaplan, D. L., Fibrous proteins and tissue engineering. *Materials Today* **2006,** 9, (12), 44-53.
19. Kawanishi, M.; Ushida, T.; Kaneko, T.; Niwa, H.; Fukubayashi, T.; Nakamura, K.; Oda, H.; Tanaka, S.; Tateishi, T., New type of biodegradable porous scaffolds for tissue-engineered articular cartilage. *Materials Science & Engineering C-Biomimetic and Supramolecular Systems* **2004,** 24, (3), 431-435.
20. Hou, Q. P.; Grijpma, D. W.; Feijen, J., Preparation of interconnected highly porous polymeric structures by a replication and freeze-drying process. *Journal of Biomedical Materials Research Part B-Applied Biomaterials* **2003,** 67B, (2), 732-740.
21. Laurencin, C. T.; Ko, F. K.; Attawia, M. A.; Borden, M. D., Studies on the development of a tissue engineered matrix for bone regeration. *Cells and materials* **1998,** 8, 175-181.
22. Mooney, D. J.; Baldwin, D. F.; Suh, N. P.; Vacanti, L. P.; Langer, R., Novel approach to fabricate porous sponges of poly(D,L-lactic-co-glycolic acid) without the use of organic solvents. *Biomaterials* **1996,** 17, (14), 1417-1422.
23. Mooney, D. T.; Mazzoni, C. L.; Breuer, C.; McNamara, K.; Hern, D.; Vacanti, J. P.; Langer, R., Stabilized polyglycolic acid fibre based tubes for tissue engineering. *Biomaterials* **1996,** 17, (2), 115-124.
24. van Tienen, T. G.; Heijkants, R. G. J. C.; Buma, P.; de Groot, J. H.; Pennings, A. J.; Veth, R. P. H., Tissue ingrowth polymers and degradation of two biodegradable porous with different porosities and pore sizes. *Biomaterials* **2002,** 23, (8), 1731-1738.
25. Horak, D.; Kroupava, J.; Slouf, M.; Dvorak, P., Poly(2-hydroxyethyl methacrylate)-based slabs as a mouse embryonic stem cell support. *Biomaterials* **2004,** 25, (22), 5249-5260.
26. Ma, P. X.; Zhang, R. Y., Microtubular architecture of biodegradable polymer scaffolds. *Journal of Biomedical Materials Research* **2001,** 56, (4), 469-477.
27. Reignier, J.; Huneault, M. A., Preparation of interconnected poly(epsilon-caprolactone) porous scaffolds by a combination of polymer and salt particulate leaching. *Polymer* **2006,** 47, (13), 4703-4717.
28. Mikos, A. G.; Temenoff, J. S., Formation of highly porous biodegradable scaffolds for tissue engineering. *Electronic journal of Biotechnology* **2000,** 3, (2).
29. Hou, Q. P.; Grijpma, D. W.; Feijen, J., Porous polymeric structures for tissue engineering prepared by a coagulation, compression moulding and salt leaching technique. *Biomaterials* **2003,** 24, (11), 1937-1947.

30. Mikos, A. G.; Thorsen, A. J.; Czerwonka, L. A.; Bao, Y.; Langer, R.; Winslow, D. N.; Vacanti, J. P., Preparation and Characterization of Poly(L-Lactic Acid) Foams. *Polymer* **1994,** 35, (5), 1068-1077.
31. Oh, S. H.; Kang, S. G.; Kim, E. S.; Cho, S. H.; Lee, J. H., Fabrication and characterization of hydrophilic poly(lactic-co-glycolic acid)/poly(vinyl alcohol) blend cell scaffolds by melt-molding particulate-leaching method. *Biomaterials* **2003,** 24, (22), 4011-4021.
32. Iannace, S.; Di Maio, E.; Nicolais, L., Preparation and characterization of polyurethane porous membranes by particulate-leaching method. *Cellular Polymers* **2001,** 20, (5), 321-338.
33. Harris, L. D.; Kim, B. S.; Mooney, D. J., Open pore biodegradable matrices formed with gas foaming. *Journal of Biomedical Materials Research* **1998,** 42, (3), 396-402.
34. Khalil, S.; Nam, J.; Sun, W., Multi-nozzle deposition for construction of 3D biopolymer tissue scaffolds. *Rapid Prototyping Journal* **2005,** 11, (1), 9-17.
35. Hutmacher, D. W.; Ng, K. W.; Kaps, C.; Sittinger, M.; Klaring, S., Elastic cartilage engineering using novel scaffold architectures in combination with a biomimetic cell carrier. *Biomaterials* **2003,** 24, (24), 4445-4458.
36. Lozinsky, V. I., Cryogels on the basis of natural and synthetic polymers: Preparation, properties and application. *Uspekhi Khimii* **2002,** 71, (6), 559-585.
37. Lozinsky, V. I.; Plieva, F. M.; Galaev, I. Y.; Mattiasson, B., The potential of polymeric cryogels in bioseparation. *Bioseparation* **2001,** 10, (4-5), 163-188.
38. De Paepe, I. Synthese van hydrogelen, op basis van biopolymeren, voor biomedische toepassingen. Ghent University, Gent, 2005.
39. Sin-hee Kim, C.-C. C., Pore structure analysis of swollen dextran-methacrylate hydrogels by SEM and mercury intrusion porosimetry. *Journal of Biomedical Materials Research* **2000,** 53, (3), 258-266.
40. Arcaute, K.; Mann, B. K.; Wicker, R. B., Stereolithography of three-dimensional bioactive poly(ethylene glycol) constructs with encapsulated cells. *Annals of Biomedical Engineering* **2006,** 34, (9), 1429-1441.
41. Lopergolo, L. C.; Lugao, A. B.; Catalani, L. H., Direct UV photocrosslinking of poly(N-vinyl-2-pyrrolidone) (PVP) to produce hydrogels. *Polymer* **2003,** 44, (20), 6217-6222.
42. Falcetta, J. J.; Park, J.; Smith, C. G. Ultraviolet absorbing hydrogels 1992.
43. Caulfield, M. J.; Hao, X.; Qiao, G. G.; Solomon, D. H., Degradation on polyacrylamides. Part II. Polyacrylamide gels. *Polymer* **2003,** 44, (14), 3817-3826.
44. Lozinsky, V. I.; Golovina, T. O.; Gusev, D. G., Study of cryostructuration of polymer systems: XIII. Some characteristic features of the behaviour of macromolecular thiols in frozen aqueous solutions. *Polymer* **2000,** 41, (1), 35-47.
45. Petrov, P.; Petrova, E.; Stamenova, R.; Tsvetanov, C. B.; Riess, G., Cryogels of cellulose derivatives prepared via UV irradiation of moderately frozen systems. *Polymer* **2006,** 47, (19), 6481-6484.
46. Lozinsky, V. I.; Morozova, S. A.; Vainerman, E. S.; Titova, E. F.; Shtilman, M. I.; Belavtseva, E. M.; Rogozhin, S. V., Study of Cryostructurization of Polymer Systems .8. Characteristic

Features of the Formation of Crosslinked Poly(Acryl Amide) Cryogels under Different Thermal Conditions. *Acta Polymerica* **1989,** 40, (1), 8-15.

47. Lozinsky, V. I.; Vainerman, E. S.; Ivanova, S. A.; Titova, E. F.; Shtilman, M. I.; Belavtseva, E. M.; Rogozhin, S. V., Study of Cryostructurization of Polymer Systems .6. The Influence of the Process Temperature on the Dynamics of Formation and Structure of Cross-Linked Polyacrylamide Cryogels. *Acta Polymerica* **1986,** 37, (3), 142-146.
48. Plieva, F.; Xiao, H. T.; Galaev, I. Y.; Bergenstahl, B.; Mattiasson, B., Macroporous elastic polyacrylamide gels prepared at subzero temperatures: control of porous structure. *Journal of Materials Chemistry* **2006,** 16, (41), 4065-4073.
49. Savina, I. N.; Mattiasson, B.; Galaev, I. Y., Graft polymerization of vinyl monomers inside macroporous polyacrylamide gel, cryogel, in aqueous and aqueous-organic media initiated by diperiodatocuprate(III) complexes. *Journal of Polymer Science Part a-Polymer Chemistry* **2006,** 44, (6), 1952-1963.
50. Zhang, X. Z.; Chu, C. C., Synthesis of temperature sensitive PNIPAAm cryogels in organic solvent with improved properties. *Journal of Materials Chemistry* **2003,** 13, (10), 2457-2464.
51. Yang, H.; Cheng, R. S.; Xie, H. F.; Wang, Z. L., The role of solvation on the conformational change during repeated freezing-thawing treatment to an extremely dilute aqueous solution of poly(vinyl alcohol). *Polymer* **2005,** 46, (18), 7557-7562.
52. Willcox, P. J.; Howie, D. W.; Schmidt-Rohr, K.; Hoagland, D. A.; Gido, S. P.; Pudjijanto, S.; Kleiner, L. W.; Venkatraman, S., Microstructure of poly(vinyl alcohol) hydrogels produced by freeze/thaw cycling. *Journal of Polymer Science Part B-Polymer Physics* **1999,** 37, (24), 3438-3454.
53. Lukas, L. A.; Surry, K. J. M.; Peters, T. M., Temperature dosimetry using MR relaxation characteristics of poly(vinyl alcohol) cryogel (PVA-C). *Magnetic Resonance in Medicine* **2001,** 46, (5), 1006-1013.
54. Lozinsky, V. I.; Damshkaln, L. G., Study of cryostructuration of polymer systems. XVII. Poly(vinyl alcohol) cryogels: Dynamics of the cryotropic gel formation. *Journal of Applied Polymer Science* **2000,** 77, (9), 2017-2023.
55. Lozinsky, V. I.; Zubov, A. L.; Titova, E. F., Poly(vinyl alcohol) cryogels employed as matrices for cell immobilization .2. Entrapped cells resemble porous fillers in their effects on the properties of PVA-cryogel carrier. *Enzyme and Microbial Technology* **1997,** 20, (3), 182-190.
56. Lozinsky, V. I.; Plieva, F. M., Poly(vinyl alcohol) cryogels employed as matrices for cell immobilization. 3. Overview of recent research and developments. *Enzyme and Microbial Technology* **1998,** 23, (3-4), 227-242.
57. Nugent, M. J. D.; Higginbotham, C. L., Investigation of the influence of freeze-thaw processing on the properties of polyvinyl alcohol/polyacrylic acid complexes. *Journal of Materials Science* **2006,** 41, (8), 2393-2404.
58. Lazaridou, A.; Biliaderis, C. G., Cryogelation of cereal beta-glucans: structure and molecular size effects. *Food Hydrocolloids* **2004,** 18, (6), 933-947.

59. Cheftel, J. C.; Thiebaud, M.; Dumay, E., Pressure-assisted freezing and thawing of foods: A review of recent studies. *High Pressure Research* **2002,** 22, (3-4), 601-611.
60. Giannouli, P.; Morris, E. R., Cryogelation of xanthan. *Food Hydrocolloids* **2003,** 17, (4), 495-501.
61. Vainerman, E. S.; Lozinsky, V. I.; Rogozhin, S. V., Study of Cryostructurization of Polymer Systems .I. Structure Formation in Solutions of Thiol-Containing Polymers under Freezing-Thawing. *Colloid and Polymer Science* **1981,** 259, (12), 1198-1201.
62. Bloch, K.; Lozinsky, V. I.; Galaev, I. Y.; Yavriyanz, K.; Vorobeychik, M.; Azarov, D.; Damshkaln, L. G.; Mattiasson, B.; Vardi, P., Functional activity of insulinoma cells (INS-1E) and pancreatic islets cultured in agarose cryogel sponges. *Journal of Biomedical Materials Research Part A* **2005,** 75A, (4), 802-809.
63. Lozinsky, V. I.; Damshkaln, L. G.; Brown, R.; Norton, I. T., Study of cryostructuration of polymer systems. XVIII. Freeze-thaw influence on water-solubilized artificial mixtures of amylopectin and amylose. *Journal of Applied Polymer Science* **2000,** 78, (2), 371-381.
64. Podorozhko, E. A.; Kurskaya, E. A.; Kulakova, V. K.; Lozinsky, V. I., Cryotropic structuring of aqueous dispersions of fibrous collagen: influence of the initial pH values. *Food Hydrocolloids* **2000,** 14, (2), 111-120.
65. Moore, M. J.; Jabbari, E.; Ritman, E. L.; Lu, L. C.; Currier, B. L.; Windebank, A. J.; Yaszemski, M. J., Quantitative analysis of interconnectivity of porous biodegradable scaffolds with micro-computed tomography. *Journal of Biomedical Materials Research Part A* **2004,** 71A, (2), 258-267.
66. Jones, A. C.; Milthorpe, B.; Averdunk, H.; Limaye, A.; Senden, T. J.; Sakellariou, A.; Sheppard, A. P.; Sok, R. M.; Knackstedt, M. A.; Brandwood, A.; Rohner, D.; Hutmacher, D. W., Analysis of 3D bone ingrowth into polymer scaffolds via micro-computed tomography imaging. *Biomaterials* **2004,** 25, (20), 4947-4954.
67. Dierick, M. Tomographic imaging techniques using cold and thermal neutron beams. Ghent University, 2005.
68. Cnudde, V. PhD Thesis. Ghent University, 2005.
69. Cnudde, V.; Masschaele, B.; Dierick, M.; Vlassenbroeck, J.; Van Hoorebeke, L.; Jacobs, P., Recent progress in X-ray CT as a geosciences tool. *Applied Geochemistry* **2006,** 21, (5), 826-832.
70. Steppe, K.; Cnudde, V.; Girard, C.; Lemeur, R.; Cnudde, J. P.; Jacobs, P., Use of X-ray computed microtomography for non-invasive determination of wood anatomical characteristics. *Journal of Structural Biology* **2004,** 148, (1), 11-21.
71. De Graef, B.; Cnudde, V.; Dick, J.; De Belie, N.; Jacobs, P.; Verstraete, W., A sensitivity study for the visualisation of bacterial weathering of concrete and stone with computerised X-ray microtomography. *Science of the Total Environment* **2005,** 341, (1-3), 173-183.
72. Dierick, M.; Masschaele, B.; Van Hoorebeke, L., Octopus, a fast and user-friendly tomographic reconstruction package developed in LabView (R). *Measurement Science & Technology* **2004,** 15, (7), 1366-1370.

73. VanVlierberghe, S.; Cnudde, V.; Dubruel, P.; Masschaele, B.; Cosijns, A.; DePaepe, I.; Jacobs, P. J. S.; VanHoorebeke, L.; Remon, J. P.; Schacht, E., Porous Gelatin Hydrogels: 1. Cryogenic Formation and Structure Analysis. *Biomacromolecules* **2007,** 8, (2), 331-337.
74. Tamari, S.; Aguilar-Chavez, A., Optimum design of gas pycnometers for determining the volume of solid particles. *Journal of Testing and Evaluation* **2005,** 33, (2), 135-138.
75. Tamari, S., Optimum design of the constant-volume gas pycnometer for determining the volume of solid particles. *Measurement Science & Technology* **2004,** 15, (3), 549-558.
76. Amore, R.; Pagani, C.; Youssef, M. N.; Netto, C. A.; Lewgoy, H. R., Polymerization shrinkage of packable resins varying the light source distance, measured by gas pycnometer. *Journal of Dental Research* **2003,** 82, 213-213.
77. Cilli, R.; Prakki, A.; Araujo, M. A. J., Utilizing gas pycnometer for measuring polymerization contraction of composite resins. *Journal of Dental Research* **2002,** 81, A259-A259.
78. McInnes, F. J.; Thapa, P.; Baillie, A. J.; Welling, P. G.; Watson, D. G.; Gibson, I.; Nolan, A.; Stevens, H. N. E., In vivo evaluation of nicotine lyophilised nasal insert in sheep. *International Journal of Pharmaceutics* **2005,** 304, (1-2), 72-82.
79. Czepirski, L.; Komorowska-Czepirska, E.; Szymonska, J., Fitting of different models for water vapour sorption on potato starch granules. *Applied Surface Science* **2002,** 196, (1-4), 150-153.
80. Cross, G. H.; Ren, Y. T.; Swann, M. J., Refractometric discrimination of void-space filling and swelling during vapour sorption in polymer films. *Analyst* **2000,** 125, (12), 2173-2175.
81. Tesch, R.; Ramon, O.; Ladyzhinski, I.; Cohen, Y.; Mizrahi, S., Water sorption isotherm of solution containing hydrogels at high water activity. *International Journal of Food Science and Technology* **1999,** 34, (3), 235-243.
82. Hobbs, P. V., *Ice physics*. Clarendon Press: Oxford, 1974.
83. Tsang, V. L.; Bhatia, S. N., Three-dimensional tissue fabrication. *Advanced Drug Delivery Reviews* **2004,** 56, (11), 1635-1647.
84. Kang, H. W.; Tabata, Y.; Ikada, Y., Effect of porous structure on the degradation of freeze-dried gelatin hydrogels. *Journal of Bioactive and Compatible Polymers* **1999,** 14, (4), 331-343.
85. Mao, J. S.; Liu, H. F.; Yin, Y. J.; Yao, K. D., The properties of chitosan-gelatin membranes and scaffolds modified with hyaluronic acid by different methods. *Biomaterials* **2003,** 24, (9), 1621-1629.
86. Aoki, H.; Taguchi, T.; Saito, H.; Kobayashi, H.; Kataoka, K.; Tanaka, J., Rheological evaluation of gelatin gels prepared with a citric acid derivative as a novel cross-linker. *Materials Science & Engineering C-Biomimetic and Supramolecular Systems* **2004,** 24, (6-8), 787-790.
87. Balakrishnan, B.; Jayakrishnan, A., Self-cross-linking biopolymers as injectable in situ forming biodegradable scaffolds. *Biomaterials* **2005,** 26, (18), 3941-3951.
88. Terao, K.; Nagasawa, N.; Nishida, H.; Furusawa, K.; Mori, Y.; Yoshii, F.; Dobashi, T., Reagent-free crosslinking of aqueous gelatin: manufacture and characteristics of gelatin gels irradiated with gamma-ray and electron beam. *Journal of Biomaterials Science-Polymer Edition* **2003,** 14, (11), 1197-1208.

89. Mwangi, J. W.; Ofner, C. M., Crosslinked gelatin matrices: release of a random coil macromolecular solute. *International Journal of Pharmaceutics* **2004,** 278, (2), 319-327.
90. Bigi, A.; Panzavolta, S.; Rubini, K., Relationship between triple-helix content and mechanical properties of gelatin films. *Biomaterials* **2004,** 25, (25), 5675-5680.
91. Boelen, E. J. H.; van Hooy-Corstjens, C. S. J.; Gijbels, M. J. J.; Bulstra, S. K.; van Ooij, A.; van Rhijn, L. W.; Koole, L. H., Preliminary evaluation of new intrinsically radiopaque hydrogels for replacing the nucleus pulposus. *Journal of Materials Chemistry* **2006,** 16, (9), 824-828.
92. Omidian, H.; Hashemi, S. A.; Sammes, P. G.; Meldrum, I., A model for the swelling of superabsorbent polymers. *Polymer* **1998,** 39, (26), 6697-6704.
93. Pourjavadi, A.; Kurdtabar, M., Collagen-based highly porous hydrogel without any porogen: Synthesis and characteristics. *European Polymer Journal* **2007,** 43, (3), 877-889.
94. Pourjavadi, A.; Sadeghi, M.; Hashemi, M. M.; Hosseinzadeh, H., Synthesis and absorbency of gelatin-graft-poly(sodium acrylate-co-acrylamide) superabsorbent hydrogel with salt and pH-responsiveness properties. *E-Polymers* **2006**.
95. Omidian, H.; Hashemi, S. A.; Sammes, P. G.; Meldrum, I., Modified acrylic-based superabsorbent polymers (dependence on particle size and salinity). *Polymer* **1999,** 40, (7), 1753-1761.
96. Zheng, J. P.; Gao, S.; Wang, J. X.; Yao, K. D., Swelling behavior of gelatin-g-methyl methacrylate copolymers. *Journal of Materials Science* **2005,** 40, (15), 4029-4033.
97. Bajpai, A. K.; Choubey, J., Release study of sulphamethoxazole controlled by swelling of gelatin nanoparticles and drug-biopolymer interaction. *Journal of Macromolecular Science-Pure and Applied Chemistry* **2005,** A42, (3), 253-275.
98. Bravo-Osuna, I.; Ferrero, C.; Jimenez-Castellanos, M. R., Water sorption-desorption behaviour of methyl methacrylate-starch copolymers: effect of hydrophobic graft and drying method. *European Journal of Pharmaceutics and Biopharmaceutics* **2005,** 59, (3), 537-548.
99. Nokhodchi, A.; Ford, J. L.; Rubinstein, M. H., Studies on the interaction between water and (hydroxypropyl)methylcellulose. *Journal of Pharmaceutical Sciences* **1997,** 86, (5), 608-615.
100. Mousia, Z.; Farhat, I. A.; Blachot, J. F.; Mitchell, J. R., Effect of water partitioning on the glass-transition behaviour of phase separated amylopectin-gelatin mixtures. *Polymer* **2000,** 41, (5), 1841-1848.
101. Bilgen, B.; Chang-Mateu, I. M.; Barabino, G. A., Characterization of mixing in a novel wavy-walled bioreactor for tissue engineering. *Biotechnology and Bioengineering* **2005,** 92, (7), 907-919.
102. Zhong, J. J.; Zhang, Z. Y., High-density cultivation of Panax notoginseng cell cultures with methyl jasmonate elicitation in a centrifugal impeller bioreactor. *Engineering in Life Sciences* **2005,** 5, (5), 471-474.
103. Peppas, N. A.; Bures, P.; Leobandung, W.; Ichikawa, H., Hydrogels in pharmaceutical formulations. *European Journal of Pharmaceutics and Biopharmaceutics* **2000,** 50, (1), 27-46.

104. Peppas, N. A.; Hilt, J. Z.; Khademhosseini, A.; Langer, R., Hydrogels in biology and medicine: From molecular principles to bionanotechnology. *Advanced Materials* **2006,** 18, (11), 1345-1360.

105. Stadler, R.; de Lucca Freitas, L., Thermoplastic elastomers by hydrogen bonding 1. Rheological properties of modified polybutadiene. *Colloid & Polymer Science* **1986,** 264, (9), 773-778.

106. Quesnel, J. P.; Mark, J. E., Rubber elasticity and characterization of networks. In *Comprehensive polymer science*, Allen, G., Ed. Pergamon: 1989; Vol. 2.

107. Wang, S. C.; Chen, B. H.; Wang, L. F.; Chen, J. S., Characterization of chondroitin sulfate and its interpenetrating polymer network hydrogels for sustained-drug release. *International Journal of Pharmaceutics* **2007,** 329, (1-2), 103-109.

108. Lee, K. Y.; Bouhadir, K. H.; Mooney, D. J., Controlled degradation of hydrogels using multi-functional cross-linking molecules. *Biomaterials* **2004,** 25, (13), 2461-2466.

109. Gopferich, A., Mechanisms of polymer degradation and erosion. *Biomaterials* **1996,** 17, (2), 103-114.

Chapter V:
Scaffolds Based on
Gelatin and Chondroitin Sulphate

1 Synthesis of scaffolds composed of gelatin and chondroitin sulphate

A key issue in the development of biomaterials is the design of a material that mimics the natural environment of cells. In the present chapter, we have therefore developed hydrogel materials that contain both a protein (gelatin) and a glycosaminoglycan (chondroitin sulphate) component.

Gelatin-chondroitin sulphate hydrogels were already applied as controlled release systems for antibacterial proteins.[1] Incorporation of chondroitin sulphate in crosslinked gelatin gels significantly increased the protein loading capacity of the gels and extended the release time.[2] Alternatively, gelatin-chondroitin sulphate-hyaluronan tri-copolymer scaffolds were, after crosslinking with EDC, applied in order to mimic natural cartilage.[3, 4] It was observed that the presence of chondroitin sulphate promoted the secretion of proteoglycan and type II collagen.[4] Bilayer gelatin-chondroitin sulphate-hyaluronan biomatrices were also studied for wound treatment. The results showed that in addition to reforming a permanent coverage with histologically normal and adequately differentiated epithelial tissue, a well-defined dermal-epidermal junction as well as collagen network in the dermis was present. As a result, the skin substitute had a positive effect on the promotion of the wound healing process and could be used to help the regeneration of full-thickness skin defects.[5, 6] Another application of the tri-copolymer scaffold is the regeneration of the human nucleus pulposus.[7] Furthermore, both microcarriers and membranes,

composed of gelatin and chondroitin sulphate, were prepared in view of different therapeutic strategies.[8-14]

Based on the broad application field of materials composed of gelatin and chondroitin sulphate, the incorporation of CS into the porous gelatin scaffolds, described in the previous chapter, could be useful since the final goal of the present work was to prepare a tissue engineering device, applicable for the regeneration of a large variety of human cells (e.g. chondrocytes).

In the present chapter, we have developed and compared different types of hydrogels based on gelatin and/or chondroitin sulphate. By combining both protein and glycosaminoglycan molecules into one porous hydrogel material, we aimed to develop biomimetic hydrogel materials. The materials developed were compared in terms of their chemical composition, 3D structure and water (vapour) uptake capacity.

Using the hydrogel precursors synthesised (chapter 2), a series of hydrogels was prepared by applying a cryogenic treatment on gel-MOD (i.e. reference), CS-MOD or combinations of both gel-MOD and CS-MOD (table 5-1).

Hydrogel Type	Gel-MOD	CS-MOD
$GIII_b$	10 w/v%	-
$GIII_bCIII_a$	10 w/v%	1 w/v%
$GIII_bCIII_b$	10 w/v%	2 w/v%
$GIII_bCIII_c$	10 w/v%	3 w/v%
$GIII_bCIII_d$	10 w/v%	5 w/v%
$CIII_e$	**-**	10 w/v%

Table 5-1: Polymer compositions of the various hydrogels developed.

In what follows, hydrogels containing gel-MOD as biopolymer are indicated as type G hydrogels. Hydrogels containing both gel-MOD and CS-MOD are indicated as type GC hydrogels. Hydrogels composed of CS-MOD only are indicated as type C hydrogels. All hydrogels were formed by gelation of (mixtures of) aqueous biopolymer solutions at room temperature, followed by radical UV-induced photo-crosslinking (photo-initiator: Irgacure 2959). Then, the chemically crosslinked

hydrogels were subjected to a cryogenic treatment. The different materials developed are summarised in table 5-1.

2 Scaffold characterization

In the present chapter, the characterization of hydrogels composed of gelatin and/or chondroitin sulphate is described. The materials are compared in terms of their (physico)chemical properties using micro-computed tomography (µ-CT), optical microscopy, atomic force microscopy (AFM), X-ray photo-electron spectroscopy (XPS), swelling experiments and dynamic vapour sorption measurements.

2.1 Hydrogel visualization

The scaffolds developed were characterized using µCT and optical microscopy to obtain information about the pore architecture and the pore size. Micro-CT measurements demonstrated that type $GIII_b$ hydrogels contained top bottom transversal channels with a decreasing pore size from top to bottom (330-20 µm) (figure 5-1, left column). The applied temperature gradient resulted in hydrogel materials with a pore size gradient.

In contrast to what was anticipated, a similar cryogenic treatment applied to hydrogels containing only CS-MOD (type $CIII_e$ hydrogels) lead to materials with deviating pore geometry: a curtain-like geometry consisting of 200 µm spaced parallel plates was observed, as indicated in figure 5-1 (right column). This is most likely due to the parallel stacking of the water-binding glycosaminoglycan chains, as depicted schematically in figure 5-2. Indications supporting this assumption were already described previously in literature.[15, 16] To the best of our knowledge, such well-defined scaffold architectures have so far only been obtained using rapid prototyping techniques.[17-19]

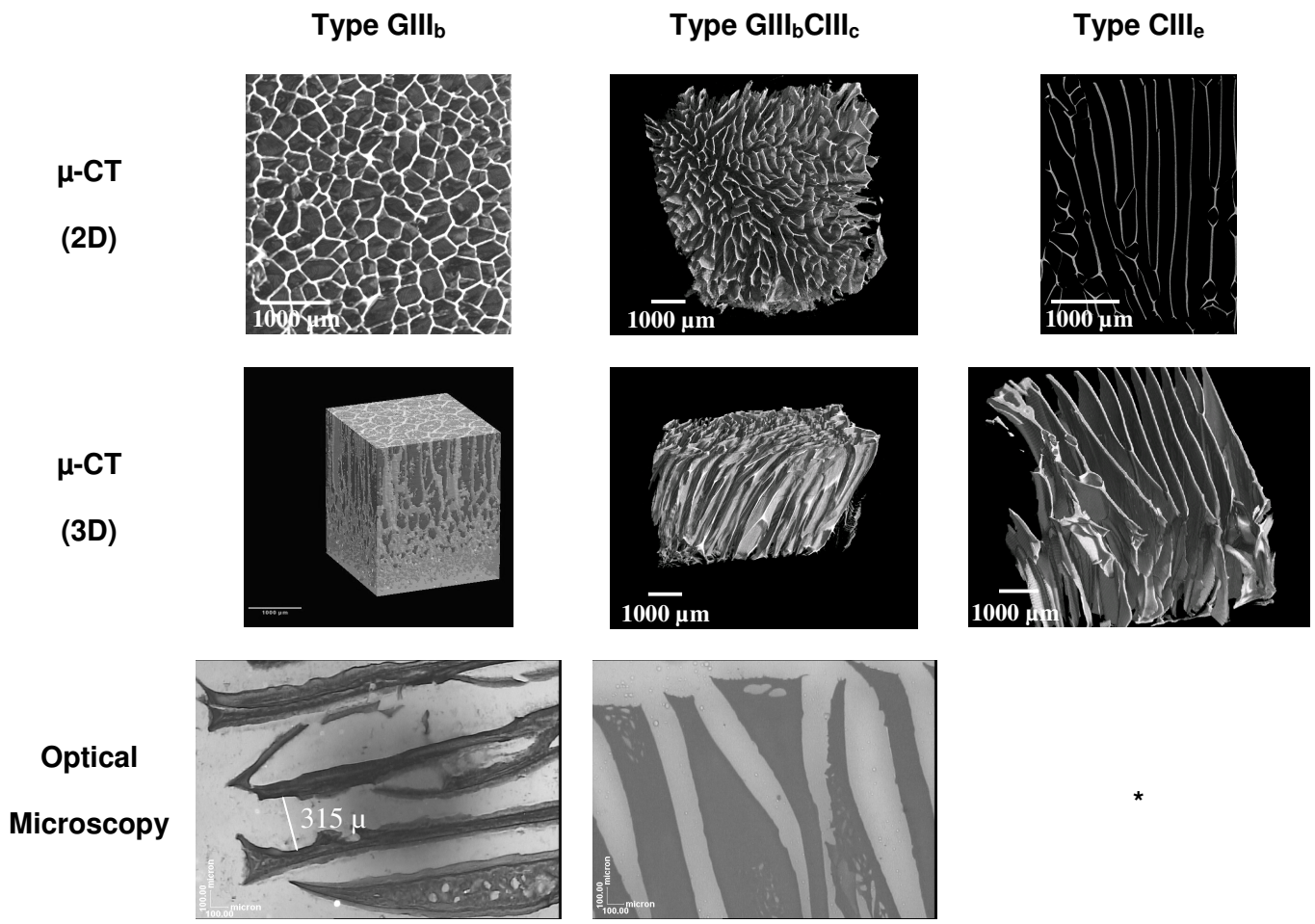

Figure 5-1: μCT (2D and 3D) and optical microscopy analysis of gel-MOD (Type GIII$_b$), CS-MOD (Type CIII$_e$) and a hydrogel containing gel-MOD and CS-MOD (Type GIII$_b$CIII$_c$). The scale bars represent 1000 μm (μ-CT) and 100 μm (optical microscopy). * = No data available (hydrogel bursted during swelling).

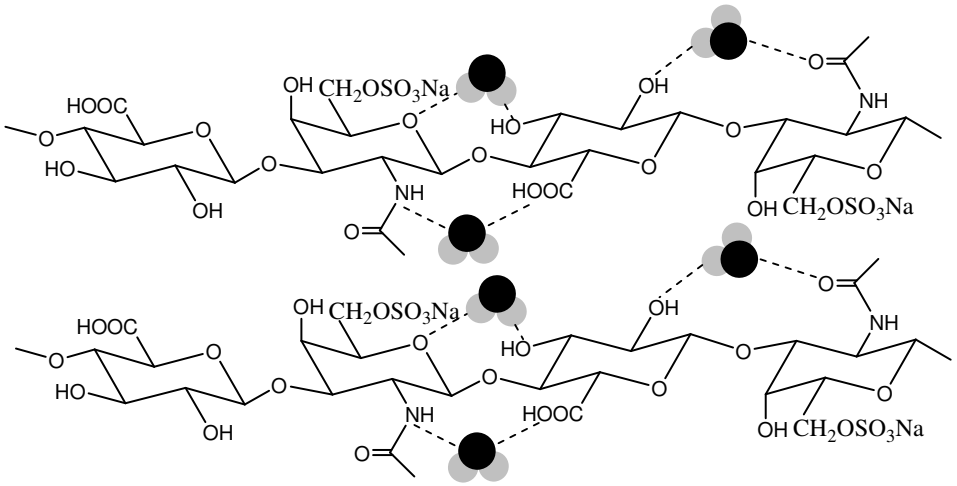

Figure 5-2: Overview demonstrating possible interactions existing between CS and water molecules.

The latter technique consists of various steps. A data processing system processes a designed scaffold model and converts it into a layered process tool path. The motion control system is driven by the layered manufacturing technique. The system can continuously lay down material in the form of line structures to create the desired model by moving the tip over a substrate in the designed path. This process can be repeated layer by layer to obtain the desired matrix.[20] However, the latter technique is rather expensive while, in the present work, the scaffolds were designed by selecting gel-MOD and/or CS-MOD, followed by applying a cryogenic treatment (with simultaneous temperature gradient) and lyophilization.

Porous materials with ordered hole structure have received increasing interest in recent years because of their potential application in the fields of electronics, photonics and life sciences.[21] There exist various strategies to produce porous structures via templating methods based on self-assembly.[22] These methods include using ordered arrays of colloidal crystals[23, 24], microphase separated block copolymers[25, 26], polymers with rod coil architecture that form honeycomb structures[27] and templating using emulsions[28] etc. The application of the porous block copolymers as templates is possible due to the formation of ordered periodic phases after microphase separation of the block copolymer. The simplest form of ordered morphology is the lamellae phase. It is typically formed when an incompatible diblock copolymer is annealed as a thin film and each type of polymer segregates into an

alternate layer stacked on top of each other. However, the latter is only achievable at nanometre scale.

The presented results clearly show that depending on the biopolymers applied, biomimetic materials with varying pore geometries can be easily developed. This unique curtain-like design offers potential for cell sheet engineering. If required, the 'curtains' could be coated in a separate step using cell-interactive peptides or proteins enabling specific cell-material interactions.

For hydrogels containing both gel-MOD and CS-MOD (type $GIII_bCIII_c$ hydrogels), a curtain-like architecture was also obtained. However, in contrast to type $CIII_e$ hydrogels, no parallel plates were observed. It could be anticipated that the observed differences were due to the lower amount of CS-MOD in type $GIII_bCIII_c$ hydrogels compared to type $CIII_e$ hydrogels.

In a subsequent part of the work, the scaffold structures were visualised after incubation in double distilled water at 37°C. In this way, we could investigate whether the scaffold architectures were preserved after *in vivo* or *in vitro* application. Unfortunately, µCT imaging on swollen hydrogels lead to blurred images due to the full hydration of the polymer chains at equilibrium swelling. This could be ascribed to differences in density or atomic number which were too small to enable visualisation by µCT. To solve this problem, freeze-sections of the swollen matrices were stained and visualized by optical microscopy (figure 5-1, bottom part). Type $GIII_b$ and type $GIII_bCIII_c$ hydrogels were sectioned respectively longitudinal and transversal. From the freeze-section images, it could be concluded that the scaffold architectures (i.e. elongated channels for type $GIII_b$ hydrogels and curtain-like for type $GIII_bCIII_c$ scaffolds) were preserved after incubating the hydrogels at body temperature. Moreover, no significant changes in pore size were observed upon comparing the freeze-dried scaffolds with the freeze-section images of swollen hydrogels. Type $CIII_e$ hydrogels were not freeze-sectioned because of their very high swelling potential, often resulting in scaffold cracking. The latter was due to the presence of sulphate groups in CS-MOD, which are able to retain large amounts of water. In addition, type $GIII_b$ and $GIII_bCIII_c$ hydrogels contained gelatin, a physical structuring polymer, which was absent in type $CIII_e$ materials.[29]

Since scaffold staining using various dyes (Alcian blue, Rhodamine B, dextran blue, Ninhydrin) did not enable a selective visualization of neither gelatin nor chondroitin sulphate, AFM was applied to study possible phase separation phenomena between both biopolymers. This might explain the mechanisms leading to the curtain-like pore architecture for type II hydrogels.

The measurements were performed on spincoated gel-MOD/CS-MOD solutions since preliminary AFM measurements indicated the requirement of flat surfaces. In addition to the globular domains of gel-MOD (figure 5-3, left part), mixtures of gel-MOD and CS-MOD contained smaller regions of phase-separated CS-MOD (figure 5-3, right part). We anticipated that both phase separation between gel-MOD and CS-MOD and the parallel stacking of the water-binding CS-MOD chains were responsible for the curtain-like scaffold architecture obtained by combining both biopolymers.

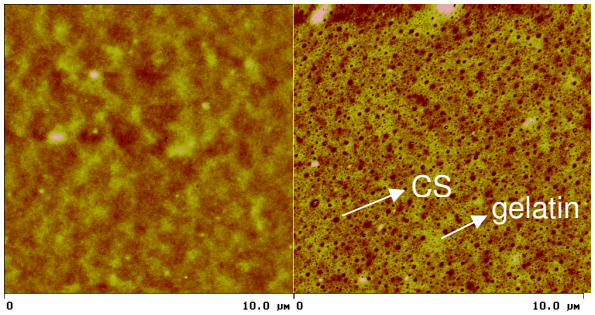

Figure 5-3: Height images of gel-MOD (left) and gel-MOD + CS-MOD films (right), obtained using AFM.

2.2 X-ray photo-electron spectroscopy (XPS)

The observed differences in pore geometry between type $GIII_b$ and $GIII_bCIII_c$ hydrogels were a first indication that both gel-MOD and CS-MOD were introduced in type $GIII_bCIII_c$ hydrogel networks. To further confirm these findings, a series of XPS measurements were performed (see table 5-2, figure 5-4). The sulphur signal appearing in all type $GIII_bCIII_c$ hydrogels confirmed the presence of CS in the developed materials. This characteristic signal was not observed for type $GIII_b$ hydrogels containing only gel-MOD. Type $GIII_b$ hydrogels exhibited higher nitrogen (10%) and no sulphur compared with type $CIII_e$ hydrogels (3% and 4% respectively). This could be ascribed to the fact that the amount of sulphur-containing amino acids

in gel-MOD is too low (0.4% of all amino acids are methionine) to be detected by XPS, which made it a useful technique for indicating the presence of CS in the newly developed hydrogels.

	Atomic composition (%)			
sample	C	N	O	S
Type $GIII_b$	72 ± 3	10 ± 3	18 ± 1	-
Type $GIII_bCIII_c$	60± 3	9 ± 1	30 ± 3	1 ± 1
Type $GIII_bCIII_c$ (inc.)	60 ± 1	11 ± 1	25 ± 1	1 ± 1
Type $CIII_e$	57 ± 3	3 ± 1	35 ± 5	4 ± 1

Table 5-2: Elemental composition of the samples determined by XPS.

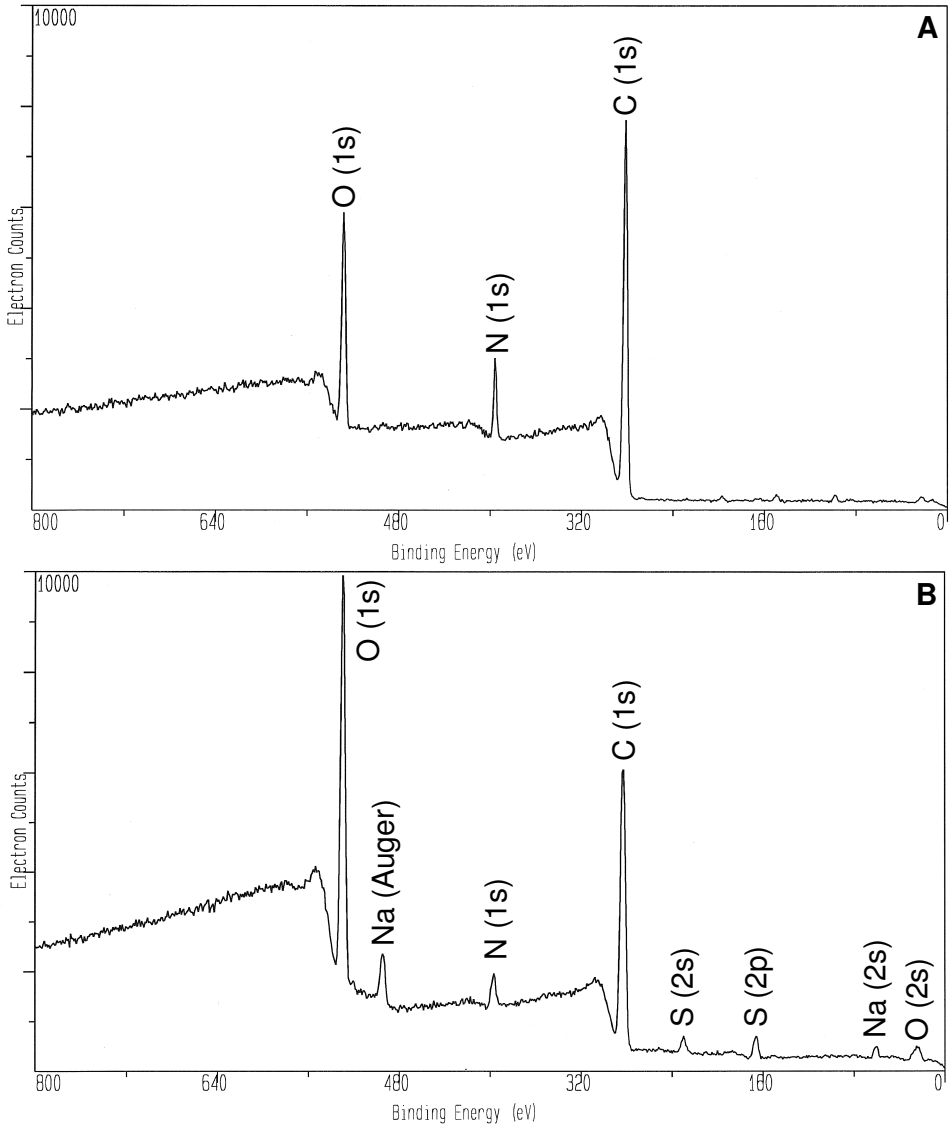

Figure 5-4: Widescan spectra of type $GIII_b$ hydrogel (A) and type $CIII_e$ scaffold (B) obtained by XPS.

Furthermore, incubation at 37°C for 24 hours revealed no significant changes in chemical composition, further indicating a successful covalent immobilisation of the CS-MOD in the type $GIII_bCIII_c$ hydrogel networks.

2.3 Water uptake capacity

For a tissue engineering scaffold, it is important to absorb body fluids and transfer nutrients and metabolites to/from implanted cells.[30] The water uptake capacity of scaffolds is significant in view of their application. Swelling could allow the pore size to increase, making the movement of cells and nutrients within the scaffolds easier.[31] On the other hand, cell adhesion could be hindered. Moreover, the gel swelling and therefore the amount of bulky water, not only depends on the porosity but also on the pore architecture, on the degree of interconnectivity and on the mechanical properties of the gel.[32]
Therefore, we studied the water uptake capacity of type $GIII_bCIII_x$ hydrogels by incubation in double distilled water at 37°C, while monitoring the water uptake at regular time points.

The polymer concentration of porous scaffolds influences the swelling capacity in two opposite ways. First, with increasing polymer concentration, the porosity decreases and the degree of crosslinking increases, both having a de-swelling effect on the scaffolds developed, as already mentioned earlier in the previous chapter (§ 3.3.1).
On the other hand, the amount of chondroitin sulphate present is in proportion with the water-binding capacity.[33, 34] Consequently, two opposing effects arise from the increase in chondroitin sulphate concentration.

Figure 5-5 indicates that the water uptake capacity at equilibrium swelling decreased with an increasing amount of CS-MOD in the hydrogels. Since CS-MOD contained a higher amount of functional groups that could be crosslinked compared to gel-MOD, a higher amount of CS-MOD in the hydrogels lead to materials with a higher crosslink density and thus a lower water uptake capacity.
In order to evaluate the effect of the CS incorporation in type $GIII_bCIII_x$ hydrogels, while excluding the influence of the polymer concentration, the water uptake of type

$GIII_c$ hydrogels was compared with type $GIII_bCIII_d$ hydrogels. From figure 5-5, it could be concluded that the incorporation of chondroitin sulphate into gelatin-based scaffolds resulted in an increase of the water uptake capacity, due to the presence of the CS sulphate groups. This was further confirmed by comparing the equilibrium swelling degree of a type $GIII_bCIII_a$ scaffold with a type $GIII_b$ hydrogel (i.e. 1300% versus 1000%).[35]

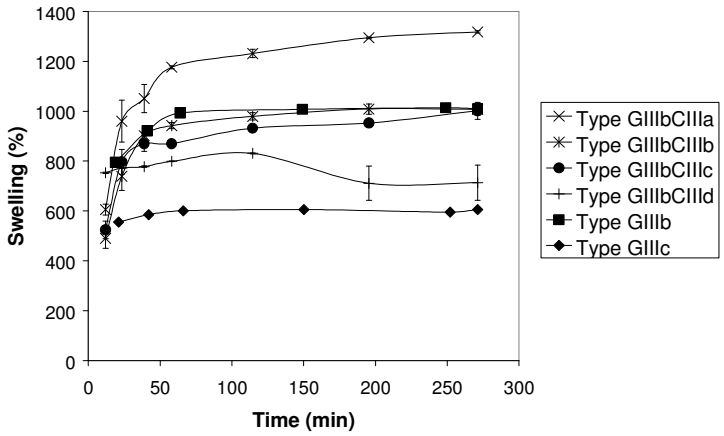

Figure 5-5: Influence of the chondroitin sulphate concentration (1 – 5 w/v%) on the hydration properties of type $GIII_bCIII_x$ hydrogels and comparison with the water uptake capacity of type $GIII_b$ and $GIII_c$ hydrogels.

2.4 Dynamic Vapour Sorption Analysis

Parameters related to water vapour sorption are very important from both a scientific and commercial points of view.[36, 37] The role of water vapour in modifying the properties of biopolymers has been studied extensively in the past.[38-40] The hydration behaviour of proteins is of great relevance since it affects the protein secondary structure formation, as well as chemical and enzymatic reactivities.[41] Knowledge of the water vapour sorption behaviour of the scaffolds developed, is required in case of commercialization. Processes including drying and packaging mainly depend on the product water activity. In many cases, the obtained isotherm can represent the sorption data for the whole range of water activities.[36, 42] The sorption behaviour of the scaffolds developed is also relevant in view of future incorporation of bio-active molecules (e.g. growth factors, fibronectin) within the porous matrices.

2.4.1 Influence of the polymer concentration

The influence of the CS-MOD concentration on the water vapour uptake capacity of type $GIII_bCIII_x$ scaffolds was studied (table 5-3).

Target RH (%)	Change in Mass (%)		
	$GIII_bCIII_a$	$GIII_bCIII_c$	$GIII_bCIII_d$
0	0	0	0
20	5.69	5.50	4.85
40	9.50	9.07	8.70
60	14.57	13.95	14.45
80	23.68	24.25	24.86

Table 5-3: Influence of CS-MOD (DS 30%) concentration on water vapour uptake capacities of type $GIII_bCIII_x$ hydrogels.

In contrast to what we anticipated based on the hydration properties (§ 2.3), it was observed that no significant difference in water vapour uptake capacity occurred between the hydrogels studied. From chapter 4 (§ 3.3.2), it was already concluded that the porosity was the most important factor influencing the water vapour uptake capacity. Consequently, scaffolds consisting of 5 w/v% CS-MOD (i.e. type $GIII_bCIII_d$) were expected to possess the lowest water vapour uptake compared to the hydrogels possessing lower CS-MOD concentrations (i.e. type $GIII_bCIII_a$ and $GIII_bCIII_c$). However, the presence of a higher amount of sulphate groups probably compensated for the porosity decrease.

2.4.2 Influence of the modification degree

Next, the influence of the modification degree of CS-MOD on the water vapour uptake was studied at 25°C. Increasing hydrogel masses during sorption were recorded as a function of the relative humidity (table 5-4).

Target RH (%)	Change in Mass (%)		
	10%	30%	40%
0	0	0	0
20	4.57	4.85	5.63
40	8.47	8.70	9.06
60	13.43	14.45	13.74
80	25.10	24.86	23.31

Table 5-4: Influence of modification degree of CS-MOD on the water vapour uptake capacities of type $GIII_bCIII_d$ hydrogels.

The water vapour uptake decreased with increasing modification degree when applying a relative humidity of 80%. When applying a lower humidity, no significant difference in sorption behaviour was observed between the various scaffolds studied.

2.5 Compression tests

As reported earlier, the goal of tissue engineering is the development of replacement tissues with compositions similar to those of native tissues, with the goal of mimicking the mechanical properties of a given native tissue.[43] Consequently, compression tests needed to be performed in order to obtain information on the mechanical properties of the materials developed.

At present, synthetic biodegradable polymers commonly used for scaffolds in tissue engineering have a limited range of mechanical properties. This limitation is a challenge to *in vivo* tissue engineering, as the cell-scaffold construct is expected to maintain or restore normal tissue biomechanics during new tissue formation.[44]

By varying the amount of added CS-MOD in combination scaffolds with gel-MOD, the mechanical properties can also be adjusted according to the application. In figure 5-6, the compression moduli of the combination scaffolds are presented as a function of the concentration CS-MOD.

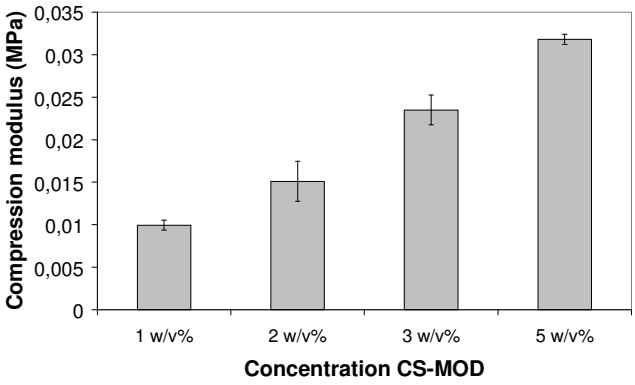

Figure 5-6: Influence of the chondroitin sulphate concentration on the compression modulus of type $GIII_bCIII_x$ scaffolds.

The compression moduli were obtained by means of a texturometer. A constant force was applied onto equilibrium swollen scaffolds with a cylindrical probe. From the slope of the initial, linear part of the stress-strain curves, the different compression moduli were obtained.

As anticipated, the compression moduli increased with increasing polymer concentration and thus with increasing degree of crosslinking. A fivefold increase in the CS-MOD concentration corresponded with a threefold increase in compression modulus.

3 Conclusion

In the present chapter, highly porous biomimetic hydrogels based on a combination of gelatin and chondroitin sulphate (CS) have been developed and characterized.
It was shown that variation of the hydrogel composition (i.e. increasing the amount of CS), lead to a modulation of the scaffold architecture. For gelatin based hydrogels, a channel-like pore morphology was obtained. CS-based hydrogels and hydrogels containing both gelatin and CS possessed a curtain-like pore architecture. We anticipated that both phase separation between gel-MOD and CS-MOD as indicated by AFM analysis and the parallel stacking of the water-binding CS-MOD chains were responsible for the curtain-like scaffold architecture. To the best of our knowledge, materials with such well defined pore geometries have not yet been reported. The materials composed of parallel plates offer a potential for a variety of applications e.g. as cell carriers. Moreover, the material can be coated with cell-interactive peptide sequences to stimulate selective cell interactions. Furthermore, it could also be applied in membrane technology to enable the transfer of only specific, preset geometrical shapes.

The scaffolds developed, both pure CS-MOD and combination scaffolds with gel-MOD, were visualized using µCT. Next, freeze-sections obtained from hydrogels, swollen to equilibrium in double distilled water at 37°C, were studied by means of optical microscopy. From the freeze-section images, it appeared that the scaffold architecture was maintained during incubation at body temperature.

Finally, the physico-chemical properties of the scaffolds developed were examined.
XPS-measurements before and after incubation at 37°C demonstrated the presence of chondroitin sulphate into the hydrogels. Furthermore, both the swelling capacities and the mechanical properties could be easily varied by changing either the polymer concentration or the modification degree of CS-MOD.

References

1. Kuijpers, A. J.; van Wachem, P. B.; van Luyn, M. J. A.; Brouwer, L. A.; Engbers, G. H. M.; Krijgsveld, J.; Zaat, S. A. J.; Dankert, J.; Feijin, J., In vitro and in vivo evaluation of gelatin-chondroitin sulphate hydrogels for controlled release of antibacterial proteins. *Biomaterials* **2000,** 21, (17), 1763-1772.
2. Kuijpers, A. J.; Engbers, G. H. M.; Meyvis, T. K. L.; de Smedt, S. S. C.; Demeester, J.; Krijgsveld, J.; Zaat, S. A. J.; Dankert, J.; Feijen, J., Combined gelatin-chondroitin sulfate hydrogels for controlled release of cationic antibacterial proteins. *Macromolecules* **2000,** 33, (10), 3705-3713.
3. Chang, C. H.; Kuo, T. F.; Lin, C. C.; Chou, C. H.; Chen, K. H.; Lin, F. H.; Liu, H. C., Tissue engineering-based cartilage repair with allogenous chondrocytes and gelatin-chondroitin-hyaluronan tri-copolymer scaffold: A porcine model assessed at 18, 24, and 36 weeks. *Biomaterials* **2006,** 27, (9), 1876-1888.
4. Chang, C. H.; Liu, H. C.; Lin, C. C.; Chou, C. H.; Lin, F. H., Gelatin-chondroitin-hyaluronan tri-copolymer scaffold for cartilage tissue engineering. *Biomaterials* **2003,** 24, (26), 4853-4858.
5. Wang, T. W.; Wu, H. C.; Huang, Y. C.; Sun, J. S.; Lin, F. H., Biomimetic bilayered gelatin-chondroitin 6 sulfate-hyaluronic acid biopolymer as a scaffold for skin equivalent tissue engineering. *Artificial Organs* **2006,** 30, (3), 141-149.
6. Wang, T. W.; Sun, J. S.; Wu, H. C.; Tsuang, Y. H.; Wang, W. H.; Lin, F. H., The effect of gelatin-chondroitin sulfate-hyaluronic acid skin substitute on wound healing in SCID mice. *Biomaterials* **2006,** 27, (33), 5689-5697.
7. Yang, S. H.; Chen, P. Q.; Chen, Y. F.; Lin, F. H., An in-vitro study on regeneration of human nucleus pulposus by using gelatin/chondroitin-6-sulfate/hyaluronan tri-copolymer scaffold. *Artificial Organs* **2005,** 29, (10), 806-814.
8. Brown, K. E.; Leong, K.; Huang, C. H.; Dalal, R.; Green, G. D.; Haimes, H. B.; Jimenez, P. A.; Bathon, J., Gelatin/chondroitin 6-sulfate microspheres for the delivery of therapeutic proteins to the joint. *Arthritis and Rheumatism* **1998,** 41, (12), 2185-2195.
9. Azhari, R.; Hirosue, S.; Leong, K. W., Chondroitin Sulfate/Gelatin Microspheres - Preparation, Characterization and Release Kinetics. *Abstracts of Papers of the American Chemical Society* **1992,** 203, 18-CELL.
10. Yonese, M.; Nakagaki, M., Physicochemical Studies of Mixed Membrane Composed of Gelatin and Chondroitin Sulfate .5. Dependence of Electrolyte Permeabilities on Membrane Charge-Density and Water-Content. *Yakugaku Zasshi-Journal of the Pharmaceutical Society of Japan* **1981,** 101, (6), 493-500.
11. Yonese, M.; Nakagaki, M., Physicochemical Studies of Mixed Membrane Composed of Gelatin and Chondroitin Sulfate .4. Membrane Charge-Density and Its Ph Dependency. *Yakugaku Zasshi-Journal of the Pharmaceutical Society of Japan* **1976,** 96, (3), 299-306.

12. Yonese, M.; Nakagaki, M., Physicochemical Studies of Mixed Membrane Composed of Gelatin and Chondroitin Sulfate .2. Effect of Chondroitin Sulfate Concentration and of Complex-Formation on Swelling. *Yakugaku Zasshi-Journal of the Pharmaceutical Society of Japan* **1975,** 95, (6), 641-647.
13. Yonese, M.; Nakagaki, M., Physicochemical Studies of Mixed Membrane Composed of Gelatin and Chondroitin Sulfate .3. Permeability of Electrolytes and Its Ph-Dependence. *Yakugaku Zasshi-Journal of the Pharmaceutical Society of Japan* **1975,** 95, (6), 665-671.
14. Yonese, M.; Nakagaki, M., Physicochemical Studies of Mixed Membrane Composed of Gelatin and Chondroitin Sulfate .1. Ph-Dependence and Anisotropy of Swelling. *Yakugaku Zasshi-Journal of the Pharmaceutical Society of Japan* **1975,** 95, (1), 75-81.
15. Almond, A., Towards understanding the interaction between oligosaccharides and water molecules. *Carbohydrate Research* **2005,** 340, (5), 907-920.
16. Seog, J.; Dean, D.; Rolauffs, B.; Wu, T.; Genzer, J.; Plaas, A. H. K.; Grodzinsky, A. J.; Ortiz, C., Nanomechanics of opposing glycosaminoglycan macromolecules. *Journal of Biomechanics* **2005,** 38, (9), 1789-1797.
17. Landers, R.; Hubner, U.; Schmelzeisen, R.; Mulhaupt, R., Rapid prototyping of scaffolds derived from thermoreversible hydrogels and tailored for applications in tissue engineering. *Biomaterials* **2002,** 23, (23), 4437-4447.
18. Khalil, S.; Nam, J.; Sun, W., Multi-nozzle deposition for construction of 3D biopolymer tissue scaffolds. *Rapid Prototyping Journal* **2005,** 11, (1), 9-17.
19. Mironov, V.; Boland, T.; Trusk, T.; Forgacs, G.; Markwald, R. R., Organ printing: computer-aided jet-based 3D tissue engineering. *Trends in Biotechnology* **2003,** 21, (4), 157-161.
20. Tsang, V. L.; Bhatia, S. N., Three-dimensional tissue fabrication. *Advanced Drug Delivery Reviews* **2004,** 56, (11), 1635-1647.
21. Hoa, M. L. K.; Lu, M. H.; Zhang, Y., Preparation of porous materials with ordered hole structure. *Advances in Colloid and Interface Science* **2006,** 121, (1-3), 9-23.
22. Peng, J.; Han, Y.; Yang, Y.; Li, B., The influencing factors on the macroporous formation in polymer films by water droplet templating. *Polymer* **2004,** 45, (2), 447-452.
23. Gates, B.; Yin, Y. D.; Xia, Y. N., Fabrication and characterization of porous membranes with highly ordered three-dimensional periodic structures. *Chemistry of Materials* **1999,** 11, (10), 2827-2836.
24. Velev, O. D.; Jede, T. A.; Lobo, R. F.; Lenhoff, A. M., Porous silica via colloidal crystallization. *Nature* **1997,** 389, (6650), 447-448.
25. Li, Z.; Zhao, W.; Liu, Y.; Rafailovich, M. H.; Sokolov, J.; Khougaz, K.; Eisenberg, A.; Lennox, R. B.; Krausch, G., Self-ordering of diblock copolymers from solution. *Journal of the American Chemical Society* **1996,** 118, (44), 10892-10893.
26. Park, M.; Harrison, C.; Chaikin, P. M.; Register, R. A.; Adamson, D. H., Block copolymer lithography: Periodic arrays of similar to 10(11) holes in 1 square centimeter. *Science* **1997,** 276, (5317), 1401-1404.

27. Jenekhe, S. A.; Chen, X. L., Self-assembly of ordered microporous materials from rod-coil block copolymers. *Science* **1999,** 283, (5400), 372-375.
28. Imhof, A.; Pine, D. J., Ordered macroporous materials by emulsion templating. *Nature* **1997,** 389, (6654), 948-951.
29. Djabourov, M., Architecture of Gelatin Gels. *Contemporary Physics* **1988,** 29, (3), 273-297.
30. Peng, L.; Cheng, X. R.; Wang, J. W.; Xu, D. X.; Wang, G., Preparation and evaluation of porous chitosan/collagen scaffolds for periodontal tissue engineering. *Journal of Bioactive and Compatible Polymers* **2006,** 21, (3), 207-220.
31. Vipin Verma, P. V. S. K. P. R. A. R. R., Fabrication of agar-gelatin hybrid scaffolds using a novel entrapment method for in vitro tissue engineering applications. *Biotechnology and Bioengineering* **2007,** 96, (2), 392-400.
32. Sannino, A.; Netti, P. A.; Mensitieri, G.; Nicolais, L., Designing microporous macromolecular hydrogels for biomedical applications: a comparison between two techniques. *Composites Science and Technology* **2003,** 63, (16), 2411-2416.
33. Daamen, W. F.; van Moerkerk, H. T. B.; Hafmans, T.; Buttafoco, L.; Poot, A. A.; Veerkamp, J. H.; van Kuppevelt, T. H., Preparation and evaluation of molecularly-defined collagen-elastin-glycosaminoglycan scaffolds for tissue engineering. *Biomaterials* **2003,** 24, (22), 4001-4009.
34. Lee, J. E.; Kim, K. E.; Kwon, I. C.; Ahn, H. J.; Lee, S. H.; Cho, H. C.; Kim, H. J.; Seong, S. C.; Lee, M. C., Effects of the controlled-released TGF-beta 1 from chitosan microspheres on chondrocytes cultured in a collagen/chitosan/glycosaminoglycan scaffold. *Biomaterials* **2004,** 25, (18), 4163-4173.
35. VanVlierberghe, S.; Dubruel, P.; Lippens, E.; Cornelissen, M.; Schacht, E., Porous gelatin cryogels for tissue engineering applications: Correlation between cryogenic parameters and physico-chemical properties. *Submitted for publication* **2007**.
36. Czepirski, L.; Komorowska-Czepirska, E.; Szymonska, J., Fitting of different models for water vapour sorption on potato starch granules. *Applied Surface Science* **2002,** 196, (1-4), 150-153.
37. Mousia, Z.; Farhat, I. A.; Blachot, J. F.; Mitchell, J. R., Effect of water partitioning on the glass-transition behaviour of phase separated amylopectin-gelatin mixtures. *Polymer* **2000,** 41, (5), 1841-1848.
38. Bravo-Osuna, I.; Ferrero, C.; Jimenez-Castellanos, M. R., Water sorption-desorption behaviour of methyl methacrylate-starch copolymers: effect of hydrophobic graft and drying method. *European Journal of Pharmaceutics and Biopharmaceutics* **2005,** 59, (3), 537-548.
39. Mann, B.; Malik, R. C., Water vapour sorption properties of buffalo milk whey protein concentrates. *Journal of Food Science and Technology-Mysore* **1996,** 33, (5), 403-406.
40. Ayranci, E., Moisture sorption of cellulose based edible films. *Nahrung-Food* **1996,** 40, (5), 274-276.
41. Nokhodchi, A.; Ford, J. L.; Rubinstein, M. H., Studies on the interaction between water and (hydroxypropyl)methylcellulose. *Journal of Pharmaceutical Sciences* **1997,** 86, (5), 608-615.

42. Tesch, R.; Ramon, O.; Ladyzhinski, I.; Cohen, Y.; Mizrahi, S., Water sorption isotherm of solution containing hydrogels at high water activity. *International Journal of Food Science and Technology* **1999,** 34, (3), 235-243.
43. Dahl, S. L. M.; Rhim, C.; Song, Y. C.; Niklason, L. E., Mechanical properties and compositions of tissue engineered and native arteries. *Annals of Biomedical Engineering* **2007,** 35, (3), 348-355.
44. Webb, A. R.; Kumar, V. A.; Ameer, G. A., Biodegradable poly(diol citrate) nanocomposite elastomers for soft tissue engineering. *Journal of Materials Chemistry* **2007,** 17, (9), 900-906.

Chapter VI:
Alternative Crosslinking Methods

1 Introduction

In literature, three mechanisms for cryogel production have been distinguished:[1]

1) Freezing before gelation
2) Freezing after gelation
3) Simultaneous freezing and gelation

In the present work, the hydrogel gelation can be subdivided into two categories. During hydrogel crosslinking, both physical entanglements inherent to gelatin and covalent bonds are introduced.

Since the water-gelatin system is rather fast-gelling, especially at polymer concentrations above 5 w/v%, it is a complicated task to perform a real cryotropic gel formation (i.e. the gel formation within the unfrozen liquid microphase). For such fast-gelling mixtures, one deals with the kinetic competition between the freezing and the 'self-gelling' processes during cooling.[2] Since the physical gelation of a 10 w/v% gelatin solution cannot be avoided when applying a cryogenic treatment, performing '*freezing before* ***physical*** *gelation*' is impossible. As a consequence, the present chapter will deal with the chemical crosslinking of gelatin after freezing or lyofilization. Up to now, the chemical crosslinking step (i.e. UV irradiation) was performed before the cryogenic treatment. As a consequence, freezing occurred after chemical crosslinking. Plieva et al. demonstrated that polyacrylamide gels prepared by freezing after gelation possessed different mechanical properties compared to cryogels developed by freezing before gelation.[1] In the present chapter, we wanted to study

whether '*freezing before* ***chemical*** *gelation*' would result into scaffolds possessing larger pore sizes compared to the gels, produced by 'freezing after gelation'.

In a first part, uncrosslinked, freeze-dried scaffolds prepared as described earlier (see chapter 4) were irradiated with UV-light (279 nm, 1 hour). Next, the crosslinking degree was evaluated by incubating the samples at 37°C in double distilled water. Since the hydrogels dissolved completely during this incubation period, alternative approaches were elaborated.

There exist different methods to crosslink polymers, as already mentioned in chapter 3 (see § 2). High energy irradiation, including gamma-, ion- and electron-beam were already applied often to crosslink polymers, for the curing of coatings and inks and to modify surfaces with reactive groups.[3]
In the present work, the effect of e-beam, redoxinitiators and 1-ethyl-3-(3-dimethylaminopropyl) carbodiimide hydrochloride (EDC) on the crosslink efficiency of the 3D scaffolds developed, was evaluated.

2 E-beam

2.1 E-beam after lyophilization

Hydrogels produced by high-energy electron irradiation possess various advantages:[4]

- ✓ Sterilization and crosslinking occurs in one step.
- ✓ Physical properties can be easily controlled by varying the applied dose.
- ✓ The electron penetration profile (i.e. the crosslink density depends on the electron penetration depth) enables the production of hydrogels possessing a soft surface, but having better mechanical properties at the opposite site, making them suitable for wound treatment applications.

First, the influence of the irradiation dose on the mechanical properties of the hydrogels, was evaluated by means of compression tests. The compression moduli were obtained from the slope of the initial, linear part of the stress-strain plots. In figure 6-1, the compression moduli are plotted as a function of the irradiation dose. From the results, it appeared that the compression moduli increased linearly with increasing irradiation dose applied. The e-beam treatments were performed in the absence of oxygen since the latter functions as a crosslink inhibitor.

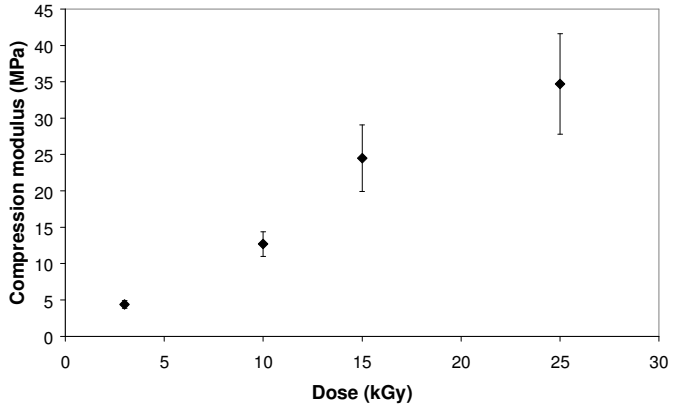

Figure 6-1: Compression moduli of type $GIII_b$ scaffolds, as a function of the irradiation dose applied.

After e-beam irradiation, the hydrogels were incubated at 37°C in double distilled water. Both the equilibrium swelling degree and the gel fraction of the incubated gelatin samples were determined and plotted as a function of the applied dose (figure 6-2).

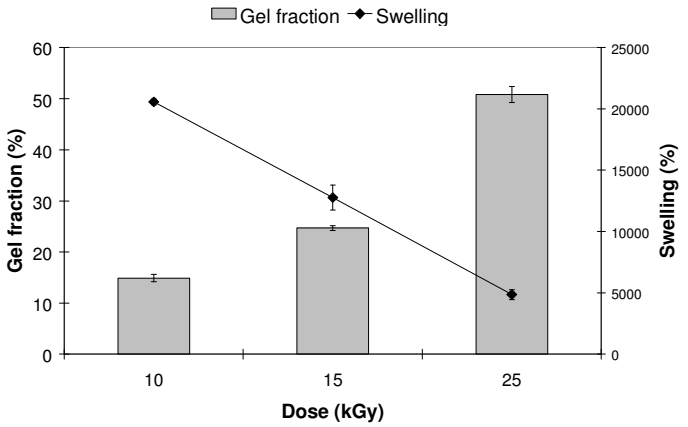

Figure 6-2: Equilibrium swelling degree and gel fraction of incubated hydrogels (type $GIII_b$) as a function of the applied dose.

From the results in figure 6-2, it was concluded that applying an irradiation dose of 25 kGy to the freeze-dried gelatin samples, resulted in scaffolds possessing a gel fraction of ± 50%. The latter implies that 50% of the polymer chains dissolved after incubation in double distilled water at 37°C. The applied dose (i.e. 25 kGy) was not increased further, based on current international standards, EN 552 and ISO 11137, recommending an irradiation dose of 25 kGy as a reference dose for terminal sterilization.[5, 6]

2.2 E-beam before lyophilization

Petrov et al already described the UV-irradiation of moderately frozen cellulose derivatives. In that study, the mechanical properties of samples, UV-treated at room temperature or irradiated at -30°C were compared. The higher crosslink efficiency after UV-irradiation at -30°C was ascribed to the polymer accumulation in the NFLMP. Due to the non-frozen solvent, the NFLMP remained liquid and the polymers retained sufficient segmental mobility to enable crosslinking.[7]
Since hydrogels possessing a gel fraction of 50%, were obtained after applying e-beam (25 kGy) on freeze-dried samples (see § 2.1), the effect of e-beam on frozen samples was also evaluated at -5°C and at -30°C.

Applying high-energy irradiation at **-30°C** did not result in a gel fraction increase. Probably, segmental mobility was partly excluded at -30°C, which hindered sufficient crosslinking. Moreover, beside crosslinking, degradation of polymer chains also occurs during e-beam treatment, as already described earlier.[8, 9]

When the crosslinking reaction was performed at **-5°C**, high gel fractions ranging from 85% to 99% were accomplished, even in the presence of oxygen. This confirmed the previous statement that sufficient segmental mobility is necessary to induce chemical crosslinking of the polymer chains. The scaffolds developed were visualized after lyophilization using µCT (see figure 6-3).

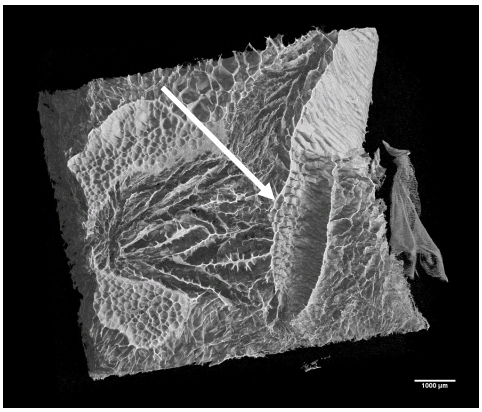

Figure 6-3: µCT image of an e-beam-treated type $GIII_b$ scaffold after freeze-drying. The scale bar represents 1000 µm.

From figure 6-3, it was observed that the pore size was in the same range compared to scaffolds prepared by 'freezing after gelation' (i.e. 330 µm ± 48 µm, see chapter 4). However, more irregularities were present within the e-beam-treated cryogels, as indicated with an arrow (see figure 6-3).

In a subsequent part of the present work, redox-initiating systems were introduced.

3 Crosslinking by use of redoxinitiators

A very effective method to generate free radicals under mild conditions is by one-electron transfer reactions, such as redox initiation.[10] A large variety of redox systems was already applied before to crosslink polymer systems.[11, 12]
In the present work, three redox systems (i.e. cerium ammonium nitrate, a combination of ammonium persulphate and TEMED and Fenton's reagent) will be applied and compared in order to crosslink gel-MOD scaffolds after implementation of a cryogenic treatment.

3.1 Cerium ammonium nitrate

Ceric salt was already applied earlier to initiate the polymerization of acrylamide.[13] The mechanism was explained by a radical process based upon Ce^{4+}-coordinated acrylamide. As a result, cerium ammonium nitrate (CAN) was evaluated as initiator for the polymerization of gel-MOD. Uncrosslinked gel-MOD hydrogels were treated cryogenically, followed by lyophilization. In a subsequent step, the freeze-dried scaffolds were swollen in an aqueous solution containing various ceric salt concentrations (5 - 10 mol%). Since the resulting scaffolds dissolved, an NMR-spectrum of gel-MOD was recorded after addition of 10 mol% CAN to study the effect of CAN on the double bonds present. From the spectrum (data not shown), it could be concluded that only 5% of the double bonds had reacted. The latter can be explained since gelatin possesses a large variety of functionalities (e.g. hydroxyls) which are sensitive to CAN.[14]

3.2 Ammonium persulphate + TEMED

Ammonium persulphate (APS) is typically used for polyacrylamide gel electrophoresis (PAGE). A mixture of acrylamide and bisacrylamide can form a chemically crosslinked polymer network in the presence of APS. N,N,N',N'-tetramethylenediamine (TEMED) functions as an accelerator for the polymerization reaction. Since incubating freeze-dried gelatin scaffolds in aqueous solutions, containing various ratios of APS and TEMED, did not result in chemical crosslinking, an alternative approach was elaborated and evaluated.

As already described earlier (§ VI.1), we wanted the chemical crosslinking to occur after the cryogenic treatment.
Consequently, APS and TEMED were added in various concentrations (5 – 40 mol%) and ratios to two series of samples, of which the first were incubated at 5°C and the second cryogenically treated, followed by incubation at -30°C. The concentrations were selected based on literature data describing the synthesis of polyacrylamide

gels at subzero temperatures.[1, 15, 16] After the lyophilization, the samples were incubated in double distilled water at 37°C to determine the crosslink efficiency. In table 6-1, chemically crosslinked (cryo)gels are indicated by 'x', while the uncrosslinked samples are marked by '-'.

Concentration APS	5°C	-30°C
5 mol%	-	-
10 mol%	-	x
20 mol%	x	x
30 mol%	x	x
40 mol%	x	x

Table 6-1: Formation of chemically crosslinked gelatin (cryo)gels.

From the results, it can be concluded that 10 mol% initiator is sufficient to enable chemical crosslinking at -30°C. Moreover, incubating these samples at 5°C did not result into the formation of chemically crosslinked hydrogels. As a consequence, a concentration of 10 mol% was selected to enable 'freezing before gelation (i.e. chemical crosslinking)' and/or 'simultaneous freezing and gelation'. The obtained gel fraction (i.e. 76%) was similar to the value obtained before, when applying a cryogenic treatment to chemically crosslinked gel-MOD hydrogels (chapter 4).
A disadvantage of this approach was that the obtained scaffolds sometimes collapsed. Moreover, the reproducibility was rather low, resulting in scaffolds possessing lower gel fractions compared to the conventional matrices.

3.3 Fenton's reagent

The metal catalysed Haber-Weiss reaction, also called Fenton reaction, has already been applied earlier for the free-radical polymerisation of hydrogel systems.[17] This redox system involves the combination of H_2O_2 and ferrous salt to generate radicals.[18] The mechanism involves a one-electron transfer from the ferrous ion to the peroxide with the dissociation of the oxygen-oxygen bond and the generation of one hydroxyl radical and one hydroxyl ion:[10]

$$Fe^{2+} + H_2O_2 \rightarrow [HO^{\cdot}\text{-}OH]Fe^{3+} \rightarrow Fe^{3+} + OH^{-} + OH^{\cdot}$$

In a subsequent step, the hydroxyl radicals can initiate the polymerization of vinyl-substituted gelatin.

Freeze-dried gelatin scaffolds were incubated during different time periods (1-24 hours) in aqueous solutions containing various amounts of initiator (2-10 mol%) in the absence or in the presence of ascorbic acid, functioning as catalyst. Since all hydrogels studied dissolved when incubating them at 37°C, it could be concluded that the scaffolds were not crosslinked chemically by the applied redox system.

In order to investigate the effect of the initiator system on the double bonds incorporated, NMR-spectra were recorded before and after addition of Fenton's reagent to gel-MOD. From the spectra, it could be concluded that only 5% of the double bonds present had reacted after addition of the redox system (data not shown).[19] Probably, the latter can be explained since gelatin possesses many other functionalities being sensitive for the redox system applied.[20]

4 Crosslinking with N-(3-dimethylaminopropyl)-N'-ethyl-carbodiimide (EDC)

Chemical crosslinking agents can be classified into non zero-length and zero-length crosslinkers.[21]

Non-zero length agents introduce poly- and bifunctional crosslinks into the network structure by bridging free amine groups of lysine and hydroxylysine, or free carboxylic acid residues of glutamic and aspartic acid of the protein molecules.

Zero-length crosslinkers introduce crosslinks without incorporation of foreign substances into the polymer, for example, by activation of the carboxylic acid groups with EDC, enabling the reaction with free amines.[22] N-Hydroxysuccinimide (NHS) is often added to the reaction mixture to improve the crosslink efficiency by reducing

side-reactions.[23-25] Crosslinking of gelatin with EDC and NHS takes place according to the mechanism in figure 6-4.

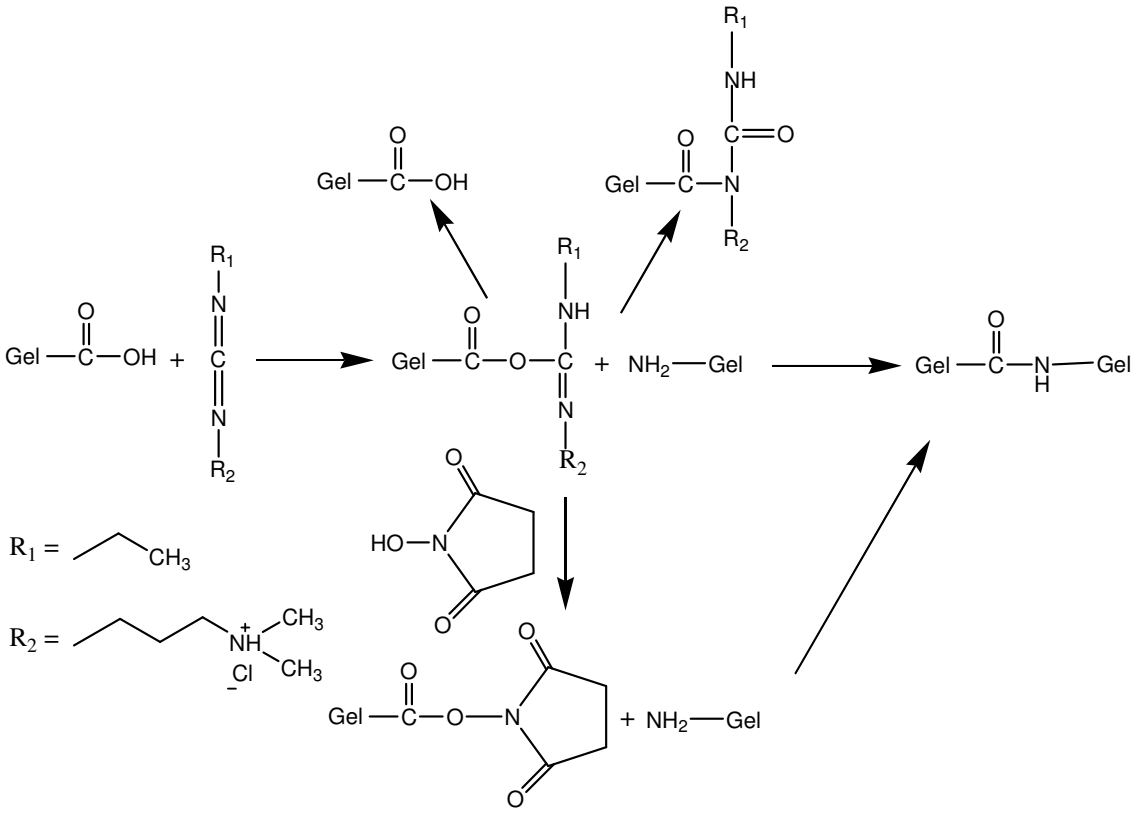

Figure 6-4: Reaction scheme for the crosslinking reaction of gelatin with EDC and NHS.

The carbodiimide activates carboxylic acid residues of aspartic and glutamic acid, with the formation of O-acylisourea groups. Next, amine groups of lysine and hydroxylysine residues can nucleophilicly attack the activated carboxylic acids, with a urea derivative as a leaving group. In order to diminish possible side reactions, such as hydrolysis and rearrangement to a stable N-acylurea, NHS can be added. All residues are water soluble and can be easily washed out after the crosslinking procedure.

It was already described earlier that the incubation of uncrosslinked gelatin-based scaffolds in aqueous solutions often resulted in matrix collapse.[26, 27] As a consequence, a mixture of acetone and water (9:1) was selected as reaction medium. Gelatin scaffolds were incubated overnight in the presence of various EDC/NHS concentrations. After washing in double distilled water, the crosslinked hydrogels were freeze-dried and characterized using SEM and µ-CT (figure 6-5).

From the SEM image, it was observed that the pore walls showed higher roughness compared to conventional hydrogels. Small pores seemed to be present on the surface of larger pores (figure 6-5, upper left). An average pore diameter of 123 µm (± 10 µm) was calculated, based on 10 pores randomly selected throughout the scaffold.

Unfortunately, from µ-CT analysis various inhomogeneous structures were observed within the 3D scaffolds (figure 6-5, bottom). The average pore diameter was 244 µm (± 75 µm), based on 10 pores randomly selected throughout the entire scaffold. The pore size, obtained using µCT was higher compared to the pore diameter calculated from SEM images. The latter can be attributed to the presence of large fractures, visualized using µCT. The relatively high deviation (i.e. 75 µm) of the pore diameter, obtained by µCT supports this explanation.

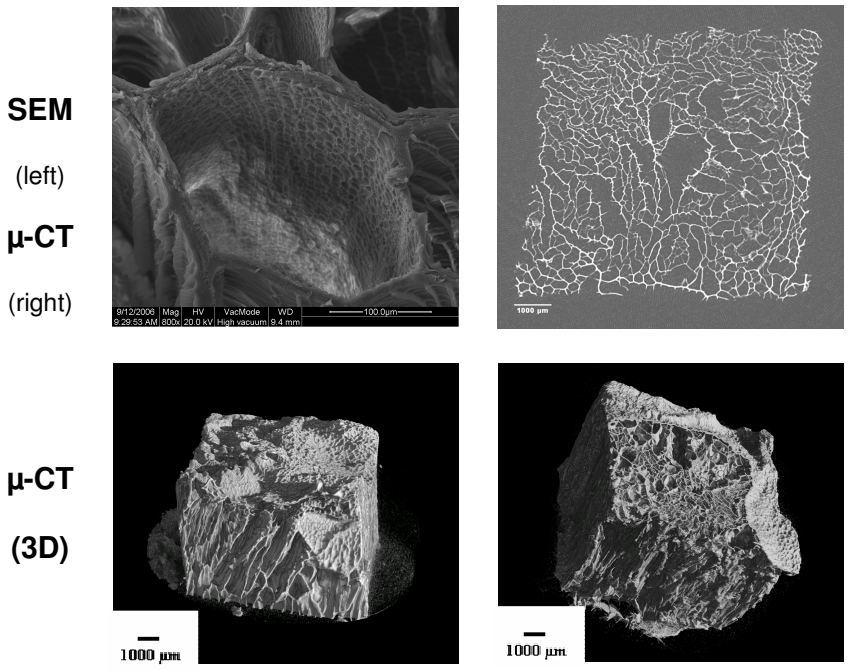

Figure 6-5: Images of the EDC-crosslinked gel-MOD scaffolds obtained with SEM and µ-CT.

The gel fraction of the scaffolds developed was 70%, thus somewhat lower compared to conventional hydrogels.

5 Conclusions

In the present chapter, alternative approaches were elaborated to enable chemical crosslinking of the frozen or freeze-dried scaffolds developed.

E-beam did not enable chemical crosslinking of lyophilized gel-MOD scaffolds nor frozen cryogels at -30°C. The lack of sufficient segmental mobility hindered the reaction of the double bonds present on the gelatin backbone. However, when performing the high-energy irradiation at -5°C, apparently enough segmental mobility within the non-frozen liquid microphase was retained enabling the chemical crosslinking after performing the cryogenic treatment.

Next, various redoxinitiators were added and their crosslink efficiency was evaluated. Cerium ammonium nitrate and Fenton's reagent were unable to chemically crosslink gel-MOD sufficiently.
Alternatively, adding ammoniumpersulphate and TEMED often resulted in the formation of scaffolds with a sufficient gel fraction (75%). However, poor reproducibility and matrix collapse indicated the need for alternative crosslink procedures.

Finally, EDC and NHS were found suitable to efficiently crosslink freeze-dried gelatin matrices. Nevertheless, the presence of inhomogeneous structures within the crosslinked 3D-scaffolds made us decide to prefer for further use of the conventional crosslinking method.

References

1. Plieva, F.; Xiao, H. T.; Galaev, I. Y.; Bergenstahl, B.; Mattiasson, B., Macroporous elastic polyacrylamide gels prepared at subzero temperatures: control of porous structure. *Journal of Materials Chemistry* **2006,** 16, (41), 4065-4073.
2. Bloch, K.; Lozinsky, V. I.; Galaev, I. Y.; Yavriyanz, K.; Vorobeychik, M.; Azarov, D.; Damshkaln, L. G.; Mattiasson, B.; Vardi, P., Functional activity of insulinoma cells (INS-1E) and pancreatic islets cultured in agarose cryogel sponges. *Journal of Biomedical Materials Research Part A* **2005,** 75A, (4), 802-809.
3. Clough, R. L., High-energy radiation and polymers: A review of commercial processes and emerging applications. *Nuclear Instruments & Methods in Physics Research Section B-Beam Interactions with Materials and Atoms* **2001,** 185, 8-33.
4. Lugao, A. B.; Malmonge, S. M., Use of radiation in the production of hydrogels. *Nuclear Instruments and Methods in Physics Research Section B: Beam Interactions with Materials and Atoms* **2001,** 185, (1-4), 37-42.
5. CEN, Sterilization of medical devices—validation and process control of sterilization by irradiation. In European Committee for Standardisation 1994; Vol. EN 552.
6. ISO, Sterilization of health care productsrequirements for validation and routine control-radiation sterilization. In International Organisation for Standardisation: 1995; Vol. ISO 11137.
7. Petrov, P.; Petrova, E.; Stamenova, R.; Tsvetanov, C. B.; Riess, G., Cryogels of cellulose derivatives prepared via UV irradiation of moderately frozen systems. *Polymer* **2006,** 47, (19), 6481-6484.
8. Filipczak, K.; Wozniak, M.; Ulanski, P.; Olah, L.; Przybytniak, G.; Olkowski, R. M.; Lewandowska-Szumiel, M.; Rosiak, J. M., Poly (epsilon-caprolactone) biomaterial sterilized by E-beam irradiation. *Macromolecular Bioscience* **2006,** 6, (4), 261-273.
9. Van Den Bulcke, A. Synthese en evaluatie van hydrogelen op basis van gelatine. 2000.
10. Sarac, A. S., Redox polymerization. *Progress in Polymer Science* **1999,** 24, (8), 1149-1204.
11. Jayakrishnan, A.; Haragopal, M.; Mahadevan, V., Polymerization of Acrylonitrile Initiated by the Redox System 2,2'-Thiodiethanol-Ce4+ in Aqueous Sulfuric-Acid. *Journal of Polymer Science Part a-Polymer Chemistry* **1981,** 19, (5), 1147-1153.
12. Sosnik, A.; Cohn, D.; San Roman, J. S.; Abraham, G. A., Crosslinkable PEO-PPO-PEO-based reverse thermo-responsive gels as potentially injectable materials. *Journal of Biomaterials Science-Polymer Edition* **2003,** 14, (3), 227-239.
13. Toru Takahashi, Y. H. I. S., Coordinated radical polymerization and redox polymerization of acrylamide by ceric ammonium nitrate. *Journal of Polymer Science Part A-1: Polymer Chemistry* **1968,** 6, (8), 2091-2102.
14. Nikishin, G. I.; Kapustina, N. I.; Kaplan, E. P., Oxidation of 1-methyl- and 1-ethylcyclohexanol with cerium ammonium nitrate. *Russian Chemical Bulletin* **1977,** 26, (7), 1420-1424.
15. Lozinsky, V. I.; Morozova, S. A.; Vainerman, E. S.; Titova, E. F.; Shtilman, M. I.; Belavtseva, E. M.; Rogozhin, S. V., Study of Cryostructurization of Polymer Systems .8. Characteristic

Features of the Formation of Crosslinked Poly(Acryl Amide) Cryogels under Different Thermal Conditions. *Acta Polymerica* **1989,** 40, (1), 8-15.

16. Lozinsky, V. I., Cryogels on the basis of natural and synthetic polymers: Preparation, properties and application. *Uspekhi Khimii* **2002,** 71, (6), 559-585.
17. Mawad, D.; Martens, P. J.; Odell, R. A.; Poole-Warren, L. A., The effect of redox polymerisation on degradation and cell responses to poly (vinyl alcohol) hydrogels. *Biomaterials* **2007,** 28, (6), 947-955.
18. Walling, C.; Eltaliaw.G, Fentons Reagent .3. Addition of Hydroxyl Radicals to Acetylenes and Redox Reactions of Vinyl Radicals. *Journal of the American Chemical Society* **1973,** 95, (3), 848-850.
19. Farahnaky, A.; Gray, D. A.; Mitchell, J. R.; Hill, S. E., Ascorbic acid and hydrogen peroxide (Fenton's reagent) induced changes in gelatin systems. *Food Hydrocolloids* **2003,** 17, (3), 321-326.
20. Ward, A. G.; Courts, A., *The science and technology of gelatin*. 1977.
21. Kuijpers, A. J.; Engbers, G. H. M.; Krijgsveld, J.; Zaat, S. A. J.; Dankert, J.; Feijen, J., Cross-linking and characterisation of gelatin matrices for biomedical applications. *Journal of Biomaterials Science-Polymer Edition* **2000,** 11, (3), 225-243.
22. Kuijpers, A. J.; Engbers, G. H. M.; van Wachem, P. B.; Krijgsveld, J.; Zaat, S. A. J.; Dankert, J.; Feijen, J., Controlled delivery of antibacterial proteins from biodegradable matrices. *Journal of Controlled Release* **1998,** 53, 235-247.
23. Mao, J. S.; Liu, H. F.; Yin, Y. J.; Yao, K. D., The properties of chitosan-gelatin membranes and scaffolds modified with hyaluronic acid by different methods. *Biomaterials* **2003,** 24, (9), 1621-1629.
24. Liu, H. F.; Yin, Y. J.; Yao, K. D.; Ma, D. R.; Cui, L.; Cao, Y. L., Influence of the concentrations of hyaluronic acid on the properties and biocompatibility of Cs-Gel-HA membranes. *Biomaterials* **2004,** 25, (17), 3523-3530.
25. Liu, H. F.; Mao, J. S.; Yao, K. D.; Yang, G. H.; Cui, L.; Cao, Y. L., A study on a chitosan-gelatin-hyaluronic acid scaffold as artificial skin in vitro and its tissue engineering applications. *Journal of Biomaterials Science-Polymer Edition* **2004,** 15, (1), 25-40.
26. Choi, Y. S.; Hong, S. R.; Lee, Y. M.; Song, K. W.; Park, M. H.; Nam, Y. S., Studies on gelatin-containing artificial skin: II. Preparation and characterization of cross-linked gelatin-hyaluronate sponge. *Journal of Biomedical Materials Research* **1999,** 48, (5), 631-639.
27. Hong, S. R.; Chong, M. S.; Lee, S. B.; Lee, Y. M.; Song, K. W.; Park, M. H.; Hong, S. H., Biocompatibility and biodegradation of cross-linked gelatin/hyaluronic acid sponge in rat subcutaneous tissue. *Journal of Biomaterials Science-Polymer Edition* **2004,** 15, (2), 201-214.

Chapter VII:
Interaction between Gelatin and Extra-Cellular Matrix Components

1 Applied techniques for studying biomolecular interactions

Since the initial cell attachment is primarily affected by the binding of adhesion molecules[1] and their subsequent mediation between the cells and the material surface, a different level of cell attachment on multiple scaffolds developed, could be related to the involvement of adhesion proteins, such as fibronectin and vitronectin present in the serum.[2-5] The latter was already observed when comparing the *in vitro* osteoblast response to gelatin/hydroxyapatite nanocomposites and the cell behaviour on conventionally mixed gelatin/hydroxyapatite composites.[6] The alkaline phosphatase activity and the osteocalcin, produced by the cells, were significantly higher on the nanocomposite scaffolds than on the conventional composite scaffolds. These improved responses are considered to result from serum protein adsorption on the nanocomposites. Similar results were obtained for poly(L-lactide-co-caprolactone), coated with fibronectin.[7]

Fibronectin is the most extensively characterized adhesive serum protein and has been generally thought to be the main cell attachment-promoting protein in serum.[8, 9] However, apparently bovine serum and plasma contain two major cell attachment-promoting proteins. Besides fibronectin, they also contain vitronectin, of which the latter accounts for more of the cell attachment-promoting activity than fibronectin.[2]

In the present work, the interaction between the scaffold material, gelatin, and the most abundant components of foetal calf serum (table 7-1) will be studied.

Component	Concentration in FCS	Iso-electric point
γ-globulin	0.1 mg/ml	6.9
lactate dehydrogenase	51.83 mU/ml	-
transferrin	0.285 mg/ml	5.3 - 5.6
albumin	3.8 mg/ml	4.7
fibronectin	0.03 mg/ml	5.5 - 6.3

Table 7-1: Overview of the most abundant components in foetal calf serum, with their respective concentrations and iso-electric points (for proteins).

Protein adsorption measurements are a necessary step in the evaluation of biomaterials. Several techniques have been used to study protein adsorption onto biomaterial surfaces, including Fourier transform infrared spectroscopy, enzyme-linked immunosorbent assay, SDS-PAGE with immunoblotting, radiolabelled proteins, atomic force microscopy, X-ray photo-electron spectroscopy (XPS), ellipsometry, surface plasmon resonance (SPR), etc.[10, 11] Each technique has its own advantages and disadvantages and their mechanisms for detecting adsorbed proteins can greatly influence their sensitivity. XPS, for example, is a useful technique for the evaluation of adsorbed protein films due to its surface sensitivity (i.e. 80-100 Å) and quantitative analysis.[12] However, XPS does not have the chemical specificity to identify different adsorbed proteins.

In the present work, multiple techniques (i.e. SPR, quartz crystal microbalance (QCM) and radiolabelling) will be utilized in order to determine the interaction between gelatin and some of the most abundant components of both the extracellular matrix and foetal calf serum.

1.1 Surface Plasmon Resonance

At the interface between two optically transparent media of different refractive indices, light is reflected back into the medium of higher refractive index, if the angle of incidence exceeds a certain critical angle. The latter phenomenon is called total internal reflection. Although the incident light is totally internally reflected, an electromagnetic field component of the light (i.e. the evanescent wave), penetrates a short distance into the medium of lower refractive index. The wave may excite

molecules close to the interface in this medium. If the light is monochromatic and p-polarized and the interface between the media is coated with a thin layer of a free-electron metal (e.g. gold), a reflectance minimum appears in the reflected light at a specific incident angle (figure 7-1). The latter is called **surface plasmon resonance** (SPR).[13]

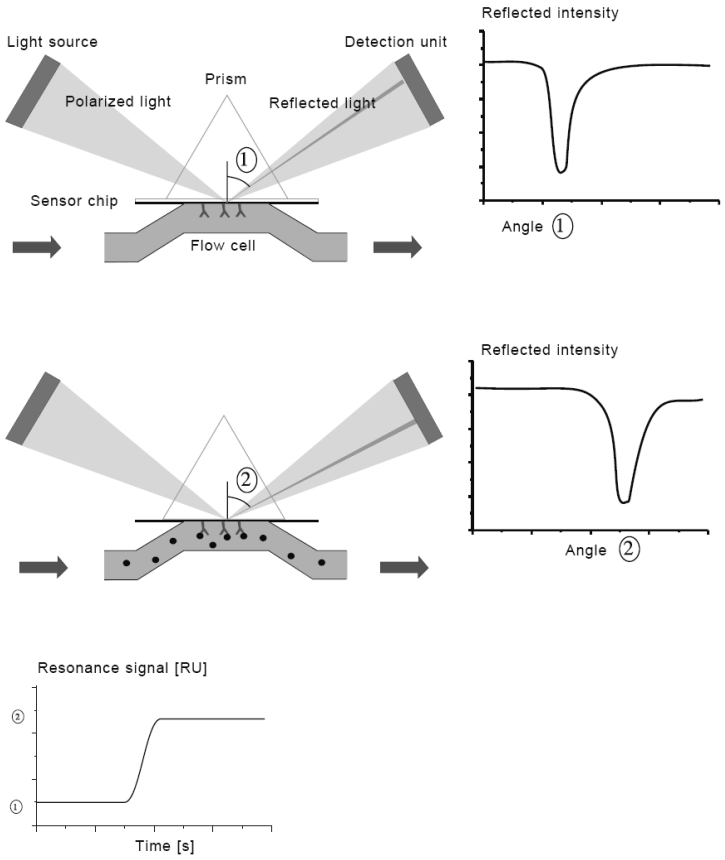

Figure 7-1: Monitoring the SPR response signal from the shift in minimum reflected intensity.

The resonance angle is very sensitive to changes in the refractive index of the thin layer, coated onto the metal surface. For example, when components adhere to a polymer film, immobilized onto a sensor chip, the resonance angle shifts to higher values (figure 7-1). The SPR response depends on the mean refractive index change, caused by the interaction of injected molecules with the substrate, coated on the gold surface.

SPR measurements can be utilized for a variety of applications[14, 15], such as in pharmaceutical industry[16, 17], to monitor antigen-antibody interactions[18-20], in medicine[21-23], for industrial applications[24, 25], in food science[26, 27], etc.

1.2. Quartz Crystal Microbalance

The **quartz crystal microbalance** (QCM) has been used for a long time to monitor thin film deposition in vacuum or gas. After it was shown that the QCM could also be used in the liquid phase,[28] the number of applications for the QCM has increased tremendously (e.g. antigen/antibody interaction, environmental screenings, polymer/protein interaction, etc.).[29-31]

A QCM consists of a thin quartz crystal, positioned between a pair of electrodes (figure 7-2). Due to the piezoelectric properties of quartz, it is possible to excite the crystal to oscillation by applying an AC voltage across its electrodes.[32]

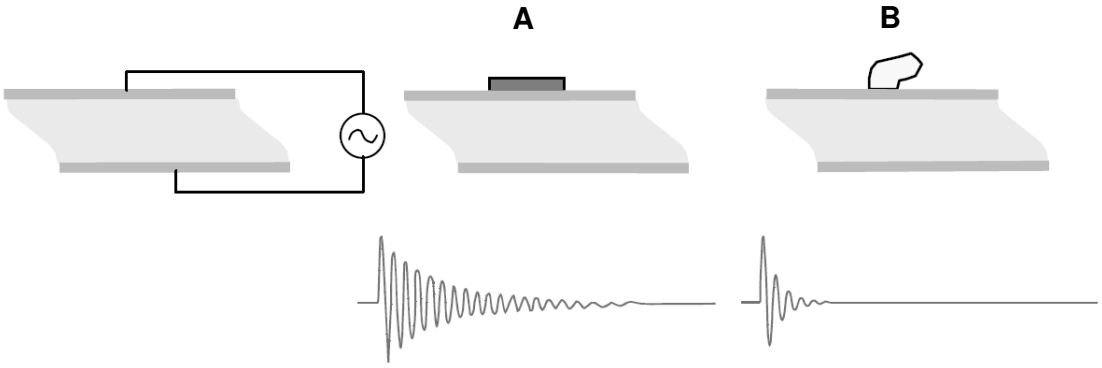

Figure 7-2: Schematic illustration of an AT-cut crystal at resonance and the decay curve of a rigid (A) and a viscoelastic sample (B).

The resonance frequency (f) of the crystal depends on the total oscillating mass, including water coupled to the oscillation. When a thin film is attached to the sensor crystal, the frequency will decrease. If the film is thin and rigid, the decrease in frequency is proportional to the film mass. In this way, the QCM operates as a very sensitive balance.

The mass of the adhering layer is calculated by means of the Sauerbrey relation:

$$\Delta m = -\frac{C\Delta f}{n}$$

with $C = 17.7$ ng Hz^{-1} cm^{-2} for a 5 MHz quartz crystal

$n = 1, 3, 5, 7$, etc. = the overtone number

Δf = the frequency shift, caused by the deposition of material on the sensor.

The thickness of the adherent layer can be calculated according to the following equation:

$$d = \frac{\Delta m}{\rho}$$

with ρ = the effective density of the attached layer

Δm = the mass deposited onto the sensor surface.

However, it also occurs that the adsorbed layer is not rigid, so the Sauerbrey relation becomes invalid. A viscoelastic film will not fully couple to the oscillation of the crystal, thus the Sauerbrey equation will underestimate the mass at the surface.[33]

A viscoelastic film dampens the crystal's oscillation (figure 7-2, part B). The dissipation of the oscillation of the quartz crystal gives an idea on the viscoelastic properties of the attached layer. The dissipation is determined according to the following equation:

$$D = \frac{E_{lost}}{2\pi E_{stored}}$$

with E_{lost} = energy dissipated (i.e. lost) during one oscillation cycle

E_{stored} = total energy stored in the oscillator.

The dissipation of a crystal can be measured by recording the response of a freely oscillating crystal, vibrating at its resonance frequency. The latter also offers the opportunity to work at both the fundamental frequency and at the overtone frequencies (e.g. 15, 25 and 35 MHz). By measuring at multiple frequencies and applying the Voight model, the adhering film can be characterized in detail.

1.3. Radiolabelling

Modification of proteins and other molecules with a radioactive element provides a means of detection that is extremely sensitive for assay, localization and imaging applications. Among the most common radiolabels for biological studies are ^{14}C, ^{32}P, ^{35}S, ^{3}H, ^{125}I and ^{131}I. In literature, fibronectin was already labelled before with iodine-125.[34, 35] **Iodine-125** decays by electron capture followed by **γ emission**. Because ^{125}I is not a particulate emitter, its use *in vivo* for imaging applications limits radiation damage to surrounding proteins, cells and tissues. It is a widely used radionuclide with a half-life of 59.4 days, emitting x-rays with a maximum energy of 35 keV. These factors make ^{125}I the most suitable iodine label for radiolabelling of biological molecules. It is produced by irradiating Xenon-124 to create Xenon-125 which then decays to form Iodine-125.
Iodine-125 is used in a variety of applications, ranging from medical research and diagnostics to medical treatment.

There are two main methods of radioiodination, commonly employed to modify proteins and other molecules:

1. direct labelling of the desired protein or other target molecule in the presence of an oxidizing agent
2. indirect labelling of the component by first labelling an intermediate compound, which is then used to perform the final modification.

In the present work, the direct labelling method is applied. The general procedure for the direct coupling of ^{125}I to a compound occurs by using an oxidizing agent. The *in situ* preparation of an electrophilic radioiodine species is essential in order to modify certain reactive sites within the desired molecules. There exist different oxidizing derivatives of N-haloamine, such as N-chlorotoluenesulfonamide (chloramine-T) or 1,3,4,6-tetrachloro-3α,6α-diphenylglycouril (IODO-GEN).[36-38] In most cases, such compounds do not harm the proteins being labelled, although reaction times should be controlled to prevent overlabelling or oxidative damage. A second methodology to create an oxidative effect is the use of an enzyme-driven system. The glucose

oxidase/lactoperoxidase reaction creates reactive iodine by the production of hydrogen peroxide from glucose with the subsequent reaction of peroxidase to form I_2 from I^-.

Formation of the electrophilic halogen species leads to the possibility to induce rapid reaction with target compounds, containing strongly activating groups such as activated aryl compounds. Particularly, substances containing aromatic ring structures, that have substituents on the ring that are electron-donating, can sufficiently activate the carbons on the ring to undergo electrophilic substitution reactions. Therefore, phenols, aniline derivatives, etc. are very susceptible to iodination. In proteins, this corresponds with tyrosine and histidine groups.[39] Tyrosine can be modified with two iodine atoms, whereas histidine can incorporate one iodine. The addition of a radioactive iodine atom to a protein molecule typically has little effect on the resultant protein activity, unless the active centre is modified in the process. The size of an iodine atom is relatively small and does not result in many steric problems with large molecules.

In the present work, IODO-GEN was applied for the radiolabelling of fibronectin. The compound is insoluble in aqueous solution, therefore making it a type of solid-phase radioiodination reagent. IODO-GEN is deposited on the inside surface of a reaction tube, prior to iodination.

The reaction of IODO-GEN with an iodine ion in solution, results in oxidation with subsequent formation of a reactive halogen species, ICl (figure 7-3). The ICl then rapidly reacts with any site within the target compound that can undergo an electrophilic substitution reaction. Since IODO-GEN is insoluble and plated on the surface of the reaction tube, it is possible to stop the reaction by simply removing the aqueous phase.

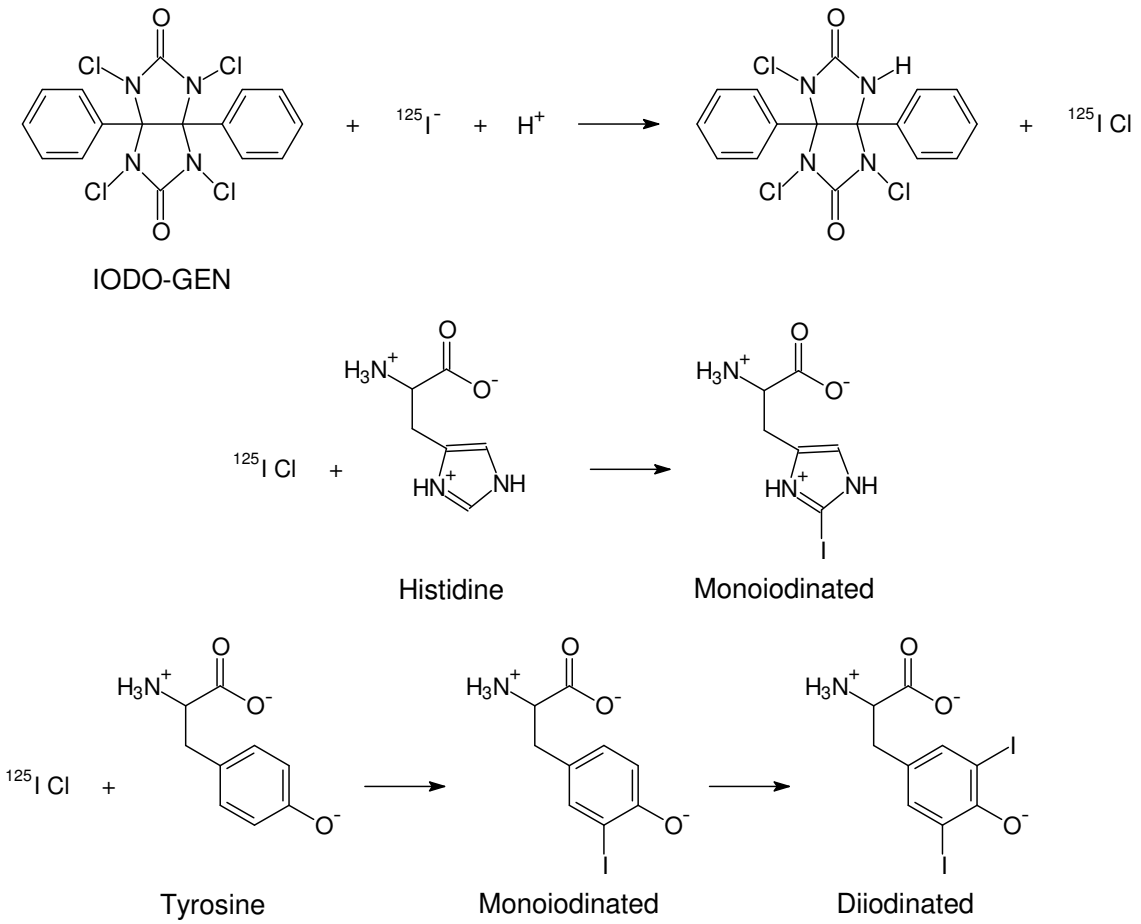

Figure 7-3: Overview of the radiolabelling of tyrosine and histidine compounds in gelatin by means of IODO-GEN.

2. Study of fibronectin - gelatin interaction

2.1. Surface Plasmon Resonance

Beside the fact that fibronectin, present in serum, could influence the cell-matrix interactions when adherence between fibronectin and the gelatin matrix would occur, there is a second reason, why the affinity between both proteins is studied in the present work.

Since the scaffolds are intended to be used as matrices for cell culture or for tissue engineering applications, the material should possess sufficient cell-interaction properties. Therefore, we investigated to what extent fibronectin could be combined with the hydrogels developed. Due to the natural gelatin binding sites on

fibronectin[40-42], an approach in which gelatin was coated with a top layer of fibronectin, was selected. The coating process was first studied by surface plasmon resonance, a technique which is very sensitive and enables real time measurement of adhesion phenomena at interfaces.[43] To study the fibronectin-gelatin interaction, gel-MOD was spincoated on an SPR sensor. In order to verify the presence of gel-MOD onto the sensor surface, ATR-IR spectra were recorded before and after spincoating (figure 7-4).

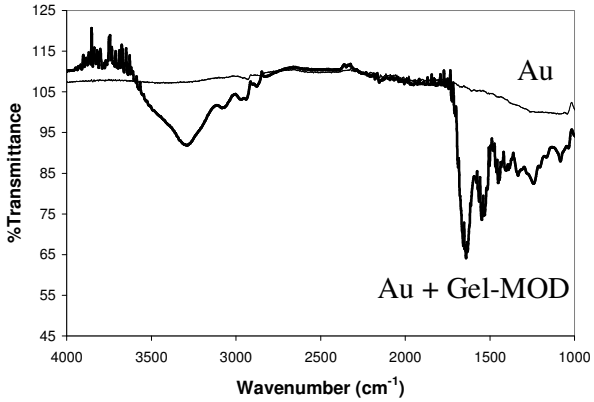

Figure 7-4: ATR-IR-spectra of a non-coated sensor chip (Au) and a gel-MOD spincoated sensorchip (Au + Gel-MOD) after incubation in running buffer at 25°C.

It was concluded that upon spincoating, the typical protein peaks (1650 cm^{-1}, 1540 cm^{-1}) appeared in the spectrum, indicating the deposition of a gelatin layer on the surface of the sensor chip. Stability studies further revealed that the coating applied was stable against the running buffer of the SPR experiment.

Contact angle measurements further revealed the presence of a gelatin layer on the SPR chip after spincoating with a 5 w/v% gel-MOD solution (figure 7-5).

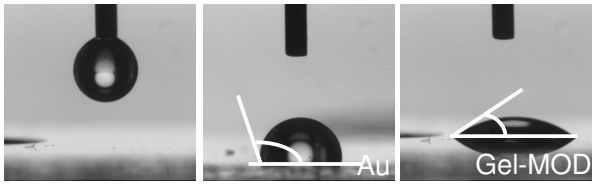

Figure 7-5: Contact angle measurements on gold and on a sensor chip, coated with gel-MOD.

The contact angle of an uncoated gold chip was 102° and that of a chip, previously spincoated with gel-MOD was 40°. The decrease in contact angle is an indication of an increased hydrophilicity of the sensor chip, after spincoating with gelatin, demonstrating the presence of the protein layer on the surface. Since surface

plasmon resonance is limited to surfaces with a thickness of ±300 nm, scanning electron microscopy was performed on a cross-section of a gold chip, coated with a gelatin layer. From figure 7-6, the film thickness was estimated to 60 nm, enabling SPR measurements to be performed.

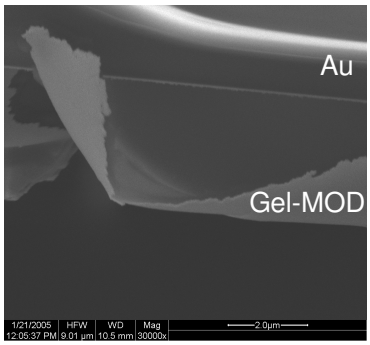

Figure 7-6: SEM image of a cross-section of a gold chip, after spincoating with gel-MOD.

After spincoating, the gelatin-coated chip was inserted in the apparatus and flushed with different concentrations of fibronectin (1-200 µg/ml). In a subsequent step, a fibronectin-antibody was passed over the surface.

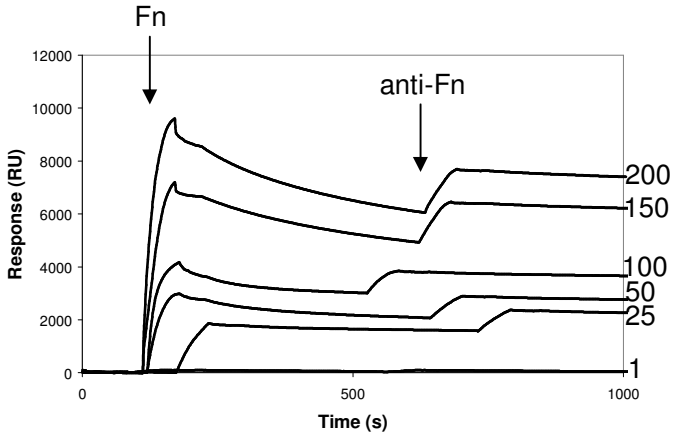

Figure 7-7: SPR-sensorgrams of the gelatin (type B)-fibronectin interaction as a function of the fibronectin concentration. The concentrations indicated in the graph are expressed in µg/ml. Upon stabilisation of the signal after fibronectin injection, anti-fibronectin was passed over the fibronectin coated surfaces (0.05 mg/ml).

From the sensorgrams, shown in figure 7-7, it can be concluded that the amount of adsorbed fibronectin increased with an increasing fibronectin concentration. This implies that the amount of adsorbed fibronectin on the gelatin hydrogels can be easily adjusted by varying the applied fibronectin concentration (e.g. by dip coating). We also observed a fibronectin-concentration related increase in the amount of

fibronectin that bound non-specifically and which was removed during the washing step. This effect was due to an increasing saturation on the surface.

In figure 7-8, the SPR response after dissociation of the gelatin-fibronectin complexes is plotted against the fibronectin concentration, which was injected. From the linear plot, it is possible to calculate the SPR response signal for other fibronectin concentrations injected onto a gelatin-coated surface.

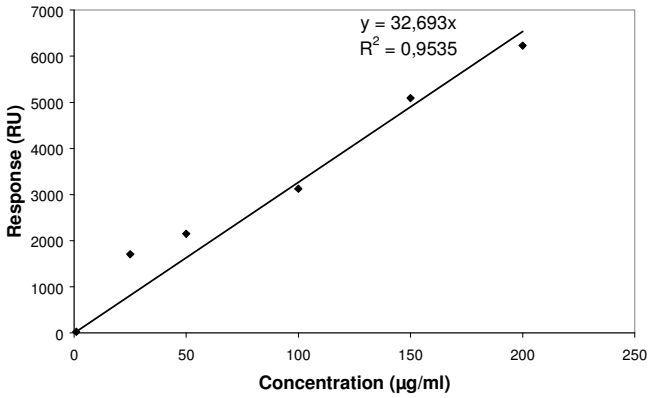

Figure 7-8: SPR response as a function of fibronectin concentration for type B gelatin.

Interestingly, the response of the anti-fibronectin did not increase significantly with the amount of fibronectin adsorbed on the surface (see figure 7-7, second signal increase). It can be anticipated that, with an increase in adsorbed fibronectin on the surface, the adopted protein orientation changed. This affected the subsequent antibody binding.

It should be considered that for SPR measurements, 2D surfaces are evaluated.

Study of the kinetics of the fibronectin – gelatin interaction

Association kinetics

The formation of a surface-bound complex between analyte A and surface-bound ligand B can be described by the following scheme:

$$A_{bulk} \underset{k_m}{\overset{k_m}{\rightleftharpoons}} A_{surface} + B \underset{k_d}{\overset{k_a}{\rightleftharpoons}} AB$$

with k_m = the rate constant for mass transport towards and away from the surface
k_a = the rate constant for association (i.e. complex formation)
k_d = the rate constant for dissociation (i.e. complex rupture)

At the beginning of the association phase, the interactions are limited by mass transport because of the large amount of binding sites, available at the surface.
If mass transport is much faster than the interaction-controlled association ($k_a[B] << k_m$), the analyte concentration at the surface is equal to its concentration in bulk and the association and dissociation constants measured, approach the constants of the interaction kinetics. Under these conditions, the reaction equation can be written as:[44]

$$\frac{d[AB]}{dt} = k_a[A][B] - k_d[AB]$$

The concentration of free ligand [B] equals the difference between the total amount of ligand at the surface $[B]_0$ and the amount of complex formed:

$$[B] = [B]_0 - [AB]$$

After substitution of [B] in the rate equation for the formation of AB, the following is obtained:

$$\frac{d[AB]}{dt} = k_a[A]([B]_0 - [AB]) - k_d[AB]$$

When the total amount of ligand $[B]_0$ is expressed as a function of the maximum analyte binding capacity of the surface, all concentrations can be expressed as SPR response in RU:

$$\frac{dR}{dt} = k_a C(R_{max}-R) - k_d R$$

with dR/dt = rate at which the SPR signal changes
C = concentration of the analyte
R_{max} = maximum analyte binding capacity in RU
R = SPR-signal in RU at time point t

The equation can then be rewritten to:

$$\frac{dR}{dt} = k_a C R_{max} - (k_a C + k_d) R$$

Rate constants can be determined by plotting dR/dt as a function of R for different analyte concentrations. Furthermore, the slope of each curve (i.e. for the different concentrations) is plotted as a function of the analyte concentration. Both k_a and k_d can be obtained from this linear plot.

Dissociation kinetics

After rinsing the analyte over the surface, the complex dissociates according to a zero-order reaction, when presuming that reassociation of dissociated analyte can be neglected:

$$\frac{dR}{dt} = -k_d R$$

After reordering and integration, the following equation is obtained:

$$\ln \frac{R_0}{R_t} = k_d (t - t_0)$$

with R_t = response at time t

R_0 = response at initial time t_0

The plot of $\ln(R_0/R_t)$ as a function of $(t - t_0)$ thus results in a linear plot with slope k_d. The association and dissociation constants, depicted in table 7-2, were calculated by means of the BIAevaluation software, version 3.1.

k_a ($M^{-1}s^{-1}$)	k_d (s^{-1})	K_A (M^{-1})
2.76×10^5	5.21×10^{-4}	5.31×10^8

Table 7-2: Association and dissociation constants for the interaction between gelatin and fibronectin.

The association constant of 5.31 x 10^8 M^{-1} is in correspondence with the association constant of 2 x 10^8 M^{-1}, corresponding to the association of fibronectin with a fibronectin-binding peptide, present in gelatin.[45] Moreover, it also corresponds to the association constant (4 x 10^8 M^{-1}) for the affinity between fibronectin and denatured collagen.[46]

Since type B gelatin and fibronectin have iso-electric points of about respectively 5 and 6, only hydrophobic interactions can occur between both proteins at physiological pH. However, there exists also an alternative gelatin type A, possessing an iso-electric point of about 8, as already mentioned in chapter 1 (§ 5.1). In addition to the hydrophobic interactions, electrostatic interactions can also occur between type A gelatin and fibronectin since these proteins are charged oppositely at physiological pH. That is why an SPR interaction study was also performed by injecting fibronectin onto a sensor chip, previously spincoated with type A gelatin. Again, experiments were performed first to verify the presence and the stability of the spincoated gelatin type A layer on the SPR chip (data not shown). Afterwards, varying concentrations of fibronectin were injected onto the gelatin-coated gold chips and the corresponding response signal was monitored, followed by injection of an antibody specific for fibronectin (figure 7-9).

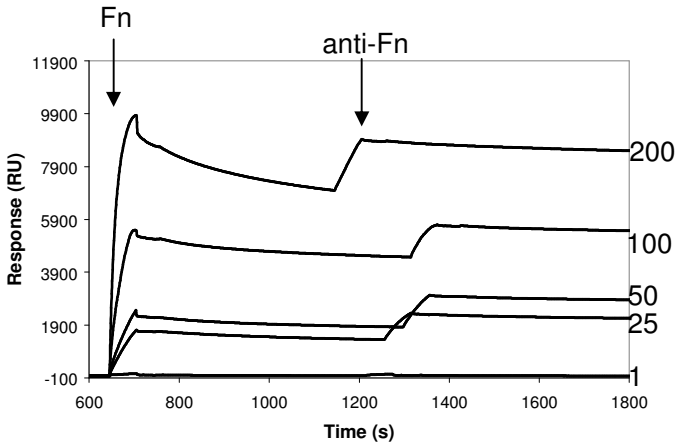

Figure 7-9: SPR-sensorgrams of the gelatin (type A)-fibronectin interaction as a function of the fibronectin concentration. The concentrations indicated in the graph are expressed in µg/ml. Upon stabilisation of the signal after fibronectin injection, anti-fibronectin was rinsed over the fibronectin coated surfaces (0.05 mg/ml).

The sensorgrams (see figure 7-9) indicate that the amount of adsorbed fibronectin again increased with an increasing fibronectin concentration. We also observed a fibronectin-concentration related increase in the amount of fibronectin that bound

non-specifically and which was removed during the washing step, similar to the results of type B gelatin.

In figure 7-10, the SPR response after dissociation of the gelatin-fibronectin complexes is again plotted against the fibronectin concentration. As could be anticipated, it was observed that the injection of fibronectin onto a type A gelatin coating resulted in a higher response signal compared to rinsing the protein over a chip, coated with type B gelatin.

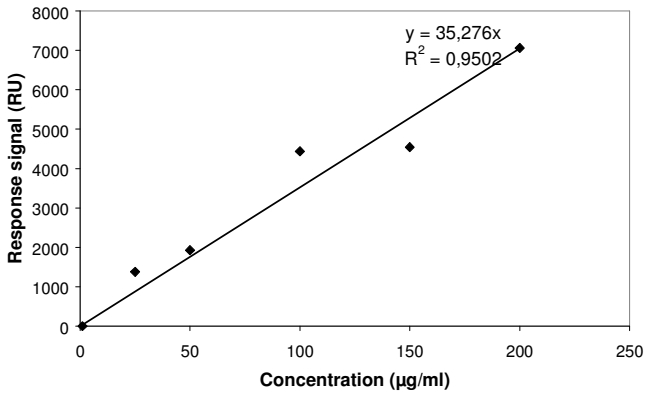

Figure 7-10: SPR response as a function of fibronectin concentration for type A gelatin.

From the results, it could be concluded that, based on the amount of fibronectin that should be incorporated, both the gelatin type and the fibronectin concentration can be varied. That is, both parameters influence the amount of incorporated fibronectin.

k_a ($M^{-1}s^{-1}$)	k_d (s^{-1})	K_A (M^{-1})
252	2.03×10^{-8}	1.24×10^{10}

Table 7-3: Association and dissociation constants for the interaction between gelatin type A and fibronectin.

From table 7-3, it appears that the association constant K_A for the interaction between type A gelatin and fibronectin is 1.24×10^{10} M^{-1}, which is higher than K_A for the system fibronectin and type B gelatin (i.e. 5.31×10^{8} M^{-1}).

2.2. Quartz crystal microbalance

An alternative technique to examine the interaction between gelatin and fibronectin is QCM. The advantage of the latter approach is that both the weight and the thickness of the deposited fibronectin layer can be determined.

Similar as for the SPR measurements (§ 2.1), QCM crystals were spincoated with gelatin type A and type B solutions (5 w/v%). Next, varying fibronectin concentrations (1 and 25 µg/ml) were passed over the sensors, when monitoring frequency and dissipation response, as depicted in figure 7-11. The results indicate that, for the low fibronectin concentration, fibronectin and anti-fibronectin adsorbed, where fibronectin adsorption lead to a smaller frequency and dissipation response, compared to anti-fibronectin.

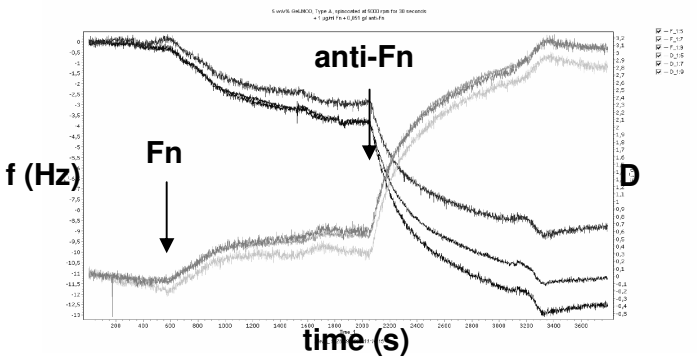

Figure 7-11: Frequency and dissipation response for three selected frequencies when injecting 1µg/ml fibronectin and 0.051 g/l anti-fibronectin on a type A gelatin-coated crystal.

In figure 7-12, the dissipation shift is plotted as a function of the frequency shift for the 5th overtone frequency. The plot gives an idea about the visco-elastic changes throughout the adsorption process. The increase in slope after injection of anti-fibronectin indicates that for the low fibronectin concentration, the initial fibronectin adsorption leads to a relatively stable product, whereas the antibody adsorption induces more visco-elasticity. The latter is also indicated by the higher dissipation values for anti-fibronectin.

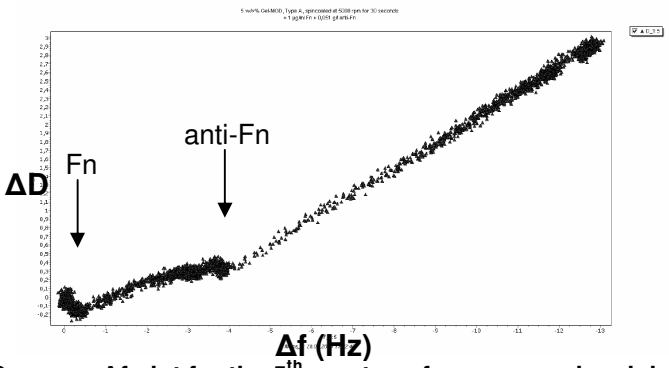

Figure 7-12: ΔD versus Δf plot for the 5th overtone frequency when injecting 1µg/ml fibronectin and 0.051 g/l anti-fibronectin on a type A gelatin-coated crystal.

Figure 7-13 shows the frequency and dissipation response for three selected frequencies when injecting 25 µg/ml fibronectin onto a crystal, coated with gelatin type A, followed by rinsing with the antibody. The first adsorption starts after 600 seconds, followed by a flushing step with PBS at 1700 seconds. Finally, anti-fibronectin is injected at 2000 seconds.

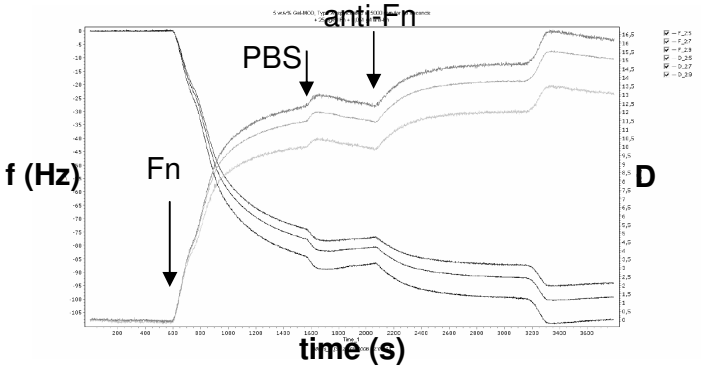

Figure 7-13: Frequency and dissipation response for three selected frequencies when injecting 25 µg/ml fibronectin and 0.051 g/l antibody on a type A gelatin-coated sensor.

When rinsing with the higher fibronectin concentration (i.e. 25 µg/ml), the frequency and dissipation response to the fibronectin uptake is higher than the response caused by the presence of the antibody onto the QCM crystal. The visco-elastic changes throughout the adsorption process were also studied for the higher fibronectin concentration (data not shown). Compared to the 1 µg/ml fibronectin, there was no significant difference between initial and following adsorption. In this case, the initial film formed by deposition of fibronectin was already much softer compared to the layer formed after rinsing with a 1 µg/ml fibronectin solution.

For all measurements, Sauerbrey and Voight masses were calculated (data not shown) and compared. The Sauerbrey mass was calculated by means of the Sauerbrey constant of 17.7 ng cm^{-2} Hz^{-1}, multiplied by the frequency shift. The Voight mass could be calculated by multiplying the modelled film thickness with the density. In the present work, we assumed the density to a reasonable value of 1050 kg/m^3, which is close to the density of water. Depending on the visco-elastic characteristics, both masses can differ in value, with the Sauerbrey mass always being lower than the Voight mass. Especially for visco-elastic films, the calculations for the Sauerbrey masses can differ quite a lot between the frequencies applied. The different responses in frequency and dissipation are an indication of the visco-elastic behaviour, since in ideal Sauerbrey films all frequencies and dissipations are identical.

In table 7-4, an overview of film thicknesses and Voight masses of all components, adsorbed on the sensor crystal, after spincoating with either gelatin type A or B, is presented. Film thicknesses and masses, represent the values in hydrated state, consequently the mass values include water, taken up by the material, after adsorption onto the QCM sensors.

		Type A gelatin		**Type B gelatin**	
		1 µg/ml	*25 µg/ml*	*1 µg/ml*	*25 µg/ml*
Fn	*thickness (nm)*	0.7	18	0.3	1
	mass (ng/cm²)	73	1837	31	105
anti-Fn	*thickness (nm)*	3	22	1.2	1.4
	mass (ng/cm²)	241	472	126	147

Table 7-4: Overview of QCM results, obtained by rinsing fibronectin and anti-fibronectin over sensor crystals, after spincoating with type A or type B gelatin.

Table 7-4 indicates that the amount of deposited fibronectin increases with an increasing fibronectin concentration. Moreover, the fibronectin adsorption is higher on type A gelatin than on type B gelatin. The latter was anticipated based on the SPR results (see § 2.1).

In some cases, the values obtained for the layer thickness is lower than the size of fibronectin itself. This can be attributed to the fact that the QCM results obtained, are

an average for the entire chip. When the chip is not completely coated, QCM underestimates the thickness of these regions of the chip which are coated.

QCM was also utilized to determine the dry mass of the spincoated gelatin. We have therefore recorded the baseline of two crystals in air, before and after coating. The difference between the frequency values is an indication of the deposited mass. All frequency values (overtones etc.) were in excellent agreement (data not shown). The deposited mass can be easily calculated using the Sauerbrey constant of 17.7 ng/cm^2/Hz, which resulted in a mass of 18 µg/cm^2 for type A gelatin and in a mass of 16 µg/cm^2 for type B gelatin.

2.3. Size exclusion chromatography

Size exclusion chromatography (SEC) was performed both on gelatin (type B) solutions and on solutions consisting of gelatin (type B) and fibronectin. The samples were dissolved in buffer and the calibration was performed by means of pullulan standards.

The resulting chromatograms are plotted in figure 7-14.

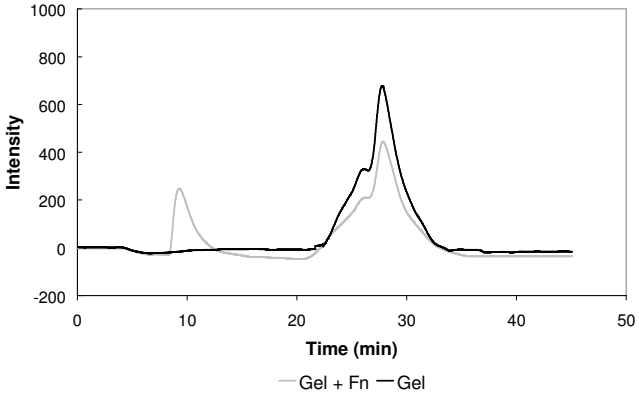

Figure 7-14: SEC chromatograms of gelatin (type B) (black) and the combination of gelatin (type B) and fibronectin (grey).

Beside the peak of pure gelatin, a second peak, having a lower retention time and thus a higher molecular weight, is present in the chromatogram, recorded from the solution with both gelatin and fibronectin. Consequently, it can be concluded that complex formation occurred between a part of the gelatin and the fibronectin added.

Since the peak intensity gives an indication of the concentration, the amount of both components in the complex can be determined.

	SAMPLES	
	Gel	**Gel + Fn**
Gel	7 mg/ml	7 mg/ml
Fn	0 mg/ml	1 mg/ml

Table 7-5: Overview of the concentrations of the individual compounds, present in the samples.

In table 7-5, the concentrations of the individual compounds, present in the samples are given. From figure 7-14, it can be concluded that 20% of the total gelatin concentration is complexed with fibronectin. This implies that 1.4 mg/ml gelatin can bind 1 mg/ml fibronectin. The latter is, of course, an estimation since SEC is a technique, based on the hydrodynamic volume, which is strongly influenced by the conformation of the polymer chains.

2.4. Radiolabelling experiments

Since QCM and SPR are dealing with interactions on surface level and SEC is concerned with protein solutions, an alternative method was utilized to study the fibronectin incorporation into the porous gelatin scaffolds, namely radiolabelling. In a first part, the fibronectin affinity for spincoated gelatin films was evaluated in order to enable correlation with the results obtained from SPR (§ 2.1) and QCM (§ 2.2) measurements. In a subsequent experiment, gelatin-based hydrogel films (1 mm thick) were prepared and their affinity for fibronectin was evaluated. Finally, the effect of pores present in the 3D-scaffolds (types $GIII_b$ and GI_b) developed on the fibronectin uptake was monitored.

The experiments were performed using radiolabelled fibronectin.

2.4.1. Fibronectin affinity for spincoated gelatin films

In a first part, glass plates were spincoated with gelatin type A and type B solutions in order to mimic the sensor chips, applied for the SPR and QCM experiments. Next, the coated glass plates were incubated with varying fibronectin concentrations (1-20 µg/ml) in PBS at room temperature. The results are shown in figures 7-15 and 7-16.

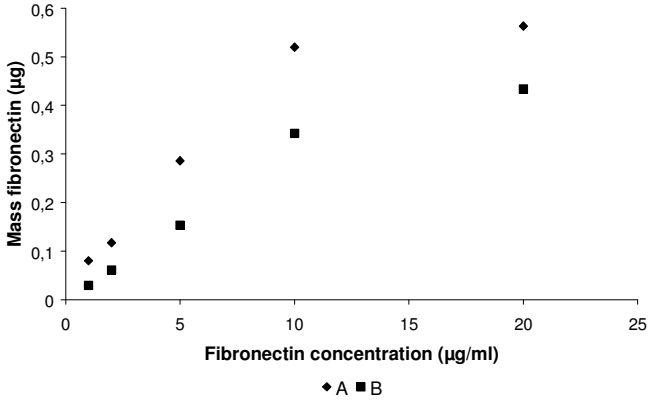

Figure 7-15: Mass of radiolabelled fibronectin deposited onto the glass plates, coated with gelatin type A and type B, as a function of the fibronectin concentration.

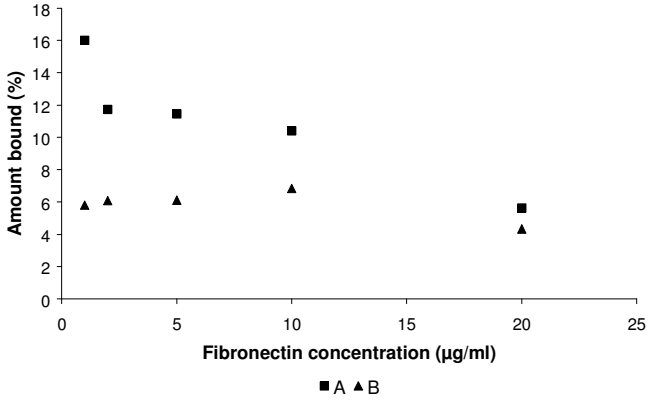

Figure 7-16: Percentage of fibronectin, bound to the gelatin-coated glass plates, of the total amount of added protein.

Figures 7-15 and 7-16 indicate that the interaction between fibronectin and type-A gelatin is higher than the affinity of type-B gelatin for fibronectin, which corresponds to the obtained SPR and QCM results.

However, the absorbance of radioactivity by the glass should also be taken into account.

2.4.2. Fibronectin affinity for gelatin-based hydrogel films

In a subsequent part of the present work, hydrogel films (Ø 6 mm x 1 mm), composed of 10 w/v% gel-MOD (type A and type B), were incubated for 1 hour in PBS at ambient temperature, in the presence of radiolabelled fibronectin (1-200 µg/ml). Next, the polymer films were washed three times in PBS. Finally, the radioactivities of the initial incubation fluid, of all washing liquids and of the gelatin pellets themselves were obtained. All experiments were performed in triplicate and the mean values are presented in the graphs below.

In figure 7-17, the mass of fibronectin, bound to the pellets, is plotted as a function of the fibronectin concentration, added to the incubation buffer.

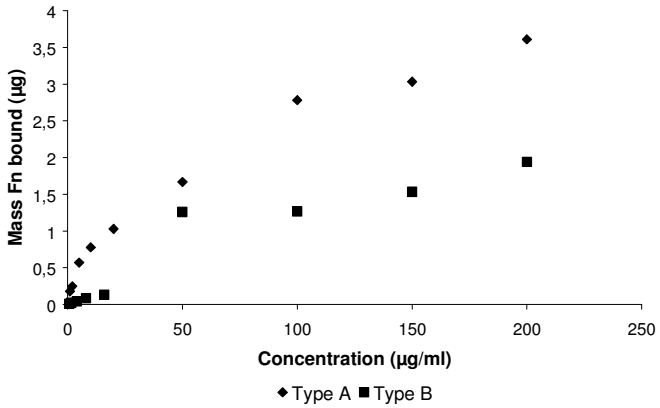

Figure 7-17: Mass of fibronectin, bound to type A and type B gelatin pellets when adding multiple fibronectin concentrations.

Figure 7-17 indicates that type A hydrogel films absorb more fibronectin compared to type B hydrogels, as anticipated. In figure 7-18, the percentage of fibonectin, bound per pellet, is plotted against the fibronectin concentration applied. From the results, it can be seen that in case of type B gelatin, a maximum exists at a fibronectin concentration of 50 µg/ml. Afterwards, the bound fraction decreases with increasing

fibronectin concentration. For type A gelatin, the bound fraction decreases logarithmically with increasing fibronectin concentration.

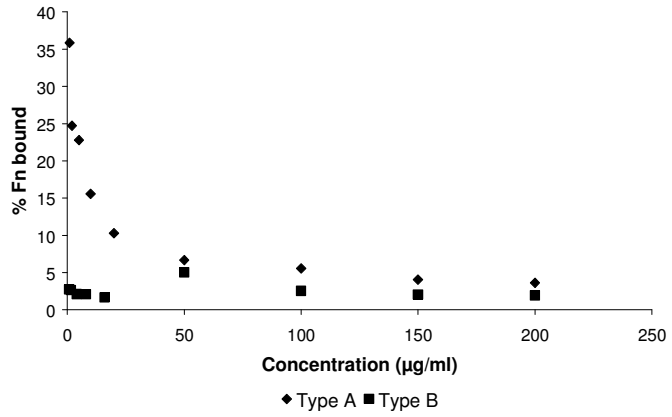

Figure 7-18: Fraction of fibronectin, bound to gelatin type A and type B pellets as a function of the fibronectin concentration added.

In table 7-6, both QCM and radiolabelling results are depicted. The mass of bound fibronectin is shown as a function of the gelatin type and the fibronectin concentration. SPR results are not included in the table below since SPR is rather a qualitative technique than a quantitative method.

		Type A gelatin		**Type B gelatin**	
		1 µg/ml	*25 µg/ml*	*1 µg/ml*	*25 µg/ml*
Mass (ng/cm^2)	*QCM*	73	1837	31	105
	Radiolabelling	239	1636	15	739

Table 7-6: Overview of adsorbed fibronectin masses obtained using QCM and radiolabelling experiments.

Table 7-6 indicates that the obtained results differ according to the technique applied. A first parameter influencing the results, is that the conformation of spincoated gelatin (cfr. QCM) differs from that of gelatin, present in hydrogel films (cfr. radiolabelling).
In addition, the deposited mass of fibronectin onto the QCM crystals, is obtained using an estimated density of 1050 kg/m^3 for the fibronectin layer.

In many cell interaction studies, reported in literature, pre-adsorbed fibronectin surfaces were observed to enhance cell attachment.[47, 48] Moreover, the effect of different pre-adsorbed fibronectin concentrations on cell attachment was observed to

be significantly different.[49] In one study, Ti surfaces, pre-adsorbed with a fibronectin concentration of 0.21 µg/mm^2, were observed to significantly increase cell attachment in comparison to uncoated surfaces and Ti surfaces, pre-adsorbed with 0.023 µg/mm^2 or 0.65 µg/mm^2 fibronectin.[50] It was suggested that fibronectin affects cell attachment by binding through cell surface receptors such as RGD and mediating adhesive interactions. It was also reported that fibronectin unfolded into an inactive conformation at a low concentration. However, at high concentrations, the unfolding was prevented by molecule packing requirements, thereby suggesting that the conformation of proteins played an important role in cell attachment.[50, 51]

In another study, adsorbed fibronectin densities enabling cell attachment on culture plastic were approximately 10-15 ng/cm^2.[8]

Consequently, the amount of fibronectin that can be incorporated through dipcoating should be sufficient to obtain scaffolds, able to support cell attachment and proliferation.

2.4.3. Fibronectin affinity for porous gelatin 3D-scaffolds

The water uptake experiments (chapter 4, § 3.3.1) indicated that the pore morphology and the pore size of the scaffolds developed, have an important influence on their water uptake capacity. Consequently, the fibronectin absorption/adsorption could also be affected by the structure properties of the porous scaffolds.

Two scaffold types, obtained by applying different cryogenic treatments, were examined for their interaction with fibronectin. Type GIII$_b$ scaffolds consisted of cone-shaped pores, with a pore size decreasing from top to bottom (330 to 20 µm) and type GI$_b$ hydrogels were composed of spherical pores, possessing a diameter of 135 µm (table 4-7). Type A and type B gel-MOD were applied subsequently in order to prepare hydrogels possessing respectively an overall positive and an overall negative charge.

Hydrogel scaffolds (Ø 6 mm x 5 mm, 10 w/v%) consisting of gel-MOD, were incubated for 1 hour in PBS at room temperature, in the presence of radiolabelled

fibronectin (1-200 µg/ml). Additionally, the scaffolds were washed three times in PBS, followed by determining the radioactivity of the initial incubation fluid, of the washing liquids and of the scaffolds themselves.

The experiments were performed twice or in triplicate, depending on the fibronectin concentration applied.

In figure 7-19, the mass of fibronectin, bound to the scaffolds, is plotted as a function of the fibronectin concentration for the various scaffold types and gelatin types studied.

The results indicated that type $GIII_b$ scaffolds contain more fibronectin than type GI_b scaffolds. The latter was anticipated since the pore size of type $GIII_b$ hydrogels at the top surface is higher than the pore size of type GI_b scaffolds. Moreover, the fibronectin uptake in type $GIII_b$ hydrogels is facilitated because of the more accessible, channel-like pore morphology. Similar results were obtained when performing swelling studies on both hydrogel types, as already discussed in chapter 4 (§ 3.3.1).

When comparing matrices, composed of type A gel-MOD with those, consisting of type B gel-MOD, it appears that type A based hydrogels contain less fibronectin than matrices, based on type B gelatin. The latter observation was not anticipated, based on previous obtained results (§ 2.4.2).

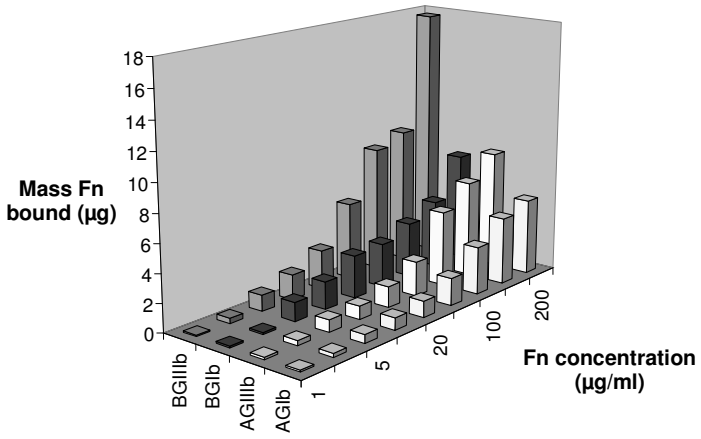

Figure 7-19: Mass of fibronectin bound to the hydrogels, as a function of the fibronectin concentration for the various scaffold types and gelatin types studied.

An important parameter influencing the fibronectin uptake, is the water uptake capacity of the scaffolds developed. Consequently, swelling experiments were performed on the scaffolds, applied in the dipcoating process (figure 7-20). The results indicated that the swelling capacity of type A gelatin scaffolds was lower than the water uptake of type B gelatin hydrogels. The latter is related to differences in processing conditions. As already described in the introduction (chapter 1), two types of gelatin can be distinguished depending on their pre-treatment. Gelatin A is processed by acidic treatment while gelatin B is processed by alkaline treatment. The alkaline pre-treatment converts glutamine and aspargine residues into glutamic acid and aspartic acid, which results in a higher carboxylic acid content for gelatin B (118/1000 amino acids) than for gelatin A (77/1000 amino acids).[52] The swelling results may be explained by the fact that at the experimental pH (7) (which is above the isoelectric point 5), gelatin B possesses a net negative charge due to $-COO^-$ groups in the molecule. These groups, present along the gelatin chains repel each other, thus producing a greater relaxation in the scaffold. This obviously results in a larger swelling of the hydrogels. Consequently, less fibronectin was incorporated into type A scaffolds compared to the type B derivatives.

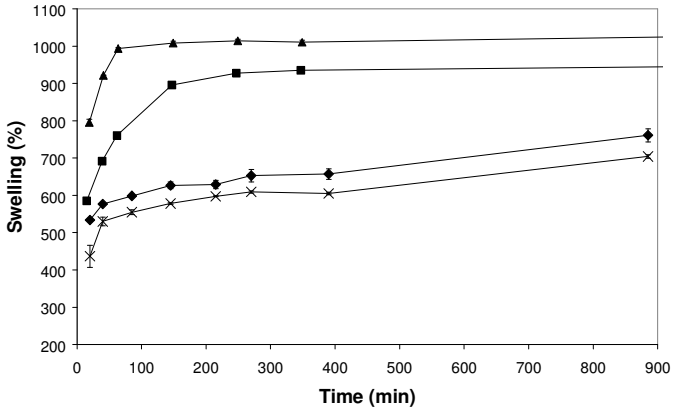

Figure 7-20: Degree of swelling as a function of time for 10 w/v% hydrogels: gel-MOD B, type $GIII_b$ (▲), gel-MOD B, type GI_b (■), gel-MOD A, type $GIII_b$ (◆) and gel-MOD A, type GI_b (✱).

The latter observation was in agreement with several studies from literature.[53-56] For example, Bajpai et al investigated the effect of the gelatin type on the release profile of sulphamethoxazole by loading the drug onto both gelatin A and B nanoparticles. The results indicated that the fractional release of the drug was much higher in the case of type B than that by type A. The latter was ascribed to the larger swelling of

the type B nanoparticles.[53] Similar results were obtained for the release of chloroquine phosphate from gelatin nanoparticles.[56]

In figure 7-21, the amount of fibronectin, bound per scaffold, is plotted as a function of the fibronectin concentration, present in the incubation liquid. From the results, it can be concluded that, in most cases, a maximum value appears, followed by a decrease in bound fraction with increasing fibronectin concentrations.

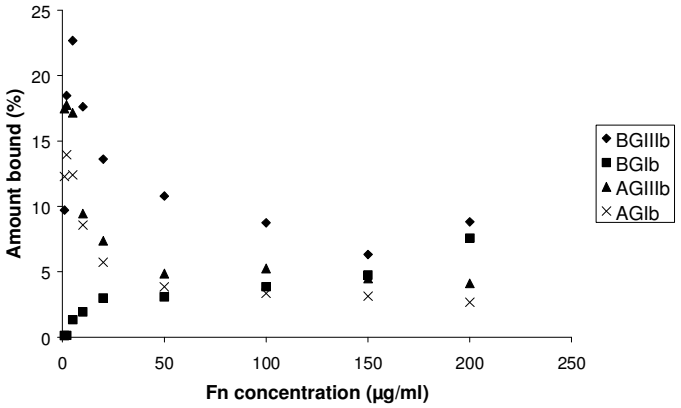

Figure 7-21: Fibronectin fraction, bound per scaffold as a function of the concentration, present in the incubation medium.

3. Study of glycosaminoglycan - gelatin interaction

Since glycosaminoglycans are major components of the extracellular matrix, their interaction with the main scaffold material (i.e. gelatin) could possibly affect the behaviour of the cells, seeded on the matrix. That is why both chondroitin sulphate and hyaluronic acid are investigated for their interaction with gelatin by means of surface plasmon resonance. The structure and properties of both polysaccharides were already described in chapter 2 (§ 4, § 5).

In literature, the interaction between proteoglycans and extracellular matrix molecules has been reported before.[57]

ECM proteins	Glycosaminoglycans								
	HA	Ch	CS-A	CS-C	CS-D	CS-E	DS	HS	Hep
Fiber-forming collagens									
Type I collagen	-	-	-	-	-	±	-	-	-
Type II collagen	-	-	-	-	-	+	-	-	-
Type III collagen	-	-	-	-	-	±	-	-	-
Type V collagen	-	-	-	-	-	+	±	-	+
FACIT collagen									
Type IX collagen	-	-	-	-	-	±	-	-	+
Sheet collagens									
Type IV collagen	-	-	-	-	-	-	-	-	-
Type VIII collagen	-	-	-	-	-	-	-	-	-
Type X collagen	-	-	-	-	-	-	-	-	-
Other collagens									
Type VI collagen	-	-	-	-	-	-	-	-	-
Type VII collagen	-	-	-	-	-	+	-	-	-
Other ECM proteins									
Fibronectin	-	-	-	-	-	-	-	-	+
Laminin	-	-	-	-	-	-	-	-	+
Vitronectin	-	-	-	-	-	-	-	-	+

Table 7-7: Interaction of glycosaminoglycans with extracellular matrix proteins (Ch, chondroitin; DS, dermatan sulphate; HS, heparin sulphate; Hep, heparin).

Most of the interactions appeared to be ionic and probably mediated by highly charged glycosaminoglycan chains of the proteoglycans. In table 7-7, an overview is presented of the interaction between glycosaminoglycans and various extracellular matrix proteins.[58]

In the present work, SPR sensor chips were coated with gelatin, followed by the injection of the glycosaminoglycan studied. The response signal, plotted in the sensorgram gives an idea on the interaction between the protein and the polysaccharide.

3.1. Chondroitin sulphate

It was already described in literature that chondroitin sulphate E has specific affinity for type V collagen.[58] The binding requires a sequence of repeating units, consisting of one glucuronic acid and one N-acetyl-galactosamine, sulphated at carbon-4 and carbon-6. Alternative oligosaccharides, consisting of other sequences, however possessing the same charge, do not interact with type V collagen.[59] The latter demonstrates that the interaction between chondroitin sulphate and gelatin depends on various parameters. Consequently, the interaction between gelatin and two types of chondroitin sulphate (i.e. type A and C) was studied by means of SPR.

In a first part of the experiment, varying concentrations of chondroitin sulphate A were injected onto a sensor chip (100-1000 µg/ml), previously spincoated with gelatin type B. In a second part, an antibody specific for chondroitin sulphate was injected in order to verify that the response was really due to the deposition of the polysaccharide onto the gelatin-coated SPR chip.

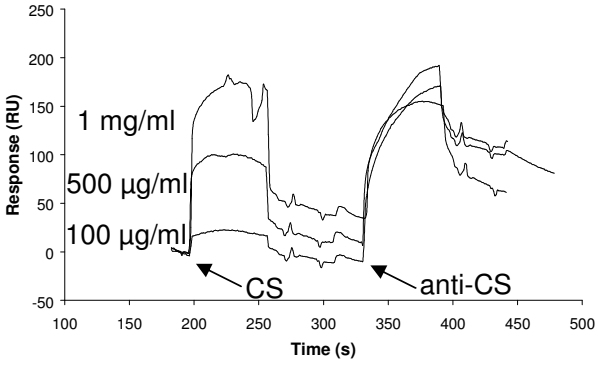

Figure 7-22: Sensorgram showing the interaction between gelatin and chondroitin sulphate A.

From figure 7-22, it appears that the affinity of chondroitin sulphate A for gelatin is rather low. However, the amount of adsorbed polysaccharide increases slightly with increasing CS concentration CS. The limited response was anticipated based on the iso-electric point of the gelatin applied (i.e. 5). Consequently, both gelatin and chondroitin sulphate were negatively charged, excluding ionic interactions. It was already reported before that there exists a weak interaction between collagen and chondroitin 4-sulphate.[60]

Apparently, the adsorbed amount of glycosaminoglycans still enabled interaction with CS antibodies, which was demonstrated by the increase in response signal after the second injection (figure 7-22).
From the results, it could also be concluded that the chemical modification (chapter II, § 4.1) and co-crosslinking of chondroitin sulphate within the gelatin hydrogels (chapter III, § 4.2), was essential to enable incorporation into the polymer scaffolds.

In a second part of the present work, an alternative type of chondroitin sulphate was evaluated for its interaction with the scaffold material (i.e. gelatin) (figure 7-23).

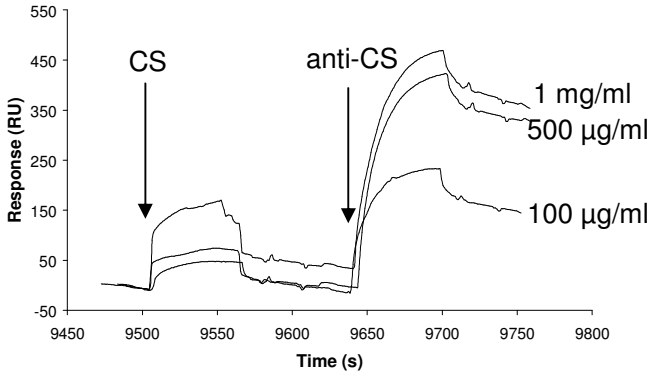

Figure 7-23: Sensorgram showing the interaction between gelatin and chondroitin sulphate C.

When comparing both types of chondroitin sulphate, type A appears to possess a somewhat higher affinity for gelatin compared to type C. However, the difference in response signal is not significant. From the results, it can also be concluded that the antibody has more affinity for chondroitin sulphate C than for CS-A.

3.2. Hyaluronic acid

In literature, there were already some indications that hyaluronic acid could bind with gelatin.[61] However, very few publications report specifically on the interaction between gelatin and HA. In the present work, the interaction between both polymers was investigated by means of surface plasmon resonance.

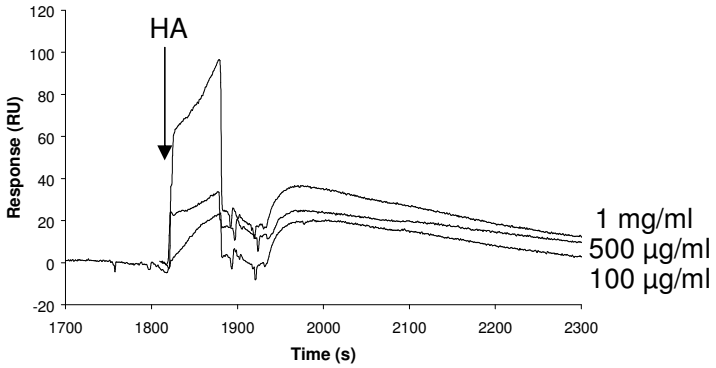

Figure 7-24: Sensorgram showing the interaction between gelatin and hyaluronic acid.

SPR sensors were again spincoated with gelatin type B, followed by rinsing the surface with various hyaluronic acid concentrations (100-1000 µg/ml). From figure 7-24, it can be seen that the interaction between gelatin and HA is rather low, similar to the interaction between gelatin and chondroitin sulphate. However, there was some HA deposition on the surface, indicated by the water uptake in the second part of the plot.

4. Study of gelatin affinity for serum components

4.1. Introduction

Protein adsorption from surrounding tissue fluids is the first phenomenon occurring after biomaterial implantation that may lead to implant integration or rejection.[62] Immediately upon contact with physiological solutions, many proteins adsorb to the implant surface, subsequently promoting nearby cells to interact with the material.[63-66] This also applies for the *in vitro* situation. Survival and growth of many cells *in vitro*, require attachment to a substratum. One of the functions of serum in culture media, is to provide adhesive proteins that mediate such attachment.[2] Studies have further demonstrated that an adsorbed protein layer usually is responsible for mediating the cell-material interaction, if cellular adhesion occurs to a synthetic material.[67] In literature, it was already described earlier that adsorption of albumin and fibrinogen onto scaffolds, composed of various polymers, improved cellular responses.[68] For example, nano-fibrous poly(L-lactic acid) scaffolds coated with fibronectin and

vitronectin, allowed >1.7 times of osteoblastic cell attachment than uncoated scaffolds.[69]

In order to interpret the cellular responses on the scaffolds developed, interaction studies were performed between the scaffold material and the major components of foetal calf serum (FCS) by means of surface plasmon resonance.

In figure 7-25, an overview is presented of the SPR response signals due to the injection of the most abundant components of foetal calf serum. The applied concentrations were the same as their concentration in the serum. Besides the constituents of FCS, the culture medium, which was used to perform *in vitro* biocompatibility studies and the medium, previously enriched with FCS, were also studied for their gelatin affinity.

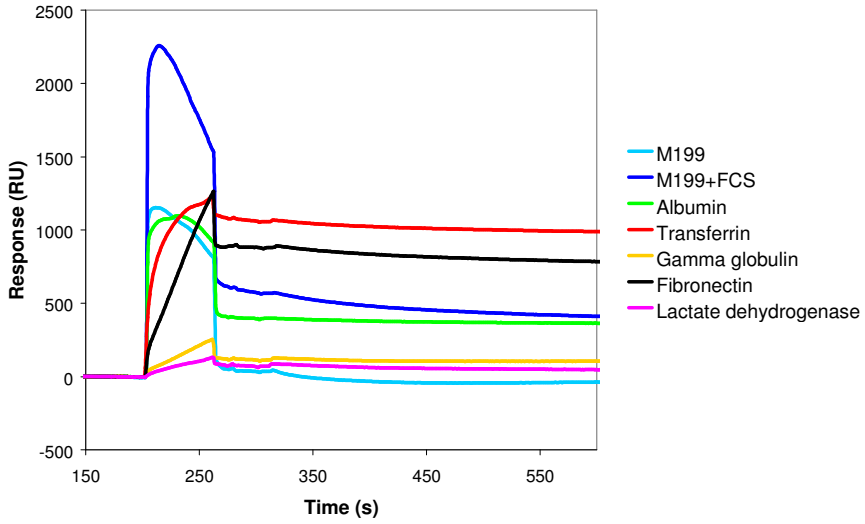

Figure 7-25: Overview of the SPR responses of the most abundant components, present in FCS, of the medium applied for the *in vitro* biocompatibility studies and of the medium enriched with FCS.

Figure 7-25 indicates that the interaction between gelatin and transferrin is higher than between gelatin and fibronectin. However, the injected concentration of fibronectin is about ten times lower than the concentration of transferrin (i.e. 0.03 versus 0.285 mg/ml). Consequently, when comparing all components of FCS, gelatin possesses the highest affinity for fibronectin. There was no baseline shift observed after injection of M199 medium, which was anticipated since the culture medium mainly contains some inorganic salts, amino acids and vitamins.

Since gelatin shows a rather high affinity for various proteins, present in the serum, it could be anticipated that, when incubating the porous scaffolds in cell culture medium, absorption of different FCS components would occur. In this case, the protein molecules would not only adsorb onto the hydrogel surface but could also diffuse into the hydrogel, as reported earlier for similar systems.[70]

4.2. γ-Globulin

Gamma globulins are a group of globularly shaped proteins in human blood plasma, including most antibodies. These antibody substances are produced as a protective reaction of the body's immune system to the invasion of disease-producing organisms.[71]

The interaction between γ-globulin and gelatin was evaluated by means of surface plasmon resonance. Various concentrations (0.025-0.2 mg/ml) of γ-globulin were rinsed over the SPR sensor surface, previously coated with gelatin. Next, the corresponding responses were recorded and plotted in a sensorgram, as demonstrated in figure 7-26.

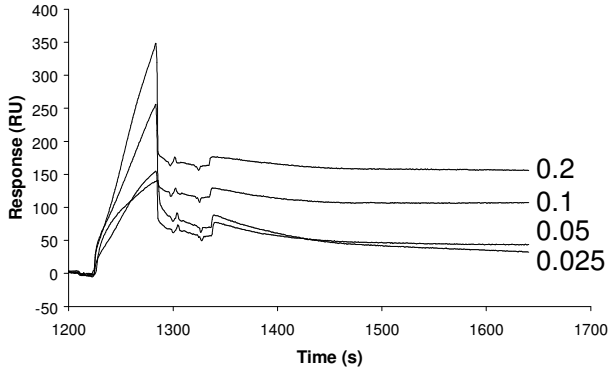

Figure 7-26: Sensorgram showing the response after injecting different concentrations of γ-globulin (0.025-0.2 mg/ml) over a gelatin-coated sensor chip.

When plotting the final response as a function of the globulin concentration, a linear plot was obtained, characterized by the following equation (data not shown):

$$R = 724c + 17$$

where R is the response signal (RU) and c equals the globulin concentration (mg/ml). Based on the kinetics theory discussed in § 2.1, a dissociation constant K_D of 5.23 x 10^{-8} M was obtained for the system gelatin/γ-globulin by means of the BIAevaluation software, version 3.1. In a final part of this chapter, an overview will be presented on the interactions between gelatin and the various FCS components (§ 4.5).

4.3. Transferrin

Transferrin is a glycoprotein, which binds iron very tightly but reversibly. It has a molecular weight of around 80,000. The interaction between transferrin and other proteins such as gelatin, has not been described previously in literature.

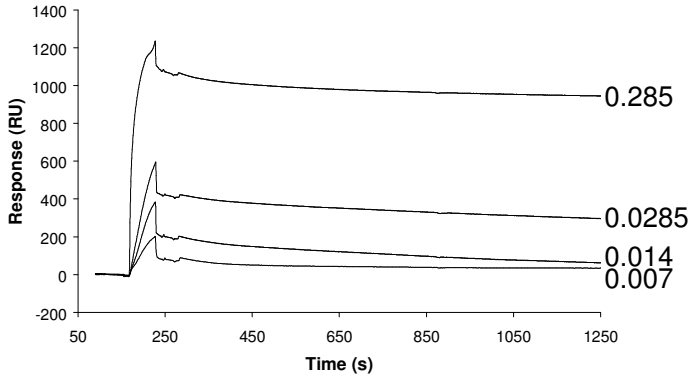

Figure 7-27: Sensorgram showing the response after injecting different concentrations of transferrin (0.007-0.285 mg/ml) over a gelatin-coated sensor chip.

Various transferrin concentrations (0.007-0.285 mg/ml) were injected onto a gelatin-coated sensor chip and the resulting sensorgrams are plotted in figure 7-27.
When plotting the final response as a function of the transferrin concentration, a linear plot was obtained, characterized by the following equation (data not shown):

$$R = 3077c + 77$$

where R is the response signal (RU) and c equals the transferrin concentration (mg/ml).
Based on the kinetics theory discussed in § 2.1, a dissociation constant K_D of 9.12 x 10^{-8} M was obtained for the system gelatin/transferrin by means of the BIAevaluation software, version 3.1.

4.4. Human Serum Albumin

Albumins are a group of proteins, constituting 60% of the proteins in blood plasma. They are important in regulating blood volume by maintaining the osmotic pressure of the blood compartment and for transporting fatty acids, hormones and other substances in the bloodstream.

In literature, it was stated before that gelatin cannot be adsorbed by albumin in solution.[72] The latter was based on the fact that gelatin did not influence the rate of albumin denaturation of albumin by shaking, at gelatin concentrations up to the gelling point.[73] If, however, albumin was initially present at a solid surface, gelatin could be adsorbed.[72] Based on those results, interaction between gelatin and albumin was anticipated, since albumin was rinsed over a gelatin-coated SPR-sensor.

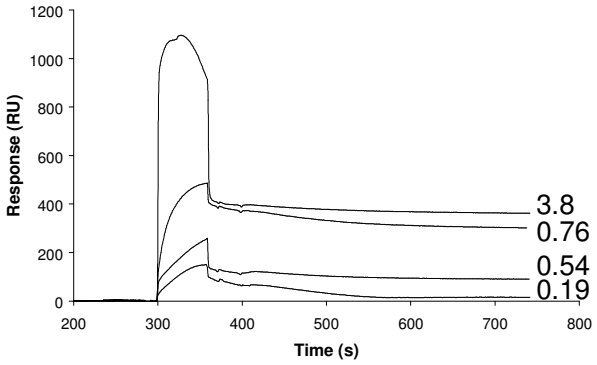

Figure 7-28: Sensorgram showing the response after injecting different concentrations of albumin (0.19-3.8 mg/ml) over a gelatin-coated sensor chip.

Various albumin concentrations (0.19-3.8 mg/ml) were applied and the resulting sensorgrams are plotted in figure 7-28.

When plotting the final response as a function of the albumin concentration, a linear plot was obtained, characterized by the following equation (data not shown):

$$R = 91c + 18$$

where R is the response signal (RU) and c equals the albumin concentration (mg/ml). Based on the kinetics theory discussed in § 2.1, a dissociation constant K_D of 4.36 x 10^{-7} M was obtained for the system gelatin/albumin by means of the BIAevaluation software, version 3.1.

4.5. Overview

In table 7-8, an overview of the most abundant proteins in foetal calf serum (FCS) is presented, with their respective dissociation constants (K_D), iso-electric points (IEP) and slopes, obtained after plotting the SPR response, as a function of the protein concentration (mg/ml) applied on a gel-MOD coated SPR sensor.

	Fibronectin	γ-Globulin	Transferrin	Albumin
K_D (M)	1.88×10^{-9}	5.23×10^{-8}	9.12×10^{-8}	4.36×10^{-7}
Slope (RUml/mg)	32693	724	3077	91
IEP	5.5-6.3	6.9	5.3-5.6	4.7

Table 7-8: Overview of the major proteins in FCS with their respective dissociation constants, slopes, when plotting the response as a function of the concentration, and iso-electric points.

Fibronectin possesses the lowest dissociation constant and highest slope, consequently gelatin has the highest affinity for fibronectin. The latter was anticipated, based on the fact that fibronectin possesses gelatin-binding sites, as already discussed earlier (§ 2).[41, 74, 75] The interactions are mainly of hydrophobic nature. Electrostatic interactions are more or less excluded, based on the iso-electric points of fibronectin and type B gelatin.

Albumin is characterized by the lowest slope and the highest dissociation constant, thus possesses the poorest interaction with gelatin. Since the iso-electric point (i.e. 4.7) is similar to that of the gelatin type applied, no electrostatic interactions were anticipated. Moreover, in literature a few studies report on only a slight interaction between both proteins.[72, 73]

When comparing transferrin and γ-globulin, transferrin appears to have a somewhat higher affinity for gelatin. Based on its iso-electric point, the interaction will be mostly hydrophobic, in contrast to the interaction between gelatin and γ-globulin, showing mainly ionic interactions.

5. Conclusions

In the present chapter, we demonstrated that gelatin interacts with various proteins, present in foetal calf serum. The latter observation is valuable since, after incubating gelatin scaffolds in culture medium, enriched with FCS, protein adsorption/absorption will occur, influencing the subsequent cell adhesion and spreading on the scaffolds developed.

A variety of techniques such as surface plasmon resonance, quartz crystal microbalance and radiolabelling experiments were utilized to perform the interaction studies. From the results, it can be concluded that various techniques lead to different results. The trend remained the same, yet the obtained values differed. Consequently, the use of different measuring techniques to evaluate a particular interaction, is essential. Moreover, when comparing the affinity for a thin gelatin coating with that for a gelatin scaffold, also differences can arise. Namely, protein diffusion within a hydrogel scaffold can occur, which is impossible for thin, coated gelatin layers. In the latter case, merely adsorption onto the surface exists.

We also demonstrated that gelatin hydrogels can be coated with cell-interactive proteins such as fibronectin. The studies revealed that the fibronectin-concentration on the hydrogel surface can be easily fine-tuned, by varying the fibronectin-concentration of the dipcoating solution.

Finally, we also observed that gelatin has a limited affinity for glycosaminoglycans such as chondroitin sulphate and hyaluronic acid. Consequently, the chemical modification and subsequent co-crosslinking of the polysaccharides with gelatin was essential in order to incorporate these polymers into the gelatin hydrogels developed earlier.

References

1. Magnani, A.; Priamo, A.; Pasqui, D.; Barbucci, R., Cell behaviour on chemically microstructured surfaces. *Materials Science and Engineering: C* **2003,** 23, (3), 315-328.
2. Hayman, E. G.; Pierschbacher, M. D.; Suzuki, S.; Ruoslahti, E., Vitronectin - a Major Cell Attachment-Promoting Protein in Fetal Bovine Serum. *Experimental Cell Research* **1985,** 160, (2), 245-258.
3. Miceli, M. V.; Newsome, D. A.; Tate, D. J., Vitronectin is responsible for serum-stimulated uptake of rod outer segments by cultured retinal pigment epithelial cells. *Investigative Ophthalmology & Visual Science* **1997,** 38, (8), 1588-1597.
4. Carsons, S. E.; Fromm, G. H., *Fibronectin in health and disease*. CRC Press: 1989.
5. Bjerrum, O. J.; Heegaard, N. H. H., *CRC Handbook of immunoblotting of proteins*. CRC Press: 1988.
6. Kim, H. W.; Kim, H. E.; Salih, V., Stimulation of osteoblast responses to biomimetic nanocomposites of gelatin-hydroxyapatite for tissue engineering scaffolds. *Biomaterials* **2005,** 26, (25), 5221-5230.
7. Zhu, Y. B.; Chian, K. S.; Chan-Park, M. B.; Mhaisalkar, P. S.; Ratner, B. D., Protein bonding on biodegradable poly(L-lactide-co-caprolactone) membrane for esophageal tissue engineering. *Biomaterials* **2006,** 27, (1), 68-78.
8. Grainger, D. W.; Pavon-Djavid, G.; Migonney, V.; Josefowicz, M., Assessment of fibronectin conformation adsorbed to polytetrafluoroethylene surfaces from serum protein mixtures and correlation to support of cell attachment in culture. *Journal of Biomaterials Science-Polymer Edition* **2003,** 14, (9), 973-988.
9. Madjar, D.; Pitaru, S.; Metzger, Z., Fcs and Fibronectin Depleted Fcs Abolish the Inhibitory Effect of Lps on Gingival Fibroblast Attachment to Collagen. *Journal of Dental Research* **1988,** 67, (4), 713-713.
10. Hook, F.; Kasemo, B.; Nylander, T.; Fant, C.; Sott, K.; Elwing, H., Variations in coupled water, viscoelastic properties, and film thickness of a Mefp-1 protein film during adsorption and cross-linking: A quartz crystal microbalance with dissipation monitoring, ellipsometry, and surface plasmon resonance study. *Analytical Chemistry* **2001,** 73, (24), 5796-5804.
11. Lassen, B.; Nimeri, G.; Golander, C. G.; Nilsson, U.; Elwing, H., Total Internal-Reflection Spectroscopy (Tirf) and Elisa for the Investigation of Protein Competition Phenomena at Rf-Polymer Surfaces. *Abstracts of Papers of the American Chemical Society* **1994,** 207, 211-COLL.
12. Browne, M. M.; Lubarsky, G. V.; Davidson, M. R.; Bradley, R. H., Protein adsorption onto polystyrene surfaces studied by XPS and AFM. *Surface Science* **2004,** 553, (1-3), 155-167.
13. Jönsson, U.; Malmqvist, M., *Real time biospecific interaction analysis*. 1992; Vol. 2, p 291-336.
14. Malmqvist, M.; Karlsson, R., Biomolecular interaction analysis: affinity biosensor technologies for functional analysis of proteins. *Current Opinion in Chemical Biology* **1997,** 1, (3), 378-383.

15. Raut, S.; Gaffney, P. J., Interaction of heparin with fibrinogen using surface plasmon resonance technology: Investigation of heparin binding site on fibrinogen. *Thrombosis Research* **1996,** 81, (4), 503-509.
16. Yu, H. N.; Munoz, E. M.; Edens, R. E.; Linhardt, R. J., Kinetic studies on the interactions of heparin and complement proteins using surface plasmon resonance. *Biochimica Et Biophysica Acta-General Subjects* **2005,** 1726, (2), 168-176.
17. Yu, D. H.; Blankert, B.; Vire, J. C.; Kauffmann, J. M., Biosensors in drug discovery and drug analysis. *Analytical Letters* **2005,** 38, (11), 1687-1701.
18. Brockhaus, M.; Ganz, P.; Huber, W.; Bohrmann, B.; Loetscher, H. R.; Seelig, J., Thermodynamic studies on the interaction of antibodies with beta-amyloid peptide. *Journal of Physical Chemistry B* **2007,** 111, (5), 1238-1243.
19. Vaisocherova, H.; Mrkvova, K.; Piliarik, M.; Jinoch, P.; Steinbachova, M.; Homola, J., Surface plasmon resonance biosensor for direct detection of antibody against Epstein-Baff virus. *Biosensors & Bioelectronics* **2007,** 22, (6), 1020-1026.
20. Karlsson, R.; Falt, A., Experimental design for kinetic analysis of protein-protein interactions with surface plasmon resonance biosensors. *Journal of Immunological Methods* **1997,** 200, (1-2), 121-133.
21. Lecaruyer, P.; Mannelli, I.; Courtois, V.; Goossens, M.; Canva, M., Surface plasmon resonance imaging as a multidimensional surface characterization instrument - Application to biochip genotyping. *Analytica Chimica Acta* **2006,** 573, 333-340.
22. Arya, S. K.; Solanki, P. R.; Singh, R. P.; Pandey, M. K.; Datta, M.; Malhotra, B. D., Application of octadecanethiol self-assembled monolayer to cholesterol biosensor based on surface plasmon resonance technique. *Talanta* **2006,** 69, (4), 918-926.
23. Du, L.; Zhang, Z. S.; Luo, X. M.; Chen, K. X.; Shen, X.; Jiang, H. L., Binding investigation of human 5-lipoxygenase with its inhibitors by SPR technology correlating with molecular docking simulation. *Journal of Biochemistry* **2006,** 139, (4), 715-723.
24. Rhodes, C.; Franzen, S.; Maria, J. P.; Losego, M.; Leonard, D. N.; Laughlin, B.; Duscher, G.; Weibel, S., Surface plasmon resonance in conducting metal oxides. *Journal of Applied Physics* **2006,** 100, (5).
25. Manera, M. G.; Leo, G.; Curri, M. L.; Comparelli, R.; Rella, R.; Agostiano, A.; Vasanelli, L., Determination of optical parameters of colloidal TiO2 nanocrystals-based thin films by using surface plasmon resonance measurments for sensing applications. *Sensors and Actuators B-Chemical* **2006,** 115, (1), 365-373.
26. Pattnaik, P.; Srivastav, A., Surface plasmon resonance - applications in food science research: A review. *Journal of Food Science and Technology-Mysore* **2006,** 43, (4), 329-336.
27. Gil, B.; Chang, Y. K.; Cho, Y. J., An application of surface plasmon resonance to evaluation of quality parameters of soybean oil during frying. *Food Science and Biotechnology* **2006,** 15, (3), 404-408.
28. Nomura, T.; Hattori, O., Determination of Micromolar Concentrations of Cyanide in Solution with a Piezoelectric Detector. *Analytica Chimica Acta* **1980,** 115, (MAR), 323-326.

29. Tammelin, T.; Osterberg, M.; Johansson, L. S.; Laine, J., Preparation of lignin and extractive model surfaces by using spincoating technique - Application for QCM-D studies. *Nordic Pulp & Paper Research Journal* **2006,** 21, (4), 444-450.
30. Sai, V. V. R.; Mahajan, S.; Contractor, A. Q.; Mukherji, S., Immobilization of antibodies on polyaniline films and its application in a piezoelectric immunosensor. *Analytical Chemistry* **2006,** 78, (24), 8368-8373.
31. Kurosawa, S.; Park, J. W.; Aizawa, H.; Wakida, S. I.; Tao, H.; Ishihara, K., Quartz crystal microbalance immunosensors for environmental monitoring. *Biosensors & Bioelectronics* **2006,** 22, (4), 473-481.
32. Cui, L.; Swann, M. J.; Glidle, A.; Barker, J. R.; Cooper, J. M., Odour mapping using microresistor and piezo-electric sensor pairs. *Sensors and Actuators B-Chemical* **2000,** 66, (1-3), 94-97.
33. Lord, M. S.; Modin, C.; Foss, M.; Duch, M.; Simmons, A.; Pedersen, F. S.; Milthorpe, B. K.; Besenbacher, F., Monitoring cell adhesion on tantalum and oxidised polystyrene using a quartz crystal microbalance with dissipation. *Biomaterials* **2006,** 27, (26), 4529-4537.
34. Bhat, V. D.; Truskey, G. A.; Reichert, W. M., Fibronectin and avidin-biotin as a heterogeneous ligand system for enhanced endothelial cell adhesion. *Journal of Biomedical Materials Research* **1998,** 41, (3), 377-385.
35. MacDonald, D. E.; Rapuano, B. E.; Deo, N.; Stranick, M.; Somasundaran, P.; Boskey, A. L., Thermal and chemical modification of titanium-aluminum-vanadium implant materials: effects on surface properties, glycoprotein adsorption, and MG63 cell attachment. *Biomaterials* **2004,** 25, (16), 3135-3146.
36. Opresko, L.; Wiley, H. S.; Wallace, R. A., Proteins Iodinated by the Chloramine-T Method Appear to Be Degraded at an Abnormally Rapid Rate after Endocytosis. *Proceedings of the National Academy of Sciences of the United States of America-Biological Sciences* **1980,** 77, (3), 1556-1560.
37. Miedzobrodzki, J.; Naidu, A. S.; Watts, J. L.; Ciborowski, P.; Palm, K.; Wadstrom, T., Effect of Milk on Fibronectin and Collagen Type-I Binding to Staphylococcus-Aureus and Coagulase-Negative Staphylococci Isolated from Bovine Mastitis. *Journal of Clinical Microbiology* **1989,** 27, (3), 540-544.
38. Lee, J. I.; Woo, S. K.; Kim, K. I.; Park, K. C.; Baek, S. H.; Yoo, Y. J.; Chung, C. H., A Method for Assaying Deubiquitinating Enzymes. *Biol. Proced. Online* **1998,** 1, 92-99.
39. Meyer-Andrews, T.; Andrews, W. W.; Baker, C. A., An Investigation Into the Removal of Enzymes from Paper Following Conservation Treatment. *The book and paper group annual* **1990,** 9.
40. Pickford, A. R.; Smith, S. P.; Staunton, D.; Boyd, J.; Campbell, I. D., The hairpin structure of the (6)F1(1)F2(2)F2 fragment from human fibronectin enhances gelatin binding. *Embo Journal* **2001,** 20, (7), 1519-1529.
41. Haas, R.; Culp, L. A., Binding of Fibronectin to Gelatin and Heparin - Effect of Surface Denaturation and Detergents. *Febs Letters* **1984,** 174, (2), 279-283.

42. Katagiri, Y.; Brew, S. A.; Ingham, K. C., All six modules of the gelatin-binding domain of fibronectin are required for full affinity. *Journal of Biological Chemistry* **2003,** 278, (14), 11897-11902.
43. Ingham, K. C.; Brew, S. A.; Erickson, H. P., Localization of a cryptic binding site for tenascin on fibronectin. *Journal of Biological Chemistry* **2004,** 279, (27), 28132-28135.
44. Green, R. J.; Frazier, R. A.; Shakesheff, K. M.; Davies, M. C.; Roberts, C. J.; Tendler, S. J. B., Surface plasmon resonance analysis of dynamic biological interactions with biomaterials. *Biomaterials* **2000,** 21, (18), 1823-1835.
45. Gao, X. Y.; Groves, M. J., Fibronectin-binding peptides. I. Isolation and characterization of two unique fibronectin-binding peptides from gelatin. *European Journal of Pharmaceutics and Biopharmaceutics* **1998,** 45, (3), 275-284.
46. Tjia, J. S.; Aneskievich, B. J.; Moghe, P. V., Substrate-adsorbed collagen and cell secreted fibronectin concertedly induce cell migration on poly(lactide-glycolide) substrates. *Biomaterials* **1999,** 20, (23-24), 2223-2233.
47. Hodde, J.; Record, R.; Tullius, R.; Badylak, S., Fibronectin peptides mediate HMEC adhesion to porcine-derived extracellular matrix. *Biomaterials* **2002,** 23, (8), 1841-1848.
48. Bergman, A. J.; Zygourakis, K., Migration of lymphocytes on fibronectin-coated surfaces: temporal evolution of migratory parameters. *Biomaterials* **1999,** 20, (23-24), 2235-2244.
49. Palecek, S. P.; Loftus, J. C.; Ginsberg, M. H.; Lauffenburger, D. A.; Horwitz, A. F., Integrin-ligand binding properties govern cell migration speed through cell-substratum adhesiveness. *Nature* **1997,** 385, (6616), 537-540.
50. Yang, Y. Z.; Glover, R.; Ong, J. L., Fibronectin adsorption on titanium surfaces and its effect on osteoblast precursor cell attachment. *Colloids and Surfaces B-Biointerfaces* **2003,** 30, (4), 291-297.
51. Yang, Y. Z.; Cavin, R.; Ong, J. L., Protein adsorption on titanium surfaces and their effect on osteoblast attachment. *Journal of Biomedical Materials Research Part A* **2003,** 67A, (1), 344-349.
52. Johns, P.; Courts, A., Relationship between collagen and gelatin. In *The science and technology of gelatin*, Academic Press: New York, 1977.
53. Bajpai, A. K.; Choubey, J., Release study of sulphamethoxazole controlled by swelling of gelatin nanoparticles and drug-biopolymer interaction. *Journal of Macromolecular Science-Pure and Applied Chemistry* **2005,** A42, (3), 253-275.
54. Kuijpers, A. J.; Engbers, G. H. M.; van Wachem, P. B.; Krijgsveld, J.; Zaat, S. A. J.; Dankert, J.; Feijen, J., Controlled delivery of antibacterial proteins from biodegradable matrices. *Journal of Controlled Release* **1998,** 53, 235-247.
55. Bessho, M.; Furuta, M.; Kojima, T.; Okuda, S.; Hara, M., Gelatin hydrogels cross-linked by gamma-ray irradiation: materials for absorption and release of dye. *Journal of Biomaterials Science-Polymer Edition* **2005,** 16, (6), 715-724.

56. Bajpai, A. K.; Jyoti, C., Design of gelatin nanoparticles as swelling controlled delivery system for chloroquine phosphate. *Journal of Materials Science: Materials in Medicine* **2006,** 17, (4), 345-358.
57. Stallcup, W. B.; Dahlin, K.; Healy, P., Interaction of the Ng2 Chondroitin Sulfate Proteoglycan with Type-Vi Collagen. *Journal of Cell Biology* **1990,** 111, (6), 3177-3188.
58. Munakata, H.; Takagaki, K.; Majima, M.; Endo, M., Interaction between collagens and glycosaminoglycans investigated using a surface plasmon resonance biosensor. *Glycobiology* **1999,** 9, (10), 1023-1027.
59. Takagaki, K.; Munakata, H.; Kakizaki, I.; Iwafune, M.; Itabashi, T.; Endo, M., Domain structure of chondroitin sulfate E octasaccharides binding to type V collagen. *Journal of Biological Chemistry* **2002,** 277, (11), 8882-8889.
60. Obrink, B.; Laurent, T. C.; Carlsson, B., Binding of Chondroitin Sulfate to Collagen. *Febs Letters* **1975,** 56, (1), 166-169.
61. Chang, N. S.; Boackle, R. J., Hyaluronic-Acid Complement Interactions .2. Role of Divalent-Cations and Gelatin. *Molecular Immunology* **1985,** 22, (8), 843-848.
62. Alves, C. M.; Reis, R. L.; Hunt, J. A., Preliminary study on human protein adsorption and leukocyte adhesion to starch-based biomaterials. *Journal of Materials Science: Materials in Medicine* **2003,** 14, (2), 157-165.
63. Garcia, A. J.; Boettiger, D., Integrin-fibronectin interactions at the cell-material interface: initial integrin binding and signaling. *Biomaterials* **1999,** 20, (23-24), 2427-2433.
64. Ito, Y.; Zheng, J.; Imanishi, Y., Enhancement of cell growth on a porous membrane co-immobilized with cell-growth and cell adhesion factors. *Biomaterials* **1997,** 18, (3), 197-202.
65. Grunkemeier, J. M.; Tsai, W. B.; McFarland, C. D.; Horbett, T. A., The effect of adsorbed fibrinogen, fibronectin, von Willebrand factor and vitronectin on the procoagulant state of adherent platelets. *Biomaterials* **2000,** 21, (22), 2243-2252.
66. Altankov, G.; Thom, V.; Groth, T.; Jankova, K.; Jonsson, G.; Ulbricht, M., Modulating the biocompatibility of polymer surfaces with poly(ethylene glycol): Effect of fibronectin. *Journal of Biomedical Materials Research* **2000,** 52, (1), 219-230.
67. Sun, T.; Norton, D.; Ryan, A. J.; MacNeil, S.; Haycock, J. W., Investigation of fibroblast and keratinocyte cell-scaffold interactions using a novel 3D cell culture system. *Journal of Materials Science: Materials in Medicine* **2007,** 18, (2), 321-328.
68. Choi, Y. J.; Choung, S. K.; Hong, C. M.; Shin, I. S.; Park, S. N.; Hong, S. H.; Park, H. K.; Park, Y. H.; Son, Y.; Noh, I., Evaluations of blood compatibility via protein adsorption treatment of the vascular scaffold surfaces fabricated with polylactide and surface-modified expanded polytetrafluoroethylene for tissue engineering applications. *Journal of Biomedical Materials Research Part A* **2005,** 75A, (4), 824-831.
69. Kyung Mi Woo, V. J. C. P. X. M., Nano-fibrous scaffolding architecture selectively enhances protein adsorption contributing to cell attachment. *Journal of Biomedical Materials Research Part A* **2003,** 67A, (2), 531-537.

70. Kato, K.; Sano, S.; Ikada, Y., Protein adsorption onto ionic surfaces. *Colloids and Surfaces B: Biointerfaces* **1995,** 4, (4), 221-230.
71. Fahey, J. L.; Horbett, A. P., Human Gamma Globulin Fractionation on Anion Exchange Cellulose Columns. *J. Biol. Chem.* **1959,** 234, (10), 2645-2651.
72. Moyer, L. S.; Moyer, E. Z., ELECTROKINETIC ASPECTS OF SURFACE CHEMISTRY. VI. THE INTERACTION OF GELATIN WITH CASEIN AND EGG ALBUMIN AT SURFACES. *J. Biol. Chem.* **1940,** 132, (1), 357-371.
73. Bull, H. B.; Neurath, H., THE DENATURATION AND HYDRATION OF PROTEINS. II. SURFACE DENATURATION OF EGG ALBUMIN. *J. Biol. Chem.* **1937,** 118, (1), 163-175.
74. Forastieri, H.; Ingham, K. C., Interaction of Gelatin with a Fluorescein-Labeled 42-Kda Chymotryptic Fragment of Fibronectin. *Journal of Biological Chemistry* **1985,** 260, (19), 10546-10550.
75. Garciapardo, A.; Gold, L. I., Further Characterization of the Binding of Fibronectin to Gelatin Reveals the Presence of Different Binding Interactions. *Archives of Biochemistry and Biophysics* **1993,** 304, (1), 181-188.

Chapter VIII:

Biological Evaluation

1 Introduction

When body tissue or an organ is severely injured, partly lost, or functions inaccurately, it is clinically treated with reconstruction surgery or organ transplantation. However, the shortage of donor organs remains a major obstacle for clinical transplantation.[1] Reconstruction surgery almost always depends on biomaterials or biomedical devices that have been artificially prepared. One often used strategy is to construct bioartificial tissues *in vitro* from cells and a support matrix and to implant the construct into the body. The cells can be autogeneic, allogeneic or xenogeneic, depending on the type of construct and the donor availability. The advantage of allogeneic or xenogeneic cells is that they can be cultured and banked in advance for use in cases in which there is not enough time to expand a patient's own cells to construct the tissue, but allogeneic and xenogeneic cells will elicit rejection if detected by the immune system.[2] It is necessary for tissue regeneration to increase the number of cells constituting the tissue as well as reconstruct a structure of extracellular matrix (ECM) to support the proliferation and differentiation of cells for regeneration induction.[3] Each tissue represents a different challenge in its production by tissue engineering. Therefore, the properties measured will vary. For example, because the blood vessel must sustain the blood pressure readily after grafting, the measurement of the mechanical resistance will be important.[4]

In vitro systems used in tissue engineering span a wide area of subject matter, from pumps and bioreactors to constructs intended for tissue or organ replacement.[5]

Gelatin-based materials have already been applied frequently in the past for tissue engineering applications. A non-exhaustive overview of the most recent publications, subdivided alphabetically by application, is summarised in the table below (table 8-1).

Application	Type of gelatin	Reference
Adipose tissue	gelatin sponge	6
Blood vessel	gelatin grafted poly(ε-caprolactone) nanofibers, VEGF immobilised gelatin, polyethylene-glycol diacrylate cross-linked gelatin, chitosan/gelatin blends, gelatin grafted PET nanofibers, gelatin coated PES fibers	7-12
Bone	hydroxyapatite chitosan/gelatin composite, gelatin coated poly(α-hydroxy acids), glutaraldehyde crosslinked gelatin, hydroxyapatite/gelatin composite, β-tricalcium phosphate/ gelatin composite, gelatin/poly(ε-caprolactone) blended nano-fibers	13-20
Cartilage	gelatin/chondoitin-6-sulfate/hyaluronan tri-copolymer, plasmid DNA immobilised chitosan-gelatin, gelatin microparticle embedded OPF hydrogels, gelatin microparticle embedded poly(D,L-lactide-ε-caprolactone)	21-25
General	transglutaminase cross-linked gelatin, proanthocyanidin cross-linked chitosan gelatin, gelatin coated poly(D,L-lactide), electrospun gelatin fibers, PHBHHx/gelatin blend, PVA/gelatin blend, PNIPAM grafted gelatin, gelatin- and fibronectin-coated PE multilayer nanofilms	26-34
Heart	gelatin coated polyurethane films	35
Intervertebral disc	gelatin/chondoitin-6-sulfate/hyaluronan tri-copolymer, gelatin, glutaraldehyde cross-linked gelatin/chondroitin-6-sulphate	36-38
Liver	cross-linked sodium alginate/gelatin	39
Muscle	gelatin grafted PCL nanofibers	40
Nerve	photo cross-linkable gelatin	41
Pancreas	gelatin grafted agarose	42
Skin	glutaraldehyde cross-linked gelatin	43

Table 8-1: Overview of biomedical applications of gelatin.

The table, based on a literature search in PubMed using gelatin and tissue engineering as keywords, clearly indicates that gelatin has a wide application range within the field of both soft and hard tissue engineering. The extensive data available on the application of gelatin as a biomaterial, however, is very scattered. Different research groups have separately evaluated gelatin-based biomaterials which differ in the applied gelatin type, crosslinking agent, additives (in case of composites), pore size, pore geometry and pore distribution.[5-42] In addition, only a limited number of cell types have been included in most studies. This makes a meaningful understanding of how one type of (gelatin) scaffold with its specific properties can be applied as a suitable substrate for a variety of cell types rather difficult.

2 Blood compatibility studies

Evaluating the influence of modified polymers on red blood cells is important before using it in blood-contact applications. Although the contact with blood is rather limited, every intervention at the site of a tissue defect, is always related with bleeding. The release of haemoglobin was used to monitor the haemolytic properties of the scaffolds developed.[44] Triton X-100 (1%) and HEPES buffer were used to provide respectively the 100 and 0% values. A selected number of porous scaffolds developed were allowed to interact with the RBC for 24h. All experiments were performed in triplicate.

According to ASTM F 756-00, materials can be classified as follows (table 8-2):[45]

Haemolysis (%) above negative control	Haemolytic grade
0-2	Non-haemolytic
2-5	Slightly haemolytic
>5	Haemolytic

Table 8-2: Classification of haemolytic grade of samples according to their haemolysis (%).

The gelatin scaffolds can be classified from non-haemolytic to slightly haemolytic, since their haemolytic indices are lower than 5% (figure 8-1).

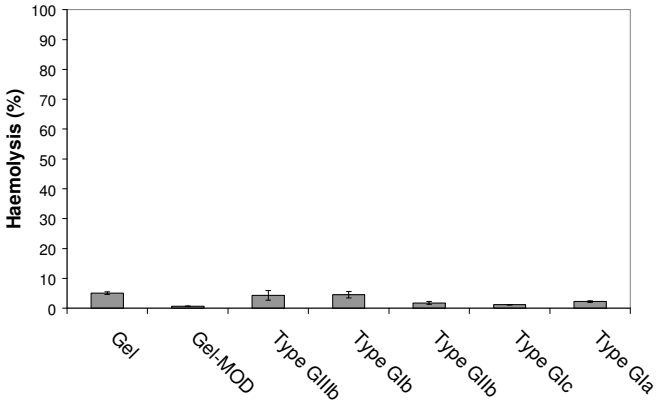

Figure 8-1: Haemolysis values of the gelatins developed.

Haemolysis is regarded as a significant screening test, since it provides quantification of small levels of plasma haemoglobin which may not be measurable under *in vivo* conditions. As reported in literature, it is not possible to define a universal level of acceptable or unacceptable amounts of haemolysis.[45] A blood-compatible material should be non-haemolytic by definition, however, in reality, several medical devices cause haemolysis. In this case, clinical benefits should overcome the risks and haemolysis values should be kept as low as possible.

Haemolysis values of CS-based scaffolds were within the same range compared to pure gelatin matrices (data not shown).

3 *In vitro* cell interaction studies

In the present work, a limited number of porous gelatin based scaffolds was screened using a panel of different human cells. The scaffolds were developed as described earlier (chapter 4, cryogenic treatment in combination with an applied temperature gradient), enabling the production of scaffolds with elongated channels throughout the material.[46] Two hydrogel types developed (i.e. type $GIII_b$ and type GI_b) were evaluated for their potential as cell carriers. The adhesion, spreading and proliferation of human cells on the porous gel-MOD hydrogels were evaluated by

confocal microscopy visualisation of calcein-acetoxy methyl ester (CAM) labelled cells.

Confocal microscopy is a microscopic technique that enables three dimensional imaging and resolution. The 3D resolution is obtained because all the light which is not coming from an in-focus plane is being blocked. The latter is achieved because there is a pinhole positioned in front of the detector (figure 8-2).

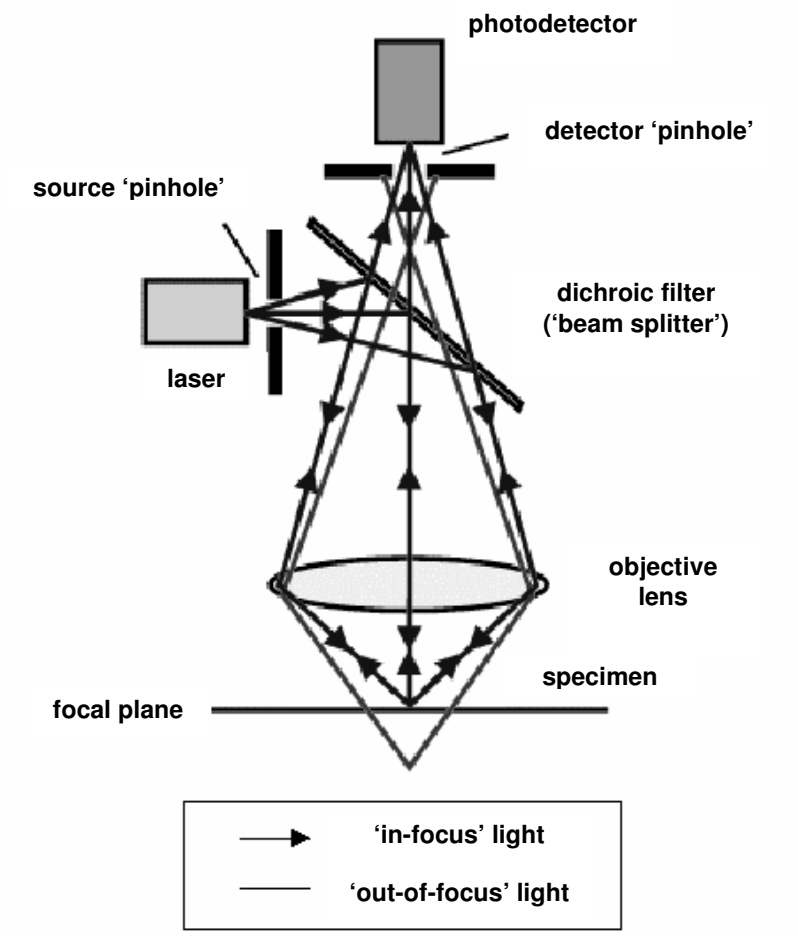

Figure 8-2: The light pathway in confocal microscopy.

In this way, all the light originating from an in-focus plane will pass freely through the pinhole, whereas light coming from an out-of-focus plane will largely be blocked by the pinhole. The light coming from the laser passes a pinhole and is reflected by a dichroic mirror and focussed by a microscope objective to a small spot on the sample. A dichroic mirror has the property that it reflects one wavelength while transmitting others. Specific dichroic mirrors can be applied for the relevant

wavelength regions of excitation and emission. When the sample is excited, it will start to emit light in a random direction.

A fraction of the emitted photons is collected by the microscope objective and imaged onto the detector. The position of the pinhole in front of the detector is such that it is in a conjugate plane with both the plane of focus of the microscope objective and the point of excitation of the laser, which is defined by the excitation pinhole. The effect of blocking out the out-of-focus contributions is also known as optical sectioning. It permits the imaging of separate (axial) slices within the specimen.[47]

The acetoxymethyl (AM) ester derivatives of fluorescent indicators and chelators make up one of the most useful groups of compounds for the study of living cells. Modification of carboxylic acids with AM ester groups results in an uncharged molecule that can permeate cell membranes. Once inside the cell, the lipophilic blocking groups are cleaved by non-specific esterases, resulting in a charged form that leaks out of cells far more slowly than its parent compound. In the case of **calcein AM**, the AM ester is colourless and non-fluorescent until hydrolyzed (figure 8-3).[48]

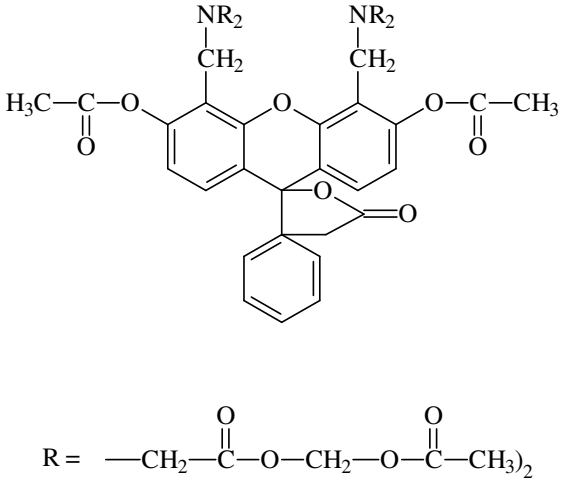

Figure 8-3: Structure of calcein acetoxymethyl ester.

3.1 Cell seeding on the hydrogels

To evaluate to what extent the induced differences in pore size and geometry affected the interaction with cells, we performed an initial *in vitro* screening of both types of scaffolds using a panel of human cells from different organ tissue origin: endothelial cells (human umbilical vein endothelial cells, HUVEC), osteoblasts (MG-63 and CAL-72), human foreskin fibroblasts, glial cells (U373-MG) and epithelial cells (HELA). For this study, more cell lines compared to primary cells were selected, since cell lines are reproducible from lab to lab. In addition, they exhibit many of the phenotypic markers of the primary cells they represent. Primary cells show donor to donor variation, are more difficult to culture and phenotype may vary from passage to passage and from lab to lab. Control pictures of the different cell types seeded on tissue culture plastic are shown in figure 8-4.

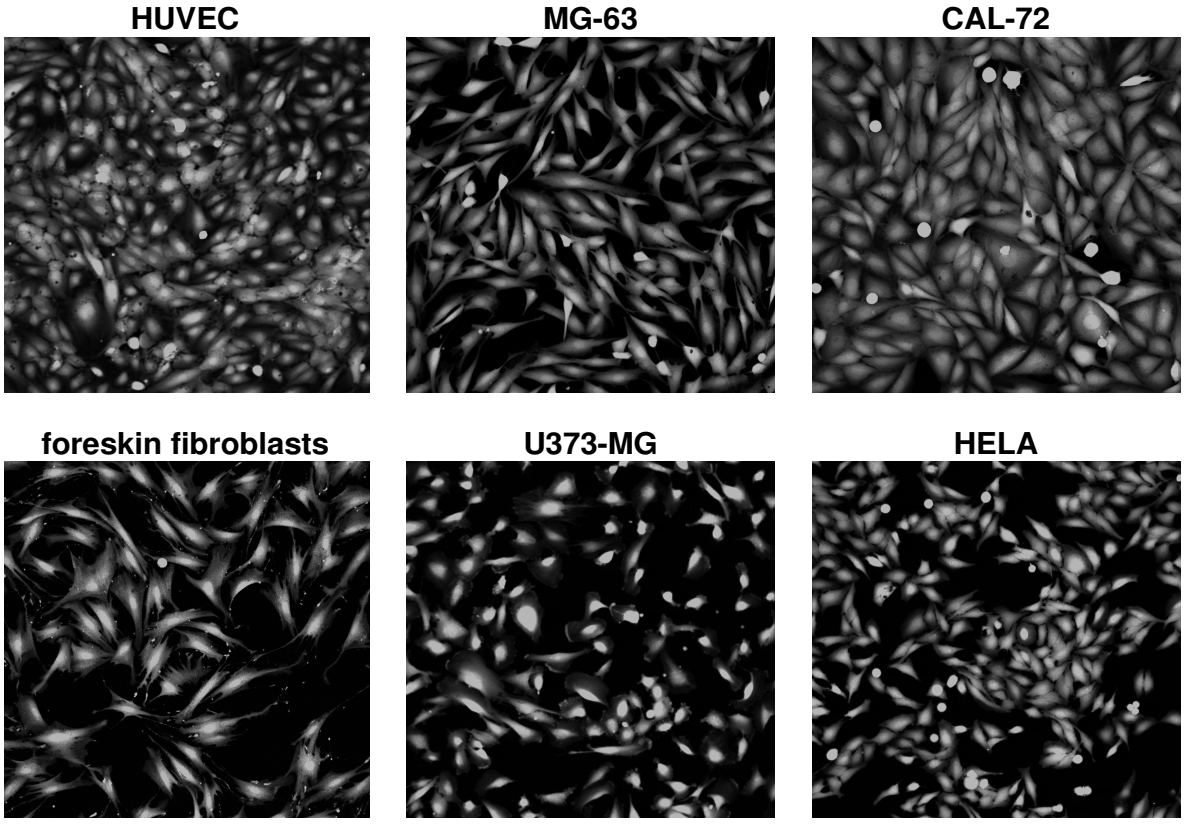

Figure 8-4: Visualisation of tissue culture plastic (TCP) seeded HUVEC, MG-63, CAL-72, foreskin fibroblasts, U373-MG and HELA. For HUVEC, the TCP was pre-coated with gelatin. Cells were stained with calcein-AM (1 µg/ml) and visualised (20X magnification) using confocal microscopy.

3.2 Cell survival and organisation on/within type GIII$_b$ hydrogels

At different incubation times after cell seeding, the cells were stained using calcein-AM as vital stain. Using this stain, only vital cells are stained. This enabled a visualisation of the cells and analysis of adhesion, spreading and proliferation after seeding on the hydrogels. The results are summarised in figures 8-5 (5x magnified) and 8-6 (10x magnified). For these preliminary experiments, cell visualisation was performed on the same side of the scaffold on which the cells were seeded. Up to 3 days after cell seeding, most HUVEC show a rounded-up morphology, whereas only a minor part of individual endothelial cells were spread out on the scaffolds. However, after one week, all cells had attached and spread-out cell morphology and the formation of cell clusters was observed. Within the hydrogel, three different types of cellular organisation could be distinguished as indicated by the numbered arrows in figure 8-6. Part of the hydrogel was covered with confluent cell layers (arrow 1 in figure 8-6). For endothelial cells, close cell-cell contacts are a requirement since these contacts control the permeability of the blood vessel wall forming a barrier for solutes, macromolecules and leukocytes.[49] In other areas of the hydrogels, HUVEC formed aligned cell entities along the pores of the hydrogels (arrow 2 in figure 8-6). Finally, in addition to the confluent cell layers and the cells aligned along the pores, a small number of single cells were also observed on the hydrogels (arrow 3 in figure 8-6).

After longer incubation times on the porous gelatin scaffolds (> 1 week), the cell density on the scaffolds gradually increased. Dividing cells spread out to cover most of the available surface area and formed nearly confluent monolayers with cell-cell contacts. As a result of the cell proliferation on the material, only confluent cell layers and aligned cell entities appeared on the material whereas the number of isolated single cells decreased. These *in vitro* studies have shown that endothelial cells remained viable for at least four weeks on the hydrogels. A further evaluation of the potential of these hydrogels for long term culturing of endothelial cells, revealed that culturing periods up to seven weeks were feasible (data not shown). The latter could have important applications in the field of bioreactor technology.

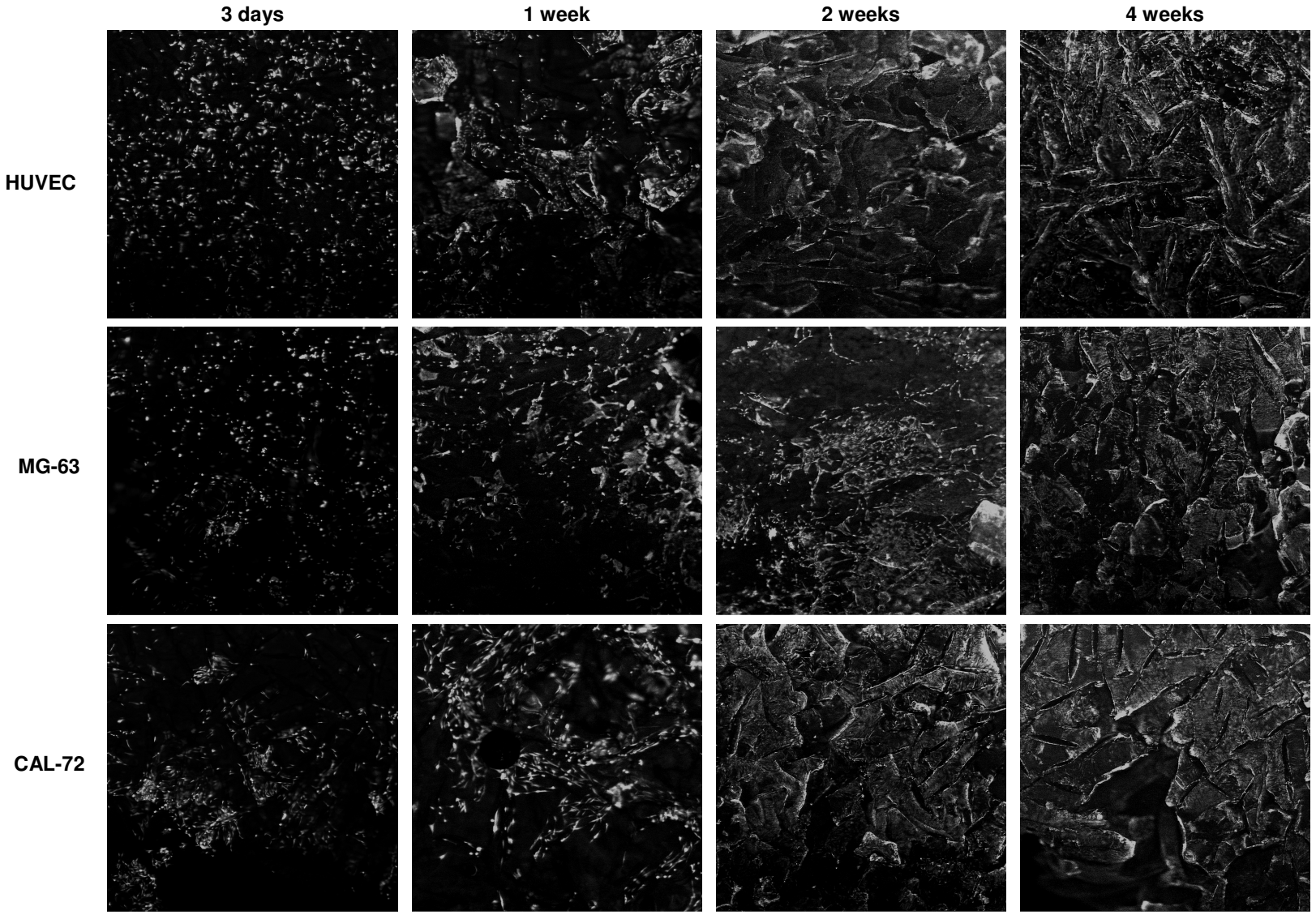

Figure 8-5: HUVEC, MG-63 and CAL-72 visualisation (5X) on type GIII$_b$ hydrogels at different time points after cell seeding.

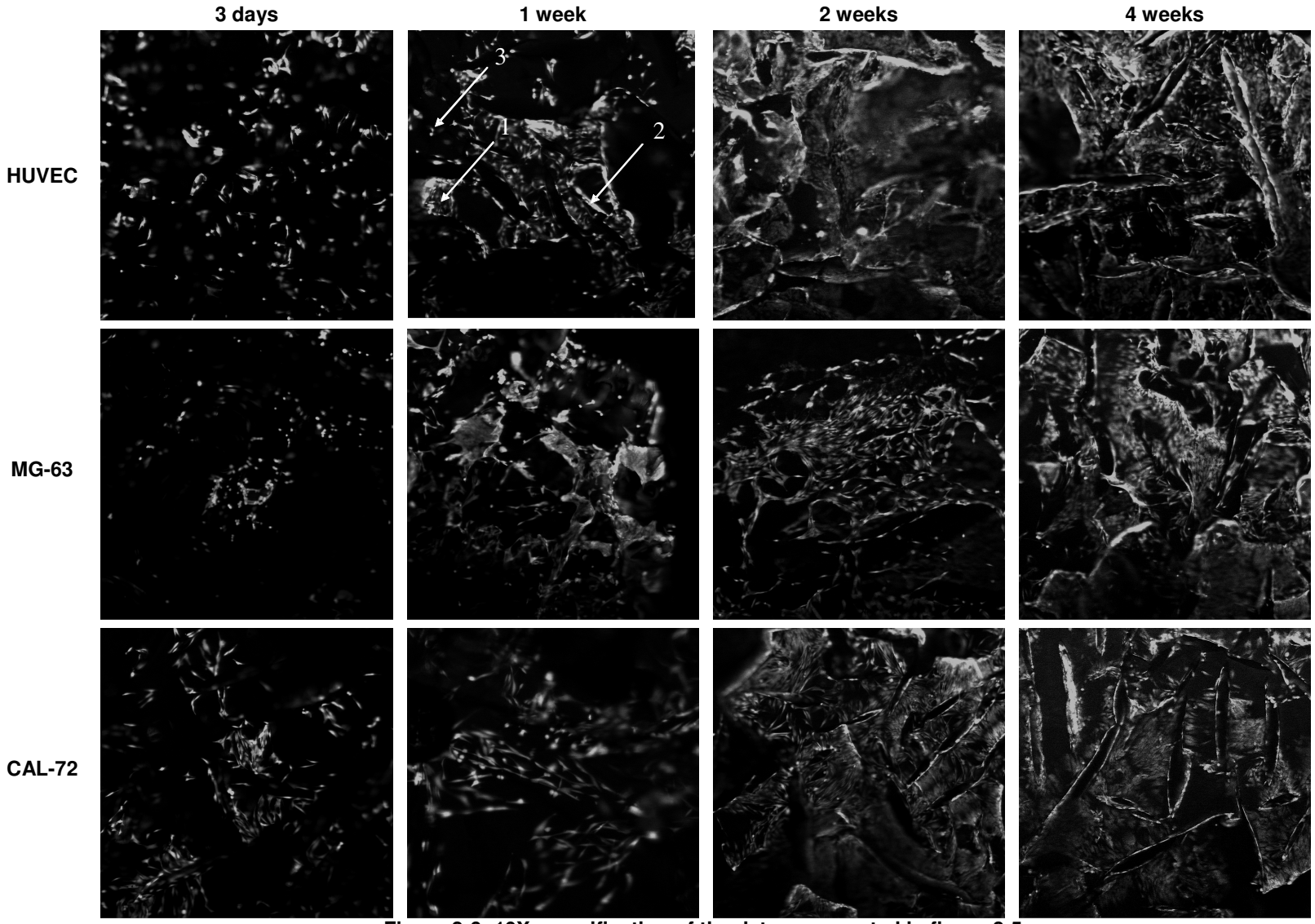

Figure 8-6: 10X magnification of the data represented in figure 8-5.

From the examination of the cell organisation on the structures (figures 8-5 and 8-6), it could be concluded that with an increasing incubation time the endothelial cells nearly covered all the available hydrogel surfaces without bridging the pores within the hydrogel structure. In those areas where pores were present, endothelial cells aligned along the pore. Additionally, further studies were also performed to determine to what extent endothelial cells have on the ability to grow into the pores of the scaffolds with time. Preliminary results indicated that HUVEC indeed grow into the pores of the scaffolds developed (figure 8-7).

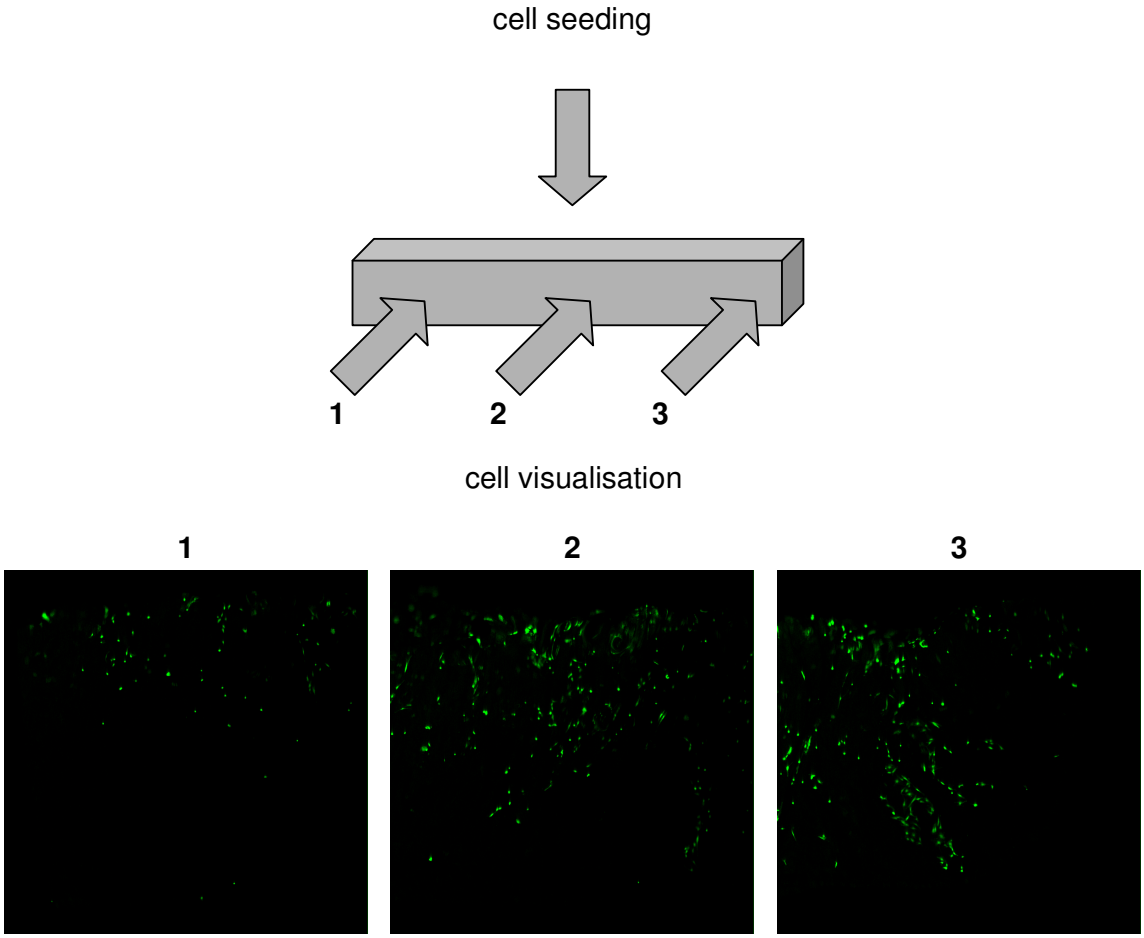

Figure 8-7: Visualisation of HUVEC on type GIII$_b$ hydrogels, 3 days after cell seeding. Cells were stained with calcein-AM (1 µg/ml) and visualised using confocal microscopy (2.5X magnification).

Compared to cell seeding on gelatin-coated cell culture flasks, the attachment and spreading of endothelial cells on the hydrogels was much slower. Endothelial cells adhered and spread on gelatin-coated cell culture plastic within 1-2 hours. Most

likely, these differences could be ascribed to the 3D character of the porous scaffolds. Upon cell seeding, the endothelial cells were not in contact with a flat polymer surface but with a complex 3D porous hydrogel. More steps may be involved in the attachment and spreading to the hydrogels compared to attachment on flat cell culture flasks which was favoured by gravity. This may explain the slower attachment and spread on the 3D materials.

In literature, it was already demonstrated that HUVEC showed different morphology on 2D chitosan surfaces than on 3D matrices. In addition, 3D cultures showed higher cell survival relative to 2D cultures. Probably, there were different factors affecting this cell behaviour.[10] In 2D substrata, cells are restricted to spread on a flat plane and the important factor affecting cellular activity is whether the substrate contains cell adhesion binding domains or not. On the contrary, 3D matrices provide spatial advantages for cell-cell and cell-matrix adhesion as well as support for cell traction. In addition, many factors such as the compliance[50], stiffness[51], hydrophilicity[52] and surface topography[53] affect various cellular processes. In 2D culture, cells are cultured on rigid surfaces coated with thin layer of matrices and stiffness that matrices possess may be primarily contributed by the surface. However, in 3D cultures, the stiffness of the scaffolds will be different than glass/TCP surfaces and may directly influence cell adhesion.[10]

For MG-63 osteoblasts, similar results were observed in terms of cell adhesion and spreading as were observed with HUVEC. Up to 3 days after cell seeding, MG-63 cells showed a rounded morphology (see figures 8-5 and 8-6). After longer incubation times, cells started to spread out and proliferate, covering the entire scaffold surface. In contrast to HUVEC-seeded hydrogels, MG-63 cells mainly formed confluent cell layers after two weeks of incubation. After four weeks *in vitro*, the number of aligned cell entities increased slightly.

In contrast with the results obtained for HUVEC and MG-63, CAL-72 cells adhered and spread on the porous gelatin hydrogels within three days after cell seeding (figures 8-5 and 8-6). The cell behaviour after longer incubation times was similar to HUVEC.

In addition to endothelial cells and osteoblasts, type $GIII_b$ hydrogels were also screened for the growth of human foreskin fibroblasts, glial cells (U373-MG) and epithelial cells (HELA). The results after 4 weeks incubation, as summarised in figure 8-8, clearly indicate that the porous gelatin scaffolds were an excellent candidate material for the (long-term) culturing of these cell types also, and the hydrogels are thus an excellent substrate for a large variety of human cells. It should be mentioned that, in contrast to the other cell types studied, human foreskin fibroblasts bridged the hydrogel pores in some areas after four weeks incubation (see arrows in figure 8-8, first column). Most likely, this can be ascribed to the high amount of extra-cellular matrix produced by these cells on the scaffolds.[54]

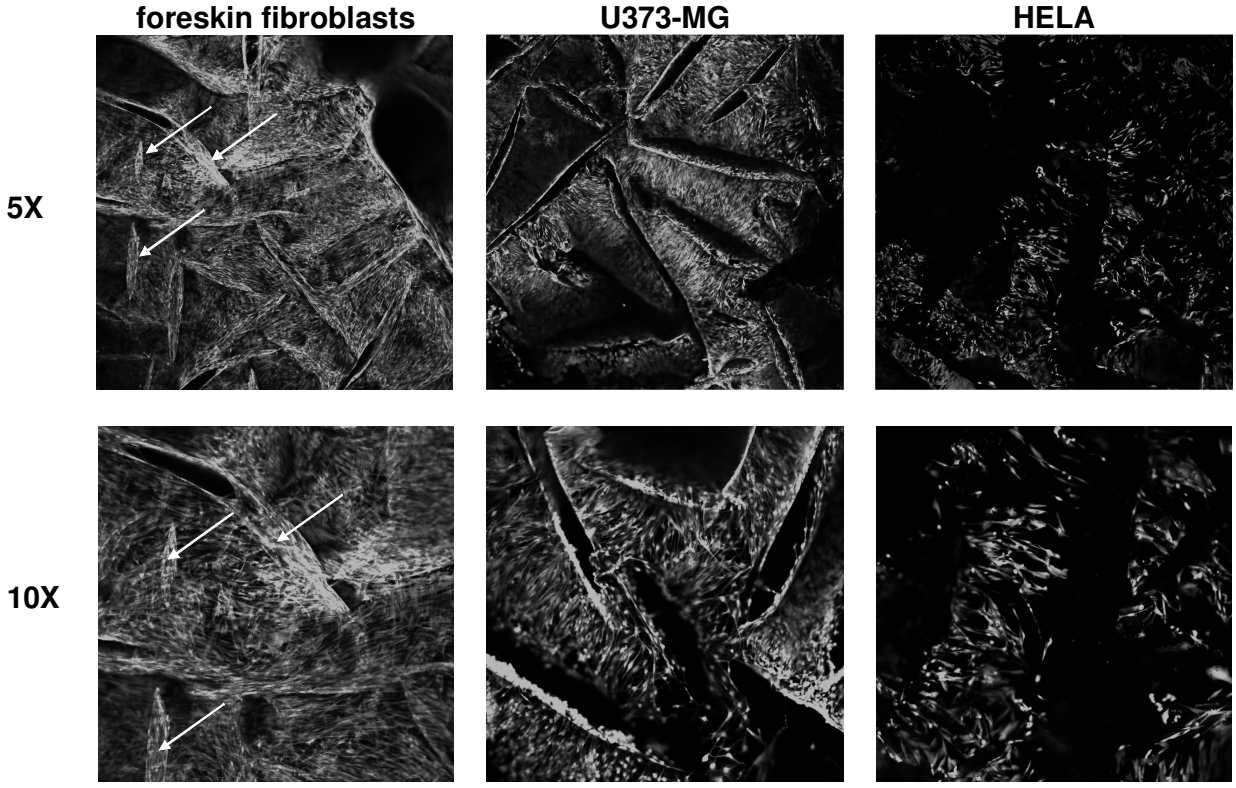

Figure 8-8: Visualisation of foreskin fibroblasts, U373-MG and HELA on type $GIII_b$ hydrogels, 4 weeks after cell seeding. Cells were stained with calcein-AM (1 µg/ml) and visualised using confocal microscopy.

3.3 Cell survival and organisation on/within type GI_b hydrogels

Since it is well known that both differences in surface chemistry and surface topography affect the interaction with cells[55], we were interested in investigating to what extent differences in pore size and pore geometry within gelatin scaffolds with the same surface chemistry, would affect the cell interaction. Type $GIII_b$ and type GI_b gelatin hydrogels were both developed starting from type B gel-MOD. Variation of the parameters used for cryogenic treatment lead to variations in pore geometry and pore size between the two scaffold types without altering the scaffold chemical composition (figure 8-1 and table 8-2).

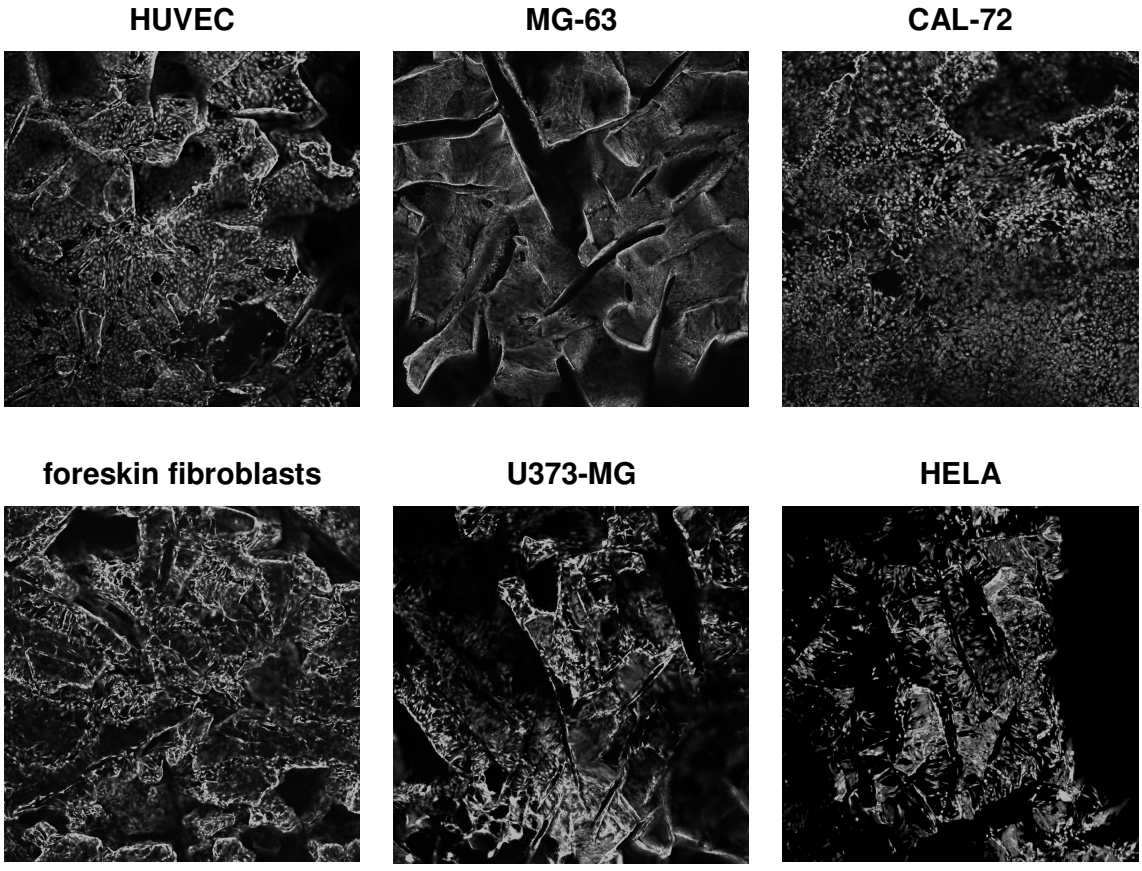

Figure 8-9: Cell visualisation (5X magnification) on type GI_b hydrogels, 4 weeks after cell seeding. Cells were stained with calcein-AM (1 µg/ml) and visualised using confocal microscopy.

The same panel of cells as described above was also seeded on gelatin hydrogels with spherical pores (135 µm in diameter, type GI_b hydrogels). The results for the

different cell types after 4 weeks incubation are summarised in figure 8-9. It was concluded that type GI_b scaffolds possessed similar properties compared to type $GIII_b$ hydrogels in terms of cell attachment, spreading and proliferation on the material.

After cell seeding, the complete hydrogel surface was covered with an increasing incubation time. It should be noted that CAL-72 osteoblasts did not show the very bright and sharp calcein-AM staining as observed for all other cell types. At present these phenomena are further being investigated, but our preliminary data indicate that mineralisation occurs at four weeks post-seeding. Namely, calcein was added to the medium, followed by measuring possible fluorescence related to calcification in the hydrogel using confocal microscopy. The results, shown in figure 8-10, clearly indicate regions were nodules can be observed. The mineralisation process might have an effect on the calcein-AM staining of cells embedded in the hydrogel.

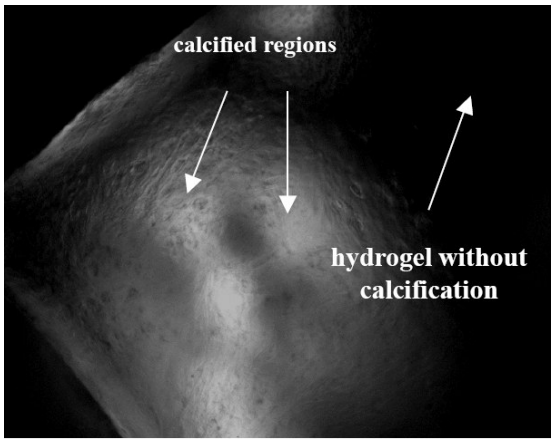

Figure 8-10: Calcified regions in type $GIII_b$ hydrogels are visualized using confocal microscopy after 4 weeks of cell seeding.

The comparative data obtained for both types of hydrogels suggested that the pore geometry and pore size of the matrix did not affect the adhesion, spreading and proliferation of cells, at least in the pore size and geometry range investigated in the present work. This could be concluded since the same type of gelatin (gel-MOD, type B) was used for the production of both scaffold types. The good cell-interactive properties of both types of porous gelatin hydrogels were not unexpected, since type B gelatin was obtained by alkaline denaturation of collagen, one of the components of the extra-cellular matrix. Chemical modification of gelatin, by derivatisation of the ε-lysine amines with methacrylamide functions and subsequent crosslinking into a 3D

network, did not affect (or at least not to a great extent) the cell-interactive properties of the material. In addition, both types of gelatin hydrogels developed, were highly porous. Preliminary results indicate that this property favours cell ingrowth and cell migration throughout the scaffold.

4 Cell differentiation

4.1 Introduction

Differentiation is a continuously regulated process and interactions between the cell and its environment play a major role in maintaining stable expression of differentiation-specific genes. An important component of the cellular environment is the extracellular matrix (ECM). Cells may be completely surrounded by ECM, as is the case for chondrocytes, or may contact the ECM only at one surface, as exemplified by epithelial and endothelial cells.[56]

Besides the interaction between endothelial cells and extracellular matrix molecules to enable cell adhesion and proliferation, the integrity of the endothelial layer is also strongly dependent on the junctions established between adjacent endothelial cells.[57] Such cell-cell adhesion is also crucial for vessels to sprout and the elongation process is mediated by a distinct series of cell surface receptors that includes PECAM-1 and VE-cadherin.[58]

Platelet endothelial cell adhesion molecule-1 (PECAM-1) is a 130-kD member of the immunoglobulin (Ig) superfamily that is expressed on the surface of circulating platelets, monocytes, neutrophils and selected T cell subsets. It is also a major constituent of the endothelial cell intercellular junction, where up to 10^6 PECAM-1 molecules are concentrated. With a few minor exceptions, PECAM-1 is not present on fibroblasts, epithelium, muscle or other nonvascular cells.[59]

PECAM-1 is a key participant in the adhesion cascade leading to extravasation of leukocytes during the inflammatory process.[59] It also establishes homophilic binding between neighboring endothelial cells and interacts with the underlying cytoskeleton.

Another important aspect is that the F-actin assembly is regulated at the cell periphery in association with changes in cell shape and spreading.[10]

The recruitment of leukocytes from the blood into the peripheral tissues in inflammation is mediated through the concerted action of different leukocyte-endothelium cell-adhesion molecules in response to various stimulatory factors (e.g. lipopolysaccharide). E-selectin, which is absent in resting endothelium, is involved on endothelial cells. Upon release of cytokines, a proinflammatory phenotype is induced in the endothelium in which a wide variety of genes, including those encoding for E-selectin, are transcribed. Selectins are thought to be responsible for the 'rolling' of leukocytes along the blood vessel wall, caused by transient and reversible interactions. The leukocyte is then guided to the site of infection by a gradient of chemoattractants. Later on, the expression levels of the different adhesion molecules decline to their original values.[60, 61]

In the present work, possible material related effects on the phenotype of seeded cells were evaluated by immunofluorescent analysis. The gene expression profile of hydrogel seeded endothelial cells for two endothelial cell selective markers (PECAM-1 and E-selectin) was compared with that of tissue culture plastic seeded cells.

4.2 Expression of endothelial cell selective markers

We investigated to what extent endothelial cells preserved their normal gene expression profile after seeding on the hydrogels. Unless intended (e.g. application of stem cells), cells seeded on a biomaterial should preserve their normal gene expression profile. For these studies, HUVEC were seeded on type $GIII_b$ and type GI_b hydrogels. At different time points, cells were fixed in MeOH/EtOH and incubated with anti-PECAM-1 or anti-E-selectin. Intra-cellular or inter-cellular localisation of both markers was studied by confocal microscopy after incubation of the hydrogels in an Alexa Fluor labelled secondary IgG antibody. It should be noted that preliminary experiments in which paraformaldehyde (4%) was used as fixation agent, were not successful. This can be ascribed to the reaction of the residual gelatin amine

functions with paraformaldehyde, in this way preventing successful crosslinking of the cellular proteins.

In a first series of experiments, HUVEC seeded on the hydrogels were screened for the expression of PECAM-1. This protein is a transmembrane cell adhesion molecule and is a major component of the endothelial cell intercellular junctions. For endothelial cells, close cell-cell contacts are a requirement since these contacts control the permeability of the blood vessel wall forming a barrier for solutes, macromolecules and leukocytes.
As control, TCP seeded HUVEC were evaluated for their PECAM-1 expression. From the results in figure 8-11, it could be concluded that PECAM-1 was mainly localised at intercellular junctions.

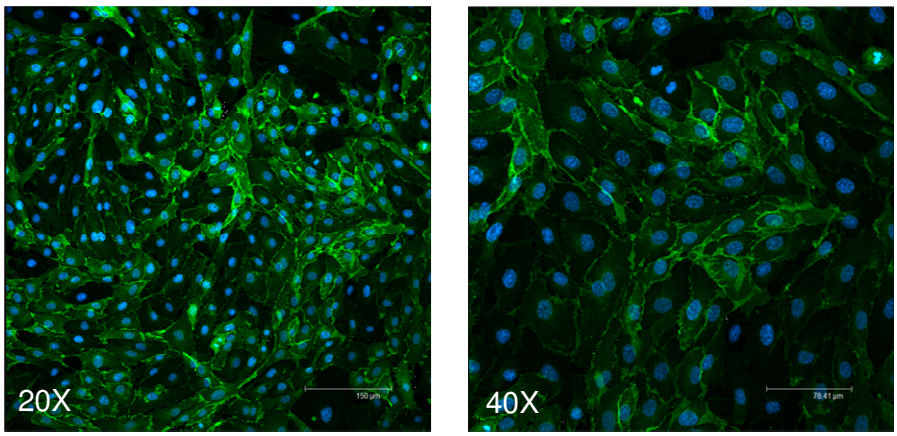

Figure 8-11: Visualisation of tissue culture plastic (TCP) seeded HUVEC, showing PECAM-1 expression. The TCP was pre-coated with gelatin. Cells were stained with DAPI and visualised using confocal microscopy.

The expression profiles observed for both types of scaffolds (figure 8-12), corresponded very well with the control samples (figure 8-11). One week after cell seeding, PECAM-1 was expressed and mainly localised at intercellular junctions.
It should be mentioned that the hydrogels studied possess a complex 3D (i.e. not flat) geometry. The number of cells shown in a picture represent the cells located in one focal plane. This number was sometimes lower than the actual number of cells present in this area, due to the fact that the scaffolds were not flat.
The data for the hydrogels confirmed those obtained during the cell attachment studies, as described in the previous paragraph (§ 2), revealing several areas of

confluent cells in which close cell-cell contacts were formed. At longer incubation times (up to 4 weeks), the PECAM-1 expression profile remained unaffected and similar to TCP seeded HUVEC.

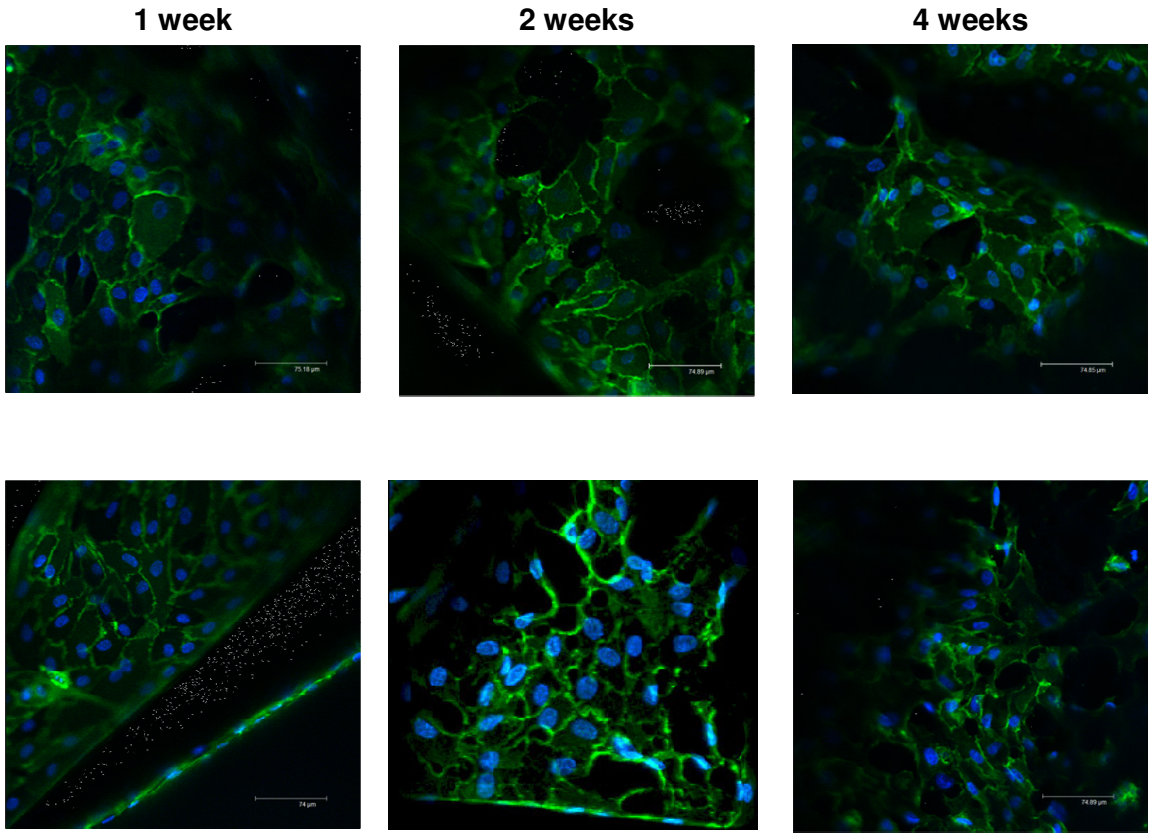

Figure 8-12: Visualisation of PECAM-1 on type $GIII_b$ hydrogels (top row) and type GI_b hydrogels (bottom row) (magnification 40X).

Although very promising, these results were somewhat surprising. Firstly, despite the very large differences in pore size and pore geometry between type $GIII_b$ and II scaffolds, HUVEC formed confluent cell layers with close cell-cell contacts and expressed PECAM-1. It was anticipated that the differences in 3D geometry would affect endothelial cell arrangement and potentially also the expression of cell adhesion molecules.

Secondly, up to three days after cell seeding HUVEC seeded on the biomaterials showed a rounded morphology. It is therefore remarkable that one week after cell seeding, confluent cell layers are formed with PECAM-1 as one of the constituents of the intercellular junctions. These results indicated that the chemical composition of

the hydrogels, which is the same for type $GIII_b$ and II, was more important than the geometry and the size of the induced pores.

It should be noted that the HUVEC 'interconnectivity' is distorted due to the fixation procedure in MeOH/EtOH causing a dehydration of the cell layers.

A second endothelial cell selective marker that was included in the present work, was E-selectin. E-selectin is a glycoprotein that is expressed in activated (stimulated) endothelial cells and binds various immune response related cells. E-selectin is a pro-inflammatory marker which is not expressed in unstimulated cells. As positive control, TCP and hydrogel seeded HUVEC which were stimulated using lipopolysaccharide (LPS, a component of the bacterial wall). The results indicated that stimulated cells, seeded on TCP or the hydrogels, exhibited high levels of E-selectin expression (figures 8-13 and 8-14). Nearly 100% of HUVEC grown on TCP and gelatin expressed the pro-inflammatory marker. This induction effect was observed for both types of gelatin scaffolds. In unstimulated cells, typically 2% of the cells expressed E-selectin.

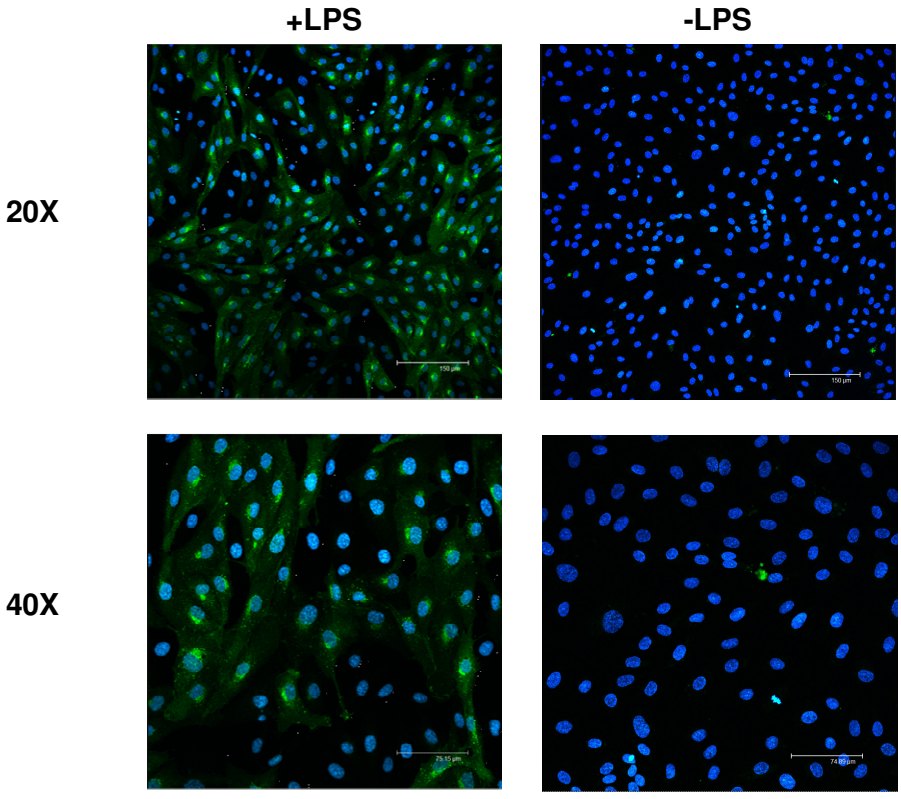

Figure 8-13: Visualisation of tissue culture plastic (TCP) seeded HUVEC, showing E-selectin expression when stimulated with LPS. The TCP was pre-coated with gelatin. Cells were stained with DAPI and visualised using confocal microscopy.

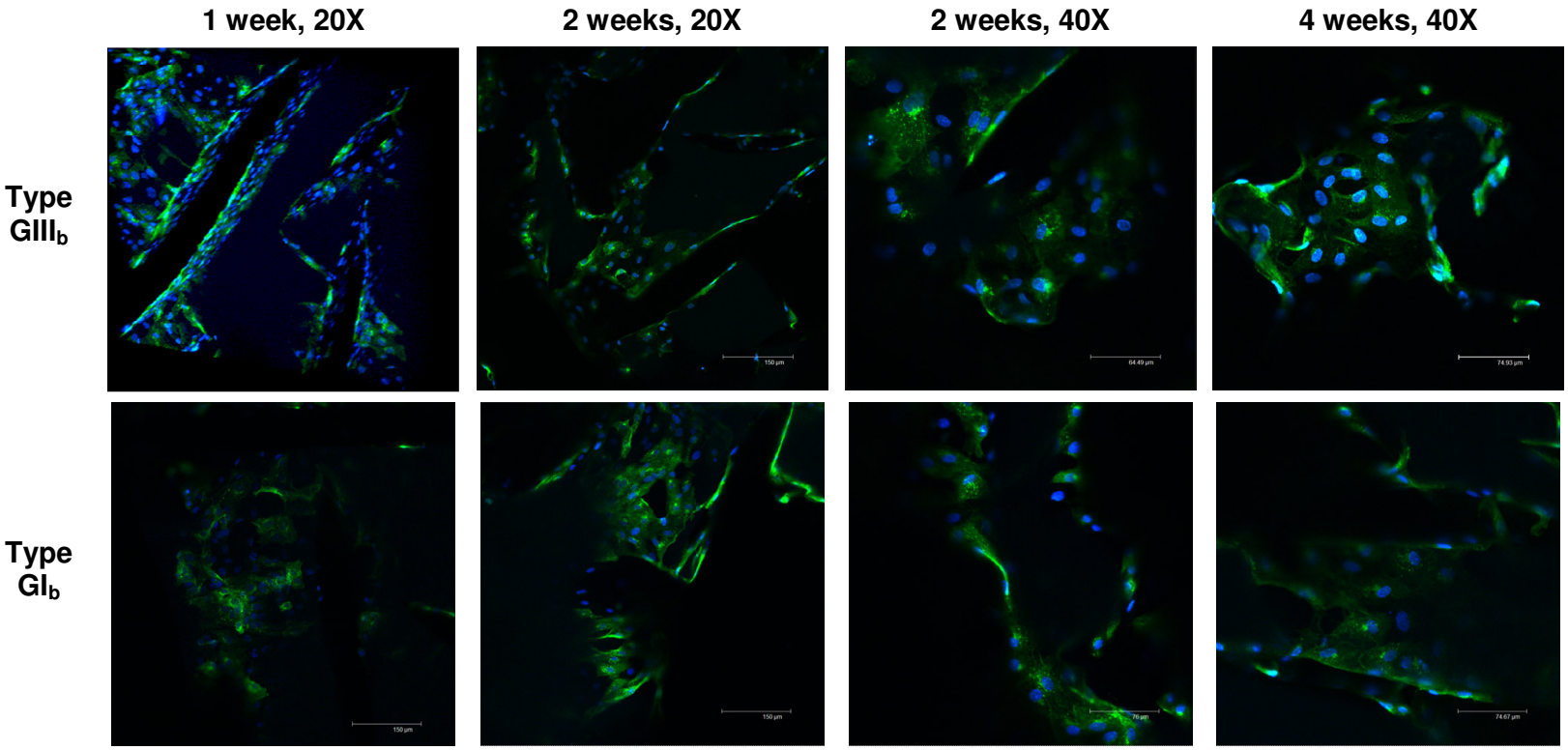

Figure 8-14: Visualisation of E-selectin expression on type GIII$_b$ hydrogels (top row) and type GI$_b$ hydrogels (bottom row).

5 Conclusion

Two types of porous gelatin hydrogels were screened for their interaction with a panel of human cells. We have shown that both types of gelatin scaffolds, differing in their pore geometry and pore size, supported the attachment and growth of human cells over longer time periods.

Summarising the gene expression results, it can be concluded that HUVEC seeded on the different biomaterials preserve a normal phenotype as compared to TCP seeded cells. HUVEC also maintain their functional properties as exhibited by the strong induction of E-selectin expression in the presence of LPS.

Finally, blood compatibility studies were performed on both gelatin- and CS-based scaffolds. Haemolysis indices of all materials developed remained within acceptable limits (<5).

References

1. Cortesini, R., Stem cells, tissue engineering and organogenesis in transplantation. *Transplant Immunology* **2005,** 15, (2), 81-89.
2. Stocum, D. L., Regenerative biology and engineering: strategies for tissue restoration. *Wound Repair and Regeneration* **1998,** 6, (4), 276-290.
3. Tabata, Y., Tissue regeneration based on tissue engineering technology. *Congenital Anomalies* **2004,** 44, (3), 111-124.
4. Germain, L.; Goulet, F.; Moulin, V.; Berthod, F.; Auger, F. A., Engineering Human Tissues for in Vivo Applications. *Annals of the New York Academy of Sciences* **2002,** 961, (1), 268-270.
5. Godbey, W. T.; Atala, A., In Vitro Systems for Tissue Engineering. *Annals of the New York Academy of Sciences* **2002,** 961, (1), 10-26.
6. Hong, L.; Peptan, I.; Clark, P.; Mao, J. J., Ex vivo adipose tissue engineering by human marrow stromal cell seeded gelatin sponge. *Annals of Biomedical Engineering* **2005,** 33, (4), 511-517.
7. Ma, Z. W.; He, W.; Yong, T.; Ramakrishna, S., Grafting of gelatin on electrospun poly(caprolactone) nanofibers to improve endothelial cell spreading and proliferation and to control cell orientation. *Tissue Engineering* **2005,** 11, (7-8), 1149-1158.
8. Ito, Y.; Hasuda, H.; Terai, H.; Kitajima, T., Culture of human umbilical vein endothelial cells on immobilized vascular endothelial growth factor. *Journal of Biomedical Materials Research Part A* **2005,** 74A, (4), 659-665.
9. Mironov, V.; Kasyanov, V.; Shu, X. Z.; Eisenberg, C.; Eisenberg, L.; Gonda, S.; Trusk, T.; Markwald, R. R.; Prestwich, G. D., Fabrication of tubular tissue constructs by centrifugal casting of cells suspended in an in situ crosslinkable hyaluronan-gelatin hydrogel. *Biomaterials* **2005,** 26, (36), 7628-7635.
10. Huang, Y.; Onyeri, S.; Siewe, M.; Moshfeghian, A.; Madihally, S. V., In vitro characterization of chitosan-gelatin scaffolds for tissue engineering. *Biomaterials* **2005,** 26, (36), 7616-7627.
11. Ma, Z. W.; Kotaki, M.; Yong, T.; He, W.; Ramakrishna, S., Surface engineering of electrospun polyethylene terephthalate (PET) nanofibers towards development of a new material for blood vessel engineering. *Biomaterials* **2005,** 26, (15), 2527-2536.
12. Unger, R. E.; Huang, Q.; Peters, K.; Protzer, D.; Paul, D.; Kirkpatrick, C. J., Growth of human cells on polyethersulfone (PES) hollow fiber membranes. *Biomaterials* **2005,** 26, (14), 1877-1884.
13. Liu, X. H.; Won, Y. J.; Ma, P. X., Surface modification of interconnected porous scaffolds. *Journal of Biomedical Materials Research Part A* **2005,** 74A, (1), 84-91.
14. Zhao, F.; Grayson, W. L.; Ma, T.; Bunnell, B.; Lu, W. W., Effects of hydroxyapatite in 3-D chitosan-gelatin polymer network on human mesenchymal stem cell construct development. *Biomaterials* **2006,** 27, (9), 1859-1867.

15. Yang, S. H.; Hsu, C. K.; Wang, K. C.; Hou, S. M.; Lin, F. H., Tricalcium phosphate and glutaraidehyde crosslinked gelatin incorporating bone morphogenetic protein - A viable scaffold for bone tissue engineering. *Journal of Biomedical Materials Research Part B-Applied Biomaterials* **2005,** 74B, (1), 468-475.
16. Kim, H. W.; Kim, H. E.; Salih, V., Stimulation of osteoblast responses to biomimetic nanocomposites of gelatin-hydroxyapatite for tissue engineering scaffolds. *Biomaterials* **2005,** 26, (25), 5221-5230.
17. Kim, H. W.; Knowles, J. C.; Kim, H. E., Hydroxyapatite and gelatin composite foams processed via novel freeze-drying and crosslinking for use as temporary hard tissue scaffolds. *Journal of Biomedical Materials Research Part A* **2005,** 72A, (2), 136-145.
18. Takahashi, Y.; Yamamoto, M.; Tabata, Y., Enhanced osteoinduction by controlled release of bone morphogenetic protein-2 from biodegradable sponge composed of gelatin and beta-tricalcium phosphate. *Biomaterials* **2005,** 26, (23), 4856-4865.
19. Takahashi, Y.; Yamamoto, M.; Tabata, Y., Osteogenic differentiation of mesenchymal stem cells in biodegradable sponges composed of gelatin and beta-tricalcium phosphate. *Biomaterials* **2005,** 26, (17), 3587-3596.
20. Zhang, Y. Z.; Ouyang, H. W.; Lim, C. T.; Ramakrishna, S.; Huang, Z. M., Electrospinning of gelatin fibers and gelatin/PCL composite fibrous scaffolds. *Journal of Biomedical Materials Research Part B-Applied Biomaterials* **2005,** 72B, (1), 156-165.
21. Chang, C. H.; Kuo, T. F.; Lin, C. C.; Chou, C. H.; Chen, K. H.; Lin, F. H.; Liu, H. C., Tissue engineering-based cartilage repair with allogenous chondrocytes and gelatin-chondroitin-hyaluronan tri-copolymer scaffold: A porcine model assessed at 18, 24, and 36 weeks. *Biomaterials* **2006,** 27, (9), 1876-1888.
22. Guo, T.; Zhao, J. N.; Chang, J. B.; Ding, Z.; Hong, H.; Chen, J. N.; Zhang, J. F., Porous chitosan-gelatin scaffold containing plasmid DNA encoding transforming growth factor-beta 1 for chondrocytes proliferation. *Biomaterials* **2006,** 27, (7), 1095-1103.
23. Park, H.; Temenoff, J. S.; Holland, T. A.; Tabata, Y.; Mikos, A. G., Delivery of TGF-beta 1 and chondrocytes via injectable, biodegradable hydrogels for cartilage tissue engineering applications. *Biomaterials* **2005,** 26, (34), 7095-7103.
24. Holland, T. A.; Bodde, E. W. H.; Baggett, L. S.; Tabata, Y.; Mikos, A. G.; Jansen, J. A., Osteochondral repair in the rabbit model utilizing bilayered, degradable oligo(poly(ethylene glycol) fumarate) hydrogel scaffolds. *Journal of Biomedical Materials Research Part A* **2005,** 75A, (1), 156-167.
25. Holland, T. A.; Tabata, Y.; Mikos, A. G., Dual growth factor delivery from degradable oligo(poly(ethylene glycol) fumarate) hydrogel scaffolds for cartilage tissue engineering. *Journal of Controlled Release* **2005,** 101, (1-3), 111-125.
26. Ito, A.; Mase, A.; Takizawa, Y.; Shinkai, M.; Honda, H.; Hata, K.; Ueda, M.; Kobayashi, T., Transglutaminase-mediated gelatin matrices incorporating cell adhesion factors as a biomaterial for tissue engineering. *Journal of Bioscience and Bioengineering* **2003,** 95, (2), 196-199.

27. Broderick, E. P.; O'Halloran, D. M.; Rochev, Y. A.; Griffin, M.; Collighan, R. J.; Pandit, A. S., Enzymatic stabilization of gelatin-based scaffolds. *Journal of Biomedical Materials Research Part B-Applied Biomaterials* **2005,** 72B, (1), 37-42.
28. Kim, S.; Nimni, M. E.; Yang, Z.; Han, B., Chitosan/gelatin-based films crosslinked by proanthocyanidin. *Journal of Biomedical Materials Research Part B-Applied Biomaterials* **2005,** 75B, (2), 442-450.
29. Zhu, H. G.; Ji, J.; Shen, J. C., Osteoblast growth promotion by protein electrostatic self-assembly on biodegradable poly(lactide). *Journal of Biomaterials Science-Polymer Edition* **2005,** 16, (6), 761-774.
30. Li, M. Y.; Mondrinos, M. J.; Gandhi, M. R.; Ko, F. K.; Weiss, A. S.; Lelkes, P. I., Electrospun protein fibers as matrices for tissue engineering. *Biomaterials* **2005,** 26, (30), 5999-6008.
31. Wang, Y. W.; Wu, Q.; Chen, G. Q., Gelatin blending improves the performance of poly(3-hydroxybutyrate-co-3-hydroxyhexanoate)films for biomedical application. *Biomacromolecules* **2005,** 6, (2), 566-571.
32. Cascone, M. G.; Lazzeri, L.; Sparvoli, E.; Scatena, M.; Serino, L. P.; Danti, S., Morphological evaluation of bioartificial hydrogels as potential tissue engineering scaffolds. *Journal of Materials Science-Materials in Medicine* **2004,** 15, (12), 1309-1313.
33. Shoji, O.; Yasuhide, N.; Takehisa, M., In vivo evaluation of poly(N-isopropylacrylamide) (PNIPAM)-grafted gelatin as an in situ-formable scaffold. *Journal of Artificial Organs* **2004,** 7, (4), 181-186.
34. Li, M. Y.; Mills, D. K.; Cui, T. H.; McShane, M. J., Cellular response to gelatin- and fibronectin-coated multilayer polyelectrolyte nanofilms. *Ieee Transactions on Nanobioscience* **2005,** 4, (2), 170-179.
35. Alperin, C.; Zandstra, P. W.; Woodhouse, K. A., Polyurethane films seeded with embryonic stem cell-derived cardiomyocytes for use in cardiac tissue engineering applications. *Biomaterials* **2005,** 26, (35), 7377-7386.
36. Yang, S.-H.; Chen, P.-Q.; Chen, Y.-F.; Lin, F.-H., An In-vitro Study on Regeneration of Human Nucleus Pulposus by Using Gelatin/Chondroitin-6-Sulfate/Hyaluronan Tri-copolymer Scaffold. *Artificial Organs* **2005,** 29, (10), 806-814.
37. Brown, R. Q.; Mount, A.; Burg, K. J. L., Evaluation of polymer scaffolds to be used in a composite injectable system for intervertebral disc tissue engineering. *Journal of Biomedical Materials Research Part A* **2005,** 74A, (1), 32-39.
38. Shu-Hua Yang, P.-Q. C. Y.-F. C. F.-H. L., Gelatin/chondroitin-6-sulfate copolymer scaffold for culturing human nucleus pulposus cells <I>in vitro</I> with production of extracellular matrix. *Journal of Biomedical Materials Research Part B: Applied Biomaterials* **2005,** 74B, (1), 488-494.
39. Balakrishnan, B.; Jayakrishnan, A., Self-cross-linking biopolymers as injectable in situ forming biodegradable scaffolds. *Biomaterials* **2005,** 26, (18), 3941-3951.

40. Williamson, M. R.; Adams, E. F.; Coombes, A. G. A., Gravity spun polycaprolactone fibres for soft tissue engineering: Interaction with fibroblasts and myoblasts in cell culture. *Biomaterials* **2006,** 27, (7), 1019-1026.
41. Eduardo, G.; aacute; mez; Yoshinobu, G.; Kengo, N.; Toru, I.; Tomio, S.; Takehisa, M., Photofabricated Gelatin-Based Nerve Conduits: Nerve Tissue Regeneration Potentials. *Cell Transplantation* **2004,** 13, 549-564.
42. Bloch, K.; Lozinsky, V. I.; Galaev, I. Y.; Yavriyanz, K.; Vorobeychik, M.; Azarov, D.; Damshkaln, L. G.; Mattiasson, B.; Vardi, P., Functional activity of insulinoma cells (INS-1E) and pancreatic islets cultured in agarose cryogel sponges. *Journal of Biomedical Materials Research Part A* **2005,** 75A, (4), 802-809.
43. Witte, R. P.; Kao, W. Y. J., Keratinocyte-fibroblast paracrine interaction: the effects of substrate and culture condition. *Biomaterials* **2005,** 26, (17), 3673-3682.
44. Dekie, L.; Toncheva, V.; Dubruel, P.; Schacht, E. H.; Barrett, L.; Seymour, L. W., Poly--glutamic acid derivatives as vectors for gene therapy. *Journal of Controlled Release* **2000,** 65, (1-2), 187-202.
45. Ferreira, P.; Pereira, R.; Coelho, J. F. J.; Silva, A. F. M.; Gil, M. H., Modification of the biopolymer castor oil with free isocyanate groups to be applied as bioadhesive. *International Journal of Biological Macromolecules* **2007,** 40, (2), 144-152.
46. VanVlierberghe, S.; Cnudde, V.; Dubruel, P.; Masschaele, B.; Cosijns, A.; DePaepe, I.; Jacobs, P. J. S.; VanHoorebeke, L.; Remon, J. P.; Schacht, E., Porous Gelatin Hydrogels: 1. Cryogenic Formation and Structure Analysis. *Biomacromolecules* **2007,** 8, (2), 331-337.
47. Robinson, J. P., Principles of confocal microscopy. In *Methods in cell biology*, Academic Press: 2001; pp 89-106.
48. Product information sheet (Molecular Probes), Acetoxy (AM) and acetate esters.
49. Dietmar, V., Molecular mechanisms that control endothelial cell contacts. *The Journal of Pathology* **2000,** 190, (3), 281-291.
50. Salacinski, H. J.; Tai, N. R.; Punshon, G.; Giudiceandrea, A.; Hamilton, G.; Seifalian, A. M., Optimal endothelialisation of a new compliant poly(carbonate-urea)urethane vascular graft with effect of physiological shear stress. *European Journal of Vascular and Endovascular Surgery* **2000,** 20, (4), 342-352.
51. Sieminski, A. L.; Hebbel, R. P.; Gooch, K. J., The relative magnitudes of endothelial force generation and matrix stiffness modulate capillary morphogenesis in vitro. *Experimental Cell Research* **2004,** 297, (2), 574-584.
52. Gao, C. Y.; Hu, X. H.; Hong, Y.; Guan, J. J.; Shen, J. C., Photografting of poly(hydroxylethyl acrylate) onto porous polyurethane scaffolds to improve their endothelial cell compatibility. *Journal of Biomaterials Science-Polymer Edition* **2003,** 14, (9), 937-950.
53. Chung, T. W.; Liu, D. Z.; Wang, S. Y.; Wang, S. S., Enhancement of the growth of human endothelial cells by surface roughness at nanometer scale. *Biomaterials* **2003,** 24, (25), 4655-4661.

54. Houglum, P., In *Therapeutic Exercise for Musculoskeletal Injuries, Human Kinetics*, second ed.; 2005.
55. Curtis, A.; Wilkinson, C., Topographical control of cells. *Biomaterials* **1997,** 18, (24), 1573-1583.
56. Adams, J. C.; Watt, F. M., Regulation of Development and Differentiation by the Extracellular-Matrix. *Development* **1993,** 117, (4), 1183-1198.
57. Liekens, S.; De Clercq, E.; Neyts, J., Angiogenesis: regulators and clinical applications. *Biochemical Pharmacology* **2001,** 61, (3), 253-270.
58. Santos, M. I.; Fuchs, S.; Gomes, M. E.; Unger, R. E.; Reis, R. L.; Kirkpatrick, C. J., Response of micro- and macrovascular endothelial cells to starch-based fiber meshes for bone tissue engineering. *Biomaterials* **2007,** 28, (2), 240-248.
59. Newman, P. J., The biology of PECAM-1. *Journal of Clinical Investigation* **1997,** 99, (1), 3-7.
60. Vandermeeren, M.; Janssens, S.; Borgers, M.; Geysen, J., Dimethylfumarate is an inhibitor of cytokine-induced E-selectin, VCAM-1, and ICAM-1 expression in human endothelial cells. *Biochemical and Biophysical Research Communications* **1997,** 234, (1), 19-23.
61. Yoshida, M.; Chien, L. J.; Yasukochi, Y.; Numano, F., Differentiation-induced transmigration of HL60 cells across activated HUVEC monolayer involves E-selectin-dependent mechanism. In *Atherosclerosis V: the Fifth Saratoga Conference*, 2000; Vol. 902, pp 307-310.

General Conclusions

The objective of the present work was to develop bio-interactive hydrogels functioning as cell carriers with the aim to induce cell migration, adhesion and proliferation. In order to fulfil these requirements, the materials developed should meet some criteria. First, highly porous materials are required to support diffusion of oxygen and nutrients towards the cells and drainage of waste products from the matrix. Second, pore interconnectivity is crucial to enable cell migration and if required angiogenesis. Finally, the interconnecting porous biomaterials should be biocompatible and, depending on the application, also biodegradable.

In the present work, gelatin was selected as a starting material since its biocompatibility and biodegradability were already demonstrated in a previous research thesis by Dr. A. Van Den Bulcke. Since gelatin is characterized by a sol-gel transition temperature of about 30°C, crosslinkable side groups (i.e. methacrylamides and thiols) were incorporated to enable chemical crosslinking. In addition to gelatin, chondroitin sulphate and hyaluronic acid were also modified with double bonds using methacrylic anhydride, as these glycosaminoglycans are important components of the extracellular matrix. The hydrogel precursors synthesized were characterized in depth using various techniques including ^{1}H-NMR spectroscopy, size exclusion chromatography and ATR-IR spectroscopy. Using the synthesis route elaborated, a series of hydrogel precursors possessing various modification degrees was prepared.

In a subsequent part of the present work, hydrogel films composed of the polymer precursors synthesized and combinations thereof were prepared and characterized using rheology, texturometry and water uptake experiments. The mechanical properties of the hydrogels developed were affected by various parameters including the storage time, the polymer concentration and the modification degree.
In addition to hydrogel formation at room temperature, gelatin cryogels were prepared by applying a cryogenic treatment. The results indicated that the implementation of successive freeze-thaw cycles induces a decrease of the critical gelation concentration.

In order for the hydrogels to be applied in the field of tissue engineering, porosity was induced using a cryogenic unit, followed by lyophilization of the frozen material. Some preliminary data on this topic were already described by Dr. I. De Paepe in her PhD thesis. The cryogenic unit developed, enabled us to vary different parameters during the cryogenic treatment (i.e. cooling rate, temperature gradient and final freezing temperature). In addition, also the effect of the gelatin concentration on the material properties was studied using micro-computed tomography, helium-pycnometry, scanning electron microscopy and optical microscopy. The results indicated that the pore size, the pore geometry and the porosity of the scaffolds developed could be easily finetuned by varying the (cryo-)parameters applied. The results obtained in the present work will be a valuable tool for research on porous scaffolds, including pore creation techniques as well as non-destructive structure analysis techniques.

In addition to radical polymerisation using a UV-active photo-initiator, alternative crosslink procedures including ebeam and redox-initiating systems were evaluated to enable chemical crosslinking of the freeze-dried scaffolds developed. The results indicated that sufficient segmental mobility was essential to obtain efficient crosslinking.

Since the final objective of the present work was to develop a widely applicable tissue engineering device, the incorporation of cell-interactive proteins including fibronectin in gelatin-based hydrogels was evaluated. Quartz crystal microbalance (QCM), surface plasmon resonance (SPR) and radiolabelling experiments indicated that fibronectin shows a high affinity for gelatin. In addition, the amount of incorporated fibronectin can be easily finetuned by varying the fibronectin concentration applied. Depending on the gelatin type applied (type A versus type B), hydrophobic or electrostatic interactions or a combination thereof existed.
In view of *in vitro* biocompatibility studies in the presence of serum-enriched medium, the affinity of various serum compounds including γ-globulin, transferrin and albumin for gelatin was also evaluated. QCM and SPR results indicated that gelatin interacts with various serum proteins potentially affecting the subsequent cell adhesion and spreading on the gelatin scaffolds developed.

We also observed a limited gelatin affinity for different glycosaminoglycans including chondroitin sulphate and hyaluronic acid.

A final important part of the present work was the evaluation of the various scaffolds prepared to function as cell carriers. Two types of porous gelatin hydrogels were screened for their interaction with a panel of human cells. The results indicated that both scaffold types, differing in their pore geometry and pore size, supported the attachment and growth of human cells over longer time periods. In addition, the gene expression profile of endothelial cells was preserved, which is a first indication that no cell differentiation occurred.

The hydrogels developed are a very promising class of biomaterials. In addition, the procedure elaborated in the present work to induce pores possessing specific pore sizes and pore geometries can be extended to other (bio)polymers to be applied as tissue engineering devices.

Chapter IX:

Experimental Part

1 Materials

- Gelatin (type B), isolated from bovine skin by an alkaline process, was kindly supplied by Rousselot, Ghent, Belgium. Gelatin samples with an approximate iso-electric point of 5, a Bloom strength of 257 and a viscosity (6.67%, 60°C) of 4.88 mPa.s were used.
- Gelatin (type A), pharmaceutical grade, isolated from porcine skin, was obtained from Rousselot, Ghent, Belgium. Gelatin samples with an approximate iso-electric point of 8.8, a Bloom strength of 202 and a viscosity (6.67%, 60°C) of 2.97 mPa.s were used.
- Methacrylic anhydride (MAA), Aldrich (Bornem, Belgium).
- Dialysis membranes Spectra/Por® 4 (MWCO 12,000-14,000 Da), Polylab (Antwerp, Belgium).
- Dialysis membranes Spectra/Por® 3 (MWCO 3,500 Da) were obtained from Polylab (Antwerp, Belgium).
- Pullulan standards (Shodex standards P-50, P-100, P-200 and P-400), S.D.K. (Showa Denko K.K.).
- 1-[4-(2-Hydroxyethoxy)-phenyl]-2-hydroxy-2-methyl-1-propane-1-one (Irgacure® 2959) was a kind gift from Ciba Speciality Chemicals N.V. (Groot-Bijgaarden, Belgium).
- Sodium phosphate (dibasic, anhydrous, p.a.), Acros (Geel, Belgium).
- Potassium hydrogen phosphate, Acros (Geel, Belgium).
- Sodium hydroxide, Merck (Darmstadt, Germany).
- Titrisol buffer pH 10, boric acid/potassium chloride-sodium hydroxide solution, tube for 500 ml buffer solution, Merck (Darmstadt, Germany).

- N-butylamine, Acros (Geel, Belgium).
- Ellman's reagent (5,5'-dithio-bis-(2-nitrobenzoic acid)), Pierce, Perbio Science (Erembodegem, Belgium).
- 2-Iminothiolane hydrochloride (Traut's reagent), Aldrich (Bornem, Belgium).
- DL-N-Acetylhomocysteine thiolactone, Acros (Geel, Belgium).
- 1,2-Phthalic dicarboxaldehyde, Acros (Geel, Belgium).
- 2-Mercaptoethanol, Merck (Darmstadt, Germany).
- L-Cysteine.HCl.H_2O, Pierce, Perbio Science (Erembodegem, Belgium).
- Hydrogen peroxide, 50 wt% solution in water, Aldrich (Bornem, Belgium).
- Dichloromethylsilane, Aldrich (Bornem, Belgium).
- Chondroitin sulphate C, sodium salt, from shark cartilage, Sigma (Bornem, Belgium).
- Chondroitin sulphate A, sodium salt, from bovine trachea, Sigma (Bornem, Belgium).
- Hyaluronic acid sodium, from human umbilical cord, Sigma (Bornem, Belgium).
- Calcium chloride (dihydrate, 77-80%), Acros (Geel, Belgium).
- Tris(hydroxymethyl)aminomethane (99,9%, ultra pure grade), Acros (Geel, Belgium).
- Sodium azide (99%), Avocado Research Chemicals Ltd. (Karlsruhe, Germany).
- Ethylene diamine tetraacetic acid (tetra sodium salt tetrahydrate), Fluka BioChemica (St. Gallen, Switzerland).
- Ammonium cerium (IV) nitrate (99%), Avocado Research Chemicals Ltd. (Karlsruhe, Germany).
- Vitamin C = Ascorbic acid, Fluka BioChemica (St. Gallen, Switzerland).
- Iron (II) D-gluconate dehydrate (98%), Aldrich (Bornem, Belgium).
- N-(3-Dimethylaminopropyl)-N'-ethylcarbodiimide hydrochloride, Aldrich (Bornem, Belgium).
- N-Hydroxysuccinimide (98%), Acros (Geel, Belgium).
- Collagenase (EC 3.4.24.3) Type IV of *Clostridium histolyticum* with collagen activity 428 U/mg (collagen digestion), Sigma Chemical Co. (St. Louis, MO, VS).
- Fibronectin from bovine plasma (0.1% solution, 1 mg/ml in 0.5 M NaCl, 0.05 M Tris and pH 7.5), Sigma-Aldrich (Bornem, Belgium).

- Polyclonal rabbit anti-human fibronectin solution (5.1 g/l), DakoCytomation (Heverlee, Belgium).
- L-Lactate dehydrogenase, Sigma (Bornem, Belgium).
- γ-Globulins, human: from cohn fraction II, III, Sigma (Bornem, Belgium).
- Albumin, human, ORHA, Behringwerke (Marburg, Germany).
- Transferrin, human, partially iron-saturated, Sigma (Bornem, Belgium).
- Monoclonal anti-chondroitin sulphate, clone CS-56, from mouse ascites fluid, Sigma (Bornem, Belgium).

2 Methods

Freeze-drying

Freeze-drying of the polymer derivatives occurred by means of a Christ freeze-dryer alpha I-5.

Size exclusion chromatography

The molecular weights were determined by means of size exclusion chromatography with a Millipore-Waters 510 pump. The detection occurred with a Waters 410 Differential Refractometer. For all polymers developed, Waters Ultrahydrogel columns 250-500-1000 (300 x 7.8 mm) at 80°C (internal temperature: 50°C) were used. Phosphate buffer (pH 7.4; 0.2 g KH_2PO_4 + 1.15 g Na_2HPO_4 / 1l H_2O) was applied as eluens. A flow rate of 0.75 ml/min was chosen. Calibration occurred by means of pullulan standards (10 mg/ml).

UV-analysis

UV-analysis was performed with an Uvikon XL spectrophotometer (Bio-Tek Instruments, BRS, Drogenbos, Belgium).

Nuclear Magnetic Resonance

^{1}H-NMR-spectra of the gelatin derivatives were recorded at 50°C in deuterated water with a Bruker WH 500 MHz instrument. The chemical shift was expressed in ppm as a function of tetramethylsilane as internal standard.

^{1}H-NMR-spectra of the chondroitin sulphate and the hyaluronic acid derivatives were recorded at room temperature in deuterated water using the same equipment as for the gelatin derivatives.

ATR-FTIR measurements

Attenuated Total Reflection Infrared analysis was performed by means of a Biorad FT-IR spectrometer FTS 575C.

UV-irradiation

An LWUV-lamp model VL-400L (Vilber Lourmat, Marne La Vallée, France), with an intensity of 10 mW/cm^2 and a wavelength range of 250-450 nm, was used for sample curing.

Rheology

The mechanical properties of the hydrogel films were evaluated using a rheometer type Physica MCR-301 (Anton Paar, Sint-Martens-Latem, Belgium).

Texturometry

Texturometrical tests were performed with a Lloyd TA500 Texture Analyser, equipped with a 100 N load cell. Hydrogel films were positioned on a flat bottom plate, having a round opening (Ø 25 mm). In order to perform different tests (e.g. TPA, fracture), a cylindrical probe (Ø 3 mm) was applied.

Optical microscopy

Optical microscopy was performed using an Axiotech 100 Reflected Light Microscope (Carl Zeiss), with reflected-light brightfield for Köhler illumination.

Scanning electron microscopy

The morphology of gold-sputtered samples was examined using the scanning electron micrographs obtained on a Fei Quanta 200F (field emission gun) scanning electron microscope.

Helium-pycnometry

Porosities were studied using a He-pycnometre type Accupyc 1330, Norcross, GA, USA. Each measurement was performed in duplicate.

Micro-computed tomography

A “Skyscan 1072” X-ray micro-tomograph was used. This compact desktop system, consisting of an X-ray shadow microscopic system and a computer with tomographic reconstruction software, generated high-resolution images for small samples (7 mm diameter). During a measurement, both the X-ray source and the detector were fixed while the sample rotates around a stable vertical axis. Samples were scanned at a voltage of 130 kV and a current of 76 µA. Random movement and multiple-frame averaging were used to minimise the Poisson noise in the images. The spot size of the Hamamatsu micro-focus tube limited the spatial resolution of the reconstructed slices to 10 µm in the X, Y and Z directions. During acquisition, X-ray radiographs were recorded at different angles during step-wise rotation between 0° and 180° around the vertical axis.

After reconstruction of the 2D cross-sections, 3D software µCTanalySIS was used in order to segment the images and determine their 3D porosity and pore size distribution. Octopus, a server/client tomography reconstruction package for parallel and cone beam geometry, was also used for analysis.

Dynamic Vapour Sorption

The influence of the hydrogel structure on the degree of water vapour sorption was examined using a Dynamic Vapour Sorption apparatus (DVS-1, Surface Measurement Systems, London, UK). The apparatus consists of a Cahn microbalance placed in a temperature-controlled housing.

Contact angle measurements

Static contact angle measurements were performed using a OCA 20 from Dataphysics (distributed by Benelux Scientific) equipped with a Hamilton syringe (500 µl). For each measurement, 1 µl of double distilled water was placed on the hydrogel surface.

X-ray photo-electron spectroscopy

The chemical composition of the different scaffold surfaces was determined using "FISONS S-PROBE", a dedicated XPS (X-ray photoelectron spectroscopy) instrument designed to give the ultimate in performance, while providing a high sample throughput. The fine focus Al-Ka source with a quartz monochromator, developed by Fisons Instruments Surface Science ensures lower background and higher sensitivity than conventional twin anode sources. All measurements were performed in a vacuum of at least 10-9 Pa. Wide and narrow-scan spectra were acquired at pass energy of 158 and 56 eV respectively. The binding energy was calibrated by the C 1s peak at 284.6 eV. The spot size used was 250 µm on 1mm. Data analysis was performed using S-PROBE software. The measured spectrum was displayed as a plot of the number of electrons (electron counts) versus electron binding energy in a fixed, small energy interval. Peak area and peak height sensitivity factors were used for the quantifications.

Atomic Force Microscopy

AFM-studies were performed with a Nanoscope IIIa Multimode (Digital Instruments, Santa Barbara, California, USA) applying 'tapping mode' in air.

Quartz Crystal Microbalance

Measurements were done using the QCM-D technique (Q-Sense E4, Q-Sense AB, Göteborg, Sweden). The Q-Sense software was used to acquire experimental data. The main feature of this package was the possibility of a mathematical fit based on a model developed by Voinova. Within the Voigt model for a viscoelastic element, this model calculated the acoustic response of the system to an applied stress.

Multiple frequency and dissipation data, preferably from three frequencies, were required for the accurate modelling.

The applied quartz crystals (5 MHz) were AT-cut and possessed a gold-coated electrode.

Surface Plasmon Resonance

The interaction between gelatin and a variety of ECM and FCS components was measured by surface plasmon resonance (SPR) measurements. The apparatus used was a Biacore-X (GE Healthcare Europe, Diegem, Belgium) equipped with an internal 500 µl Hamilton syringe.

Statistical analysis

Statistical analysis was performed using the student *t*-test. Two values were considered to be significantly different when $p < 0.05$.

3 Chapter II: Synthesis and characterization of the hydrogel precursors

Synthesis of gel-MOD

After swelling of 100 g gelatin (35 mmol ε-amine-sidegroups of lysine and hydroxylysine) in 1 l phosphate buffer (pH 7.8) for one hour, the solution was heated to 40°C. When a homogeneous gelatin solution was obtained, one equivalent of methacrylic anhydride (5.66 ml, 0.038 mol) was added. The reaction mixture was stirred vigorously for one hour at 40°C. Next, the mixture was diluted with 1 l double distilled water and transferred in dialysis membranes (Spectra/Por® 4, MWCO 12,000-14,000 Da). After one day of dialysis in water at 40°C, the obtained derivative was freeze-dried.

Gel-MOD with other modification degrees was obtained by analogous synthesis with different concentrations of methacrylic anhydride.

Characterization of gel-MOD

^{1}H NMR-spectra of modified gelatin were recorded at 40°C in deuterated water. The degree of substitution can be obtained after comparison of the integrations of the characteristic peaks of the methacrylamide-substituent (5.62 ppm and 5.85 ppm) and the integration of a peak of amino acids, which are not involved in the modification (e.g. Val + Leu + Ile at 1.12 ppm). Based on the known amino acid composition of the gelatin applied, the degree of substitution can be calculated, as indicated by the following equation:

$$\text{DS (\%)} = 0.3836 \text{ mol} \times (\text{integration at 5.7 ppm} / \text{integration at 1.1 ppm}) \times (100 / 0.0385 \text{ mol})$$

Synthesis of thiolated gelatin

After swelling of 5 g gelatin (1.75 mmol ε-amine-sidegroups of lysine and hydroxylysine) in 50 ml carbonate buffer (pH 10), the solution was heated to 40°C. When a homogeneous gelatin solution was obtained, 1 mM EDTA (0.015 g) was added in order to complex any metals present, to avoid catalysis of the oxidation reaction. Next, an excess of N-acetyl-homocysteine thiolactone (5 equivalents, 1.51 g) was added. The reaction mixture was stirred vigorously for three hours at 40°C. Subsequently, the mixture was diluted with 50 ml double distilled water and transferred in dialysis membranes (Spectra/Por® 4, MWCO 12,000-14,000 Da). After one day of dialysis in water at 40°C, the thiolated gelatin was freeze-dried.

Both the reaction and the dialysis were performed under argon atmosphere.Gelatin-SH with lower modification degrees were obtained by analogous synthesis with lower concentrations of N-acetyl-homocysteine thiolactone.

Alternatively, thiolation of gelatin (5 g) also occurred by adding traut's reagent (2 equivalents, 0.523 g) to gelatin, previously dissolved in phosphate buffer (pH 8) at 40°C. The reaction proceeded for 45 minutes, followed by dialysis and lyophilization.

Characterization of thiolated gelatin

Determination of modification degree

Direct method

First, a stock solution was prepared, composed of 4.5 mg Ellman's reagent in 1 ml phosphate buffer (pH 8), containing 1 mmol EDTA. For the preparation of the thiolated-gelatin solutions, freeze-dried samples were applied. Protein suspensions (1 mg/ml double distilled water) were heated for 2 hours at 40°C until a homogeneous solution was obtained. To 250 µl heated protein solution (250 µl H_2O for blank), 50 µl stock solution and 2.5 ml reaction buffer were added successively. After mixing thoroughly, the solution was incubated at 35°C for 15 minutes. Finally, the absorption was measured at 412 nm and 37°C. All experiments were performed in triplicate.
Similar measurements were performed, in which the gelatin solutions were replaced by a series of solutions with known concentrations of thiol groups. A calibration curve, based on a dilution series (0.25 mM to 1.5 mM) of cysteine, was formulated.

Indirect method

20 mg ortho-phthalic dialdehyde (OPA) was dissolved in 10 ml ethanol. Next, the mixture was diluted to 50 ml with double distilled water. A second stock solution, containing 25 µl 2-mercaptoethanol in 50 ml borate buffer (pH 10) was then prepared. To 50 µl heated gelatin solution (1 g / 40 ml double distilled water), 950 µl double distilled water, 1500 µl mercaptoethanol solution and 500 µl of the second stock solution were added subsequently, followed by vigorously mixing. Finally, the absorbance at 335 nm was measured compared to a blank (i.e. mixture with water in stead of gelatin) at 37°C. All measurements were performed in triplicate.

Analogous measurements were performed with n-butylamine (0.002 M to 0.01 M) standards to obtain a calibration curve. Calculation of the amount of free amine groups, remaining after the modification, enabled the determination of the modification degree of gelatin-SH.

Determination of average molecular weight

Seven mg thiolated gelatin was dissolved in 1 ml phosphate buffer (pH 7.4) at 40°C. The average molecular weight and the molecular weight dispersity were obtained by means of size exclusion chromatography (SEC) at 80°C. Calibration occurred by means of pullulan standards.

Synthesis of CS-MOD

Chondroitin sulphate (1 g, 2 mmol disaccharide repeating units, 6 mmol hydroxyl functions, type C, Sigma-Aldrich) was dissolved in 50 ml double distilled water at room temperature. Subsequently, an excess methacrylic anhydride (8.94 ml, 60 mmol, Sigma-Aldrich) was added dropwise. Simultaneously, the pH of the reaction mixture was adjusted to 8, by adding NaOH (5 N). The methacrylic acid/NaOH ratio was 1. The mixture was then stirred at room temperature for 2 hours. Finally, the solution was diluted with 50 ml double distilled water and transferred to a dialysis membrane (Spectra/Por® 3, Polylab, MWCO 3500 Da, 3 days), followed by lyophilization.

CS-MOD with lower modification degrees was obtained by adding lower amounts of methacrylic anhydride.

Characterization of CS-MOD

Determination of degree of substitution

The ^{1}H-NMR spectrum of CS-MOD was recorded at room temperature in deuterated water using a Bruker WH 500 MHz. The degree of substitution was calculated comparing the integrations (I) of the characteristic peaks of the methacrylate-substituent ($I_{1.95\ ppm}$, $I_{5.76\ ppm}$ and $I_{6.19\ ppm}$) and the methyl group from the CS N-acetyl group ($I_{2.04\ ppm}$) using the following equation:

$$DS\ (\%) = 3 \times 100 \times I_{5.7\ ppm} / (I_{1.95\ ppm} + I_{2.04\ ppm} - 3 \times I_{5.7\ ppm})$$

Determination of average molecular weight

Ten mg chondroitin sulphate methacrylate was dissolved in 1 ml phosphate buffer (pH 7.4) at room temperature. The average molecular weight and the molecular weight dispersity were obtained by means of size exclusion chromatography (SEC) at 80°C. Calibration occurred by means of pullulan standards.

Synthesis of HA-MOD

0.05 g hyaluronic acid was dissolved in 10 ml double distilled water at room temperature. Next, an excess methacrylic anhydride (10 equivalents, 803 µl) was added dropwise. Simultaneously, the pH of the reaction mixture was adjusted to 8, by adding NaOH (5 N). The ratio between the added amounts of methacrylic anhydride and NaOH was 1 to 1.12. The mixture was then stirred at room temperature for 2 hours. Finally, the solution was diluted with 10 ml double distilled water and transferred to dialysis membranes (Spectra/Por® 4, MWCO 12,000-14,000 Da), followed by lyophilization.
HA-MOD with lower modification degrees was obtained by adding lower amounts of methacrylic anhydride.

Characterization of HA-MOD

Determination of degree of substitution

^{1}H NMR-spectra of HA-MOD were recorded at room temperature in deuterated water. The degree of substitution could be obtained after comparison of the integrations of the characteristic peaks of the methacrylate-substituent (1.98 ppm, 5.78 ppm and 6.21 ppm) and the integration of the characteristic peak corresponding to the methyl groups in native HA (2.06 ppm). Consequently, the degree of substitution could be calculated, as indicated by the following equation:

DS (%) = 100 x (integration at 5.78 ppm) /
((sum of integrations at 1.98 and 2.06 ppm – 3 x (integration at 5.78 ppm)) / 3)

4 Chapter III: Preparation and characterization of hydrogel films

Hydrogel preparation

Gel-MOD hydrogels

Room temperature

Gel-MOD DS 65% (1 g) was dissolved in 10 ml double distilled water at 40°C. Next, the photoinitiator Irgacure® 2959 (5 µmol, 2 mol% to the methacrylamides) was added, followed by injection of the mixture between two parallel glass plates, separated by a 1 mm thick silicone spacer (figure 9-1).

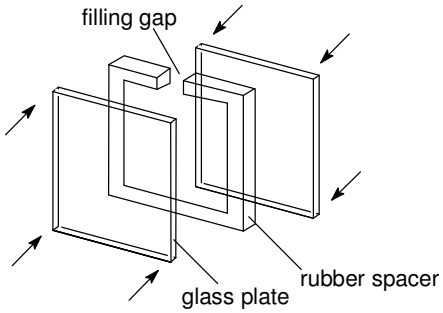

Figure 9-1: Cast for the preparation of 1 mm thick hydrogel films.

Finally, the hydrogel was irradiated with UV-light (276 nm, 10 mW/cm^2) for 20 minutes on both sides. Crosslinked hydrogels were stored at 5°C until their evaluation.

Cryogels

Aqueous gelatin solutions with varying concentrations (0.2 - 2 w/v %) were prepared by adding double-distilled water to gelatin at 40°C. One freeze-thaw cycle included storage in the freezer at -30°C during 24 hours, followed by 24-hours storage in the

fridge at 5°C. As controls, non-frozen hydrogels were kept in the fridge at 5°C for the same incubation time.

For the cryogels developed, possible effects of the cryogenic parameters applied (cooling rate, freezing temperature, thawing rate) were also evaluated.

The cooling rate and freezing temperature were programmed using a Julabo, type FP40-ME (Julabo, Seelbach, Germany). In order to evaluate the influence of the cooling rate on the cryogels developed, all materials were cooled from 21°C to -20°C at a certain speed (0.1 - 1°C/min). Next, the samples were heated to 5°C at a thawing rate of 0.5°C/min. Finally, the scaffolds were stored in the fridge overnight at 5°C.

Gels with a varying thawing rate were prepared by freezing them first for 30 minutes at -20°C. Next, the cryogels were thawed to 2°C with a varying speed (0.06 – 1°C/min) and stored overnight in the fridge at 5°C.

Beside the physically crosslinked cryogels, chemically crosslinked cryogels were also prepared. To an aqueous solution of gel-MOD (DS 60%), 2 mol% photo-initiator Irgacure® 2959, as calculated to the methacrylamide side chains, was added. Gels were UV-cured in situ, during rheology, using a Novacure 2100 spot curing system (EXFO Photonic Solutions Inc., Hampshire, UK).

Hydrogels based on gel-SH

Gel-SH DS 70% (1.5 g) was dissolved in 10 ml double distilled water at 40°C. Next, hydrogen peroxide (0.5 equivalents, 14 µl) was added, followed by injection of the mixture between two silanized glass plates (figure 9-1).

Silanization occurred by incubating the glass plates overnight into an aqueous solution of 2 v/v% H_2SO_4/HNO_3, followed by an overnight incubation in toluene, containing 10 v/v% trimethylsilylchloride.

Disulfide crosslinked gelatin hydrogels were stored at 5°C until their evaluation.

Hydrogels based on CS-MOD

Chondroitin sulphate methacrylate (0.1-1g) with various modification degrees (5%-40%) was dissolved in 20 ml double distilled water at room temperature. Next, the photoinitiator Irgacure® 2959 (2 mol% to the methacrylates) was added, followed by injection of the mixture between silanized glass plates (figure 9-1). Finally, the hydrogel was irradiated with UV-light (276 nm, 10 mW/cm^2) for 20 minutes on both sides or crosslinked in situ during rheology.
Crosslinked hydrogels were stored at 5°C until their evaluation.

Hydrogel characterization

Dynamic oscillation measurements

The visco-elastic properties of the **hydrogels** were evaluated by means of dynamic oscillation measurements at small deformations according to the following procedures:

Deformation scan: The linear visco-elastic range was determined by isothermal measurements (20°C) of the elasticity and viscosity modulus G' and G'' as a function of the deformation ($\gamma = 0.01 \rightarrow 1$) and at constant frequency (1 Hz).
Frequency scan: Mechanical spectra were recorded at a constant deformation of 0.1% strain in the frequency range of 0.1-10 Hz at 20°C.
Time scan: The gelation of the polymer mixture was followed as a function of time and temperature. The other parameters (1 Hz, 0.1% strain and $F_N = 0.1$ N) were kept constant.
Temperature scan: The temperature dependence of the elasticity modulus G' or the viscosity modulus G'' was measured by oscillation shear measurements during heating or cooling in the range of 20°C to 60°C (rate = 3.9°C/min). These measurements were performed at a constant frequency (1 Hz) and at a constant deformation (0.1% strain).

Cryogels were evaluated according to the following procedure. Oscillation measurements were performed using two parallel plates, with the upper plate having a diameter of 50 mm. Amplitude scans were performed at 5°C, at a frequency of 1 Hz and with a gap of 0.5 mm. Mechanical spectra were obtained at 5°C, using a strain of 0.5% and a gap of 0.5 mm. G' and G'' were measured by means of oscillation rheology.

Swelling experiments

Hydrogel films (1 mm thick, Ø 32 mm) were, after weighing, incubated in 80 ml double distilled water, containing NaN_3, at 37°C. At regular time points, the swollen discs were removed, dipped gently with paper and weighed. The measurements were expressed as %swelling and calculated, based on the following formula:

$$\text{swelling (\%)} = [(W_{ht} - W_{d0}) / W_{d0}] \times 100\%$$

W_{d0} is the weight of dry gel at the initial time 0, W_{ht} is the weight of hydrated gel at time t.

If the hydrogels are utilized directly from the cast and the swelling studies are thus started with hydrated hydrogel films, extra discs, taken from the respective hydrogels, needed to be dried. The dry weight W_{d0} at time 0, needed for the calculation of the swelling percentage, could be obtained based on this second hydrogel series.
After equilibrium swelling (e.g. overnight), the hydrogel discs were removed, freeze-dried and weighed again. The loss of dry mass of the hydrogel during incubation at 37°C, enabled the calculation of the polymer gel fraction. The equation is based on the mass of the dry gel after incubation (= W_{de}) and the initial mass of the dry gel before incubation (= W_{d0}). Swelling experiments always were performed in triplicate.

$$\text{gel fraction (\%)} = (W_{de} / W_{d0}) \times 100\%$$

Texturometrical analysis

The hydrogel films (5 cm x 5 cm x 1 mm thick) were applied in the centre of the flat bottom plate with round excision (Ø 25 mm). The polymers were fixed onto the plate by applying a second plate with round excision (Ø 25 mm) on the gelatin films. The measurements were generally performed in triplicate at 21°C.

When performing 'texture profile analysis' tests (TPA-test), the hydrogel was compressed twice with a cylindrical probe (Ø 3 mm) over a distance of 3 mm with a rate of 20 mm/min.
When performing fracture tests, the cylindrical probe compressed the gel once until fracture occurred (20 mm/min). In the present work, fracture was defined as a decrease of the maximum force with 20%.

5 Chapter IV: Preparation and characterization of gelatin scaffolds

Scaffold preparation

Gel-MOD with a degree of substitution of 60% was selected. As an example, the synthesis of 10 w/v% gelatin is given. In a typical experiment, 1 g modified gelatin was dissolved in 10 ml distilled water at 40°C, containing 2 mol% photo-initiator Irgacure® 2959 as calculated to the methacrylamide side chains. The solution was then injected into the mould of the cryo-unit (figure 3-22), after which the solution was allowed to gel for 1 hour at room temperature. In a final curing step, the hydrogel was exposed to UV-light (276 nm, 10 mW/cm^2) for 2 hours.
After placing the chemically crosslinked hydrogel in the cryo-unit, the temperature of freezing and the cooling rate were programmed with a Julabo, type FP40-ME. Under the bottom of the mould, a Peltier element (also known as thermo electric cooler, TEC) was positioned. This device enables a temperature gradient of maximum 30°C to be established between the top and the bottom of the mould. The TEC used, was

a DuraTec DT12 type from Marlow industries. The aluminum heat exchangers and the electronic TEC controller were designed, built and assembled by the technical workshop (CWFW) of the Ghent University – Faculty of Sciences. For the samples obtained by applying a temperature gradient, the temperature at the top of the mould was the highest. After incubating the sample for one hour at the final freezing temperature, the frozen hydrogel was transferred to a freeze-dryer to remove the ice crystals, resulting in a porous scaffold.

Gelatin scaffolds with a dissolvable skin were prepared as described earlier. Before applying the cryogenic treatment, a 10 w/v % solution of non-modified gelatin was injected on the top and the bottom of the chemically crosslinked hydrogel, which was positioned in the mould of the cryo-unit. The resulting layer was 0.5 mm in thickness on a 5 mm thick hydrogel. After cryogenic treatment and freeze-drying of the hydrogels, the samples were incubated in deionised water at 40°C for 5 hours. Freeze-sections of the incubated scaffolds were made with a microtome and studied using optical microscopy.

Scaffold characterization

Water uptake capacity

Freeze-dried gelatin samples (1 x 1 x 0.5 cm^3) were weighed and then immersed in 80 ml double distilled water at 37°C, in the presence of sodium azide to prevent bacterial growth. At regular time points, the hydrogels were removed from the solution, dipped gently with paper and weighed again. The degree of swelling was calculated, as described earlier in the present chapter.

All data points are the mean of three separate measurements.

Dynamic vapour sorption analysis

The influence of the hydrogel structure on the degree of water vapour sorption was examined using a Dynamic Vapour Sorption apparatus. All experiments were

performed at 25°C or at 37°C. Dry nitrogen was passed through water in order to give 100% relative pressure of the solvent. The relative pressure of water flowing via the sample was controlled via a computer program which controls the appropriate flow to the wet (100% relative pressure water) and dry side (dry nitrogen).

Mechanical testing of hydrogels

The mechanical properties of the hydrogels, swollen to equilibrium, were studied using a TA500 Texture Analyser. The samples (1 x 1 x 0.5 cm^3) were compressed by a cylinder (3 mm diameter) until a strain of 20% was reached. Next, the stress (MPa) corresponding to each strain (%) was plotted. The compression modulus was calculated from the slope of the initial linear part of the compression curve. Each measurement was performed in triplicate.

In vitro degradation of hydrogels

The *in vitro* degradation behaviour of the hydrogels was studied by incubating the freeze-dried samples (Ø 0.8 x 0.5 cm) in 0.5 ml Tris-HCl buffer (0.1 M, pH 7.4) in the presence of 0.005 % w/v NaN_3 and 5 mM $CaCl_2$ at 37°C. After 1 hour, 0.5 ml collagenase (200 U/ml), dissolved in Tris-HCl buffer, was added. At different time intervals, the degradation was stopped by addition of 0.1 ml EDTA solution (0.25 M) and subsequent cooling of the sample on ice. Next, the hydrogels were washed three times during ten minutes with ice-cooled Tris-HCl buffer and three times with double-distilled water. The partially degraded scaffolds were tested for their mechanical properties using a texturometer. The corresponding compression moduli were calculated and plotted as a function of the degradation time. After texturometry analysis, the hydrogels were freeze-dried for the determination of the gel fraction (i.e. the polymer fraction that remains after degradation), as described earlier.

6 Chapter V: Preparation and characterization of scaffolds based on chondroitin sulphate and gelatin

Scaffold preparation

Using the gel-MOD and CS-MOD hydrogel precursors, different types of hydrogels were developed. As an example, the 10 w/v% gel-MOD hydrogels (further referred to as type I hydrogels) were obtained by dissolving 1 g gelatin type B, previously modified with methacrylamide side groups, in 10 ml double distilled water at 40°C containing 2 mol% photo-initiator Irgacure® 2959, as calculated to the amount of methacrylamide side chains. The solution was then injected into the mould of a cryo-unit, after which the solution was allowed to gel for 1 hour at room temperature. In a final step, the hydrogel was exposed to UV-light (276 nm) for 2 hours, followed by applying a cryogenic treatment (cooling range on top side: 21°C until -30°C, cooling rate: 0.15°C/min). In addition, a temperature gradient (T_{top} - T_{bottom} = 30°C) between top and bottom of the scaffold was applied during the freezing step. After incubating the sample for one hour at the final freezing temperature, the frozen hydrogel was transferred to a freeze-dryer to remove the ice crystals, resulting in a porous scaffold. CS-MOD based scaffolds and hydrogels containing both gel-MOD and CS-MOD (further referred to as respectively type III and type II scaffolds) were developed by applying the same procedure as for the gel-MOD hydrogels. For type II hydrogels, the amount of CS-MOD was varied between 1 - 5 w/v%, while keeping the gel-MOD concentration constant (10 w/v%).

Characterization

Phase separation phenomena upon mixing gel-MOD and CS-MOD were studied by AFM. Glass slides (ø 1 cm) were spincoated with aqueous solutions of 5 w/v% gel-MOD with or without 1 w/v% CS-MOD during 90 seconds at 6000 rpm. Next, AFM-studies were performed on the spincoated glass slides with a Nanoscope IIIa Multimode applying the 'tapping mode' in air.

7 Chapter VI: Alternative crosslinking procedures

E-beam

Gel-MOD with a degree of substitution of 60% was selected. 1 g modified gelatin was dissolved in 10 ml distilled water at 40°C. The solution was then injected into the mould of the cryo-unit, after which the solution was allowed to gel for 1 hour at room temperature. Finally, the samples were treated cryogenically as described in the previous paragraph.

Both frozen and freeze-dried samples were irradiated in the absence of oxygen. The samples were irradiated with electrons from a 15 MeV linear electron accelerator. This accelerator delivered electron beams with a well-defined energy in the range 3-15 MeV and with an average power up to 5 kW. For electron irradiation, an 80 µA 10 MeV beam traversed a water-cooled vacuum window and 80 cm of air, so that the lateral dose distribution was flattened by scattering. The electrons that interacted with the samples had an energy of 8 MeV (that is 10 MeV minus the energy-loss in the vacuum window). The average duration for a 25 kGy irradiation was 400 s. Before every irradiation, a dosimetric calibration was performed.

Crosslinking by use of redoxinitiators

Cerium ammonium nitrate

10 w/v% gel-MOD hydrogels were prepared as described earlier. Freeze-dried scaffolds (1 g) were immersed in 20 ml double distilled water in the presence of 10 mol% (13 mg) cerium ammonium nitrate for varying incubation times (1 – 24 h).

Alternatively, 10 mol% cerium ammonium nitrate (13 mg) was added to 10 ml double distilled water, containing 1 g gel-MOD at 40°C. Finally, a cryogenic treatment was applied, followed by lyophilization and ^{1}H-NMR analysis.

Ammonium persulphate + TEMED

1.4 g gel-MOD was dissolved in 14 ml double distilled water at 40°C in the presence of 10 mol% ammonium persulphate (8 mg) and 26 µl TEMED. Next, a series of samples was treated cryogenically as described earlier, followed by overnight incubation at -30°C and lyophilization. A second series of samples was incubated overnight at 5°C without applying a previous cryogenic treatment.
Finally, the gel fractions were determined after incubation of the freeze-dried samples in double distilled water at 37°C.

Fenton's reagent

Cryo-treated and freeze-dried gel-MOD scaffolds (1 g) were incubated for 1 to 24 hours in 20 ml double distilled water in the presence of 10 mol% iron (II) D-gluconate dihydrate (12 mg) and 7.2 µl H_2O_2. Additionally, 44 mg ascorbic acid was added in a second series of experiments.
Finally, the gel fractions were determined after incubation of the freeze-dried samples in double distilled water at 37°C.
Alternatively, 10 mol% iron (II) D-gluconate dihydrate (12 mg) and 7.2 µl H_2O_2 (with and without 44 mg ascorbic acid) were added to 10 ml double distilled water, containing 1 g gel-MOD at 40°C. Finally, a cryogenic treatment was applied, followed by lyophilization and ^{1}H-NMR analysis.

Crosslinking with EDC

Cryogenically treated and freeze-dried gelatin scaffolds were incubated overnight in 9:1 acetone/H_2O mixtures (25 ml) in the presence of 45 mg EDC with or without 5.4 mg NHS. Next, the scaffolds were washed two times in double distilled water, followed by freeze-drying and characterization using SEM and µ-CT.

8 Chapter VII: Interaction between gelatin and extra-cellular matrix components

Surface plasmon resonance

The interaction between gelatin and various ECM components was measured by surface plasmon resonance (SPR) measurements. All measurements were performed at 25°C using phosphate buffer (0.05 M, pH = 7.4). The flow rate was set to 50 µl/min. The sensor surface was spincoated using 90 µl of an aqueous 5 w/v% gel-MOD (degree of substitution 60%) solution at a speed of 6000 rpm during 90 seconds. The presence of gelatin on the sensor chip after spincoating and the stability of the applied layer after incubation in SPR running buffer, was confirmed by ATR-FTIR measurements (Biorad FT-IR spectrometer FTS 575C) and contact angle measurements.

After spincoating, the gelatin coated sensor was inserted into the apparatus. After stabilisation of the baseline, 50 µl of various concentrations of a protein/glycosaminoglycan solution was injected. In a final step, after stabilisation of the signal, 50 µl of an antibody solution (50 mg/l for anti-fibronectin and 200x dilution of stock for anti-chondroitin sulphate) was injected. All values reported are relative to a reference flow channel.

Quartz Crystal Microbalance

Measurements were done using the QCM-D technique (Q-Sense E4, Q-Sense AB, Göteborg, Sweden). Multiple frequency and dissipation data, preferably from three frequencies, were required for the accurate modelling. QCM crystals were spincoated with 90 µl of a 5 w/v% gel-MOD (degree of substitution 60%) solution at a speed of 6000 rpm during 90 seconds. Next, the gelatin coated sensors were inserted into the QCM apparatus. After stabilisation of the baseline (600 s), various fibronectin concentrations (1 and 25 µg/ml) were rinsed over the surface during 1100 s. After

1700 s, the system was flushed with PBS and after 2000 s, anti-fibronectin (0.051 g/l) was injected during 1300 s. All experiments were performed at 25°C.

Radiolabelling experiments

The labelled fibronectin (^{125}I-Fn) was obtained by following a specific protocol described below.

Approximately 1 mg fibronectin was incubated with carrier-free 10 µl ^{125}I (1 mCi) in a reaction vessel (5 ml) coated with ? µg iodogen for 15 minutes at room temperature. The reaction mixture was then removed from the oxidant and free radioactivity was removed by gel filtration through PD-10 columns (?) equilibrated with PBS. The specific radioactivity obtained immediately after labelling was 1.12 µCi per µg protein. The stock solution was finally diluted with PBS to the final concentrations, used in the experiments.

Hydrogel films (Ø 7 mm, type A and type B) and hydrogel scaffolds (0.5 mm thickness, Ø 7 mm) were incubated for 1 hour in respectively 500 µl and 1 ml phosphate buffered saline (pH 7.4) (PBS), containing various iodine-labelled fibronectin concentrations (1-200 µg/ml). Next, the hydrogels were removed and washed three times in 500 µl PBS for 5 minutes. Finally, the radioactivity of the incubating solution, the three washing solutions and the hydrogels was measured. The mass of bound fibronectin was determined based on the counts of the hydrogels compared to the total amount of added counts (i.e. from incubating and washing solutions). All experiments were performed in triplicate.

Water uptake capacity study

Freeze-dried gelatin samples (1 x 1 x 0.5 cm^3) were weighed and then immersed in 80 ml double distilled water at 37°C, in the presence of sodium azide to prevent bacterial growth. At regular time points, the hydrogels were removed from the solution, dipped gently with paper and weighed again. The hydration properties were calculated using the following equation:

$$\% \text{ Swelling} = [(W_t - W_0)/W_0] \times 100\%$$

W_0 = initial weight of the dry scaffold

W_t = weight of the hydrated/swollen hydrogel at time point t.

All data points were the mean of three separate measurements.

9 Chapter VIII: *Biological Evaluation*

Blood compatibility studies

The RBC were isolated from horse blood and washed three times with HEPES buffer (20 mM, 150 mM NaCl, pH 7.4) at room temperature. A 2% RBC solution was used within 24h after collection. The various scaffolds (Ø 0.5 cm) were added to the RBC and the solutions were allowed to stand for 24h at 37°C. The supernatants were centrifuged at 4000 rpm for 5 min. Haemolysis was investigated and quantified by measuring the haemoglobin release at 545 nm. The readings were compared with Triton X-100 (1%) and HEPES buffer which provided respectively the 100 and 0% values, so that haemolysis could be assessed according to the formula:

$$\text{haemolysis (\%)} = \frac{A_{sample} - A_{blank}}{A_{100\%\,haemolysis}} \text{ x } 100\%$$

Cell cultivation

The *in vitro* cell biocompatibility of both types of scaffolds was evaluated by applying a panel of human cells on the hydrogels: endothelial cells (human umbilical vein endothelial cells, HUVEC), osteoblasts (MG-63 and CAL-72), human foreskin fibroblasts, glial cells (U373-MG) and epithelial cells (HELA). All cells used were typically passaged twice weekly. HUVEC were isolated from umbilical veins as described earlier by Jaffe et al. The HUVEC were propagated in M199 medium

(Sigma) supplemented with 20% foetal calf serum (FCS) (PAA), 1% Penicillin/Streptomycin (Gibco), 0.34% Glutamax (Gibco), 25 µg/ml endothelial cell growth factor (Beckton Dickinson) and 25 µg/ml sodium heparin (Sigma-Aldrich) at 37°C (5% CO_2) on gelatin-coated (Sigma-Aldrich, 0.2 %) cell culture surfaces. All experiments were performed with cells in passage 2 or 3.

MG-63 and U373-MG were cultured in EMEM (Minimum Essential Medium Eagle, Sigma) supplied with 10% FCS, 1% Penicillin/Streptomycin (Gibco) and 1% Glutamax (Gibco) at 37°C (5% CO_2).

CAL-72 and human foreskin fibroblasts were cultured in DMEM (Dulbecco's Modified Eagle Medium, Sigma) supplied with 10% FCS, 1% Penicillin/Streptomycin (Gibco) and 2% Glutamax (Gibco) at 37°C (5% CO_2).

HELA cells were cultured in RPMI medium (Gibco) supplied with 5% FCS, 1% Penicillin/Streptomycin (Gibco) and 1% Glutamax (Gibco) at 37°C (5% CO_2).

Cell seeding on the hydrogels

Prior to cell seeding, the freeze-dried hydrogels were incubated in cell culture medium with serum for two hours at room temperature. The swollen hydrogels were then cut with a scalpel to 15 mm x 4 mm x 3 mm (L x W x H) cubes. For all experiments, the initial number of cells seeded on the biomaterial (L x W x H, 15 mm x 4 mm x 3 mm) was 160,000. Cell seeding was performed by drop seeding. For type I hydrogels, cells were seeded at the site of the largest pores. To immerse the gelatin hydrogels completely with medium and thus to prevent them from floating, the hydrogels were 'fixed' to the bottom of 6-well plates using silicone flexiPERM rings (Vivascience). The amount of medium required to prevent the flexiPERM rings (and thus the hydrogels) from floating was 3 ml. After one day, the flexiPERM rings were removed and the hydrogel samples were transferred to a 12 well plate, flipped and incubated with 2 ml fresh medium. Culture medium was changed twice a week.

Cell visualization within the hydrogels

Cells seeded on the hydrogel were visualised within the gelatin hydrogels at different time points using confocal microscopy. Cell-seeded hydrogels were first incubated with calcein-AM (1 µg/ml) for 5-10 minutes at 37°C in the dark. Calcein-AM is a cell-permeable compound which is taken up by viable cells and subsequently hydrolysed by intra-cellular esterases. Upon hydrolysis, calcein-AM becomes highly fluorescent and cell-impermeable which make it suited for vital cell visualisation purposes. After the incubation step, the hydrogels were transferred into a petri-dish for confocal microscopy analysis (Leica TCS NT).

Immunofluorescent staining of cell seeded hydrogels

At different time points after cell seeding, HUVEC were fixed by incubating the cell-seeded hydrogels in a MeOH/EtOH mixture (2/1) for 10 minutes at room temperature. After a washing step with PBS (3 times, 5 minutes in total), the cells were incubated with the first antibody (either mouse anti-E-selectin or mouse anti-PECAM-1, 1:50 dilution in 1% PBS/BSA) for one hour at room temperature. After the second washing step with PBS, the cells were incubated with the second antibody (goat anti-mouse Alexa 488, 1:1000 dilution in 1% PBS/BSA) for one hour in the dark at room temperature. After the third washing step with PBS, cell nuclei were stained with DAPI for 5 minutes in the dark at room temperature. After a final washing step with PBS, E-selectin or PECAM-1 were visualized using confocal microscopy. For the gene expression studies, HUVEC seeded on gelatin coated tissue culture plastic were taken as controls. For the E-Selectin expression studies, HUVEC seeded hydrogels and HUVEC seeded on gelatin coated tissue culture plastic stimulated for 4 hours using lipopolysaccharide (LPS, 1:1000 dilution in cell medium from a 1 mg/ml LPS stock) were selected as additional controls.

Appendix

List of publications

1. Van Vlierberghe S, Dubruel P, Lippens E, Masschaele B, Van Hoorebeke L, Cornelissen M, Unger R, Kirkpatrick CJ, Schacht E. Toward modulating the architecture of hydrogel scaffolds: Curtains versus channels. Journal of Materials Science – Materials in Medicine 2008; 19:1459-1466, SCI = 1.562
2. Van Vlierberghe S, Cnudde V, Dubruel P, Masschaele B, Cosijns A, De Paepe I, Jacobs P, Van Hoorebeke L, Remon JP, Schacht E. Porous Gelatin Hydrogels: 1. Cryogenic Formation and Structure Analysis. Biomacromolecules 2007; 8:331-337, SCI = 3.664
3. Dubruel P, Unger R, Van Vlierberghe S, Cnudde V, Jacobs P, Schacht E, Kirkpatrick, C.J. Porous Gelatin Hydrogels: 2. In Vitro Cell Interaction Study. Biomacromolecules 2007; 8:338-344, SCI = 3.664
4. Van Vlierberghe S, Dubruel P, Lippens E, Cornelissen M, Schacht E. Correlation between cryogenic parameters and physico-chemical properties of porous gelatin cryogels. Journal of Biomaterials Science – Polymer Edition 2008; submitted, SCI = 1.6
5. Van Vlierberghe S, De Wael K, Busschop H, Adriaensen A, Van der Eycken J, Schacht E, Dubruel P. Ozonisation and cyclic voltammetry as efficient methods for the regeneration of gelatin coated SPR chips. Macromolecular Bioscience 2008; submitted, SCI = 2.521
6. Van Vlierberghe S, Dubruel P, Schacht E. Effect of cryogenic treatment on the mechanical properties of gelatin hydrogels. Cryogenics 2008; submitted, SCI = 0.927